



City Research Online

City, University of London Institutional Repository

Citation: Tang, K. Y. (1999). Double-Diffusive Convection in a Vertical Slot. (Unpublished Doctoral thesis, City, University of London)

This is the accepted version of the paper.

This version of the publication may differ from the final published version.

Permanent repository link: <https://openaccess.city.ac.uk/id/eprint/30764/>

Link to published version:

Copyright: City Research Online aims to make research outputs of City, University of London available to a wider audience. Copyright and Moral Rights remain with the author(s) and/or copyright holders. URLs from City Research Online may be freely distributed and linked to.

Reuse: Copies of full items can be used for personal research or study, educational, or not-for-profit purposes without prior permission or charge. Provided that the authors, title and full bibliographic details are credited, a hyperlink and/or URL is given for the original metadata page and the content is not changed in any way.

Double-Diffusive Convection in a Vertical Slot

Kit Yee Tang

A thesis submitted for the degree of
Doctor of Philosophy

City University
Department of Mathematics
London

20th May 1999

Contents

1	Introduction	1
2	Description of the Problem	8
2.1	The Continuity Equation	8
2.2	Equation of Motion	10
2.3	Temperature Equation	12
2.4	Salinity Equation	13
2.5	Formulation of Governing Equations	14
2.6	Non-dimensionalisation	15
2.7	Dimensionless Stream Function	17
2.8	The Background State	18
2.9	Stability Analysis	23
2.10	Eigenvalue Problem	24
3	Full Numerical Method and Results	26
3.1	Runge-Kutta Scheme	26
3.2	Full Numerical Results	28
3.3	Oscillatory Branch and $Ra_S \ll 1$ Solution	35
4	Comparison of Galerkin Method	39
4.1	Galerkin Method	40

5	Asymptotics	57
5.1	Large Ra_S with $\alpha \neq 0$	58
5.2	Small α	68
5.3	Large Ra_T	83
5.4	Thermal Convection and Small Ra_S	95
6	Conclusion	112
	Appendix A: Full Numerical Method	120
	Appendix B: Galerkin Approach	127
B.1	Orthogonal Properties	128
B.2	Integrals for ψ	129
B.3	Integrals for T	138
B.4	Integrals for S	139
B.5	Abbreviated Integrals	143
	Appendix C: Small α	154
C.1	Solution ψ_0	154
C.2	Function $f(Ra_S, \tau)$	157
C.3	Function $g(Ra_S, \tau)$	159
	References	164

Acknowledgements

I am greatly indebted to my supervisor, Dr. Oliver S. Kerr, for his invaluable suggestions, patience and critical review of the thesis. He has provided inspiration, encouragement and research opportunity that helped develop my initial understanding of double-diffusive convection. I would like to thank Prof. P.G. Daniels for his assistance during the early investigation of thermal convection in a vertical slot. I also want to express my gratitude to my husband and family for their continuous support. My research work is supported by SERC grants to the City University (London).

Abstract

For decades there has been considerable interest in flows which can become convectively unstable due to differential diffusion in thermohaline convection. We consider the stability of the steady motion of a stably stratified fluid in an infinite vertical slot generated by a temperature difference across the boundaries. In particular, we are interested in the case where the instabilities are affected by a vertical salt gradient, where salt diffuses more slowly than heat.

The disturbances at marginal instability when a salinity gradient in a slot was subject to differential heating were previously examined by Thangam, Zebib & Chen (1981). We attempt to re-produce their results for the stability boundary using two independent numerical approaches, the Runge-Kutta scheme and the Galerkin method. Our results indicate there are various instability regimes in the linear analyses and most are stationary except for one small curved section on the stability boundary that gives oscillatory solutions. Our results also show that the oscillatory solutions reported by Thangam *et al.* are erroneous. This is confirmed by Young & Rosner (1998) in their recent paper.

We have identified four different asymptotic regimes on the stability boundary. One of these, the limit of a strong salinity gradient, has previously been analysed by Thorpe, Hutt & Soulsby (1969). Other asymptotic regimes including the limits of small wave number, large thermal Rayleigh number and weak salinity gradient are also analysed. These four cases represent almost the entire boundary that separates the stable and unstable modes for double-diffusive instabilities in a vertical slot.

Chapter 1

Introduction

For almost forty years, there has been considerable interest in the field of double-diffusive convection. This is the study of convection in fluids driven by gradients of two components with different molecular diffusivities. The archetypal example is salt and heat which both affect the density. When gradients of two such components are present even in a stably stratified fluid convection can occur. Since the most widely considered combination is that of heat with high diffusivity and salt with low diffusivity, this process is also known as ‘thermohaline’ or ‘thermosolutal’ convection.

In double-diffusive systems, the form of motions in the fluid depends on whether the driving source is initiated by the faster or slower diffusive component. The two simple situations in figure 1.1 illustrate the characteristics in two possible types of motion. The first case was considered by Stommel, Arons & Blanchard (1956). They considered a long narrow pipe inserted vertically through a region of the ocean where warm salty water overlies colder fresher denser water. The upward-pumping water quickly becomes the same temperature as its surroundings at the same level, while it remains fresher and so is less dense. The relative buoyancy of the water in the pipe drives the water up, and a salt fountain would continue to flow for as long as a vertical

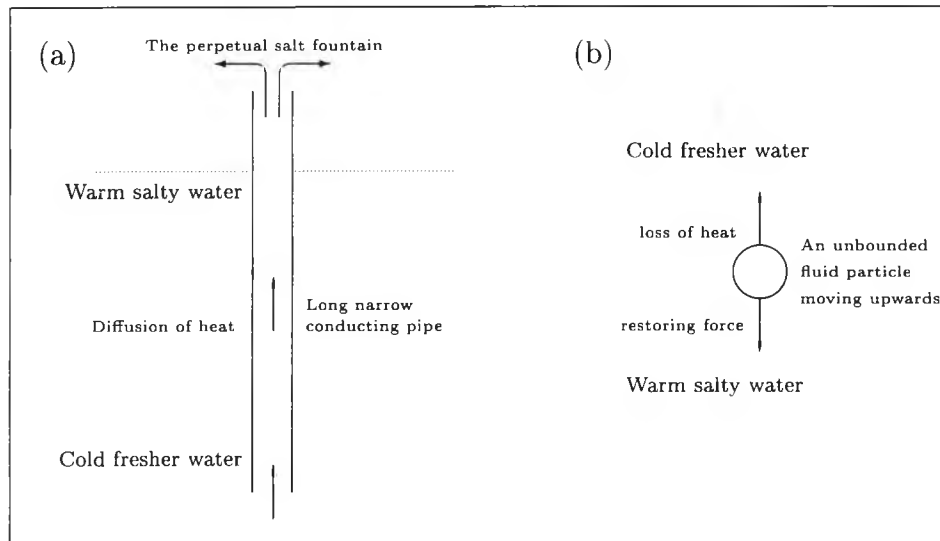


Figure 1.1: Outlining the two cases of fluid motion where the opposing vertical gradients of heat and salt are considered. (a) shows the salt fountain and (b) gives the oscillatory motion.

salinity gradient is there to supply the potential energy. The converse situation looks at a fluid particle which is displaced upwards in an environment where warm salty water is underneath cold fresher water. Such a particle tends to lose heat faster than salt so it is heavier than its surroundings. Therefore it tends to fall back to its original position due to buoyancy effects and then overshoots. It is possible that the overshoot will be greater than the initial displacement, and so the disturbance can grow. The motion produced is oscillatory where heat is the driving component.

A major discovery was made by Stern (1960) who realised the lower diffusivity of salt removed the need for a pipe, as salt remains in the upward moving fluid. He realised that in the first situation down-flowing warm salty water loses heat but not salt to the surrounding cold fresher water, thereby becoming denser and accelerating downwards. Cold fresher up-flowing water gains thermal buoyancy and so accelerates upwards. Long narrow convection cells called 'salt fingers' are formed due to the rapid diffusion of heat relative to salt. In the second situation, with warm salty water under cool fresh water,

it was Stern who first noted the possibility of oscillatory instability due to the loss of heat giving rise to an enhanced restoring force and hence growing oscillations. This is known as the 'diffusive instability'.

Although the theoretical discovery of double-diffusive phenomena was credited to Stern for salt fingers, the first salt finger experiment was in fact performed by Jevons (1857) in his study motivated by cloud observations. He appreciated the importance of thermal conduction to the instability when he introduced warm sugar water over cold fresh water. Rayleigh (1883) was inspired by Jevons' work to examine stratified fluids in which the effects of heat and solute diffusion were neglected. In this work he was first to derive the expression for the buoyancy frequency for internal waves. Almost a century after Jevons' insight, the paper by Stommel *et al.* on the perpetual salt fountain was published. These authors were close to understanding the finger instability, but it was Stern, their co-worker, who independently derived the theory behind double-diffusive convection.

The importance of double-diffusive convection in applications to oceanography was initially recognised in the 1960s. This period marked the beginning of major ocean experiments to confirm the existence of double-diffusive convection in the Mediterranean outflow and in the Caribbean Sea. Thermohaline stratification in the Atlantic underneath the warm and salty Mediterranean outflow was reported by Tait & Howe (1968, 1971). Fingers have been observed in the deep ocean by Williams (1974) and double-diffusive processes in the Gulf stream (Williams, 1981). Evidence indicated much of the ocean is unstable to double-diffusive processes and seems to be affected by their presence. Both salt fingers and diffusive convection are active ocean mixing processes. Much of the main thermocline of the mid- and low-latitude ocean

is unstable to salt fingers, and double-diffusive intrusions are likely an important lateral mixing agent in some areas (Schmitt, 1994). The presence of double-diffusive mixing has significant implications for the thermohaline circulation and thus the ocean climate as well. The complicated nature of the convection in the largely unexplored ocean which covers most of the Earth is one of the concerns of the study of oceanography. This area of research has been growing almost exponentially since its recognition. Many new applications of the basic phenomenology continue to rise in fields as diverse as geophysics, astrophysics, metallurgy and chemistry. Examples include the effects of magma chambers to the layering of igneous rock, convection due to solar radiation, convection in mushy layers during solidification (Huppert, 1990), convection of the Earth's mantle and at the core-mantle boundary.

A broad view of double-diffusive convection is given by Huppert & Turner (1981), Schmitt (1994) and Brandt & Fernando (1996).

It is well known that horizontal temperature and salinity gradients can drive double-diffusive instabilities in fluids. These instabilities have been investigated by various people looking at many different configurations. The linear stability of a stratified horizontal fluid layer has been reported by Stern (1960), Wallin (1964), Veronis (1965), Nield (1967), Baines & Gill (1969) and Turner (1974). Experiments involving opposing vertical gradients of two solutes in a container with a sloping boundary are due to Turner & Chen (1974), Chen & Wong (1974), Chen (1975) and Linden & Webber (1977). Another type of experiment containing a stable solute gradient being heated along a vertical or sloping boundary has been looked at by Thorpe, Hutt & Soulsby (1969), Hart (1971, 1973), Chen & Sandford (1977), Paliwal (1979) and Paliwal & Chen (1980). The instability of a finite front confined between two

different types of fluid was examined by Ruddick & Turner (1979), Holyer, Jones, Priestly & Williams (1987) and Ruddick (1992). Other experiments which have instabilities that occur at a single vertical wall of some semi-infinite body of fluid were done by Chen, Briggs & Wirtz (1971), Chen & Skok (1974), Huppert & Turner (1980), Huppert & Josberger (1980), Narusawa & Suzukawa (1981), Huppert, Kerr & Hallworth (1984), Chereskin & Linden (1986), Tanny & Tsinober (1988, 1989) and Schladow, Thomas & Koseff (1992). These investigations have looked at the effects of horizontal gradients in fluids with the presence of either vertical salinity gradients or the combination of salinity and temperature gradients in the vertical direction. Some examined the additional effect of rotation on the instabilities at a heated boundary.

The theoretical work on double diffusive instabilities driven by horizontal gradients can be categorised into four areas: (1) Instabilities as a result of infinite uniform horizontal and vertical gradients were examined by Stern (1967), Toole & Georgi (1981), McDougall (1985), Holyer (1983) and Walsh & Ruddick (1994). (2) Instabilities of horizontal gradients in a finite front located in an infinite body of fluid by Niino (1986) and Yoshida, Nagashima & Niino (1989). (3) Instabilities from a single sidewall by Kerr (1989, 1990, 1996). And, (4) Instabilities for a slot by Thorpe, Hutt & Soulsby (1969), Hart (1971), Chen & Sandford (1977), Thangam, Zebib & Chen (1981), Kerr (1995) and Young & Rosner (1998).

The last category is the interest of our research. We will examine the linear stability of a salinity gradient in an infinite vertical slot based on the first theoretical paper by Thangam, Zebib & Chen (1981). Our work is inspired by Tanny & Tsinober (1988) who used the slot stability boundary of

Thangam *et al.* to compare their single sidewall heating problem. In Tanny & Tsinober's analysis of their experimental results they found the stability diagram of their single boundary problem is similar to that of a linear salinity gradient heated differentially in a vertical narrow slot when the salinity gradient was relatively strong. The stability criterion for heating strong salinity gradients was found by Thorpe, Hutt & Soulsby (1969) for heating a slot and by Kerr (1989) for heating at a single boundary, but not for other situations when the salt Rayleigh number, a measure of the salinity stratification, decreases. With zero salinity stratification in a heated slot, this is the case of a thermally driven problem which has been examined by many authors since Batchelor (1954), including Mizushima & Gotoh (1976), Bergholz (1978) and Daniels (1987). Tanny & Tsinober showed that there was some correlation between their experiments with a single boundary and the stability boundary found by Thangam *et al.* We hope to identify all the modes of linear instability for a slot and to see if they will give insight into modes for a single boundary when Ra_S , the salt Rayleigh number, is *not* large.

In chapter 2 we discuss the four fundamental equations and how to formulate the governing equations for the linear stability of the fluid in a vertical slot when there is a constant temperature difference imposed across the walls. In chapter 3 we present the results of numerical calculations for the stability boundary. These calculations were performed using a Runge-Kutta scheme. In chapter 4 a second Galerkin approach was employed to find the solutions for weak salinity gradient and the oscillatory branch of solutions. In chapter 5 four different sections of the stability boundary will be identified and the asymptotic analysis corresponding to each of these regimes will be examined. One section involving the limit of a strong salinity gradient has already been analysed by Thorpe, Hutt & Soulsby (1969). The analyses including the lim-

its of small wave number, large thermal Rayleigh number and weak salinity gradient are separately given. Finally, conclusions of the theoretical study in this slot problem are given in chapter 6. Details of some of the techniques used in the numerical schemes and some lengthy mathematical expressions derived in the asymptotic are included in the appendices.

Chapter 2

Description of the Problem

We begin by outlining the fundamental equations to be used in this double-diffusive problem. This gives physical understanding of the fluid motion which is driven by the presence of two diffusive components. We follow the usual convention for thermohaline convection so that the faster diffusive component is known as “heat” while the slower diffusive one is referred to as “salt”. In the linear analysis of vertical slot convection, we formulate the stability equations and then discuss the results obtained for the various instabilities in subsequent chapters.

A brief introduction is given to the four fundamental equations that govern the motion of the fluid, the dispersion of salinity, the temperature diffusion and the continuity of the fluid. In the following sections dimensional quantities are indicated by an asterisk.

2.1 The Continuity Equation

With the principle that mass is conserved, we consider an arbitrary volume V of fluid of any shape and of finite size. This volume is fixed in space and is bounded by a surface \bar{S} . Fluid moves into or out of the volume at points over

its surface. Any one point on the surface is described by the fluid velocity \mathbf{u}^* and the elemental surface area $d\bar{\mathbf{S}}$ (note, $d\bar{\mathbf{S}} \equiv \mathbf{n} d\bar{S}$, where \mathbf{n} is a unit vector perpendicular to the surface at $d\bar{S}$). The mass flow of a moving fluid across a fixed surface is the product $\rho^* \mathbf{u}^* \cdot d\bar{\mathbf{S}}$ where ρ^* is the fluid density. When both \mathbf{u}^* and $d\bar{\mathbf{S}}$ point in the direction out of the volume, giving a positive product then this indicates an outflow. In turn, an inflow is denoted by \mathbf{u}^* pointing into the volume and so the above product is negative. In the case when the mass flow is leaving the volume, this outward mass flow from V is given by

$$\int_{\bar{S}} \rho^* \mathbf{u}^* \cdot d\bar{\mathbf{S}}, \quad (2.1.1)$$

and this is equal to the rate of decrease of mass inside the volume

$$-\frac{d}{dt^*} \int_V \rho^* dV. \quad (2.1.2)$$

Since the volume considered is fixed in space and the limits of integration for the above integrals are constant, the time derivative can be placed inside the integral. Hence, the conservation of mass gives

$$\int_V \frac{\partial \rho^*}{\partial t^*} dV + \int_{\bar{S}} \rho^* \mathbf{u}^* \cdot d\bar{\mathbf{S}} = 0. \quad (2.1.3)$$

Applying the divergence theorem from vector calculus, the surface integral in (2.1.3) can be expressed as a volume integral. This gives

$$\int_V \frac{\partial \rho^*}{\partial t^*} dV + \int_V \nabla \cdot (\rho^* \mathbf{u}^*) dV = 0, \quad (2.1.4)$$

or

$$\int_V \left\{ \frac{\partial \rho^*}{\partial t^*} + \nabla \cdot (\rho^* \mathbf{u}^*) \right\} dV = 0. \quad (2.1.5)$$

If we assume that the integrand is continuous then the only way such an integral can be zero for all arbitrary volumes V is if the integrand is zero at all points. Hence, this gives the general expression representing the mass conservation for a fluid in which both \mathbf{u}^* and ρ^* are functions of position,

$$\frac{\partial \rho^*}{\partial t^*} + \nabla \cdot (\rho^* \mathbf{u}^*) = 0. \quad (2.1.6)$$

This is known as the continuity equation. A different form of equation (2.1.6) is obtained by expanding the divergence term and the operator D/Dt^* (which is a time derivative following the motion of the fluid, or a material derivative). The two terms together make up the material derivative of the density:

$$\frac{D\rho^*}{Dt^*} + \rho^* \nabla \cdot \mathbf{u}^* = 0. \quad (2.1.7)$$

In this form the equation may be interpreted in terms of the changes in the volume of a given mass of fluid. A fluid is said to be incompressible when the density of an element of fluid is not affected by changes in the pressure. The density of the fluid in a mass element may change as a result of molecular conduction of heat or of a solute into the element. However, in most cases the effect of heat or solute conduction in the fluid is negligible compared to the original density and so the fluid is usually treated as incompressible. This implies the density of each mass element of the fluid remains approximately constant. Thus, for an incompressible fluid, the rate of change of ρ^* following the motion is close to zero, that is

$$\frac{D\rho^*}{Dt^*} = 0. \quad (2.1.8)$$

The continuity equation then takes the simple form

$$\nabla \cdot \mathbf{u}^* = 0. \quad (2.1.9)$$

2.2 Equation of Motion

This equation representing Newton's second law of motion, is based on the principle that the rate of change of momentum of a fluid particle is equal to the sum of forces acting on it. With the velocity of the fluid given by $\mathbf{u}^* = (u^*, v^*, w^*)$, we can write down the conservation form of $\rho^* D\mathbf{u}^*/Dt^*$, the rate of change of momentum per unit volume following the fluid to be

$$\rho^* \frac{D\mathbf{u}^*}{Dt^*} = \rho^* \frac{\partial \mathbf{u}^*}{\partial t^*} + \rho^* \mathbf{u}^* \cdot \nabla \mathbf{u}^*. \quad (2.2.1)$$

We consider forces related to the velocity field that are due to pressure and to viscous action. For fluids which are assumed to be Newtonian (where the shear stress is proportional to the velocity gradients), the momentum equation with the pressure p^* , and the acceleration due to gravity $\mathbf{g}^* = (0, 0, -g^*)$, can be written as

$$\rho^* \frac{D\mathbf{u}^*}{Dt^*} = \rho^* \frac{\partial \mathbf{u}^*}{\partial t^*} + \rho^* \mathbf{u}^* \cdot \nabla \mathbf{u}^* = -\nabla p^* + \rho^* \mathbf{g}^* + \mu \nabla^2 \mathbf{u}^*. \quad (2.2.2)$$

This is known as the Navier-Stokes equation. The axes for x^* and y^* are in the horizontal plane and z^* is vertically upwards. The last term is the result of molecular viscosity μ in which μ is assumed to be independent of the temperature and salinity concentration. For small density variations, we can linearize the dependence of ρ^* on the temperature T^* and salinity S^* so

$$\rho^* = \rho_o^* [1 - \alpha_T (T^* - T_o^*) + \beta (S^* - S_o^*)], \quad (2.2.3)$$

where $\alpha_T = -\rho_o^{*-1} \left(\frac{\partial \rho^*}{\partial T^*} \right)_{S^*, p^*}$ is the coefficient of thermal expansion and $\beta = \rho_o^{*-1} \left(\frac{\partial \rho^*}{\partial S^*} \right)_{T^*, p^*}$ is the relative density change due to change in the salinity. In the Boussinesq approximation where density variations are assumed to be important only in the buoyancy term, we can apply the density relation of (2.2.3) into the Navier-Stokes equation to give

$$\rho_o^* \frac{D\mathbf{u}^*}{Dt^*} = -\nabla p^* + \rho_o^* [1 - \alpha_T (T^* - T_o^*) + \beta (S^* - S_o^*)] \mathbf{g}^* + \mu \nabla^2 \mathbf{u}^*, \quad (2.2.4)$$

where the inertia term, $\rho^* D\mathbf{u}^*/Dt^*$ is replaced by $\rho_o^* D\mathbf{u}^*/Dt^*$. If we introduce the modified pressure

$$p^* = p_1^* - \rho_o^* g^* z^*, \quad (2.2.5)$$

then the Boussinesq momentum equation reduces to

$$\frac{D\mathbf{u}^*}{Dt^*} = -\frac{1}{\rho_o^*} \nabla p_1^* - [\alpha_T (T^* - T_o^*) - \beta (S^* - S_o^*)] \mathbf{g}^* + \nu \nabla^2 \mathbf{u}^*, \quad (2.2.6)$$

where $\nu = \mu/\rho_o^*$ is the kinematic viscosity.

2.3 Temperature Equation

The equation for energy is

$$\rho^* \frac{DE^*}{Dt^*} = \nabla(K^* \nabla T^*) - p^* \nabla \cdot \mathbf{u}^* + \Omega^*, \quad (2.3.1)$$

where E^* is the internal energy per unit mass of the fluid, Ω^* the rate of viscous dissipation per unit volume of fluid and K^* the thermal conductivity. In most circumstances the rate of heat generation by viscous dissipation is small when compared with the heat being transferred in the fluid by molecular conduction so Ω^* can be neglected. We also assume K^* to be constant. This is an appropriate approximation when temperature differences are small. If the assumption that $\nabla \cdot \mathbf{u}^* = 0$ is used, then (2.3.1) reduces to

$$\rho^* \frac{DE^*}{Dt^*} = K^* \nabla^2 T^*. \quad (2.3.2)$$

In heated salty water, mass diffusion resulting from a temperature gradient is termed the Soret effect so that the internal energy increases as the temperature rises, producing a salinity gradient. However, this is not important in most problems involving heat and salt in water. If we assume the change in E^* depends linearly on temperature only and not on the salinity then

$$\Delta E^* = c(T^* - T_o^*), \quad (2.3.3)$$

where E^* is the enthalpy (at constant pressure) and c is the specific heat capacity of the fluid. This linear dependence can be written as

$$\frac{DE^*}{Dt^*} = c \frac{DT^*}{Dt^*}. \quad (2.3.4)$$

Substituting this result into (2.3.2) gives

$$\rho^* c \frac{DT^*}{Dt^*} = K^* \nabla^2 T^*. \quad (2.3.5)$$

Hence,

$$\frac{DT^*}{Dt^*} = \kappa_T \nabla^2 T^*, \quad (2.3.6)$$

where $\kappa_T = K^* / \rho^* c$ is the thermal diffusivity.

2.4 Salinity Equation

Consider the salt carried in any volume of fluid, V . The rate of increase of the salt inside V is equal to the inward flux of salt entering V . This gives

$$\frac{\partial}{\partial t^*} \int_V S^* dV = - \int_{\tilde{S}} \mathbf{S}_f^* \cdot \mathbf{n} d\tilde{S}, \quad (2.4.1)$$

where \tilde{S} is the closed surface bounding a region of volume of salt, \mathbf{n} the outward normal to the surface and \mathbf{S}_f^* the flux of salt moving across the surface. Assuming that temperature gradients do not drive salinity gradients as in the Soret effect, the distribution of salt is determined by its advection by moving fluid and by its diffusion between fluid particles. Hence,

$$\int_V \frac{\partial S^*}{\partial t^*} dV = - \int_{\tilde{S}} (S^* \mathbf{u}^* - \kappa_S \nabla S^*) \cdot \mathbf{n} d\tilde{S}, \quad (2.4.2)$$

where $S^* \mathbf{u}^*$ is the advection of salt by fluid velocity, $\kappa_S \nabla S^*$ is the diffusion due to molecular diffusivity. We assume κ_S can be taken to be constant. Applying the divergence theorem to the surface integral in (2.4.2) then

$$\int_V \frac{\partial S^*}{\partial t^*} dV = - \int_V \nabla \cdot (S^* \mathbf{u}^* - \kappa_S \nabla S^*) dV, \quad (2.4.3)$$

giving

$$\int_V \left(\frac{\partial S^*}{\partial t^*} + \nabla S^* \cdot \mathbf{u}^* + S^* \nabla \cdot \mathbf{u}^* - \kappa_S \nabla^2 S^* \right) dV = 0, \quad (2.4.4)$$

which is true for any volume of fluid. Since this volume integral is zero for arbitrary volume V then if the integrand is continuous it must be zero.

Therefore,

$$\frac{\partial S^*}{\partial t^*} + \nabla S^* \cdot \mathbf{u}^* + S^* \nabla \cdot \mathbf{u}^* - \kappa_S \nabla^2 S^* = 0. \quad (2.4.5)$$

Again assuming that $\nabla \cdot \mathbf{u}^* = 0$, the salinity equation becomes

$$\frac{\partial S^*}{\partial t^*} + \mathbf{u}^* \cdot \nabla S^* = \frac{DS^*}{Dt^*} = \kappa_S \nabla^2 S^*. \quad (2.4.6)$$

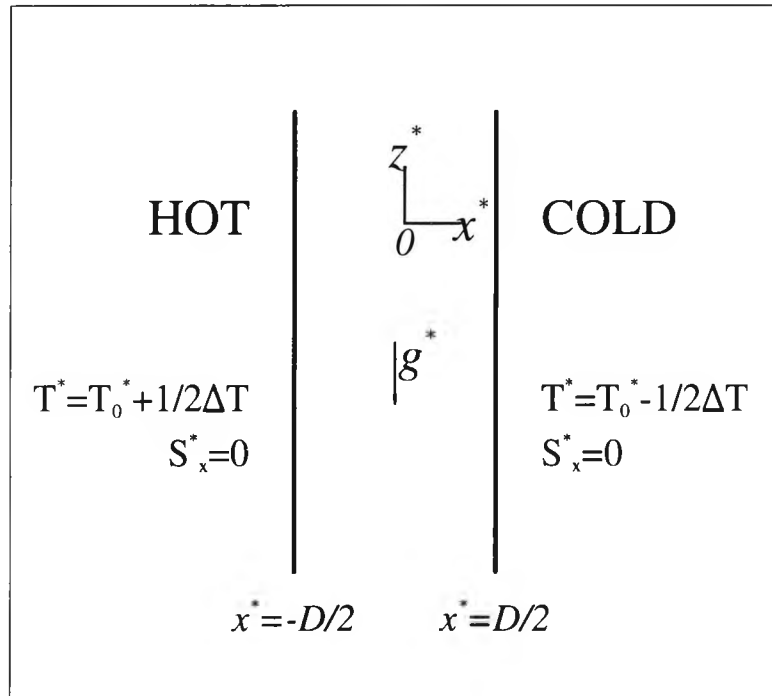


Figure 2.1: Schematic diagram of the configuration under consideration.

2.5 Formulation of Governing Equations

The problem that we are concerned with consists of an incompressible fluid confined between two differentially heated rigid walls that stand vertically and are parallel to each other. The two walls are impermeable to salt and are perfect heat conductors, while the applied temperature difference across them is ΔT . The distance which separates the two walls is D . The configuration set up is shown in figure 2.1 which also indicates the axial directions of the co-ordinate system.

In the undisturbed state, there is an imposed constant salinity gradient in the vertical direction, $\Phi_o = \partial S_o^* / \partial z^*$, and a constant temperature gradient in the lateral direction. We denote the pressure, density, salinity and temperature by p^* , ρ^* , S^* and T^* respectively. All variables with an asterisk indicate that the measurements are in dimensional form. The four governing

equations with dimensional quantities are

$$\nabla \cdot \mathbf{u}^* = 0, \quad (2.5.1)$$

$$\frac{D\mathbf{u}^*}{Dt^*} = -\frac{1}{\rho_o^*} \nabla p_1^* - [\alpha_T(T^* - T_o^*) - \beta(S^* - S_o^*)] \mathbf{g}^* + \nu \nabla^2 \mathbf{u}^*, \quad (2.5.2)$$

$$\frac{DT^*}{Dt^*} = \kappa_T \nabla^2 T^*, \quad (2.5.3)$$

$$\frac{DS^*}{Dt^*} = \kappa_S \nabla^2 S^*. \quad (2.5.4)$$

The hot wall is located at $x^* = -D/2$ and the cold wall at $x^* = D/2$. Thus the boundary conditions are

$$T^* = T_o^* \pm \Delta T/2, \quad S_x^* = 0, \quad u^* = v^* = w^* = 0 \quad \text{on} \quad x^* = \mp D/2. \quad (2.5.5)$$

2.6 Non-dimensionalisation

We shall non-dimensionalise equations (2.5.1) to (2.5.5) subject to the following scalings:

$$\begin{aligned} x &= \frac{x^*}{D}; & \mathbf{u} &= \frac{D}{\kappa_T} \mathbf{u}^*; & t &= \frac{\kappa_T}{D^2} t^*; \\ T &= \frac{T^* - T_o^*}{\Delta T}; & S &= \frac{S^* - S_o^*}{D |\Phi_o|}; & p &= \frac{D^2}{\rho_o^* \kappa_T^2} p_1^*. \end{aligned} \quad (2.6.1)$$

First of all, the continuity equation (2.5.1) is simply refined as $\nabla \cdot \mathbf{u} = 0$.

The momentum equation (2.5.2) becomes

$$\frac{\kappa_T^2}{D^3} \frac{D\mathbf{u}}{Dt} = -\frac{\kappa_T^2}{D^3} \nabla p - [\alpha_T T \Delta T - \beta S D |\Phi_o|] \mathbf{g}^* + \nu \frac{\kappa_T}{D^3} \nabla^2 \mathbf{u}. \quad (2.6.2)$$

This can be re-arranged to give

$$\frac{D\mathbf{u}}{Dt} = -\nabla p + Pr(Ra_T T - Ra_S S) \mathbf{z} + Pr \nabla^2 \mathbf{u}, \quad (2.6.3)$$

where

$$Ra_T = \frac{g \alpha_T \Delta T D^3}{\kappa_T \nu}, \quad (2.6.4)$$

is the thermal Rayleigh number,

$$Ra_S = \frac{g\beta D^4 |\Phi_o|}{\kappa_T \nu}, \quad (2.6.5)$$

the salinity Rayleigh number and,

$$Pr = \frac{\nu}{\kappa_T}, \quad (2.6.6)$$

the Prandtl number. Similarly, the diffusive equation of temperature (2.5.3) when non-dimensionalised becomes

$$\frac{DT}{Dt} = \nabla^2 T, \quad (2.6.7)$$

and the salinity equation (2.5.4) becomes

$$\frac{DS}{Dt} = \frac{\kappa_S}{\kappa_T} \nabla^2 S = \tau \nabla^2 S, \quad (2.6.8)$$

where $\tau = \kappa_S/\kappa_T$ is the Lewis number (salt/heat diffusivity ratio). With this scaling, the imposed non-dimensionalised vertical salinity gradient is -1 .

The non-dimensionalised set of governing equations with Boussinesq approximations are

$$\frac{D\mathbf{u}}{Dt} = -\nabla p + Pr(Ra_T T - Ra_S S)\hat{\mathbf{z}} + Pr \nabla^2 \mathbf{u}, \quad (2.6.9)$$

$$\frac{DT}{Dt} = \nabla^2 T, \quad (2.6.10)$$

$$\frac{DS}{Dt} = \tau \nabla^2 S, \quad (2.6.11)$$

$$\nabla \cdot \mathbf{u} = 0, \quad (2.6.12)$$

with boundary conditions

$$T = \pm \frac{1}{2}, \quad S_x = u = v = w = 0 \quad \text{on} \quad x = \mp \frac{1}{2}. \quad (2.6.13)$$

2.7 Dimensionless Stream Function

We shall derive the momentum, temperature and salinity equations in terms of the stream function ψ for the fluid velocity. Since the slot is assumed to be infinitely long in the y -direction, the effect of the lateral boundaries between the hot and cold walls can be ignored. We consider fluid motion in the x - z plane only and the velocity component in the y direction is zero, i.e. $\mathbf{u} = (u, 0, w)$. For the case of two-dimensional motion, the concept of streamlines (curves everywhere parallel to the direction of the flow) can be related to the continuity equation. This continuity equation for incompressible flow may be written as

$$\frac{\partial u}{\partial x} + \frac{\partial w}{\partial z} = 0. \quad (2.7.1)$$

For u and w to satisfy the continuity relationship, we can introduce a stream function defined by the equations

$$u = \frac{\partial \psi}{\partial z} \quad \text{and} \quad w = -\frac{\partial \psi}{\partial x}, \quad (2.7.2)$$

where ψ is a function of x and z .

The momentum equation (2.6.9) can be written as three equations for the components in x -, y - and z -directions. These equations of motion are

$$\frac{\partial u}{\partial t} + u \frac{\partial u}{\partial x} + w \frac{\partial u}{\partial z} = -\frac{\partial p}{\partial x} + Pr \nabla^2 u, \quad (2.7.3)$$

$$0 = -\frac{\partial p}{\partial y} \quad \Rightarrow \quad p = p(x, z, t), \quad (2.7.4)$$

$$\frac{\partial w}{\partial t} + u \frac{\partial w}{\partial x} + w \frac{\partial w}{\partial z} = -\frac{\partial p}{\partial z} + Pr \nabla^2 w + Pr(Ra_T T - Ra_S S). \quad (2.7.5)$$

The pressure term is removed by cross-differentiation in the x - and z -momentum equations

$$\left[\frac{\partial}{\partial t} + u \frac{\partial}{\partial x} + w \frac{\partial}{\partial z} - Pr \nabla^2 \right] \left(\frac{\partial u}{\partial z} - \frac{\partial w}{\partial x} \right) + Pr \left(Ra_T \frac{\partial T}{\partial x} - Ra_S \frac{\partial S}{\partial x} \right) = 0. \quad (2.7.6)$$

The above equation is substituted with the stream function relation from (2.7.2) to obtain this equation for ψ

$$\left[\frac{1}{Pr} \left(\frac{\partial}{\partial t} + \frac{\partial \psi}{\partial z} \frac{\partial}{\partial x} - \frac{\partial \psi}{\partial x} \frac{\partial}{\partial z} \right) - \nabla^2 \right] \nabla^2 \psi = Ra_S \frac{\partial S}{\partial x} - Ra_T \frac{\partial T}{\partial x}. \quad (2.7.7)$$

Now examining the temperature equation (2.6.10) and this can be expanded to

$$\frac{\partial T}{\partial t} + \mathbf{u} \cdot \nabla T = \nabla^2 T, \quad (2.7.8)$$

giving,

$$\frac{\partial T}{\partial t} + \frac{\partial \psi}{\partial z} \frac{\partial T}{\partial x} - \frac{\partial \psi}{\partial x} \frac{\partial T}{\partial z} = \nabla^2 T. \quad (2.7.9)$$

An analogous approach is adopted in the salinity equation (2.6.11) to yield

$$\frac{\partial S}{\partial t} + \frac{\partial \psi}{\partial z} \frac{\partial S}{\partial x} - \frac{\partial \psi}{\partial x} \frac{\partial S}{\partial z} = \tau \nabla^2 S. \quad (2.7.10)$$

The resulting three equations for the two-dimensional flow are

$$\left[\frac{1}{Pr} \left(\frac{\partial}{\partial t} + \frac{\partial \psi}{\partial z} \frac{\partial}{\partial x} - \frac{\partial \psi}{\partial x} \frac{\partial}{\partial z} \right) \nabla^2 - \nabla^4 \right] \psi = Ra_S \frac{\partial S}{\partial x} - Ra_T \frac{\partial T}{\partial x}, \quad (2.7.11)$$

$$\left[\frac{\partial}{\partial t} + \frac{\partial \psi}{\partial z} \frac{\partial}{\partial x} - \frac{\partial \psi}{\partial x} \frac{\partial}{\partial z} - \nabla^2 \right] T = 0, \quad (2.7.12)$$

$$\left[\frac{\partial}{\partial t} + \frac{\partial \psi}{\partial z} \frac{\partial}{\partial x} - \frac{\partial \psi}{\partial x} \frac{\partial}{\partial z} - \tau \nabla^2 \right] S = 0. \quad (2.7.13)$$

2.8 The Background State

In many double-diffusive problems with boundaries, steady background states do not exist. An example is the investigation by Linden & Webber (1977) of the unsteady flow along a sloping single boundary in a stratified fluid where the stratification was due to both salt and heat gradients. The unsteadiness is due to the difference in the diffusivities of salinity and temperature, and could only be avoided if the diffusion rates were the same, i.e. the salt/heat

diffusivity ratio was one.

For the infinite vertical slot with lateral heating a steady state solution does exist. This steady state solution was obtained by Thangam, Zebib & Chen (1981). The background state is found by looking for time-independent solutions for (2.7.11) to (2.7.13). In addition, there is no variation in the z -direction, i.e. $\frac{\partial}{\partial z} = \frac{\partial^2}{\partial z^2} = 0$, and no horizontal velocity $u = 0$. Since there is no dependency on either t or z , all the equations concerned will be reduced to ordinary differential equations (ODEs).

With these assumptions in place, the equation for stream function (2.7.11) simplifies to

$$-\frac{d^4\psi}{dx^4} = Ra_S \frac{dS}{dx} - Ra_T \frac{dT}{dx}. \quad (2.8.1)$$

Expressing this in terms of the vertical velocity, $w = -d\psi/dx$ gives

$$\frac{d^3w}{dx^3} + Ra_T \frac{dT}{dx} - Ra_S \frac{dS}{dx} = 0. \quad (2.8.2)$$

The equations of temperature and salinity, (2.7.12) and (2.7.13), become

$$\frac{d^2T}{dx^2} = 0, \quad (2.8.3)$$

$$\tau \frac{d^2S}{dx^2} + w = 0. \quad (2.8.4)$$

We overline and attach the subscript o to indicate the solutions to the steady-state background problem:

$$\frac{d^3\overline{w}_o}{dx^3} + Ra_T \frac{d\overline{T}_o}{dx} - Ra_S \frac{d\overline{S}_o}{dx} = 0, \quad (2.8.5)$$

$$\frac{d^2\overline{T}_o}{dx^2} = 0, \quad (2.8.6)$$

$$\frac{d^2\overline{S}_o}{dx^2} + \frac{1}{\tau}\overline{w}_o = 0, \quad (2.8.7)$$

with boundary conditions

$$\overline{T}_o = \pm \frac{1}{2}; \quad \frac{d\overline{S}_o}{dx} = 0; \quad \overline{w}_o = 0 \quad \text{on} \quad x = \mp \frac{1}{2}. \quad (2.8.8)$$

The solution to (2.8.6) is

$$\overline{T}_o = -x. \quad (2.8.9)$$

Combining (2.8.5) with both (2.8.7) and (2.8.9), we can write the equation for \overline{S}_o as

$$\tau \frac{d^5 \overline{S}_o}{dx^5} + Ra_S \frac{d\overline{S}_o}{dx} + Ra_T = 0. \quad (2.8.10)$$

This has the general solution

$$\begin{aligned} \overline{S}_o(x) = & A' - \frac{Ra_T}{Ra_S} x \\ & + B' \cosh Mx \cos Mx + C' \cosh Mx \sin Mx \\ & + D' \sinh Mx \cos Mx + E' \sinh Mx \sin Mx, \end{aligned} \quad (2.8.11)$$

where

$$M = \left(\frac{Ra_S}{4\tau} \right)^{\frac{1}{4}}, \quad (2.8.12)$$

and A', B', C', D' and E' are constants. The symmetry of the problem indicates the function $\overline{S}_o(x)$ is odd, and so $A' = B' = E' = 0$. Thus the general solution reduces to

$$\overline{S}_o(x) = C' \cosh Mx \sin Mx + D' \sinh Mx \cos Mx - \frac{Ra_T}{Ra_S} x. \quad (2.8.13)$$

The no-flux boundary conditions require $\overline{S}'_o(\pm 1/2) = 0$. These two conditions are analogous, giving

$$\begin{aligned} C' \sinh \frac{M}{2} \sin \frac{M}{2} + C' \cosh \frac{M}{2} \cos \frac{M}{2} + D' \cosh \frac{M}{2} \cos \frac{M}{2} \\ - D' \sinh \frac{M}{2} \sin \frac{M}{2} = \frac{Ra_T}{MRa_S}. \end{aligned} \quad (2.8.14)$$

When the condition that $\overline{w}_o = 0$ on $x = \pm 1/2$ is substituted into (2.8.7) it produces the further constraint

$$\frac{d^2 \overline{S}_o}{dx^2} = 0 \quad \text{on} \quad x = \pm \frac{1}{2}. \quad (2.8.15)$$

When (2.8.13) is differentiated twice and then substituted into (2.8.15) it gives

$$D' = C' \frac{\sinh \frac{M}{2} \cos \frac{M}{2}}{\cosh \frac{M}{2} \sin \frac{M}{2}}. \quad (2.8.16)$$

We can now solve for C' and D' using (2.8.14) and (2.8.16) so

$$C' = \frac{Ra_T \sin \frac{M}{2} \cosh \frac{M}{2}}{M Ra_S (\sinh \frac{M}{2} \cosh \frac{M}{2} + \cos \frac{M}{2} \sin \frac{M}{2})}, \quad (2.8.17)$$

and

$$D' = \frac{Ra_T \sinh \frac{M}{2} \cos \frac{M}{2}}{M Ra_S (\sinh \frac{M}{2} \cosh \frac{M}{2} + \cos \frac{M}{2} \sin \frac{M}{2})}. \quad (2.8.18)$$

The horizontal background salinity gradient is

$$\frac{d\bar{S}_o}{dx} = \frac{Ra_T}{Ra_S} \left[-1 + \frac{Q}{\sinh \frac{M}{2} \cosh \frac{M}{2} + \cos \frac{M}{2} \sin \frac{M}{2}} \right], \quad (2.8.19)$$

where

$$\begin{aligned} Q = & \sin \frac{M}{2} \cosh \frac{M}{2} \sinh Mx \sin Mx \\ & + \sin \frac{M}{2} \cosh \frac{M}{2} \cosh Mx \cos Mx \\ & + \sinh \frac{M}{2} \cos \frac{M}{2} \cosh Mx \cos Mx \\ & - \sinh \frac{M}{2} \cos \frac{M}{2} \sinh Mx \sin Mx. \end{aligned} \quad (2.8.20)$$

This equation for Q can be re-arranged to give the form used by Thangam *et al.*:

$$Q = -\frac{1}{2} [\cosh M_1 \sin M_2 - \cosh M_2 \sin M_1 + \sinh M_2 \cos M_1 - \sinh M_1 \cos M_2], \quad (2.8.21)$$

where $M_1 = Mx + \frac{M}{2}$ and $M_2 = Mx - \frac{M}{2}$. Thus we can rewrite (2.8.19) as

$$\frac{d\bar{S}_o}{dx} = -\frac{Ra_T}{4\tau M^4} \left[1 + \frac{Q_1}{\sinh M + \sin M} \right] \quad (2.8.22)$$

where $Q_1 = -2Q$ and $Ra_S = 4\tau M^4$. The background velocity is found by differentiating (2.8.22) once and using (2.8.7) to give

$$\bar{w}_o = \frac{Ra_T (\sinh M_1 \sin M_2 - \sin M_1 \sinh M_2)}{2M^3 (\sinh M + \sin M)}. \quad (2.8.23)$$

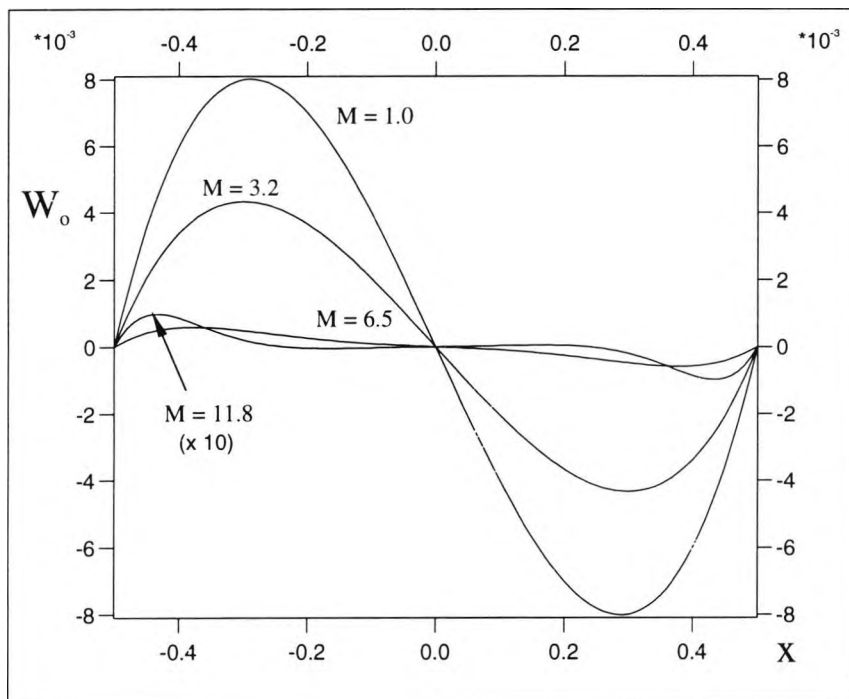


Figure 2.2: The background velocity profile across the slot is shown as a function of $M = (Ra_S/4\tau)^{1/4}$ where \bar{w}_o is antisymmetric about $x = 0$. The velocity for $M = 11.8$ has been multiplied by a factor of 10.

These are the background states given by Thangam *et al.* and they depend on the single parameter

$$M = \left(\frac{Ra_S}{4\tau} \right)^{1/4}. \quad (2.8.24)$$

Figures 2.2 and 2.3 show how the profiles of \bar{w}_o and \bar{S}_{ox} change for any given value of M (which depends on Ra_S). As Ra_S increases the background vertical velocity decreases in magnitude and the motion becomes confined in the boundary layer near the walls. The background horizontal salinity gradient approaches to a constant at the core of the slot as Ra_S becomes large, with an adjustment to the zero-flux boundary conditions at the thin boundary layer near the walls. The background temperature profile is linear and so it is not shown here. These background profiles are shown in the earlier work by Hart (1971) with good agreement made in comparison to our results but have opposite signs. This outcome is expected since we have used

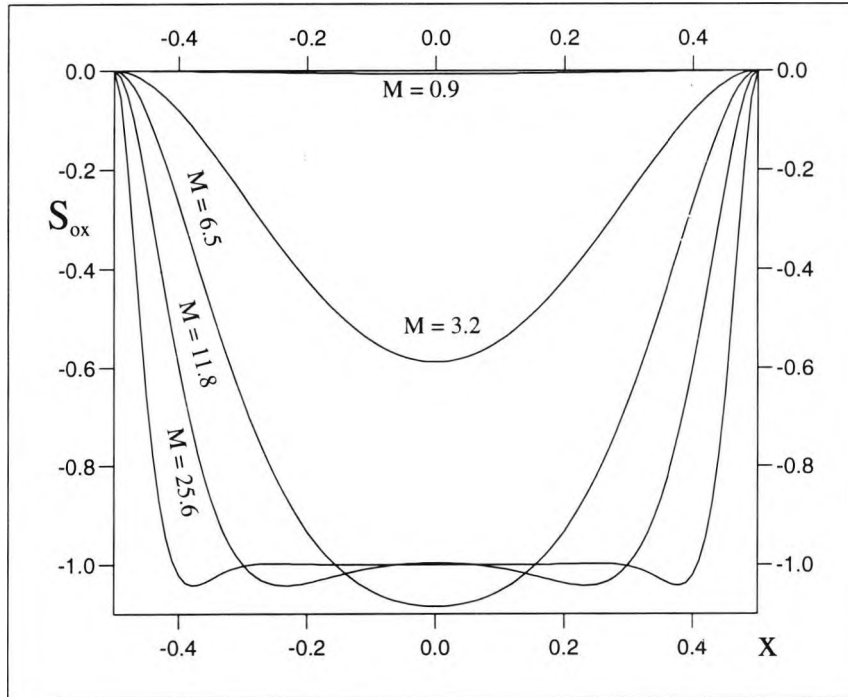


Figure 2.3: A similar background profile for the horizontal salinity gradient is also shown to depend on the parameter M as defined in figure 2.2 but $\overline{S_{ox}}$ is symmetric about $x = 0$.

the convention that the hotter wall is at $x = -1/2$ while Hart had the cooler wall there.

2.9 Stability Analysis

We now turn our interest to the investigation of the behaviour of perturbations to the steady state. These perturbed quantities are denoted by $\psi'(x, z, t)$, $T'(x, z, t)$ and $S'(x, z, t)$ and evolve with time as well as depend on x and z . We take

$$\psi(x, z, t) = - \int \overline{w_o} dx + \psi'(x, z, t), \quad (2.9.1)$$

$$T(x, z, t) = \overline{T_o}(x) + T'(x, z, t), \quad (2.9.2)$$

$$S(x, z, t) = -z + \overline{S_o}(x) + S'(x, z, t). \quad (2.9.3)$$

The $-z$ term in the salinity comes from the constant vertical salinity gradient. The above results are substituted into the set of governing equations (2.7.11) to (2.7.13). We can then linearize these equations by neglecting terms which are products of two perturbation terms. This gives the perturbation equations

$$\frac{1}{Pr} \nabla^2 \frac{\partial \psi'}{\partial t} + \frac{\overline{w}_o}{Pr} \nabla^2 \frac{\partial \psi'}{\partial z} - \frac{1}{Pr} \left(\frac{\partial \psi'}{\partial z} \frac{\partial^2 \overline{w}_o}{\partial x^2} \right) - \nabla^4 \psi' + Ra_T \frac{\partial T'}{\partial x} - Ra_S \frac{\partial S'}{\partial x} = 0, \quad (2.9.4)$$

$$\frac{\partial T'}{\partial t} - \frac{\partial \psi'}{\partial z} + \overline{w}_o \frac{\partial T'}{\partial z} - \nabla^2 T' = 0, \quad (2.9.5)$$

$$\frac{\partial S'}{\partial t} + \frac{\partial \overline{S}_o}{\partial x} \frac{\partial \psi'}{\partial z} + \overline{w}_o \frac{\partial S'}{\partial z} + \frac{\partial \psi'}{\partial x} - \tau \nabla^2 S' = 0. \quad (2.9.6)$$

2.10 Eigenvalue Problem

Insight into the development of small disturbances can be gained by resolving ψ' , T' and S' from (2.9.4) to (2.9.6) into Fourier modes in the vertical direction. Since all coefficients are time independent each mode will depend exponentially on time with an exponent which may be complex. We will use complex notation. It will be assumed that the real part of solutions will be taken to find the final physical solutions. We will drop the explicit mention of taking the real part in the future.

Since the perturbation equations are linear, we can follow the evolution of each Fourier mode independently. The Fourier modes of ψ' , T' and S' can be expressed as

$$\begin{aligned} \psi'(x, z, t) &= \check{\psi}(x) e^{i\alpha z + \sigma t}, \\ T'(x, z, t) &= \check{T}(x) e^{i\alpha z + \sigma t}, \\ S'(x, z, t) &= \check{S}(x) e^{i\alpha z + \sigma t}, \end{aligned} \quad (2.10.1)$$

where $\check{\psi}(x)$, $\check{T}(x)$ and $\check{S}(x)$ are the corresponding eigenfunctions for the streamlines, temperature and salinity. The real parameter α is the vertical wave number in the z -direction and σ the growth rate, which may be complex, i.e. $\sigma = \sigma_r + i\sigma_i$. When (2.10.1) is substituted into equations (2.9.4) to (2.9.6) we can derive the equation for each mode:

$$\frac{\sigma}{Pr}(D^2 - \alpha^2)\check{\psi} + \frac{i\alpha}{Pr} \left\{ \overline{w_o}(D^2 - \alpha^2)\check{\psi} - D^2\overline{w_o}\check{\psi} \right\} - (D^2 - \alpha^2)^2\check{\psi} + Ra_T D\check{T} - Ra_S D\check{S} = 0, \quad (2.10.2)$$

$$(D^2 - \alpha^2)\check{T} + i\alpha(\check{\psi} - \overline{w_o}\check{T}) - \sigma\check{T} = 0, \quad (2.10.3)$$

$$\tau(D^2 - \alpha^2)\check{S} - i\alpha\check{\psi}D\overline{S_o} - i\alpha\overline{w_o}\check{S} - D\check{\psi} - \sigma\check{S} = 0, \quad (2.10.4)$$

with boundary conditions

$$\check{\psi} = D\check{\psi} = \check{T} = D\check{S} = 0 \quad \text{on} \quad x = \pm \frac{1}{2}. \quad (2.10.5)$$

Here $D = d/dx$. Henceforth $\check{\psi}$, \check{T} and \check{S} will be replaced by ψ , T and S for notational convenience. The condition $\psi = 0$ at the walls comes from the requirement that there is no flux through the walls ($u = 0$). The solutions to these equations for the eigenvalue problem will be investigated in the subsequent chapters.

Chapter 3

Full Numerical Method and Results

In this chapter we hope to find the marginal stability curve for the linear eigenvalue problem of double diffusive convection in a vertical slot. This problem was previously examined by Thangam, Zebib & Chen (1981). The numerical approach adopted by these authors was different from the way we first solve this system of equations. They used a Galerkin method which we will examine in chapter 4. Here we use a Runge-Kutta scheme in an attempt to reproduce their numerical results for the stability boundary. The use of a Runge-Kutta scheme will allow us to examine the relative magnitudes of the different terms in the differential equations with greater ease. It also enables us to investigate possible asymptotic regimes by removing selected terms from the governing equations in a simple way.

3.1 Runge-Kutta Scheme

The Runge-Kutta scheme is often chosen for solving ordinary differential equations and the most common one in use is of order four. This means

the local truncation error of this method is of $O(dx^5)$ where dx is the step length. The derivatives in the system of differential equations are expressed in terms of first-order equations such that $\mathbf{y}' = \mathbf{f}(x, \mathbf{y})$ where \mathbf{y} is a vector with any number of elements in the system. These are then numerically calculated based on the classical four-stage formula:

$$y_{k+1} = y_k + \frac{k_1}{6} + \frac{k_2}{3} + \frac{k_3}{3} + \frac{k_4}{6}, \quad (3.1.1)$$

where

$$k_1 = dx f(x, y_k), \quad (3.1.2)$$

$$k_2 = dx f(x + dx/2, y_k + k_1/2), \quad (3.1.3)$$

$$k_3 = dx f(x + dx/2, y_k + k_2/2), \quad (3.1.4)$$

$$k_4 = dx f(x + dx, y_k + k_3). \quad (3.1.5)$$

A shooting method is used to ensure that we satisfy the boundary conditions at both walls. This shooting method involves a matrix manipulation of some of the initial conditions to get some boundary conditions correct at the far wall before using Newton's method (or Broyden's algorithm) to ensure that we satisfy the remaining conditions by varying the chosen eigenvalue(s). For example, vary Ra_T for obtaining steady instability and vary both σ_i and Ra_T for oscillatory instability. The numerical scheme is able to vary the vertical wave number in order to find the minimum point of any given eigenvalue. For example, in the case of steady instability, this scheme may calculate the minimum value of Ra_T and the corresponding α for a given value of Ra_S . In addition, the corresponding growth rate, σ_i , is given when Broyden's algorithm is used to look for non-steady solutions. Further details of the numerical scheme for solving the full problem are documented in Appendix A.

3.2 Full Numerical Results

The full problem of (2.10.2) to (2.10.5) gives rise to steady instabilities if $\sigma_i = 0$. Otherwise, if $\sigma_i \neq 0$ it gives rise to oscillatory solutions. The problem is dependent upon several parameters: the salt Rayleigh number (Ra_S), the thermal Rayleigh number (Ra_T), the vertical wave number (α), the Prandtl number (Pr) and finally the Lewis number (τ). These parameters are all closely associated with the eigenvalue σ , the growth rate. In this numerical investigation, the Prandtl and Lewis numbers are taken to be 6.7 and 0.01 respectively. These values are appropriate for the classical heat and salt combination in water of double-diffusive convection. We have taken $Pr = 6.7$ because this value was used in the double-diffusive problem for a vertical slot by Thangam, Zebib & Chen (1981). This value corresponds to T_o^* of around 22°C in pure water (Batchelor, 1967 pp. 597).

Initially we look for the value of Ra_T that gives a neutral state for a given value of α and Ra_S . We then vary α in order to find the minimum value of Ra_T and the corresponding α for each value of Ra_S . From this, some neutral curves describing the characteristics of the wave number, Ra_S and Ra_T can be found.

Figures 3.1 and 3.2 illustrate the relationship between Ra_T and α as Ra_S is varied between 25 and 10^4 . It shows how the location of the minimum moves. The first shows the minimum for small magnitude of Ra_S and the other highlights the changing phase of the minimum as Ra_S increases. All the curves in the range $10 \leq Ra_S \leq 64.3$ show a steady decline towards the Ra_T axis. The gradient of these curves increases rapidly when the wave number is greater than 4. The critical value of Ra_T found in this zone lies in the vicinity of zero α . We know that solutions to the full stability equations

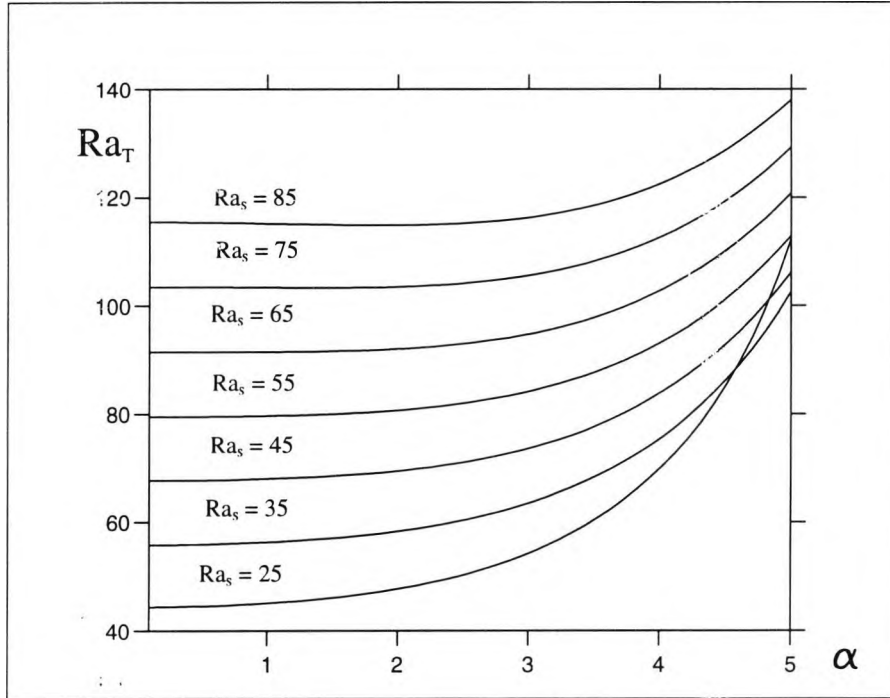


Figure 3.1: Graph of the critical thermal Rayleigh number, Ra_T , against the vertical wave number, α , for moderately small salt Rayleigh numbers.

cannot be found if α is exactly zero. In this case the equations for the flow are equivalent to those of the background flow (2.8.5), (2.8.6) and (2.8.7), but with no temperature difference between the walls. The only solution in this case is the trivial solution with ψ , T and S all zero. Thus the values of Ra_T on the axis at $\alpha = 0$ which the stability boundary approaches is not the minimum Ra_T for steady convection, but it is the greatest lower bound for values of Ra_T where steady convection can take place. In these cases we estimate the value of Ra_T for the lower boundary of marginal stability by fitting a quadratic of the form $Ra_T = A + B\alpha^2$ through the two nearest points to $\alpha = 0$. This gives the formula:

$$Ra_T = Ra_{T_1} - \frac{1}{3}(Ra_{T_2} - Ra_{T_1}),$$

where Ra_{T_1} and Ra_{T_2} are the values for marginal stability evaluated at $\alpha = \delta\alpha$ and $\alpha = 2\delta\alpha$ respectively where $\delta\alpha$ is small (we take $\delta\alpha = 0.001$).

As Ra_s passes through 63.4, an interesting transition occurs which is more

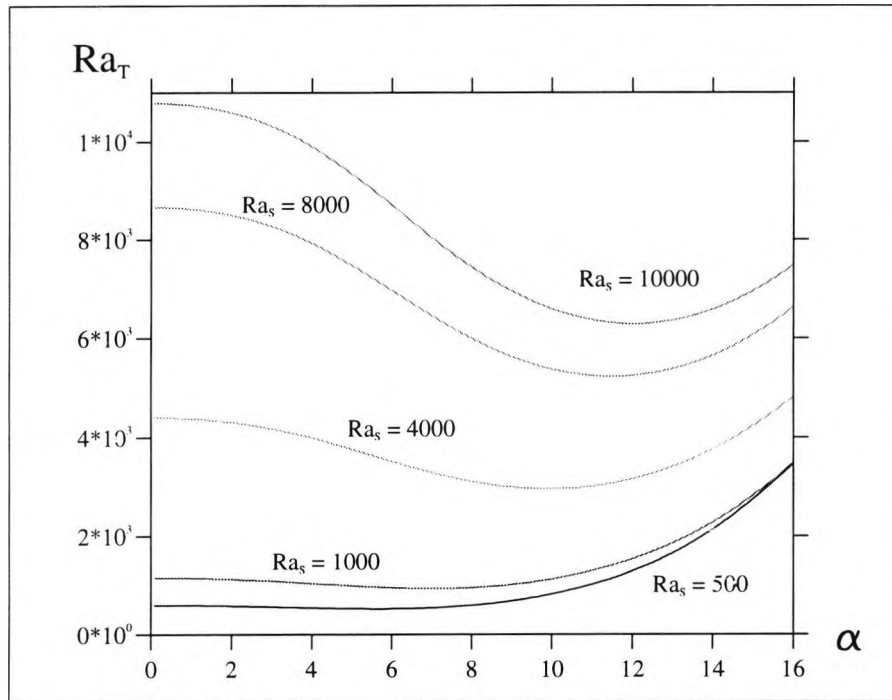


Figure 3.2: Graph of the critical value of Ra_T against α for some large salt Rayleigh numbers.

clearly seen in figure 3.2. The minimum shifts towards the right away from the origin. This time, the minima become more distinct with wave number increasing above 16. These neutral curves are again following a similar pattern as the smaller salt Rayleigh number where they are disappearing off to infinity with increasing wave number.

Graphs indicating the critical values of Ra_T and α against Ra_S are displayed in figures 3.3 and 3.4. Each minimum corresponds to the marginal stability of the system as Ra_S is varied. For values of Ra_T less than the minimum the fluid is stable to all infinitesimal disturbances. For values greater than this initial value there is always an unstable mode, i.e. the fluid is unstable to infinitesimal disturbances. It also shows how the critical value of the wave number increases with the increasing value of Ra_S . The increase in the critical wave number and Ra_T is caused by the damping effect of the vertical stratification as Ra_S increases.

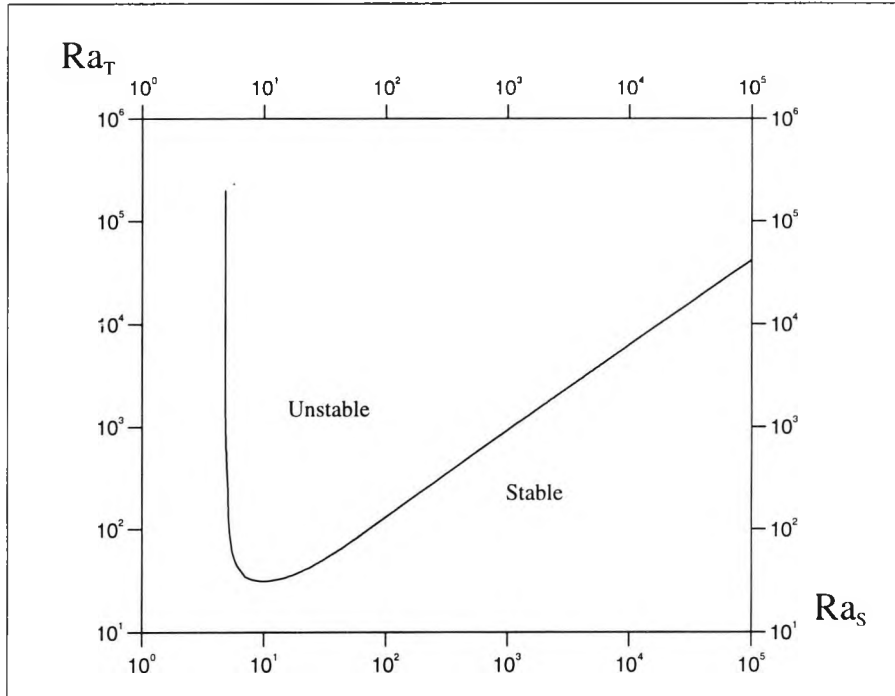


Figure 3.3: $Pr = 6.7$ and $\tau = 0.01$ are used to establish the neutral stability curve of Ra_T and Ra_S . These steady solutions are found using the Runge-Kutta scheme. This shows the unstable and stable regions over the stationary branches of solutions.

In figure 3.3 it can be seen that near $Ra_S = 4.7703$, the boundary is almost vertical. This vertical branch of solutions separates stable regimes on the left from unstable regimes on the right. It is found by fixing Ra_T and varying both Ra_S and α in the Runge-Kutta scheme thus finding the minimum value of Ra_S for instabilities from a given value of Ra_T . This boundary extends downwards until reaching a minimum near $Ra_S = 10$. The destabilization for this vertical region is attributed by Thangam *et al.* to the large difference between the diffusivity ratio of heat and salt and so the fluid motion within the slot is creating the local buoyancy to give instability. However, it will be shown to be caused by a different mechanism in the large Ra_T section of chapter 5. The critical wave number becomes zero as Ra_S falls under 63.4 as shown in figure 3.4 and then remains at zero until Ra_S reaches about 5. It then curves and forms a sharp peak which corresponds to values taken on

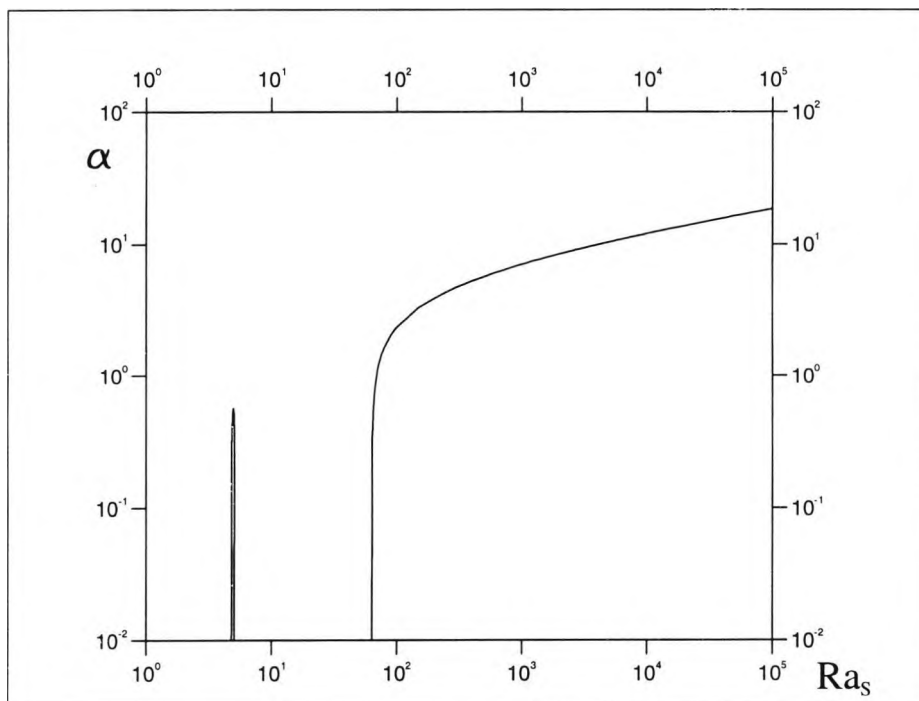


Figure 3.4: Another neutral curve showing the relation between α and Ra_S , found by using the Runge-Kutta scheme.

the near vertical part of the curve in figure 3.3. An alternative depiction of the relation between α and Ra_T is shown in figure 3.5. There seems to be a maximum point at $\alpha = 0.541$ and $Ra_T = 506$. The part of the curve on the right decreases linearly in this logarithmic plot, indicating α decays as Ra_T^{-1} .

The stability curve in figure 3.3 is essentially the same as that of Thangam *et al.* for values of Ra_S greater than 10, but differences in results obtained for $4.7703 < Ra_S < 10$ are found. For comparison with the results of Thangam *et al.*, their stability curve is reproduced in figure 3.6. We have found a steady vertical boundary at $Ra_S = 4.7703$ and this is a continuous extension from the part of the stability curve with Ra_S greater than 10. This vertical boundary lies in the region that Thangam *et al.* found was stable to infinitesimal perturbations. We failed to find the oscillatory solutions as shown in Thangam *et al.*'s stability curve. In addition, the Runge-Kutta scheme also failed to calculate small Ra_S results. This failure of the numerical scheme is

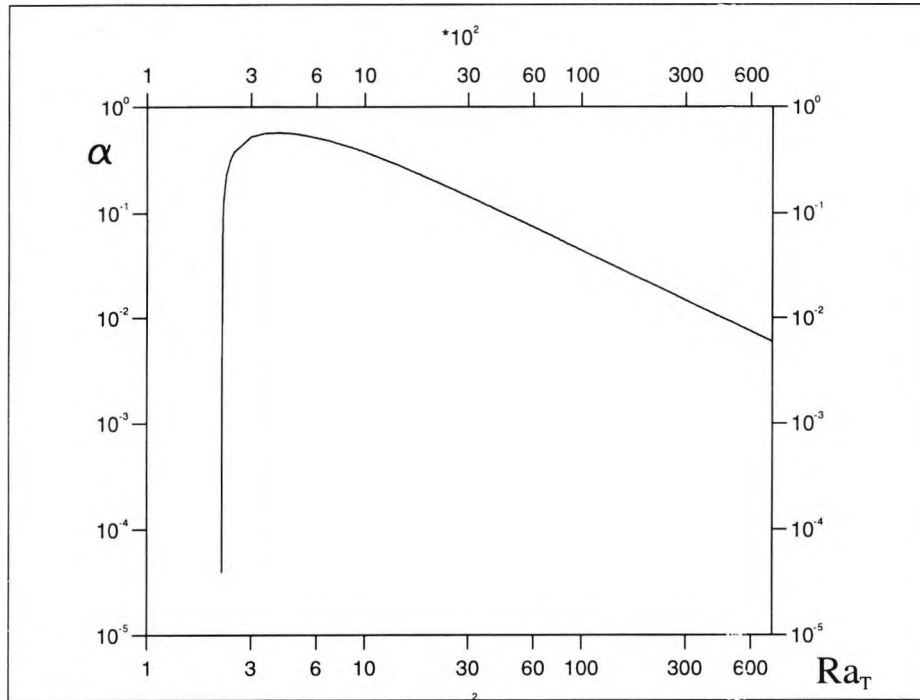


Figure 3.5: This neutral curve showing the behaviour of α and Ra_T in the vertical boundary, is found by fixing Ra_T in the Runge-Kutta scheme.

examined in the next section.

Instabilities in the absence of a salinity gradient occur for $Ra_T > 52715$ (Vest & Arpaci, 1969). It can be seen that the presence of a salinity gradient greatly enhances instability. We shall see later in chapter 5 that these instabilities are driven by the horizontal salinity gradient set up by the background flow which is driven by the imposed temperature difference.

The streamlines, salinity and temperature perturbations across a vertical slot were also examined. Typical examples of such contour-plots showing these periodic instabilities for the case $Ra_S = 10^3$ are shown in figures 3.7, 3.8 and 3.9. Other examples including cases on parts of the stability boundary not found by the Runge-Kutta scheme are shown in the next chapter. The counter-rotating convective cells are symmetrical about the origin as expected in a system with linear gradients. This background motion has warm salty

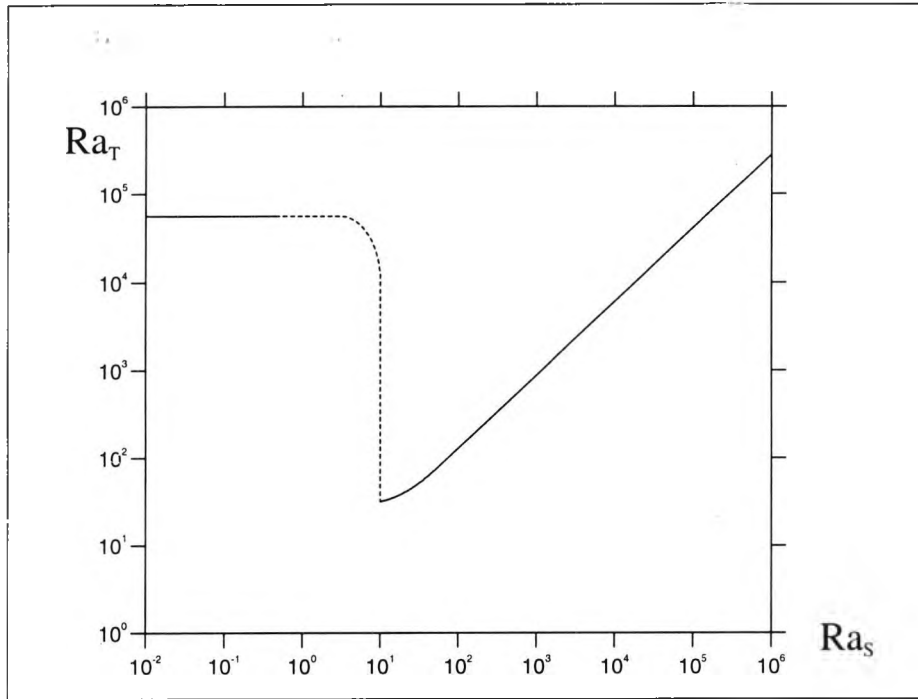


Figure 3.6: Neutral stability curve from Thangam, Zebib & Chen (1981). $Pr = 6.7$ and $\tau = 1/101$ are taken in their solutions for the stationary (solid line) and oscillatory (dashed line) branches.

fluid ascending in $-\frac{1}{2} < x < 0$ and cold fresh fluid descending in $0 < x < \frac{1}{2}$. As the fluid diverts away from the hot wall and moves into the cooler environment, its heat dissipation is significantly faster than the loss of its salt. This in effect creates a greater weight in the fluid which becomes heavier than its surrounding and so the fluid sinks. In contrast, the fluid coming from the cold region which is gradually heated up becomes fresher, and tends to rise upwards. When the streamlines and isotherms are superimposed, it is clear that the convective motion is transporting heat to the cold wall and cold water to the hot wall. Similarly the salinity perturbations appear much larger than the temperature perturbations because the heat contrasts diffuse faster than salinity by a hundredfold. The presence of a vertical salinity gradient causes an increase in salt concentration in areas of upward velocity and a reduction in areas of downward velocity.

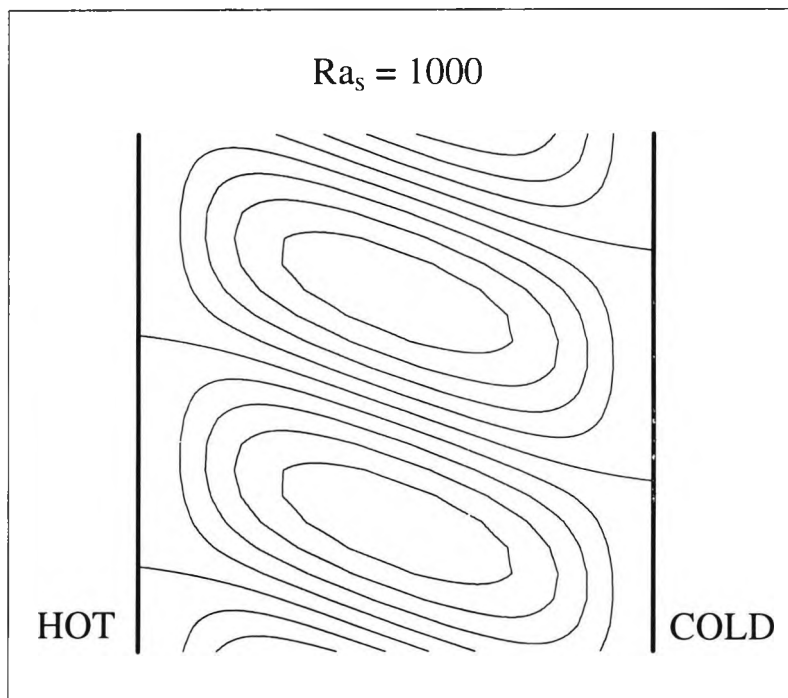


Figure 3.7: Graph of the streamlines of the perturbations for marginal stability at the critical value of α . Here x is in the range from -0.5 to 0.5 with the same ratio as the vertical walls. The contours of the stream function are ranging from -0.01 to 0.01 in steps of 0.002 .

3.3 Oscillatory Branch and $Ra_S \ll 1$ Solution

As previously mentioned, the Runge-Kutta scheme failed to find the oscillatory solutions as described by Thangam, Zebib & Chen (1981) and the small Ra_S solutions. Here we will briefly mention the methods used in looking for them.

We tackled the oscillatory region by substituting Broyden's algorithm to find the common zero of a pair of functions of two variables in place of Newton's method. This latter method only sets one of the last two boundary conditions to zero while the second is simultaneously satisfied due to symmetry in the slot problem in steady convection. This Broyden's algorithm is used for approximating solutions of the non-linear system: $\mathbf{F}(\mathbf{x}) = \mathbf{0}$ when the initial approximation \mathbf{x} is given. Here, $\mathbf{F}(\mathbf{x})$ has components which are the last two boundary conditions of $T_r(1/2) = T_i(1/2) = 0$ and the components

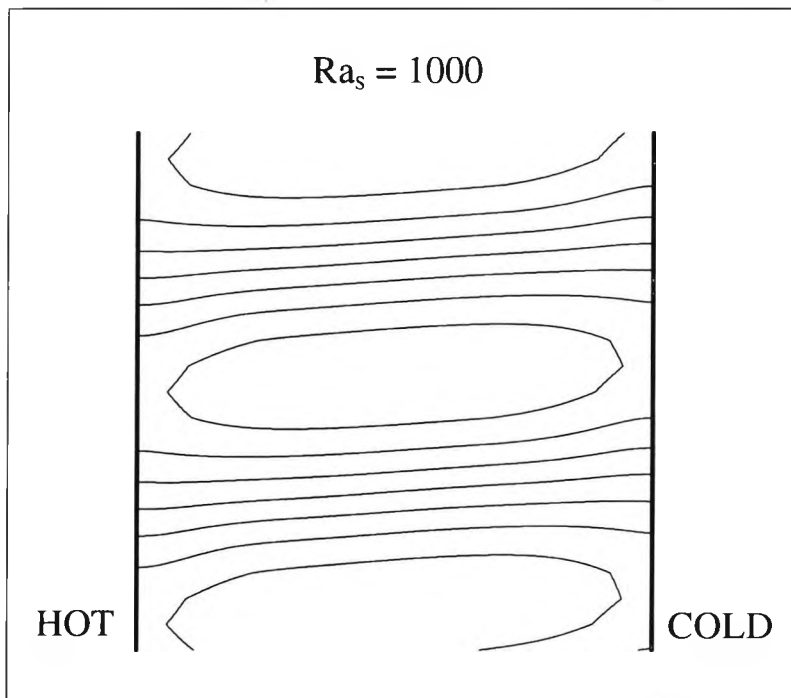


Figure 3.8: Graph of the salinity perturbations for marginal stability at the critical value of α . The lines of constant salinity perturbation are at levels from -0.1 to 0.1 in steps of 0.02 .

of \mathbf{x} are Ra_T and σ_i . It can be seen in Appendix A that six of the eight boundary conditions are satisfied based on the shooting method and we subsequently use this Broyden's algorithm to satisfy these last two temperature boundary conditions on the right wall by varying both Ra_T and σ_i . A (2×2) Jacobian matrix representing the initial approximation to the temperature boundary conditions was set up before leading to the computation of its inverse and other necessary matrix multiplication. Full details can be found in Burden, Faires and Reynolds (1981, pp. 458-460). These calculations should be iterated for a number of times until both Ra_T and σ_i converge at some point. This should ultimately find the critical values of Ra_T , α , and the corresponding growth rate σ_i for any fixed value of Ra_S .

The above algorithm needs a reasonable initial guess for Ra_T and α to converge. In the absence of knowledge about the magnitude of the frequency of the growth rate when using the above numerical scheme, a large range of

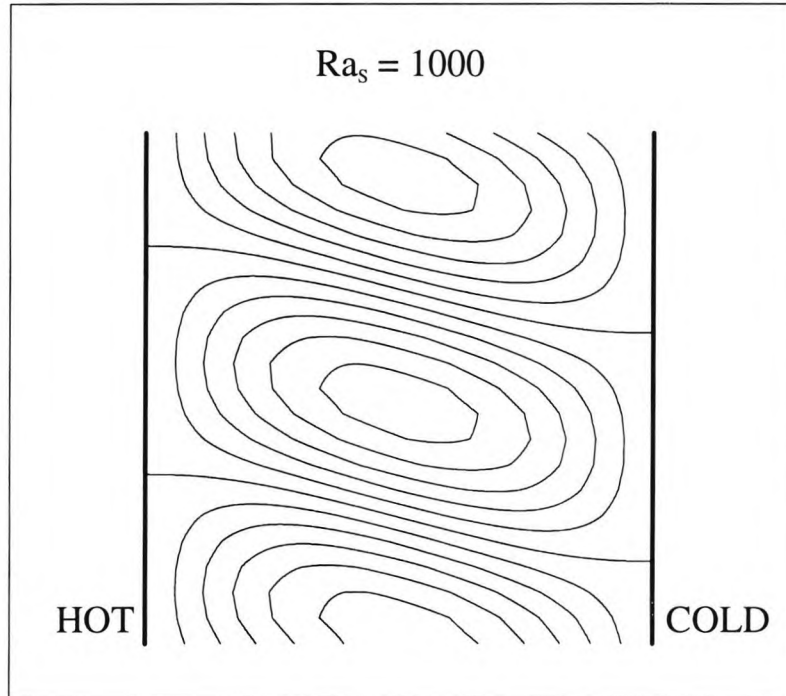


Figure 3.9: Graph of the temperature perturbations for marginal stability at the critical value of α . The lines of constant temperature perturbation are plotted at levels from -0.01 to 0.01 with stepsize of 0.002 .

possible frequencies were tried. It was not possible to locate any solutions corresponding to oscillatory instability or any of those overstable solutions suggested by Thangam *et al.* However, the Runge-Kutta scheme with Broyden's algorithm will only converge to produce oscillatory solutions when the initial guesses for the growth rate, Ra_T and α have assigned values very close to the actual solutions. This means the numerical scheme is weak for finding independent oscillatory solutions but is able to produce steady solutions when σ_i is zero. Therefore, it could only be used for confirmation of some known oscillatory results. An independent Galerkin approach of chapter 4 (which was used by Thangam *et al.*) is able to find oscillatory solutions in the range $2.0256 \leq Ra_S \leq 4.7703$. This new finding indicates mistakes exist in the results of Thangam *et al.* for oscillatory solutions.

Furthermore, the next part of the stability curve with weaker salinity gra-

dients where Thangam *et al.* found steady convection, cannot be found by using the Runge-Kutta scheme. This numerical scheme failed to find solutions for any given choice of boundary conditions at the left wall as the solutions always grew to large values by the time they reached the right wall. The reason for this problem will be discussed further in the thermal convection and small Ra_S section of chapter 5.

The vertical part of the oscillatory solutions reported by Thangam *et al.* with Ra_S about 10 cannot be found by this Runge-Kutta scheme. Instead, a similar branch of steady solutions is found for Ra_S about 4.7703. It is because of the failure in the Runge-Kutta scheme to find solutions in the case of small salinity gradient and, for verification of the results obtained for $4.7703 < Ra_S < 10$ which differed from Thangam *et al.*, that we employed their Galerkin method. This is discussed in the subsequent chapter. Most importantly, this second method is able to complete the full stability curve for the part that the Runge-Kutta scheme was unable to calculate. This includes the $Ra_S \ll 1$ region and the overstable branch of solutions.

Chapter 4

Comparison of Galerkin

Method

The fourth order Runge-Kutta scheme combined with a standard shooting method was first used to investigate the marginal stability curve of the full problem as described in chapter 3. However, solutions for Ra_S below 4.7703 could not be found by this numerical scheme. Also, results found between $Ra_S = 4.7703$ and $Ra_S = 10$ were different from those of Thangam, Zebib & Chen (1981). It was decided that verification of the results of the previous chapter was needed by using a method independent of the Runge-Kutta scheme, so a Galerkin method was employed following the approach of Thangam *et al.* in their paper. This is a technique that has been used in other double-diffusive problems. For example, the linear stability investigation by Paliwal & Chen (1980) for a stratified fluid contained in an inclined slot subject to a temperature difference. This independent numerical study is the subject of this chapter.

The Galerkin method is not only useful for the confirmation of our previous results, it is also proved successful in generating solutions for the difficult region where the salinity gradient is weak. In this sensitive region,

the Runge-Kutta scheme failed to find solutions for parameters under consideration ($Pr = 6.7$ and $\tau = 0.01$). As we shall see later, the problems experienced include boundary layers that developed at the walls and at the centre of the slot, and stiff behaviour found elsewhere due to a large magnitude term in the salinity equation. In fact, the uniform resolution introduced across the slot width by the expansion functions used by Thangam *et al.* in their Galerkin approach has an advantage for this problem as it maintains resolution in the middle of the slot. A similar numerical scheme used by Young & Rosner (1998) involving the use of Chebyshev polynomials concentrates the resolution adjacent to the boundaries and therefore it is possible that their numerical scheme is slightly less appropriate to the problem in this case. The reason for the failure in the shooting method will become clearer in chapter 5 when we discuss the asymptotic for the small salt gradient regime.

4.1 Galerkin Method

In principle, the Galerkin method is a special case of the more general method called the Method of Weighted Residuals. This technique expands the unknown solution ψ , T or S in a complete set of orthogonal trial functions with adjustable coefficients. These coefficients are then determined so as to give the best solution of the system of stability equations. To accomplish this, the assumed (or unknown) solutions are substituted into the stability equations and the residuals are set approximately to zero to give the best values of the unknown coefficients. In the Galerkin method, the chosen trial functions are expanded in a complete set, indicating the trial functions are used as weighting functions and so the residuals are made orthogonal to the respective trial functions. It is best to choose trial functions that will automatically satisfy the boundary conditions of the problem.

This Galerkin approach was used by Paliwal & Chen (1980) in their theoretical study of double-diffusive instabilities in an inclined slot as well as by Thangam *et al* for a vertical slot. Below are the expansions substituted into the stability problem of (2.10.2) to (2.10.4) where the set of orthogonal functions chosen satisfies the appropriate boundary conditions in (2.10.5). The variables ψ , T and S are expressed in terms of their trial functions:

$$\psi = \sum_{n=1}^{\infty} a_{2n-1} \left\{ \frac{\cosh \mu_{2n-1} x}{\cosh \frac{1}{2} \mu_{2n-1}} - \frac{\cos \mu_{2n-1} x}{\cos \frac{1}{2} \mu_{2n-1}} \right\} + a_{2n} \left\{ \frac{\sinh \mu_{2n} x}{\sinh \frac{1}{2} \mu_{2n}} - \frac{\sin \mu_{2n} x}{\sin \frac{1}{2} \mu_{2n}} \right\}, \quad (4.1.1)$$

$$T = \sum_{n=1}^{\infty} b_{2n-1} \cos(2n-1)\pi x + b_{2n} \sin(2n)\pi x, \quad (4.1.2)$$

$$S = \sum_{n=1}^{\infty} c_{2n-1} \cos 2(n-1)\pi x + c_{2n} \sin(2n-1)\pi x, \quad (4.1.3)$$

where μ_{2n-1} and μ_{2n} are respectively zeros of

$$\tanh\left(\frac{1}{2}\mu_{2n-1}\right) + \tan\left(\frac{1}{2}\mu_{2n-1}\right) = 0, \quad (4.1.4)$$

and

$$\coth\left(\frac{1}{2}\mu_{2n}\right) - \cot\left(\frac{1}{2}\mu_{2n}\right) = 0. \quad (4.1.5)$$

These expansions, (4.1.1) to (4.1.3), are also used to derive the derivatives required in the stability equations. The stability problem with the substituted expansions is then made into a system of residual equations by multiplying the appropriate trial function and integrating across the slot. This gives the integrals

$$\int_{-\frac{1}{2}}^{\frac{1}{2}} \{\text{LHS of (2.10.2)}\} \left\{ \frac{\cosh \mu_{2m-1} x}{\cosh \frac{1}{2} \mu_{2m-1}} - \frac{\cos \mu_{2m-1} x}{\cos \frac{1}{2} \mu_{2m-1}} \right\} dx = 0, \quad (4.1.6)$$

$$\int_{-\frac{1}{2}}^{\frac{1}{2}} \{\text{LHS of (2.10.2)}\} \left\{ \frac{\sinh \mu_{2m} x}{\sinh \frac{1}{2} \mu_{2m}} - \frac{\sin \mu_{2m} x}{\sin \frac{1}{2} \mu_{2m}} \right\} dx = 0, \quad (4.1.7)$$

$$\int_{-\frac{1}{2}}^{\frac{1}{2}} \{\text{LHS of (2.10.3)}\} \cos(2m-1)\pi x dx = 0, \quad (4.1.8)$$

$$\int_{-\frac{1}{2}}^{\frac{1}{2}} \{\text{LHS of (2.10.3)}\} \sin(2m)\pi x dx = 0, \quad (4.1.9)$$

$$\int_{-\frac{1}{2}}^{\frac{1}{2}} \{\text{LHS of (2.10.4)}\} \cos 2(m-1)\pi x dx = 0, \quad (4.1.10)$$

$$\int_{-\frac{1}{2}}^{\frac{1}{2}} \{\text{LHS of (2.10.4)}\} \sin(2m-1)\pi x dx = 0. \quad (4.1.11)$$

In each case, the trial functions are either odd or even in x . The terms that arise from substituting the expansions into (2.10.2) to (2.10.4) can also be readily split into odd and even functions of x and so many terms can be seen to integrate to zero. This leads to some reduction in work. The resulting integrals are products of perturbation quantities with some containing the implicit form of the background state which are evaluated explicitly and are shown in Appendix B. This subsequently produces an infinite system of linear homogeneous algebraic equations.

In the case of the stream function equation, the integrals involving multiplication by the even trial functions in the ψ expansion give

$$\begin{aligned} & \left[\mu_{2m-1}^4 + \alpha^4 - 2\alpha^2 \mu_{2m-1}^2 H_1 \right] a_{2m-1} \\ & + \left[-\frac{i\alpha}{Pr} \mu_{2m}^2 H_2 + \frac{i\alpha^3}{Pr} H_3 + \frac{i\alpha}{Pr} H_4 \right] a_{2m} \\ & - Ra_T(2m\pi) H_5 b_{2m} + Ra_S(2m-1)\pi H_6 c_{2m} \\ & + \sum_{n \neq m}^{\infty} -2\alpha^2 \mu_{2n-1}^2 H_7 a_{2n-1} \\ & + \left\{ -\frac{i\alpha}{Pr} \mu_{2n}^2 H_8 + \frac{i\alpha^3}{Pr} H_9 + \frac{i\alpha}{Pr} H_{10} \right\} a_{2n} \\ & - Ra_T(2n\pi) H_{11} b_{2n} + Ra_S(2n-1)\pi H_{12} c_{2n} \\ & = \sigma \left[\left\{ -\frac{\alpha^2}{Pr} + \frac{\mu_{2m-1}^2}{Pr} H_1 \right\} a_{2m-1} + \sum_{n \neq m}^{\infty} \frac{\mu_{2n-1}^2}{Pr} H_7 a_{2n-1} \right], \quad (4.1.12) \end{aligned}$$

and the corresponding equation from the integrals involving the odd trial

functions in the expansion for ψ give

$$\begin{aligned}
& \left[\mu_{2m}^4 + \alpha^4 - 2\alpha^2 \mu_{2m}^2 H_{14} \right] a_{2m} \\
& + \left[-\frac{i\alpha}{P_r} \mu_{2m-1}^2 H_{13} + \frac{i\alpha^3}{P_r} H_{15} + \frac{i\alpha}{P_r} H_{16} \right] a_{2m-1} \\
& + Ra_T(2m-1)\pi H_{17} b_{2m-1} - Ra_S 2(m-1)\pi H_{18} c_{2m-1} \\
& + \sum_{n \neq m}^{\infty} \left\{ -\frac{i\alpha}{P_r} \mu_{2n-1}^2 H_{19} + \frac{i\alpha^3}{P_r} H_{21} + \frac{i\alpha}{P_r} H_{22} \right\} a_{2n-1} \\
& \quad - 2\alpha^2 \mu_{2n}^2 H_{20} a_{2n} + Ra_T(2n-1)\pi H_{23} b_{2n-1} \\
& \quad - Ra_S 2(n-1)\pi H_{24} c_{2n-1} \\
& = \sigma \left[\left\{ -\frac{\alpha^2}{P_r} + \frac{\mu_{2m}^2}{P_r} H_{14} \right\} a_{2m} + \sum_{n \neq m}^{\infty} \frac{\mu_{2n}^2}{P_r} H_{20} a_{2n} \right], \tag{4.1.13}
\end{aligned}$$

where the integrals H_1 to H_{24} for ψ are given by

$$H_1 = \int_{-1/2}^{1/2} \left(\frac{\cosh \mu_{2m-1} x}{\cosh \frac{1}{2} \mu_{2m-1}} + \frac{\cos \mu_{2m-1} x}{\cos \frac{1}{2} \mu_{2m-1}} \right) \left(\frac{\cosh \mu_{2m-1} x}{\cosh \frac{1}{2} \mu_{2m-1}} - \frac{\cos \mu_{2m-1} x}{\cos \frac{1}{2} \mu_{2m-1}} \right) dx, \tag{4.1.14}$$

$$H_2 = \int_{-1/2}^{1/2} \overline{w}_o \left(\frac{\sinh \mu_{2m} x}{\sinh \frac{1}{2} \mu_{2m}} + \frac{\sin \mu_{2m} x}{\sin \frac{1}{2} \mu_{2m}} \right) \left(\frac{\cosh \mu_{2m-1} x}{\cosh \frac{1}{2} \mu_{2m-1}} - \frac{\cos \mu_{2m-1} x}{\cos \frac{1}{2} \mu_{2m-1}} \right) dx, \tag{4.1.15}$$

$$H_3 = \int_{-1/2}^{1/2} \overline{w}_o \left(\frac{\sinh \mu_{2m} x}{\sinh \frac{1}{2} \mu_{2m}} - \frac{\sin \mu_{2m} x}{\sin \frac{1}{2} \mu_{2m}} \right) \left(\frac{\cosh \mu_{2m-1} x}{\cosh \frac{1}{2} \mu_{2m-1}} - \frac{\cos \mu_{2m-1} x}{\cos \frac{1}{2} \mu_{2m-1}} \right) dx, \tag{4.1.16}$$

$$H_4 = \int_{-1/2}^{1/2} D^2 \overline{w}_o \left(\frac{\sinh \mu_{2m} x}{\sinh \frac{1}{2} \mu_{2m}} - \frac{\sin \mu_{2m} x}{\sin \frac{1}{2} \mu_{2m}} \right) \left(\frac{\cosh \mu_{2m-1} x}{\cosh \frac{1}{2} \mu_{2m-1}} - \frac{\cos \mu_{2m-1} x}{\cos \frac{1}{2} \mu_{2m-1}} \right) dx, \tag{4.1.17}$$

$$H_5 = \int_{-1/2}^{1/2} \cos(2m)\pi x \left(\frac{\cosh \mu_{2m-1} x}{\cosh \frac{1}{2} \mu_{2m-1}} - \frac{\cos \mu_{2m-1} x}{\cos \frac{1}{2} \mu_{2m-1}} \right) dx, \tag{4.1.18}$$

$$H_6 = \int_{-1/2}^{1/2} \cos(2m-1)\pi x \left(\frac{\cosh \mu_{2m-1} x}{\cosh \frac{1}{2} \mu_{2m-1}} - \frac{\cos \mu_{2m-1} x}{\cos \frac{1}{2} \mu_{2m-1}} \right) dx, \tag{4.1.19}$$

$$H_7 = \int_{-1/2}^{1/2} \left(\frac{\cosh \mu_{2n-1}x}{\cosh \frac{1}{2}\mu_{2n-1}} + \frac{\cos \mu_{2n-1}x}{\cos \frac{1}{2}\mu_{2n-1}} \right) \left(\frac{\cosh \mu_{2m-1}x}{\cosh \frac{1}{2}\mu_{2m-1}} - \frac{\cos \mu_{2m-1}x}{\cos \frac{1}{2}\mu_{2m-1}} \right) dx, \quad (4.1.20)$$

$$H_8 = \int_{-1/2}^{1/2} \bar{w}_o \left(\frac{\sinh \mu_{2n}x}{\sinh \frac{1}{2}\mu_{2n}} + \frac{\sin \mu_{2n}x}{\sin \frac{1}{2}\mu_{2n}} \right) \left(\frac{\cosh \mu_{2m-1}x}{\cosh \frac{1}{2}\mu_{2m-1}} - \frac{\cos \mu_{2m-1}x}{\cos \frac{1}{2}\mu_{2m-1}} \right) dx, \quad (4.1.21)$$

$$H_9 = \int_{-1/2}^{1/2} \bar{w}_o \left(\frac{\sinh \mu_{2n}x}{\sinh \frac{1}{2}\mu_{2n}} - \frac{\sin \mu_{2n}x}{\sin \frac{1}{2}\mu_{2n}} \right) \left(\frac{\cosh \mu_{2m-1}x}{\cosh \frac{1}{2}\mu_{2m-1}} - \frac{\cos \mu_{2m-1}x}{\cos \frac{1}{2}\mu_{2m-1}} \right) dx, \quad (4.1.22)$$

$$H_{10} = \int_{-1/2}^{1/2} D^2 \bar{w}_o \left(\frac{\sinh \mu_{2n}x}{\sinh \frac{1}{2}\mu_{2n}} - \frac{\sin \mu_{2n}x}{\sin \frac{1}{2}\mu_{2n}} \right) \left(\frac{\cosh \mu_{2m-1}x}{\cosh \frac{1}{2}\mu_{2m-1}} - \frac{\cos \mu_{2m-1}x}{\cos \frac{1}{2}\mu_{2m-1}} \right) dx, \quad (4.1.23)$$

$$H_{11} = \int_{-1/2}^{1/2} \cos(2n)\pi x \left(\frac{\cosh \mu_{2m-1}x}{\cosh \frac{1}{2}\mu_{2m-1}} - \frac{\cos \mu_{2m-1}x}{\cos \frac{1}{2}\mu_{2m-1}} \right) dx, \quad (4.1.24)$$

$$H_{12} = \int_{-1/2}^{1/2} \cos(2n-1)\pi x \left(\frac{\cosh \mu_{2m-1}x}{\cosh \frac{1}{2}\mu_{2m-1}} - \frac{\cos \mu_{2m-1}x}{\cos \frac{1}{2}\mu_{2m-1}} \right) dx, \quad (4.1.25)$$

$$H_{13} = \int_{-1/2}^{1/2} \bar{w}_o \left(\frac{\cosh \mu_{2m-1}x}{\cosh \frac{1}{2}\mu_{2m-1}} + \frac{\cos \mu_{2m-1}x}{\cos \frac{1}{2}\mu_{2m-1}} \right) \left(\frac{\sinh \mu_{2m}x}{\sinh \frac{1}{2}\mu_{2m}} - \frac{\sin \mu_{2m}x}{\sin \frac{1}{2}\mu_{2m}} \right) dx, \quad (4.1.26)$$

$$H_{14} = \int_{-1/2}^{1/2} \left(\frac{\sinh \mu_{2m}x}{\sinh \frac{1}{2}\mu_{2m}} + \frac{\sin \mu_{2m}x}{\sin \frac{1}{2}\mu_{2m}} \right) \left(\frac{\sinh \mu_{2m}x}{\sinh \frac{1}{2}\mu_{2m}} - \frac{\sin \mu_{2m}x}{\sin \frac{1}{2}\mu_{2m}} \right) dx, \quad (4.1.27)$$

$$H_{15} = \int_{-1/2}^{1/2} \bar{w}_o \left(\frac{\cosh \mu_{2m-1}x}{\cosh \frac{1}{2}\mu_{2m-1}} - \frac{\cos \mu_{2m-1}x}{\cos \frac{1}{2}\mu_{2m-1}} \right) \left(\frac{\sinh \mu_{2m}x}{\sinh \frac{1}{2}\mu_{2m}} - \frac{\sin \mu_{2m}x}{\sin \frac{1}{2}\mu_{2m}} \right) dx, \quad (4.1.28)$$

$$H_{16} = \int_{-1/2}^{1/2} D^2 \bar{w}_o \left(\frac{\cosh \mu_{2m-1}x}{\cosh \frac{1}{2}\mu_{2m-1}} - \frac{\cos \mu_{2m-1}x}{\cos \frac{1}{2}\mu_{2m-1}} \right) \left(\frac{\sinh \mu_{2m}x}{\sinh \frac{1}{2}\mu_{2m}} - \frac{\sin \mu_{2m}x}{\sin \frac{1}{2}\mu_{2m}} \right) dx, \quad (4.1.29)$$

$$H_{17} = \int_{-1/2}^{1/2} \sin(2m-1)\pi x \left(\frac{\sinh \mu_{2m}x}{\sinh \frac{1}{2}\mu_{2m}} - \frac{\sin \mu_{2m}x}{\sin \frac{1}{2}\mu_{2m}} \right) dx, \quad (4.1.30)$$

$$H_{18} = \int_{-1/2}^{1/2} \sin 2(m-1)\pi x \left(\frac{\sinh \mu_{2m}x}{\sinh \frac{1}{2}\mu_{2m}} - \frac{\sin \mu_{2m}x}{\sin \frac{1}{2}\mu_{2m}} \right) dx, \quad (4.1.31)$$

$$H_{19} = \int_{-1/2}^{1/2} \overline{w}_o \left(\frac{\cosh \mu_{2n-1}x}{\cosh \frac{1}{2}\mu_{2n-1}} + \frac{\cos \mu_{2n-1}x}{\cos \frac{1}{2}\mu_{2n-1}} \right) \left(\frac{\sinh \mu_{2m}x}{\sinh \frac{1}{2}\mu_{2m}} - \frac{\sin \mu_{2m}x}{\sin \frac{1}{2}\mu_{2m}} \right) dx, \quad (4.1.32)$$

$$H_{20} = \int_{-1/2}^{1/2} \left(\frac{\sinh \mu_{2n}x}{\sinh \frac{1}{2}\mu_{2n}} + \frac{\sin \mu_{2n}x}{\sin \frac{1}{2}\mu_{2n}} \right) \left(\frac{\sinh \mu_{2m}x}{\sinh \frac{1}{2}\mu_{2m}} - \frac{\sin \mu_{2m}x}{\sin \frac{1}{2}\mu_{2m}} \right) dx, \quad (4.1.33)$$

$$H_{21} = \int_{-1/2}^{1/2} \overline{w}_o \left(\frac{\cosh \mu_{2n-1}x}{\cosh \frac{1}{2}\mu_{2n-1}} - \frac{\cos \mu_{2n-1}x}{\cos \frac{1}{2}\mu_{2n-1}} \right) \left(\frac{\sinh \mu_{2m}x}{\sinh \frac{1}{2}\mu_{2m}} - \frac{\sin \mu_{2m}x}{\sin \frac{1}{2}\mu_{2m}} \right) dx, \quad (4.1.34)$$

$$H_{22} = \int_{-1/2}^{1/2} D^2 \overline{w}_o \left(\frac{\cosh \mu_{2n-1}x}{\cosh \frac{1}{2}\mu_{2n-1}} - \frac{\cos \mu_{2n-1}x}{\cos \frac{1}{2}\mu_{2n-1}} \right) \left(\frac{\sinh \mu_{2m}x}{\sinh \frac{1}{2}\mu_{2m}} - \frac{\sin \mu_{2m}x}{\sin \frac{1}{2}\mu_{2m}} \right) dx, \quad (4.1.35)$$

$$H_{23} = \int_{-1/2}^{1/2} \sin(2n-1)\pi x \left(\frac{\sinh \mu_{2m}x}{\sinh \frac{1}{2}\mu_{2m}} - \frac{\sin \mu_{2m}x}{\sin \frac{1}{2}\mu_{2m}} \right) dx, \quad (4.1.36)$$

$$H_{24} = \int_{-1/2}^{1/2} \sin 2(n-1)\pi x \left(\frac{\sinh \mu_{2m}x}{\sinh \frac{1}{2}\mu_{2m}} - \frac{\sin \mu_{2m}x}{\sin \frac{1}{2}\mu_{2m}} \right) dx. \quad (4.1.37)$$

These 24 integrations are evaluated explicitly in Appendix B.

Following a similar procedure, the algebraic equations obtained by multiplying the terms in the temperature expansion by the even and odd functions in T and integrating are

$$\begin{aligned} & - \frac{1}{2} \left[(2m-1)^2 \pi^2 + \alpha^2 \right] b_{2m-1} + i\alpha F_1 a_{2m-1} - i\alpha F_2 b_{2m} \\ & + \sum_{n \neq m}^{\infty} [i\alpha F_3 a_{2n-1} - i\alpha F_4 b_{2n}] = \sigma \left[\frac{1}{2} b_{2m-1} \right], \end{aligned} \quad (4.1.38)$$

$$\begin{aligned} & - \frac{1}{2} \left[(2m)^2 \pi^2 + \alpha^2 \right] b_{2m} + i\alpha F_5 a_{2m} - i\alpha F_6 b_{2m-1} \\ & + \sum_{n \neq m}^{\infty} [i\alpha F_7 a_{2n} - i\alpha F_8 b_{2n-1}] = \sigma \left[\frac{1}{2} b_{2m} \right]. \end{aligned} \quad (4.1.39)$$

Similarly, the algebraic equations found for the salinity expansion are

$$\begin{aligned} & - \frac{T}{2} \left[4(m-1)^2 \pi^2 + \alpha^2 \right] c_{2m-1} - i\alpha G_1 a_{2m-1} - i\alpha G_2 c_{2m} - \mu_{2m} G_3 a_{2m} \\ & + \sum_{n \neq m}^{\infty} [-i\alpha G_4 a_{2n-1} - i\alpha G_5 c_{2n} - \mu_{2n} G_6 a_{2n}] = \sigma \left[\frac{1}{2} c_{2m-1} \right], \end{aligned} \quad (4.1.40)$$

$$\begin{aligned}
& - \frac{\tau}{2} \left[(2m-1)^2 \pi^2 + \alpha^2 \right] c_{2m} - i\alpha G_7 a_{2m} - i\alpha G_8 c_{2m-1} - \mu_{2m-1} G_9 a_{2m-1} \\
& + \sum_{n \neq m}^{\infty} [-i\alpha G_{10} a_{2n} - i\alpha G_{11} c_{2n-1} - \mu_{2n-1} G_{12} a_{2n-1}] = \sigma \left[\frac{1}{2} c_{2m} \right]. \quad (4.1.41)
\end{aligned}$$

The eight integrals, F_1 to F_8 , for the temperature and the twelve integrals for the salinity, G_1 to G_{12} , are given by

$$F_1 = \int_{-1/2}^{1/2} \left(\frac{\cosh \mu_{2m-1} x}{\cosh \frac{1}{2} \mu_{2m-1}} - \frac{\cos \mu_{2m-1} x}{\cos \frac{1}{2} \mu_{2m-1}} \right) \cos(2m-1)\pi x \, dx, \quad (4.1.42)$$

$$F_2 = \int_{-1/2}^{1/2} \bar{w}_o \sin(2m)\pi x \cos(2m-1)\pi x \, dx, \quad (4.1.43)$$

$$F_3 = \int_{-1/2}^{1/2} \left(\frac{\cosh \mu_{2n-1} x}{\cosh \frac{1}{2} \mu_{2n-1}} - \frac{\cos \mu_{2n-1} x}{\cos \frac{1}{2} \mu_{2n-1}} \right) \cos(2m-1)\pi x \, dx, \quad (4.1.44)$$

$$F_4 = \int_{-1/2}^{1/2} \bar{w}_o \sin(2n)\pi x \cos(2m-1)\pi x \, dx, \quad (4.1.45)$$

$$F_5 = \int_{-1/2}^{1/2} \left(\frac{\sinh \mu_{2m} x}{\sinh \frac{1}{2} \mu_{2m}} - \frac{\sin \mu_{2m} x}{\sin \frac{1}{2} \mu_{2m}} \right) \sin(2m)\pi x \, dx, \quad (4.1.46)$$

$$F_6 = \int_{-1/2}^{1/2} \bar{w}_o \cos(2m-1)\pi x \sin(2m)\pi x \, dx, \quad (4.1.47)$$

$$F_7 = \int_{-1/2}^{1/2} \left(\frac{\sinh \mu_{2n} x}{\sinh \frac{1}{2} \mu_{2n}} - \frac{\sin \mu_{2n} x}{\sin \frac{1}{2} \mu_{2n}} \right) \sin(2m)\pi x \, dx, \quad (4.1.48)$$

$$F_8 = \int_{-1/2}^{1/2} \bar{w}_o \cos(2n-1)\pi x \sin(2m)\pi x \, dx, \quad (4.1.49)$$

and,

$$G_1 = \int_{-1/2}^{1/2} D\bar{S}_o \left(\frac{\cosh \mu_{2m-1} x}{\cosh \frac{1}{2} \mu_{2m-1}} - \frac{\cos \mu_{2m-1} x}{\cos \frac{1}{2} \mu_{2m-1}} \right) \cos 2(m-1)\pi x \, dx, \quad (4.1.50)$$

$$G_2 = \int_{-1/2}^{1/2} \bar{w}_o \sin(2m-1)\pi x \cos 2(m-1)\pi x \, dx, \quad (4.1.51)$$

$$G_3 = \int_{-1/2}^{1/2} \left(\frac{\cosh \mu_{2m} x}{\sinh \frac{1}{2} \mu_{2m}} - \frac{\cos \mu_{2m} x}{\sin \frac{1}{2} \mu_{2m}} \right) \cos 2(m-1)\pi x \, dx, \quad (4.1.52)$$

$$G_4 = \int_{-1/2}^{1/2} D\overline{S}_o \left(\frac{\cosh \mu_{2n-1}x}{\cosh \frac{1}{2}\mu_{2n-1}} - \frac{\cos \mu_{2n-1}x}{\cos \frac{1}{2}\mu_{2n-1}} \right) \cos 2(m-1)\pi x dx, \quad (4.1.53)$$

$$G_5 = \int_{-1/2}^{1/2} \overline{w}_o \sin(2n-1)\pi x \cos 2(m-1)\pi x dx, \quad (4.1.54)$$

$$G_6 = \int_{-1/2}^{1/2} \left(\frac{\cosh \mu_{2n}x}{\sinh \frac{1}{2}\mu_{2n}} - \frac{\cos \mu_{2n}x}{\sin \frac{1}{2}\mu_{2n}} \right) \cos 2(m-1)\pi x dx, \quad (4.1.55)$$

$$G_7 = \int_{-1/2}^{1/2} D\overline{S}_o \left(\frac{\sinh \mu_{2m}x}{\sinh \frac{1}{2}\mu_{2m}} - \frac{\sin \mu_{2m}x}{\sin \frac{1}{2}\mu_{2m}} \right) \sin(2m-1)\pi x dx, \quad (4.1.56)$$

$$G_8 = \int_{-1/2}^{1/2} \overline{w}_o \cos 2(m-1)\pi x \sin(2m-1)\pi x dx, \quad (4.1.57)$$

$$G_9 = \int_{-1/2}^{1/2} \left(\frac{\sinh \mu_{2m-1}x}{\cosh \frac{1}{2}\mu_{2m-1}} + \frac{\sin \mu_{2m-1}x}{\cos \frac{1}{2}\mu_{2m-1}} \right) \sin(2m-1)\pi x dx, \quad (4.1.58)$$

$$G_{10} = \int_{-1/2}^{1/2} D\overline{S}_o \left(\frac{\sinh \mu_{2n}x}{\sinh \frac{1}{2}\mu_{2n}} - \frac{\sin \mu_{2n}x}{\sin \frac{1}{2}\mu_{2n}} \right) \sin(2m-1)\pi x dx, \quad (4.1.59)$$

$$G_{11} = \int_{-1/2}^{1/2} \overline{w}_o \cos 2(n-1)\pi x \sin(2m-1)\pi x dx, \quad (4.1.60)$$

$$G_{12} = \int_{-1/2}^{1/2} \left(\frac{\sinh \mu_{2n-1}x}{\cosh \frac{1}{2}\mu_{2n-1}} + \frac{\sin \mu_{2n-1}x}{\cos \frac{1}{2}\mu_{2n-1}} \right) \sin(2m-1)\pi x dx. \quad (4.1.61)$$

The general form of the 6 algebraic equations in (4.1.12), (4.1.13) and (4.1.38) to (4.1.41) can be written in a more compact format as a matrix equation:

$$A\mathbf{x} = \sigma B\mathbf{x}, \quad (4.1.62)$$

where A and B are infinite matrices. In order to solve the problem a truncation level, N , is introduced, making the system numerically tractable. Both A and B are defined as $(3N \times 3N)$ matrices with complex elements and the vector \mathbf{x} is a column of unknown coefficients made up of the coefficients a_i , b_i and c_i . The matrix B is not diagonal and certainly not the identity matrix (cf. Thangam *et al.* equation (3.4)). The elements of matrices A and B are functions of the parameters Pr , τ , Ra_S , Ra_T and α .

For a given set of values of the parameters of this problem, the solution to the matrix eigenvalue problem given by the truncation of (4.1.62) may be determined using a NAG Routine (F02GJF). This library routine calculates all the eigenvalues σ , and if requested, all the corresponding eigenvectors of the complex eigenproblem. For marginal instability, we look for where the largest real part of all the eigenvalues changes sign from negative (decaying disturbance) to positive (growing disturbance). In addition, the accompanying imaginary part, σ_i , indicates stationary instability when $\sigma_i = 0$ or oscillatory instability when $\sigma_i \neq 0$. Sometimes σ has a very small imaginary part due to numerical rounding errors. True complex eigenvalues occur in conjugate pairs in this problem, so any eigenvalue with a small imaginary part but no conjugate pair would mean that it must be an approximation to a real eigenvalue. An iteration scheme similar to the Newton's method originally used by the Runge-Kutta scheme (see details in Appendix A), is set up in order to determine, say, the minimum for Ra_T and the corresponding α for any given Ra_S .

The complete picture of the marginal stability curve is given in figure 4.1, showing the boundary between stable and unstable modes. These numerical solutions of both stationary and oscillatory branches are respectively indicated by solid and dashed lines in this Ra_S - Ra_T plane. This version of marginal stability curve is clearly different to that of Thangam *et al.* in figure 3.6 when Ra_S lies between 0.45 and 10. Other parts of the curve are essentially the same. At $Ra_S = 0.45$, Thangam *et al.* found a transition to oscillatory solutions. However, the primary mode of instability continues to be steady beyond this point and slowly rises upwards to meet the next region at $Ra_S = 2.0256$. In this next region the instability is no longer stationary but overstable. This oscillatory branch then continues to curve downwards

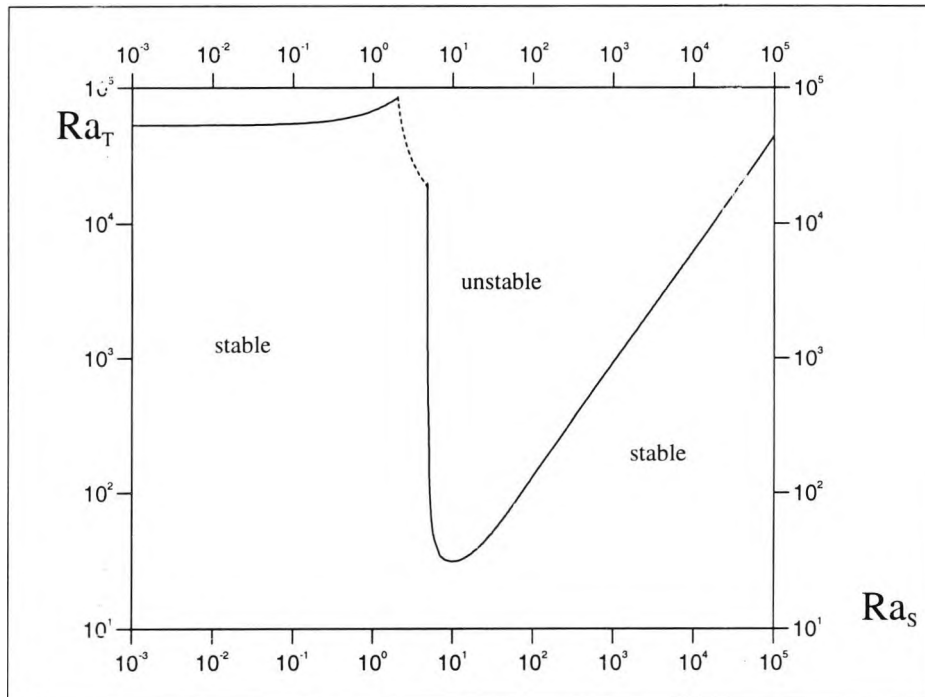


Figure 4.1: The complete version of the marginal stability curve for $Pr = 6.7$ and $\tau = 0.01$ are considered. Only a small section indicated by dashed line is the oscillatory branch and others are all stationary branches.

until it reaches $Ra_S = 4.7703$. Here there is an almost vertical boundary which takes over and the value of Ra_T decreases rapidly until reaching a minimum near $Ra_S = 10$. The solutions found for this vertical boundary revert to being stationary. This contradicts the existence of the overstable solutions claimed by Thangam *et al.* and confirms the previous results found in the previous chapter by the Runge-Kutta scheme for Ra_S between 4.7703 and 10. The recent paper by Young & Rosner (1998) verified our findings although a slightly different value of the Prandtl number was used. It has been found for lower values of N , for example 48, that some parts of the stability boundary seem to be oscillatory although the true solution should be non-oscillatory (see below). This misleading result was recorded in the drafts of Young and Rosner's paper where they reported the small rising section of the neutral curve (on the left hand side) just before the point $Ra_S = 2.0256$ was oscillatory. Fortunately, we were able to point out this error to Young and Rosner,

and their results were corrected before publication.

Contour plots of the perturbations streamlines, temperature and salinity are shown in figures 4.2–4.5. These show the instabilities along different parts of the stability boundary to the left of the minimum (see figure 4.1). In each case the hot wall is on the left and the cold wall is on the right. Contour plots for an example to the right of the minimum have been shown in the previous chapter. Each of these shows a complete period of the instability in the vertical direction. In figure 4.2 is shown the instability on the vertical portion of the boundary. These instabilities have a very long vertical scale and have been compressed by a factor of 100. The heat diffuses very rapidly in the horizontal direction and so the temperature perturbation is very small and has little effect on the density. In figures 4.3 and 4.4 are shown instabilities on the oscillatory part of the boundary. The first has $\sigma_i > 0$ and so represents a downward travelling instability, while the second has $\sigma_i < 0$ and is upward travelling. These instabilities are centred on the upward and downward flowing parts of the background flow respectively. The contour spacings on these two figures are the same, but using a normalisation of $\psi''(-1/2) = 1$ means that these modes which are not symmetrical about the centre of the slot have different maximum values and hence number of contours. Lastly, figure 4.5 shows the instability on top left portion of the stability boundary. The most notable feature of instabilities on this portion of the boundary is the large narrow peak in the salinity at the centre of the slot. The physical mechanism behind these instabilities is discussed further in chapter 5.

Most of the oscillatory solutions given by Thangam *et al.* for Ra_S between 0.45 and 10 were not found here. The only part showing initial oscillatory instability is indicated by a dashed line which occupies a small portion of the

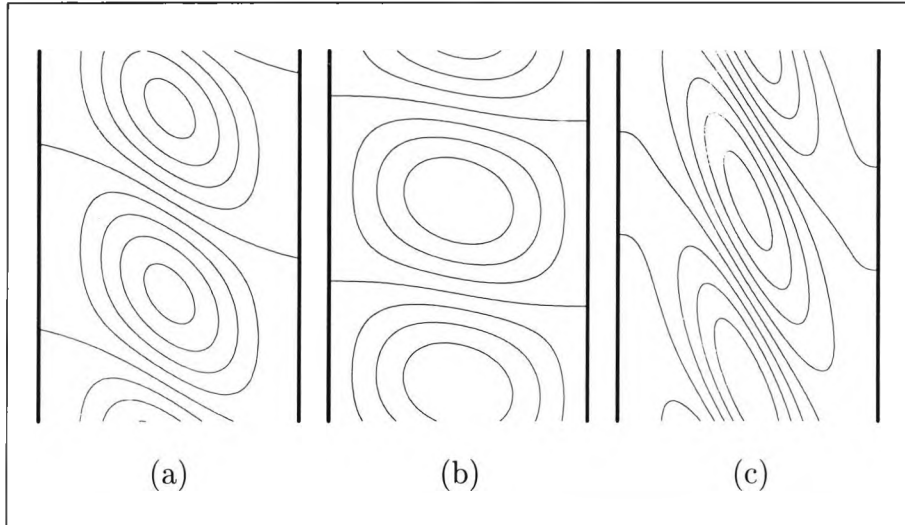


Figure 4.2: Contour plots for $Ra_S = 4.77065$ and $Ra_T = 10\,000$ showing perturbations of the (a) streamlines, (b) temperature and (c) salinity are for the steady case at marginal instability. These contours are taken in steps of 0.01, 0.00004 and 0.7 respectively and have been compressed by a factor of 100 in the vertical. The hot wall is on the left and the cold wall is on the right.

stability boundary. These oscillatory solutions continue to penetrate into the unstable region, giving a local minimum point on the curve of critical Ra_T as a function of wave number. The stability boundary of Ra_T as a function of α is shown in figure 4.6. The fluid in the slot is unstable in the region enclosed by the solid line and above the dashed line. There are no unstable modes in the region inbetween. The transition to instability along the dashed line is oscillatory and there is a local minimum at $Ra_T = 14\,057$ and $\alpha = 2.2416$. However, the global minimum is clearly on the steady branch for a much lower $Ra_T = 31.571$. Thus steady instabilities would always be observed and this is shown in figure 4.1. The minimum on the oscillatory branch is clearly different to the oscillatory result reported by Thangam *et al.* for $Ra_S = 10$. However, these oscillatory solutions can no longer be found beyond $Ra_S = 15.5$ or for Ra_T much below 12 000. In other words, no oscillatory solutions have been found between this value of Ra_T and the minimum for any instability at $Ra_T = 31.571$. Thus, the extensive search made for oscillatory solutions as reported by Thangam *et al.* in this region using the

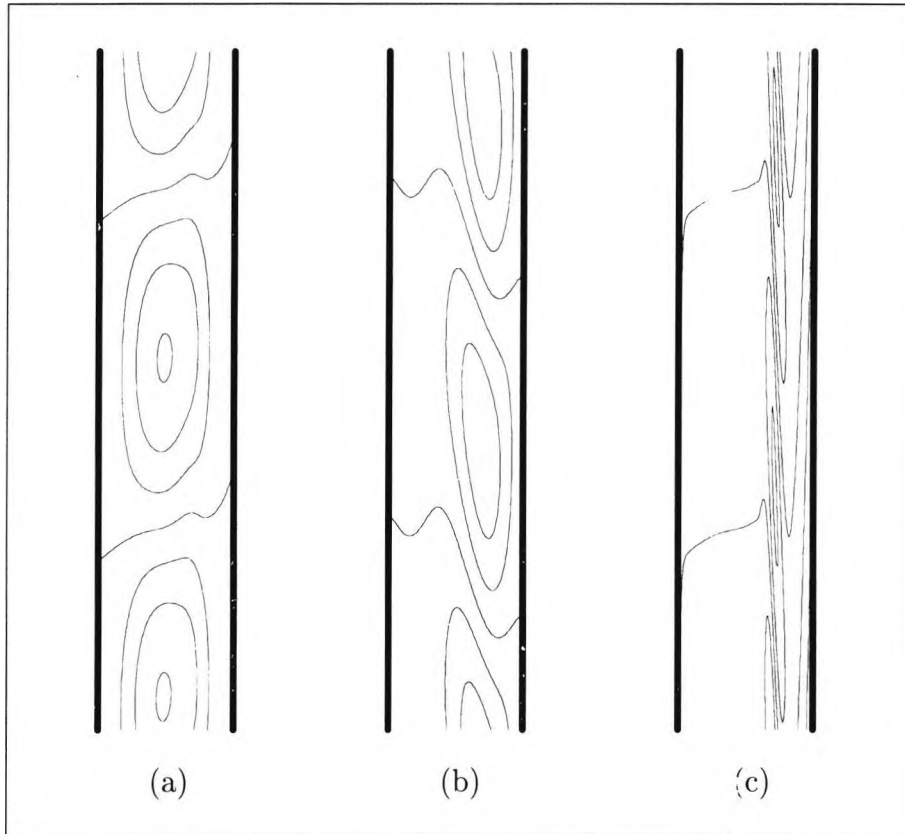


Figure 4.3: Contour plots for $Ra_S = 3$ and $Ra_T = 30230$ showing perturbations of the (a) streamlines, (b) temperature and (c) salinity are for the oscillatory case at marginal instability. These contours representing the positive eigenvalue are taken in steps of 0.01, 0.02 and 4 respectively. This mode has $\sigma_i > 0$ and so represents a downward moving instability.

Runge-Kutta scheme was doomed to failure.

It is in no doubt that the second numerical approach involving the expansion method confirms the results obtained earlier by the Runge-Kutta scheme. The comparison procedure is carried out by considering some known solutions for the critical Ra_T and α for any given values of Ra_S . We then check to see if the largest real part of the eigenvalue changes sign or not. If so, we have shown the two approaches agree and produce the same results.

The accuracy of solutions depends on the truncation level, N , chosen in the matrix system for the expansions of ψ , T and S . The choice of the trun-

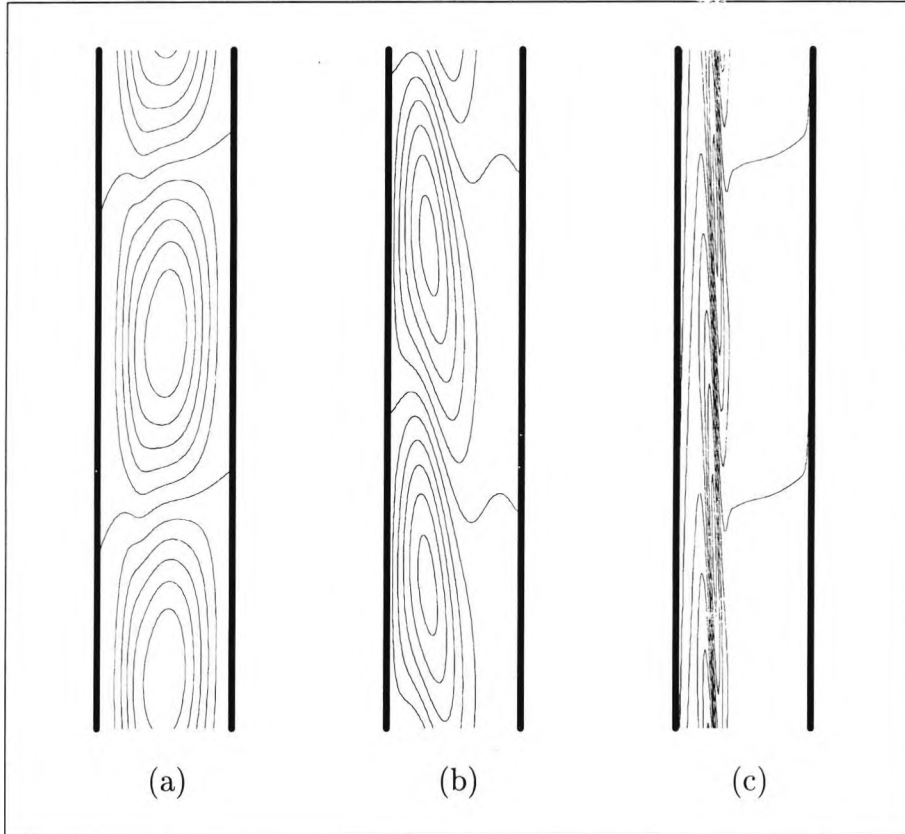


Figure 4.4: These contour plots are for the same situation as in figure 4.3 except that $\sigma_i < 0$ is shown here and the instabilities move upwards. The same contour spacings are used.

N	$Ra_S = 1.0$	$Ra_S = 0.1$	$Ra_S = 0.01$	$Ra_S = 0.001$
24	57979.172	53288.817	52773.197	52721.124
30	Not found	53511.629	52795.320	52723.364
48	66665.399	54052.185	52848.487	52728.680
72	67255.831	54093.822	52852.502	52729.080
96	67255.932	54093.828	52852.503	52729.080

Table 4.1: A table of the critical value of Ra_T calculated for different truncation levels, N , for small values of Ra_S .

cation level! N is determined by the part of the marginal stability curve being considered. The most difficult part of the curve on which to perform calculations was the steady small Ra_S part of the curve. The critical values of Ra_T found for various values of N with different values of Ra_S is shown in

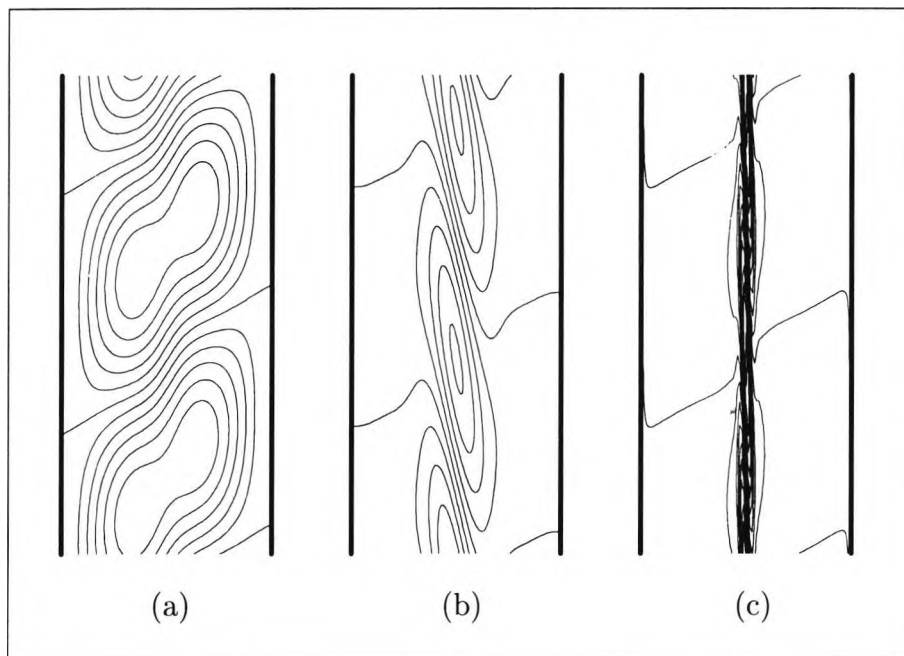


Figure 4.5: Contour plots for $Ra_S = 0.1$ and $Ra_T = 54093$ showing perturbations of the (a) streamlines, (b) temperature and (c) salinity are for the steady case at marginal instability. These contours are taken in steps of 0.0025, 0.0004 and 1 respectively.

table 4.1. For all cases shown here, the solution converges when $N = 96$. In the case with $N = 48$, the solution to the small salinity gradient problem is noticeably different to the $N = 96$ solution for $Ra_S = 1$. This difference becomes small as Ra_S tends to zero when the critical value for the thermally driven slot problem emerges. On all other parts of the neutral curve using 48 terms in the expansions gives good convergence in the results. This choice of $N = 48$ is an improved truncation level on that used by Thangam *et al.* in their expansions; their maximum level was $N = 30$ and was used in their oscillatory results while in other regions they often used $N = 16$. With $N = 72$ the solutions obtained for Ra_S up to 1.0 give very good agreement with the $N = 96$ results. As Ra_S increases further, the results seem to diverge more, indicating a higher N is necessary to obtain satisfactory solutions of the salinity equation along the steady branch. This condition is expected since the salinity expansions would need sufficient resolution to adequately resolve the boundary layer that exists at the centre of the slot with its sharp

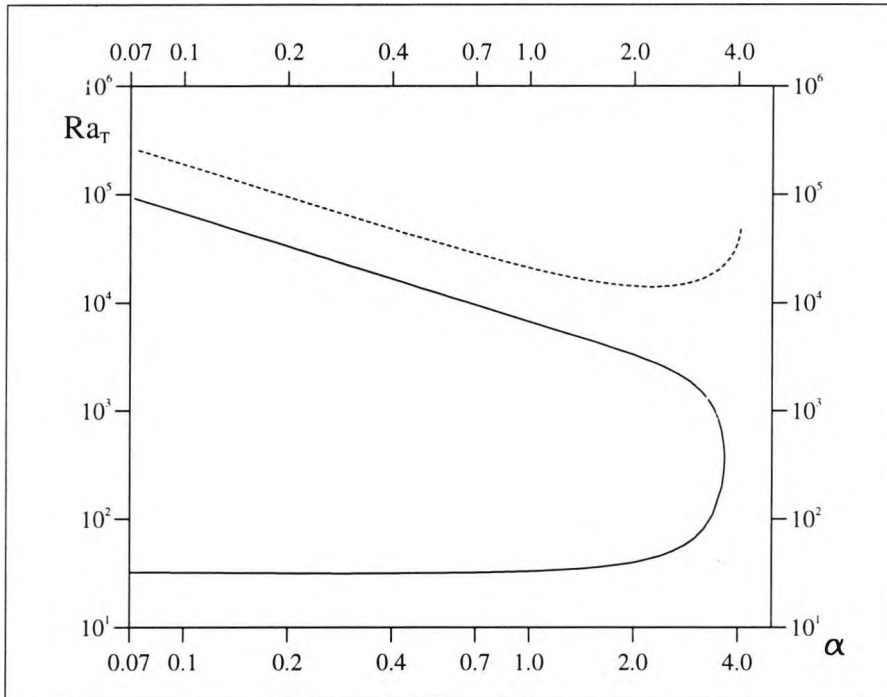


Figure 4.6: When $Ra_S = 10$, the minimum point for the (dashed) oscillatory solutions are indicated on the right while the other minimum point where instability is steady for zero α solutions is shown on the left as a solid line.

peak in the salinity. This is discussed in chapter 5 for the boundary layer problem in the limit of small Ra_S . Care must be taken when choosing N for $0.45 < Ra_S < 2.0256$ because if N is not sufficiently large the marginal solutions often seem to be oscillatory. It is found that on parts of the stability boundary where solutions are obtainable using both approaches, the solutions nearly always agree to five significant figures or more.

It seems that our results are partially different to those of Thangam *et al.* due to their truncation level being insufficient to obtain numerical convergence to the correct solution. The choice of truncation level is particularly important in the case of small Ra_S where solutions are changing between overstable and stationary branches. This may explain why the stationary vertical boundary was not found in Thangam *et al.*'s results and the shape of the oscillatory branch was different. The choice for $N = 24$ or 30 produces solutions far from the solutions found with $N = 96$. The reason why

Thangam *et al.* did not find the steady solutions for $4.7703 < Ra_S < 10$, is not clear.

The marginal instability curve is finally complete and the next chapter examines the asymptotic of the four regimes found on the different parts of this graph.

Chapter 5

Asymptotics

In this chapter we look at the full linear problem for a slot using asymptotic analysis. There are several regimes which describe the onset of instability in the heat and salt system as the salt Rayleigh number is varied. We will use this analysis to examine the physical processes involved that represent the significant features found in thermohaline convection in a vertical slot. In each case we attempt to derive a reduced model representing only the essential characteristics of that regime. Each reduced model is produced by investigating the different leading order balances in the full problem. This establishes various sections of the theoretical asymptotic behaviour for marginal stability, giving the vertical wave number and the corresponding salt and thermal Rayleigh numbers.

The neutral stability curve in figure 5.1 is divided into five different regions. The corresponding graph of α as a function of Ra_S is shown in figure 5.2. The majority of the curve is stationary except for region 4, marking the transition to an overstable instability. Only four asymptotic regimes are identified as shown by the different limits on the stability curve. We first examine the previously studied problem of strong salinity stratification (region 1) and then extend our findings by examining the weaker salinity gradient problems

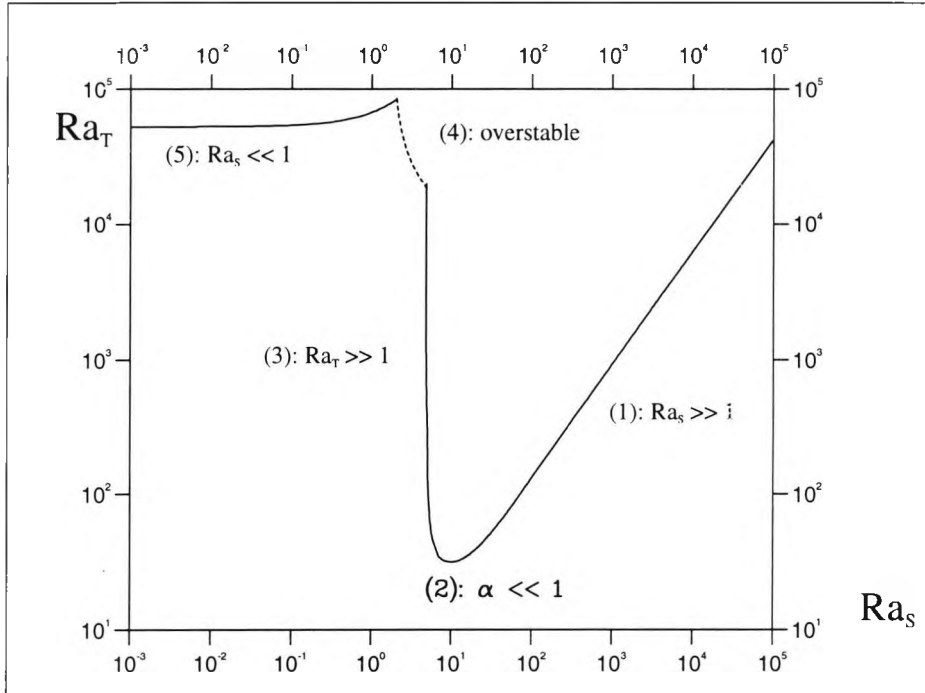


Figure 5.1: The neutral stability curve with $Pr = 6.7$ and $\tau = 0.01$. Each region which lends itself to an asymptotic analysis, is described by the appropriate limit. Stationary solutions are marked with solid lines and overstable with a dashed line.

which we will discuss in subsequent sections.

5.1 Large Ra_S with $\alpha \neq 0$

This regime involving strong salinity gradient in a differentially heated vertical slot has been examined by Thorpe, Hutt & Soulsby (1969) and then extended by Hart (1971). In this regime the salt Rayleigh number is considered large and the wave number is non-zero. This regime corresponds to the part of the neutral curve marked with region 1 in figure 5.1. This region alone is considered in figure 5.3 and is compared with the results obtained from the large Ra_S reduced model.

There are two reasons why we include this section on an asymptotic regime which was thoroughly investigated during the last three decades. For one, this problem for large Ra_S is a learning channel to the initial understanding of

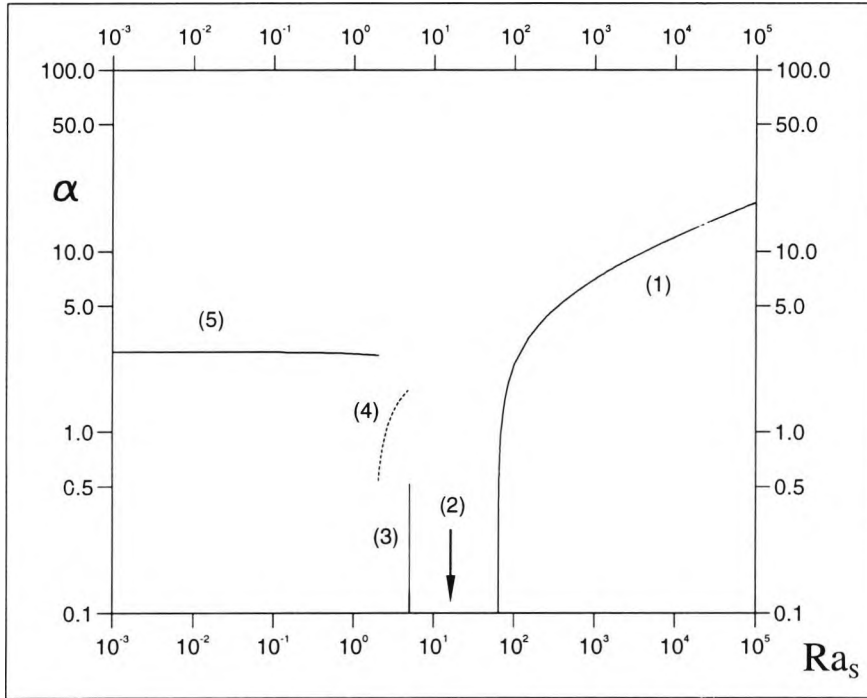


Figure 5.2: A graph of α as a function of Ra_S where the stationary solutions are marked with solid lines and the overstable with a dashed line for the different regions.

double-diffusive problem for a slot. This knowledge becomes useful when making analysis in other complex problems involving weaker salinity concentration. Secondly, it is useful to present asymptotic results for the linear theory for the slot problem that covers as much of the range of Ra_S as possible for later discussions.

We propose to determine all the dominant terms found in the linearised equations of ψ , T and S for the case of $Ra_S \gg 1$ by looking at each equation separately as outlined in (2.10.2) to (2.10.5) for the full problem where σ is set to zero. We consider all the terms in turn to obtain approximations corresponding to the modulus of their real and imaginary parts across the interval of $x = -1/2$ to $x = 1/2$. There are in total 17 such terms to be computed containing the real and imaginary parts of each term in the governing equations. We shall denote the 8 terms from the equation of ψ as

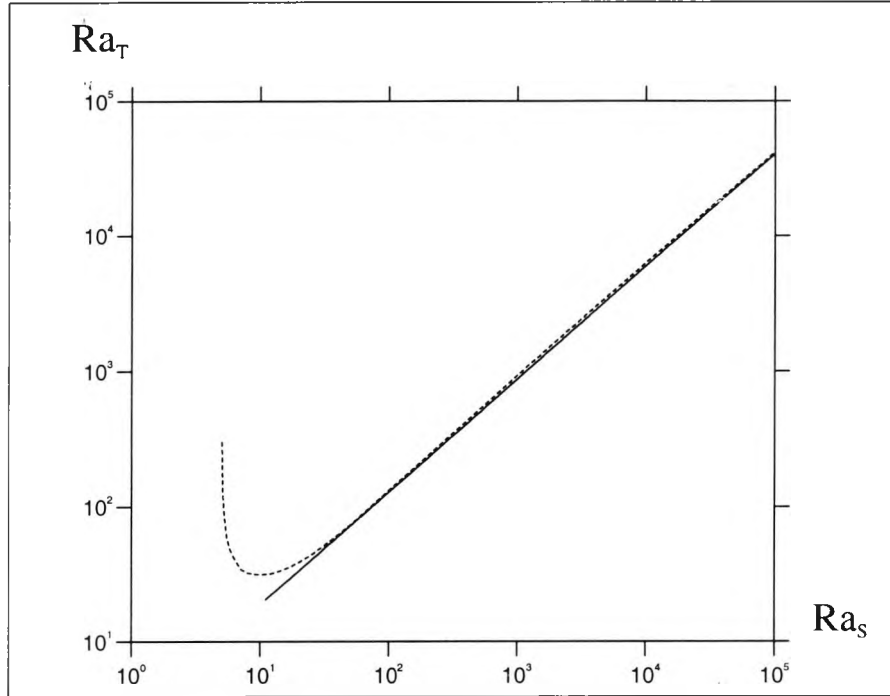


Figure 5.3: Graph showing the full (dashed) and reduced (solid) models that give good agreement in region 1.

$$\begin{aligned}
 \text{term 1} &= D^4\psi; & \text{term 2} &= 2\alpha^2 D^2\psi, \\
 \text{term 3} &= \alpha^4\psi; & \text{term 4} &= \alpha\bar{w}_o D^2\psi/Pr, \\
 \text{term 5} &= \alpha^3\bar{w}_o\psi/Pr; & \text{term 6} &= \alpha D^2\bar{w}_o\psi/Pr, \\
 \text{term 7} &= Ra_T DT; & \text{term 8} &= Ra_S DS.
 \end{aligned}$$

Similarly, the four terms from the temperature equation are

$$\begin{aligned}
 \text{term 9} &= D^2T; & \text{term 10} &= \alpha^2 T, \\
 \text{term 11} &= \alpha\psi; & \text{term 12} &= \alpha\bar{w}_o T,
 \end{aligned}$$

and the remaining five terms for the salinity equation are

$$\begin{aligned}
 \text{term 13} &= D^2S; & \text{term 14} &= \alpha^2 S, \\
 \text{term 15} &= \alpha D\bar{S}_o\psi/\tau; & \text{term 16} &= \alpha\bar{w}_o S/\tau, \\
 \text{term 17} &= D\psi/\tau.
 \end{aligned}$$

The investigation of the 17 terms sheds some light on their significance in the regime. The corresponding curves are drawn across the slot so every term

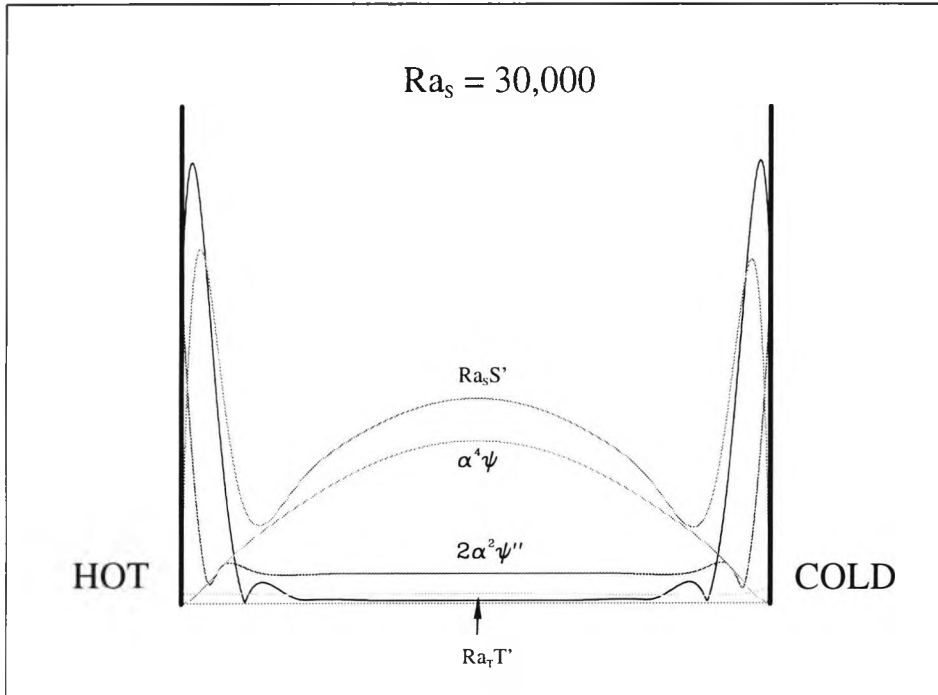


Figure 5.4: The modulus of terms describing the stream function are plotted in the range from $x = -1/2$ to $x = 1/2$. Four terms are highlighted for their significance across the slot as Ra_S gets large.

can be compared in the equations of ψ , T and S in figures 5.4 to 5.6 for $Ra_S = 30\,000$. In figure 5.4, the four important terms in the stream function are highlighted but the term $2\alpha^2 D^2\psi$ becomes less significant as Ra_S increases and can be neglected. Figures 5.5 and 5.6 reveal the magnitudes of the terms for the temperature and salinity equations respectively. It appears that the temperature terms are reduced to two and then three dominant terms are captured in the salinity equation. In fact, all the curves shown suggest the boundary layers become less significant when Ra_S is large. It is noted that horizontal diffusion is not important in the bulk of fluid but will become significant in thin boundary layers near the walls. These boundary layers do not play an important role in the leading order asymptotic (Hart, 1971).

Now we can eliminate terms which are insignificant from the full problem and only retain those ones dominating the flow between the two walls. The

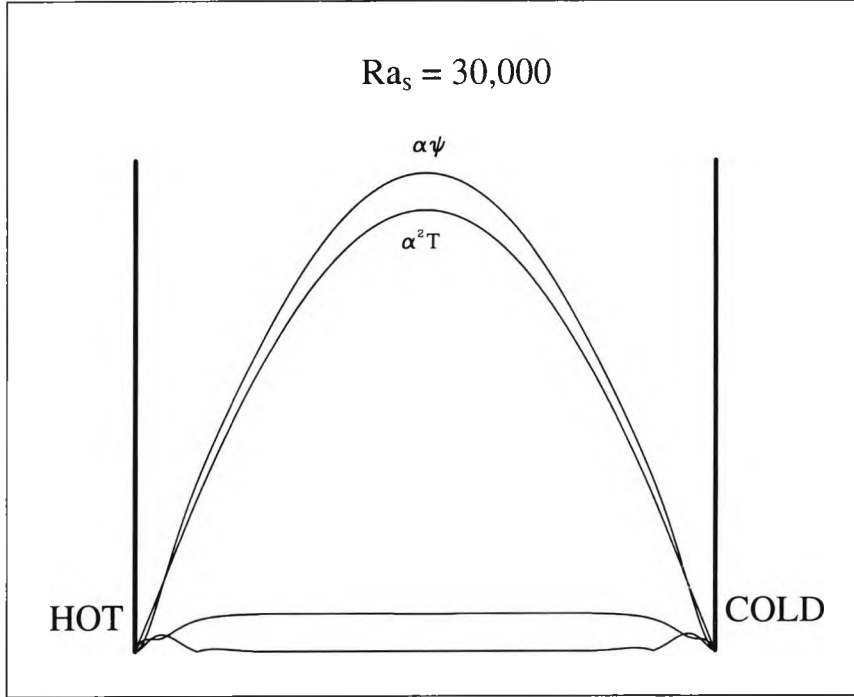


Figure 5.5: The modulus of terms describing the temperature are plotted in the range from $x = -1/2$ to $x = 1/2$. The two terms which are important within the two walls as Ra_S becomes large are indicated.

reduced model representing the $Ra_S \gg 1$ regime where $\alpha \neq 0$ is found to be

$$\alpha^4 \psi - Ra_T DT + Ra_S DS = 0, \quad (5.1.1)$$

$$-\alpha^2 T + i\alpha\psi = 0, \quad (5.1.2)$$

$$-\tau\alpha^2 S - i\alpha\psi D\bar{S}_o - D\psi = 0. \quad (5.1.3)$$

The leading order terms for large Ra_S can also be derived under the assumption that the vertical scale is much smaller than the horizontal scale. This is observed to be the case in experiments conducted by Thorpe *et al.* and Chen, Briggs & Wirtz (1971). We shall see later this corresponds to the condition that the vertical Chen scale ($\alpha_T \Delta T / \beta |\Phi_o|$) is much less than the slot width, D and $|\Phi_o|$ is the vertical salinity gradient. Here we have to emphasize that α_T is the coefficient of thermal expansion in order to avoid confusion with the vertical wave number.

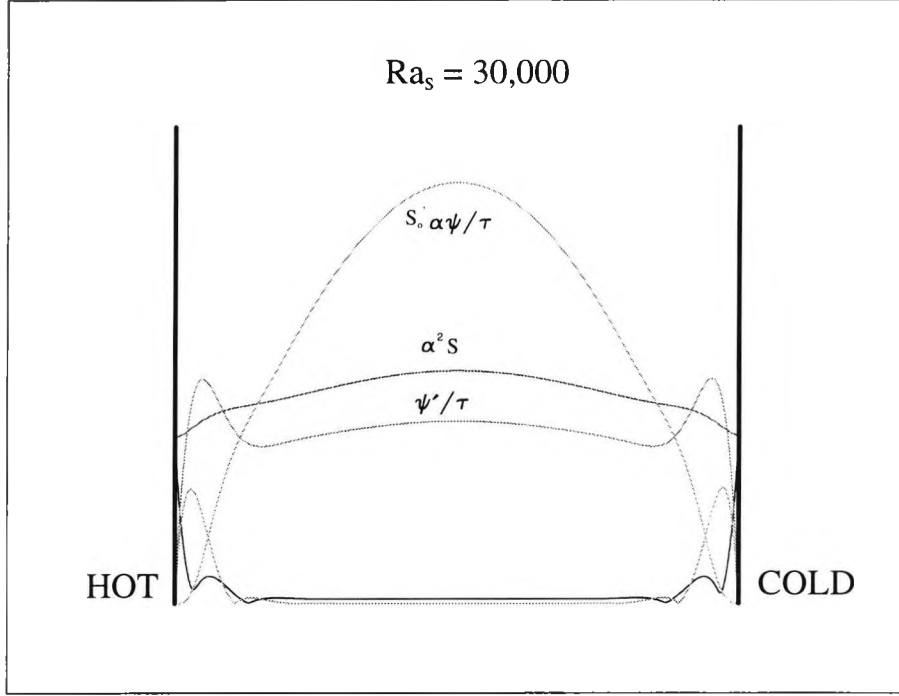


Figure 5.6: The modulus of terms describing the salinity are plotted in the range from $x = -1/2$ to $x = 1/2$. Three dominant terms are found between the walls as Ra_s becomes large. These are indicated.

The salinity equation (5.1.3) for the background salinity gradient is of leading order $D\bar{S}_o \approx -Ra_T/4\tau M^4$ in the core of the slot. This is obtained from the expansion for large M in

$$D\bar{S}_o \simeq \frac{-Ra_T}{4\tau M^4} \left[1 + e^{M(x-\frac{1}{2})} \sin\left(Mx - \frac{M}{2}\right) - e^{-M(x+\frac{1}{2})} \sin\left(Mx + \frac{M}{2}\right) - e^{M(x-\frac{1}{2})} \cos\left(Mx - \frac{M}{2}\right) - e^{-M(x+\frac{1}{2})} \cos\left(Mx + \frac{M}{2}\right) \right]. \quad (5.1.4)$$

The similar expansion for background velocity is

$$\bar{w}_o \simeq \frac{Ra_T}{2M^3} \left[e^{M(x-\frac{1}{2})} \sin\left(Mx - \frac{M}{2}\right) + e^{-M(x+\frac{1}{2})} \sin\left(Mx + \frac{M}{2}\right) \right], \quad (5.1.5)$$

showing $\bar{w}_o \rightarrow 0$ in the slot core. At the leading order, the core has a constant salinity gradient ($= -Ra_T/4\tau M^4$) and the boundary layers are thickness M^{-1} , decaying exponentially far away from the walls. From (5.1.2) and (5.1.3) we write respectively

$$DT = \frac{iD\psi}{\alpha}, \quad (5.1.6)$$

$$DS = \frac{1}{\tau\alpha^2} \left[\frac{i\alpha Ra_T D\psi}{4\tau M^4} - D^2\psi \right], \quad (5.1.7)$$

and these results are substituted into (5.1.1) giving

$$\alpha^4\psi - \frac{iRa_T}{\alpha} D\psi + \frac{Ra_S}{\tau\alpha^2} \left[\frac{i\alpha Ra_T D\psi}{4\tau M^4} - D^2\psi \right] = 0. \quad (5.1.8)$$

Dividing throughout by $Ra_S/\tau\alpha^2$ gives,

$$D^2\psi + D\psi \left[\frac{i\tau\alpha Ra_T}{Ra_S} - \frac{i\alpha Ra_T}{4\tau M^4} \right] - \frac{\tau\alpha^6\psi}{Ra_S} = 0. \quad (5.1.9)$$

We then replace Ra_S with $4\tau M^4$ and factor out $i\alpha Ra_T$ in the second term to give,

$$D^2\psi - \frac{i\alpha Ra_T(1-\tau)}{4\tau M^4} D\psi - \frac{\alpha^6\psi}{4M^4} = 0. \quad (5.1.10)$$

The solution ψ is of the form

$$\psi = Be^{\beta x} + Ce^{\gamma x}, \quad (5.1.11)$$

where β, γ are given by

$$\frac{1}{2} \left[\frac{i\alpha Ra_T(1-\tau)}{4\tau M^4} \pm \sqrt{\frac{-\alpha^2 Ra_T^2(1-\tau)^2}{16\tau^2 M^8} + \frac{\alpha^6}{M^4}} \right]. \quad (5.1.12)$$

The boundary condition of $\psi = 0$ on $x = \pm 1/2$ is used to provide the two expressions:

$$Be^{-\frac{1}{2}\beta} + Ce^{-\frac{1}{2}\gamma} = 0, \quad Be^{\frac{1}{2}\beta} + Ce^{\frac{1}{2}\gamma} = 0. \quad (5.1.13)$$

These can be combined to give the condition for the existence of solutions that

$$Be^{-\frac{1}{2}\beta}(e^\beta - e^\gamma) = 0. \quad (5.1.14)$$

If β, γ are real then $\beta = \gamma$ is trivial in the solutions but if β, γ are considered complex then we have

$$\beta - \gamma = 2n\pi i, \quad (5.1.15)$$

or alternatively the roots are replaced by (5.1.12),

$$\left[\frac{-\alpha^2 Ra_T^2(1-\tau)^2}{16\tau^2 M^8} + \frac{\alpha^6}{M^4} \right]^{\frac{1}{2}} = 2n\pi i. \quad (5.1.16)$$

Squaring both sides,

$$\frac{-\alpha^2 Ra_T^2 (1-\tau)^2}{16\tau^2 M^8} + \frac{\alpha^6}{M^4} = -4n^2\pi^2, \quad (5.1.17)$$

to give the expression of Ra_T ,

$$Ra_T^2 = \frac{\tau^2 M^4}{\alpha^2 (1-\tau)^2} [16\alpha^6 + 64n^2\pi^2 M^4]. \quad (5.1.18)$$

For the case of marginal stability we take $dRa_T/d\alpha = 0$. When (5.1.18) is differentiated with respect to α we obtain the expression for α

$$\frac{\tau^2 M^4}{(1-\tau)^2} \left[64\alpha^3 - \frac{128n^2\pi^2 M^4}{\alpha^3} \right] = 0, \quad (5.1.19)$$

giving

$$\alpha^6 = 2n^2\pi^2 M^4. \quad (5.1.20)$$

The expression for α in (5.1.20) is then put into the expression of Ra_T in (5.1.18) to give

$$Ra_T^2 = \frac{\tau^2 M^4}{(2n^2\pi^2 M^4)^{\frac{1}{3}} (1-\tau)^2} [16(2n^2\pi^2 M^4) + 64n^2\pi^2 M^4], \quad (5.1.21)$$

and this is minimized when $n = 1$ so that the smallest value of Ra_T is given by

$$Ra_T^6 = \frac{432\pi^4 Ra_S^5 \tau}{(1-\tau)^6}. \quad (5.1.22)$$

Consequently, the critical values for both the thermal Rayleigh number and the wave number describing the marginal stability in the regime of $Ra_S \gg 1$ are

$$Ra_T = (432\pi^4)^{\frac{1}{6}} Ra_S^{\frac{5}{6}} \frac{\tau^{\frac{1}{6}}}{(1-\tau)}, \quad (5.1.23)$$

and,

$$\alpha = \pi^{\frac{1}{3}} \left(\frac{Ra_S}{2\tau} \right)^{\frac{1}{6}}. \quad (5.1.24)$$

Thorpe *et al.* were first to examine the leading order asymptotic behaviour of this regime with both vertical and horizontal temperature-salinity gradients across the slot. Their asymptotic relation for marginal instability in

this regime is $Ra_T = 2.76Ra_S^{\frac{5}{6}}$ which is equivalent to equation (5.1.23). This analysis was extended by Hart who concentrated on the higher order effects of the boundary layers at the walls.

We can use the result for the critical α to find the physical height of the instability. We can express this wave number as

$$\alpha = \frac{2\pi D}{h}, \quad (5.1.25)$$

where h is the physical height of instability and D the slot width. With the physical quantities substituted for Ra_S in (5.1.24), we write

$$\frac{2\pi D}{h} = \pi^{\frac{1}{3}} \left(\frac{1}{2\tau} \frac{g\beta|\Phi_o|D^4}{\kappa_T\nu} \right)^{\frac{1}{6}}, \quad (5.1.26)$$

to determine the physical height,

$$h = 2\pi^{\frac{2}{3}} \left[\frac{2\kappa_S\nu}{g\beta|\Phi_o|} D^2 \right]^{\frac{1}{6}}. \quad (5.1.27)$$

We shall eliminate the horizontal scale D , in favour of the positive quantities involving the temperature and salinity gradients. From equation (5.1.22) we derive the expression

$$D^2 = \frac{g(\alpha_T\Delta T)^6(1-\tau)^6}{432\pi^4\tau(\beta|\Phi_o|)^5\kappa_T\nu}. \quad (5.1.28)$$

When this is substituted into (5.1.27) it gives

$$h = 2\pi^{\frac{2}{3}} \left[\frac{2\kappa_S\nu}{g\beta|\Phi_o|} \frac{g(\alpha_T\Delta T)^6(1-\tau)^6}{432\pi^4\tau(\beta|\Phi_o|)^5\kappa_T\nu} \right]^{\frac{1}{6}}, \quad (5.1.29)$$

which simplifies to

$$h = \sqrt{\frac{2}{3}}(1-\tau) \left[\frac{\alpha_T\Delta T}{\beta|\Phi_o|} \right]. \quad (5.1.30)$$

The quantity in the brackets, $\alpha_T\Delta T/\beta|\Phi_o|$, is the Chen scale. The convection cells in this regime take the form of thin almost horizontal layers whose vertical scale is approximately the Chen scale (see Chen, Briggs & Wirtz, 1971).

As the convective instabilities in this regime are constrained by this Chen scale in the vertical direction and the slot width in the horizontal direction, the theoretical result given here is also of some relevance to the mechanistic argument of Kerr (1989). This argument is based on a linear stability analysis of a semi-infinite body of fluid with a vertical salinity gradient heated from a single sidewall and it can similarly be applied here to a vertical slot. The non-dimensional parameter Q that was introduced in his analysis is related to the thermal Rayleigh number as observed in the case of Rayleigh-Bénard convection. However, the parameter

$$Q = \frac{(1 - \tau)^6 g(\alpha_T \Delta T)^6}{\nu \kappa_S D^2 (\beta |\Phi_{o1}|)^5}, \quad (5.1.31)$$

that governs the instabilities in this regime is determined by two length scales: the width of the slot and the vertical Chen scale. The horizontal scale in the context of a vertical slot is the slot width, D , and in Kerr's problem, the thermal diffusion distance from the single wall is $(\kappa_T t)^{\frac{1}{2}}$, where t is the dimensional time since the onset of heating. For strong salinity stratification in a vertical slot, instability starts to occur when $Q = 432\pi^4$ which is equivalent to the result of Thorpe *et al.* and Hart. Kerr also determined the next order perturbation of Q for the sidewall heating problem, which is the square of the ratio of the Chen scale to the horizontal length scale with an extra factor of $(1 - \tau)$. In the context of the variables used here, this expansion parameter is equivalently $((1 - \tau)Ra_T/Ra_S)^2$. In this regime where both temperature and salinity perturbations play an important role in the leading order asymptotic, the length scale for the diffusion of T and S is the same.

Our numerical results show good agreement with the above theoretical asymptotic for large Ra_S as shown in figure 5.3. For values around $Ra_S = 10^3$, a slight divergence is observed between the full and asymptotic estimates but

this difference diminishes as Ra_S increases. The asymptotic curve continues to agree with the full results as far down the solution branch as about $Ra_S = 30$ and this is the point where the next asymptotic regime for region 2 is appropriate. This exceptionally good agreement down to this value is probably entirely fortuitous. As we know α is assumed large under the $Ra_S \gg 1$ regime, therefore large α solutions are not appropriate in the small α regime. We shall see in the next section that at $Ra_S = 30$ the small α approximation is the appropriate approximation.

5.2 Small α

This section focuses on the bottom curved part of the marginal stability boundary that corresponds to small α . This is region 2 indicated in figure 5.1. For values of $Ra_S > 10$, our neutral curve has essentially the same shape as that of Triangam, Zebib & Chen (1981) but we found different results to their stability curve between the region of $0.45 \leq Ra_S \leq 10$. They only produced overstable solutions between the two limits.

The solution found on this boundary as highlighted in figure 5.7, is characterized by the vertical wave number becoming small. This is evidently supported by the results in the α - Ra_T plane in figure 3.1 where we observed a transition showing the decrease in the values of Ra_S . This gives the corresponding minimum close to the origin where α tends to zero. Figure 3.4 also gives the plot of α and Ra_S , showing the trace of α which is disappearing into the horizontal axis just after the left narrow peak. In fact, there are no zero growth rate solutions on this stability boundary of region 2 as solutions do not exist for $\alpha = 0$. Above the boundary there are always growing solutions and zero growth rate solutions. Therefore we propose to determine solutions in the limit of $\alpha \rightarrow 0$ for the asymptotic in region 2.

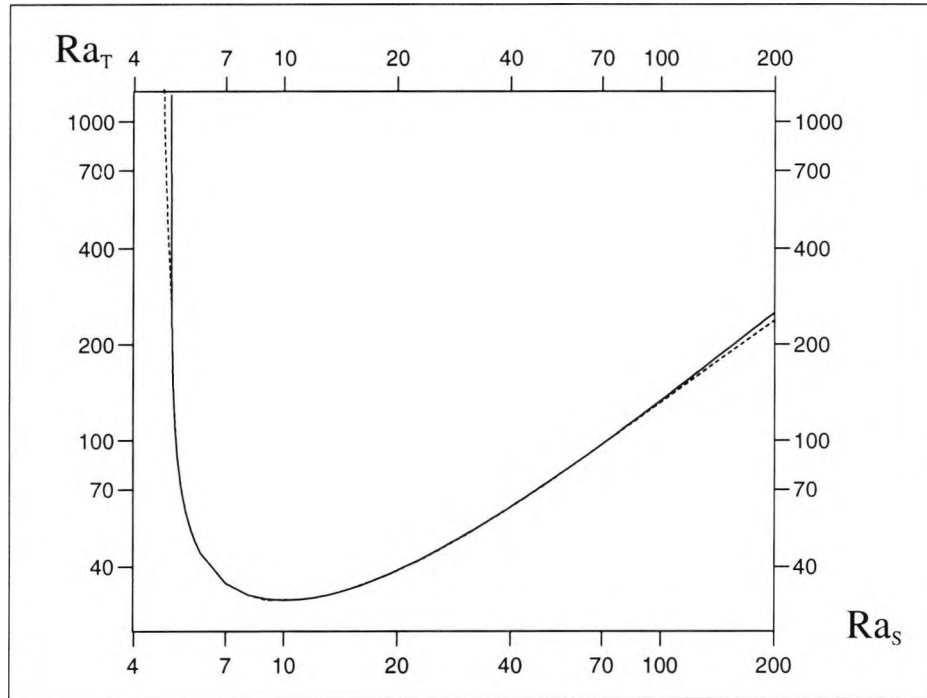


Figure 5.7: In the $\alpha \ll 1$ limit of region 2, a good comparison is shown between the full and reduced numerical results. Dashed line for the full model and solid for the asymptotic result.

The way of finding a reduced model for small α is to retain those dominant terms across the slot for these values of Ra_S when α becomes smaller. The technique in finding these significant terms is the same as that explained in the previous section of large Ra_S asymptotic. The labelled curves for $Ra_S = 10$ in figures 5.8 and 5.9 are the important terms for the equations of ψ and T . Both the stream function and temperature similarly indicate that there are two dominant terms found in the core of the slot. These terms balance each other so closely that the curves are indistinguishable. A different profile is revealed in figure 5.10. Although symmetry is visible about the line $x = 0$ for all significant salinity terms, they grow relatively large away from the core and decay quickly into the cold and hot walls. These curves are simply two smooth symmetrical peaks found in the confined slot. We will later see that the reason for this distribution is the terms in the salinity equation are odd functions about $x = 0$.

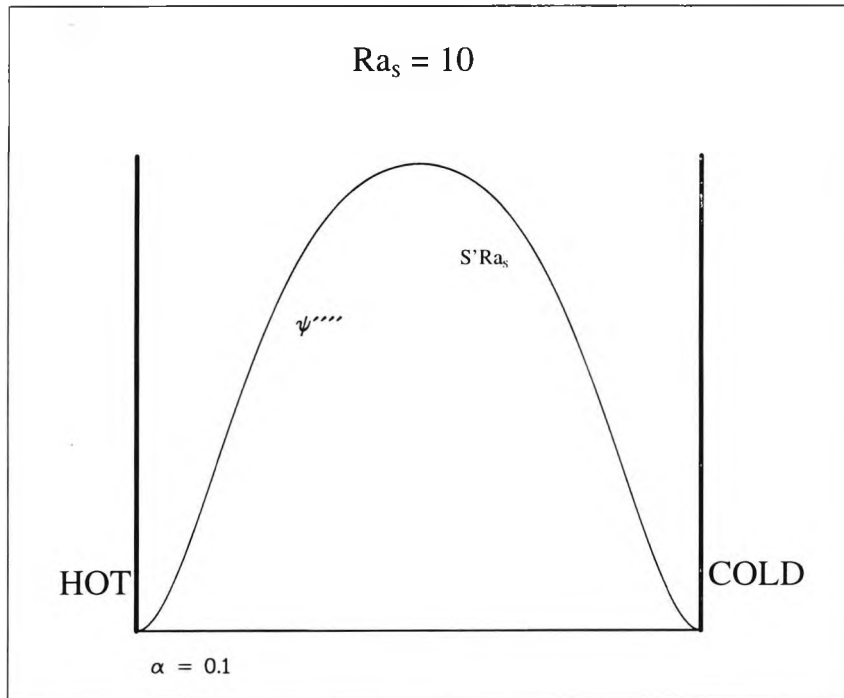


Figure 5.8: The modulus of the stream function illustrates two important terms across the slot in the region of small α .

When the reduced model is established from the above graphical examination, the reduced system of equations can be solved numerically using the Runge-Kutta method. This helps confirm the results in the next approach where we use an analytical method to obtain the asymptotic for this small α regime.

In order to determine a suitable reduced model for the small α case, we can also examine the scaling for the important parameters and variables that produce suitable balances. For example, we can take

$$\begin{aligned}
 Ra_T = O(1), \quad Ra_S = O(1), \quad \psi = O(1), \\
 T = O(\alpha^a) \quad \text{and} \quad S = O(\alpha^b)
 \end{aligned}
 \tag{5.2.1}$$

as $\alpha \rightarrow 0$, where the unknowns a and b are to be determined so as to give a satisfactory balance in the slot. We hope to find zero growth rate (time-independent) solutions in the limit $\alpha \rightarrow 0$ using the full problem in (2.10.2)

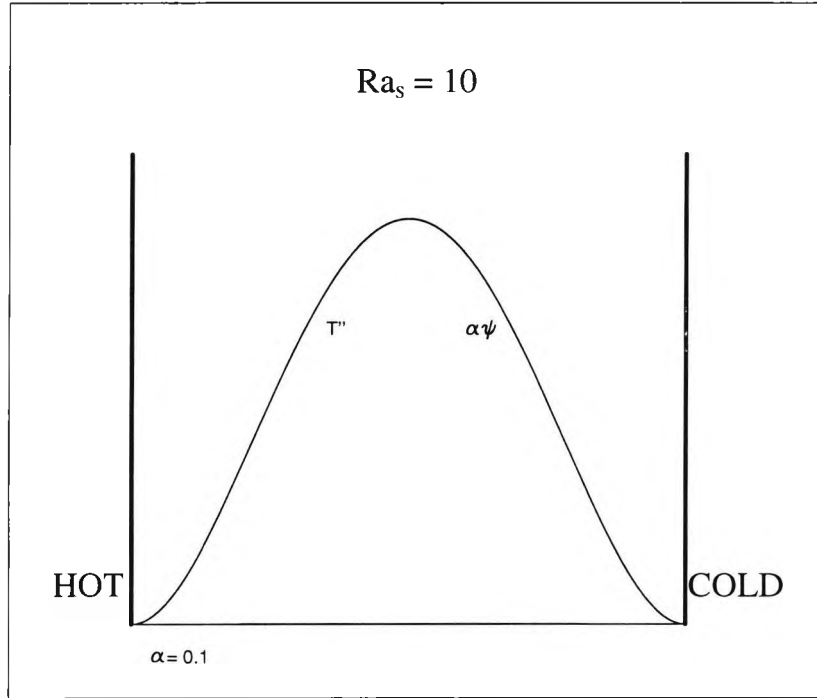


Figure 5.9: The modulus of the important temperature terms are shown across the two walls in the small α regime.

to (2.10.4). We first look at the magnitude of each term in the governing equations using the scaling as defined above. Each term in the equations of ψ , T and S is then expressed in powers of α as shown:

$$\begin{array}{cccccc}
 D^4\psi & - & 2\alpha^2 D^2\psi & + & \alpha^4\psi & - & \frac{i\alpha}{Pr}\overline{w}_o D^2\psi & + & \frac{i\alpha^3}{Pr}\overline{w}_o\psi \\
 \vdots & & \vdots & & \vdots & & \vdots & & \vdots \\
 O(\alpha^0) & & O(\alpha^2) & & O(\alpha^4) & & O(\alpha^1) & & O(\alpha^3) \\
 & & & & & & & & \\
 & + & \frac{i\alpha}{Pr}D^2\overline{w}_o\psi & - & Ra_T DT & + & Ra_S DS & = & 0, \\
 & & \vdots & & \vdots & & \vdots & & \\
 & & O(\alpha^1) & & O(\alpha^a) & & O(\alpha^b) & & (5.2.2)
 \end{array}$$

$$\begin{array}{cccccc}
 D^2T & - & \alpha^2 T & + & i\alpha\psi & - & i\alpha\overline{w}_o T & = & 0, \\
 \vdots & & \vdots & & \vdots & & \vdots & & \\
 O(\alpha^a) & & O(\alpha^{2+a}) & & O(\alpha^1) & & O(\alpha^{1+a}) & & (5.2.3)
 \end{array}$$

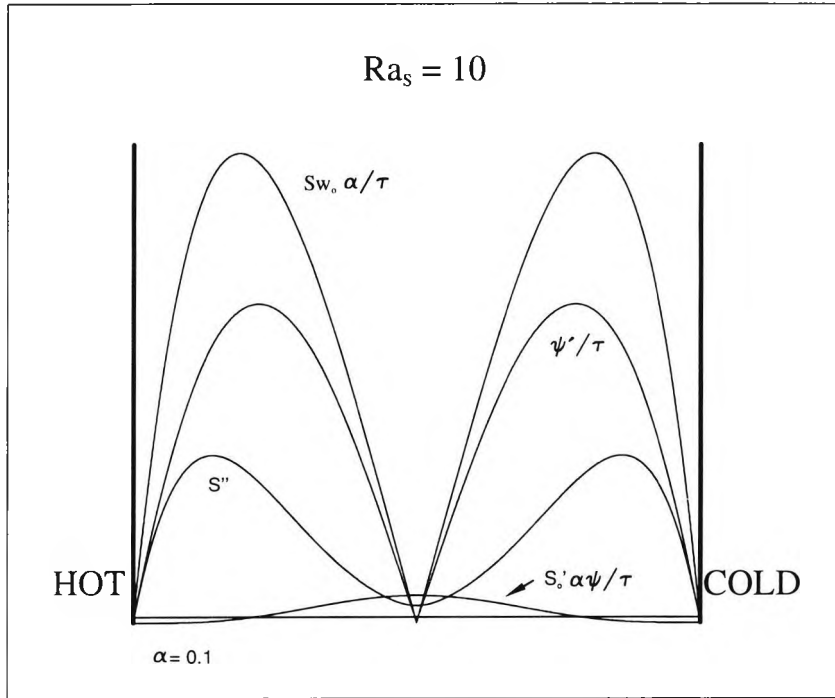


Figure 5.10: The modulus of the dominant salinity terms across the slot are shown in the graph for the case of small α .

and

$$\begin{array}{cccccc}
 \tau D^2 S & - & \tau \alpha^2 S & - & i \alpha D \bar{S}_o \psi & - & i \alpha \bar{w}_o S & - & D \psi & = & 0. \\
 \vdots & & \\
 O(\alpha^b) & & O(\alpha^{2+b}) & & O(\alpha^1) & & O(\alpha^{1+b}) & & O(\alpha^0) & &
 \end{array} \quad (5.2.4)$$

If terms clearly not of leading order are eliminated, we obtain the remaining terms for ψ , T and S with orders

$$\begin{array}{ccc}
 D^4 \psi & - & Ra_T DT & + & Ra_S DS & = & 0, \\
 \vdots & & \vdots & & \vdots & & \\
 O(\alpha^0) & & O(\alpha^a) & & O(\alpha^b) & &
 \end{array} \quad (5.2.5)$$

$$\begin{array}{ccc}
 D^2 T & + & i \alpha \psi & = & 0, \\
 \vdots & & \vdots & & \\
 O(\alpha^a) & & O(\alpha^1) & &
 \end{array} \quad (5.2.6)$$

Here we shall pose an expansion for

$$\begin{aligned}\psi &= \psi_0 + \alpha \psi_1 + \dots, \\ S &= \alpha^{-1} S_{-1} + S_0 + \alpha S_1 + \dots,\end{aligned}\tag{5.2.12}$$

with S_{-1} a constant. We use the boundary condition $\psi''(-1/2) = 1$ to define the scale of the perturbations therefore the leading order term, ψ_0 , is of order one. The leading order problem satisfies the following equations:

$$\begin{aligned}D^4\psi_0 + Ra_S DS_0 &= 0, \\ \tau D^2 S_0 - i\bar{w}_o S_{-1} - D\psi_0 &= 0.\end{aligned}\tag{5.2.13}$$

The first equation is differentiated once and is used to eliminate S_0 from the second. The subsequent ordinary differential equation (ODE) for ψ_0 is

$$D^5\psi_0 + \frac{Ra_S}{\tau} D\psi_0 + i\frac{Ra_S}{\tau} \bar{w}_o S_{-1} = 0.\tag{5.2.14}$$

This inhomogeneous ODE is solved by obtaining its complementary and particular solutions. We know ψ_0 is an even function and therefore any odd terms in the solution are eliminated such that ψ_0 is the combination of

$$\begin{aligned}\psi_{0_{CF}} &= A' + B' \cosh Mx \cos Mx + C' \sinh Mx \sin Mx, \\ \text{and } \psi_{0_{PI}} &= D' x \sinh Mx \cos Mx + E' x \cosh Mx \sin Mx.\end{aligned}\tag{5.2.15}$$

The corresponding boundary conditions $\psi_0 = D\psi_0 = D^4\psi_0 = 0$ on $x = \pm 1/2$ are used to determine A', B', C', D' and E' in the solution, ψ_0 . The technique in solving ψ_0 is given in Appendix C. For the benefit of simplification in the work to follow we write the solution of ψ_0 in the following way:

$$\psi_0 = i S_{-1} Ra_T \left\{ \begin{array}{l} A + B \cosh Mx \cos Mx + C \sinh Mx \sin Mx \\ + D x \sinh Mx \cos Mx + E x \cosh Mx \sin Mx. \end{array} \right\}\tag{5.2.16}$$

where

$$A = \frac{-1}{4M^4},$$

$$\begin{aligned}
B &= \frac{4(\sinh M + \sin M)^2 - \sinh \frac{M}{2} \sin \frac{M}{2} C_1}{16M^4(\sinh M + \sin M)^2 \cosh \frac{M}{2} \cos \frac{M}{2}}, \\
C &= \frac{C_1}{16M^4(\sinh M + \sin M)^2}, \\
C_1 &= 8 \cos \frac{M}{2} \cosh \frac{M}{2} - 4 \cos \frac{3M}{2} \cosh \frac{M}{2} \\
&\quad + 4 \sin \frac{M}{2} \sinh \frac{3M}{2} - 4 \sin \frac{3M}{2} \sinh \frac{M}{2} \\
&\quad - 4 \cos \frac{M}{2} \cosh \frac{3M}{2} - M \cos \frac{M}{2} \sinh \frac{3M}{2} \\
&\quad - M \cos \frac{M}{2} \sinh \frac{M}{2} + M \sin \frac{3M}{2} \cosh \frac{M}{2} \\
&\quad + M \sin \frac{M}{2} \cosh \frac{M}{2}, \\
D &= \frac{-\sin \frac{M}{2} \cosh \frac{M}{2}}{4M^3(\sinh M + \sin M)}, \\
E &= \frac{\sinh \frac{M}{2} \cos \frac{M}{2}}{4M^3(\sinh M + \sin M)}. \tag{5.2.17}
\end{aligned}$$

This solution for ψ_0 becomes useful when we integrate the full salinity equation across the slot. We shall recall the full salinity equation which is

$$\tau D^2 S - \tau \alpha^2 S - i\alpha D \overline{S}_o \psi - i\alpha \overline{w}_o S - D\psi = 0. \tag{5.2.18}$$

The integration across the slot for each term gives

$$\begin{aligned}
\int_{-\frac{1}{2}}^{\frac{1}{2}} \tau D^2 S dx &= \int_{-\frac{1}{2}}^{\frac{1}{2}} \tau (D^2 S_0 + \alpha D^2 S_1 + \dots) dx \\
&= \tau [DS_0 + \alpha DS_1 + \dots]_{-\frac{1}{2}}^{\frac{1}{2}} = 0 \quad \text{at all orders,} \tag{5.2.19}
\end{aligned}$$

$$\begin{aligned}
\int_{-\frac{1}{2}}^{\frac{1}{2}} \tau \alpha^2 S dx &= \int_{-\frac{1}{2}}^{\frac{1}{2}} \tau \alpha^2 (\alpha^{-1} S_{-1} + S_0 + \alpha S_1 + \dots) dx \\
&= \tau \alpha S_{-1} + O(\alpha^2), \tag{5.2.20}
\end{aligned}$$

$$\int_{-\frac{1}{2}}^{\frac{1}{2}} i\alpha D \overline{S}_o \psi dx = \int_{-\frac{1}{2}}^{\frac{1}{2}} i\alpha D \overline{S}_o \psi_0 dx + O(\alpha^2), \tag{5.2.21}$$

$$\begin{aligned}
\int_{-\frac{1}{2}}^{\frac{1}{2}} i \alpha \overline{w}_o S dx &= \int_{-\frac{1}{2}}^{\frac{1}{2}} i \overline{w}_o S_{-1} dx + \int_{-\frac{1}{2}}^{\frac{1}{2}} i \alpha \overline{w}_o S_0 dx + O(\alpha^2) \\
&= \int_{-\frac{1}{2}}^{\frac{1}{2}} i S_{-1} (-\tau D^2 \overline{S}_o) dx + \int_{-\frac{1}{2}}^{\frac{1}{2}} i \alpha \overline{w}_o S_0 dx + O(\alpha^2) \\
&= i \alpha \int_{-\frac{1}{2}}^{\frac{1}{2}} \overline{w}_o S_0 dx + O(\alpha^2), \tag{5.2.22}
\end{aligned}$$

$$\int_{-\frac{1}{2}}^{\frac{1}{2}} D\psi dx = [\psi_0 + \alpha \psi_1 + \dots]_{-\frac{1}{2}}^{\frac{1}{2}} = 0 \quad \text{at all orders.} \tag{5.2.23}$$

From the above terms we get contributions in

$$-\tau \alpha S_{-1} - i \alpha \int_{-\frac{1}{2}}^{\frac{1}{2}} D\overline{S}_o \psi_0 dx - i \alpha \int_{-\frac{1}{2}}^{\frac{1}{2}} \overline{w}_o S_0 dx + O(\alpha^2) = 0. \tag{5.2.24}$$

The leading order terms give

$$\begin{aligned}
&\tau \alpha S_{-1} + i \alpha \int_{-\frac{1}{2}}^{\frac{1}{2}} D\overline{S}_o \psi_0 dx + i \alpha \int_{-\frac{1}{2}}^{\frac{1}{2}} \overline{w}_o S_0 dx \\
&= \tau \alpha S_{-1} + \frac{\alpha S_{-1} Ra_T^2 f(Ra_S, \tau)}{4 \tau M^4} \\
&\quad + \frac{\alpha S_{-1} Ra_T^2 g(Ra_S, \tau)}{Ra_S M^3 (\sinh M + \sin M)} = 0, \tag{5.2.25}
\end{aligned}$$

where $f(Ra_S, \tau)$ and $g(Ra_S, \tau)$ are the expressions found from the two integrals respectively. With further reduction, an expression for Ra_T describing marginal stability is obtained:

$$Ra_T^2 = \frac{-\tau^2}{\frac{f}{4M^4} + \frac{g}{4M^7(\sinh M + \sin M)}}, \tag{5.2.26}$$

where both functions of f and g are governed by the salt Rayleigh number and the Lewis number, but they only appear in the combination $Ra_S/\tau = 4M^4$.

The derivation of f and g is included in Appendix C. With A , B , C , D and E from (5.2.17), the full version found for function f is

$$\begin{aligned}
f(Ra_S, \tau) &= A + B \left(\frac{\cosh \frac{M}{2} \sin \frac{M}{2} + \sinh \frac{M}{2} \cos \frac{M}{2}}{M} \right) \\
&+ C \left(\frac{\cosh \frac{M}{2} \sin \frac{M}{2} - \sinh \frac{M}{2} \cos \frac{M}{2}}{M} \right)
\end{aligned}$$

$$\begin{aligned}
& + D \left(\frac{\cosh \frac{M}{2} \cos \frac{M}{2} + \sinh \frac{M}{2} \sin \frac{M}{2}}{2M} - \frac{\cosh \frac{M}{2} \sin \frac{M}{2}}{M^2} \right) \\
& + E \left(\frac{-\cosh \frac{M}{2} \cos \frac{M}{2} + \sinh \frac{M}{2} \sin \frac{M}{2}}{2M} + \frac{\sinh \frac{M}{2} \cos \frac{M}{2}}{M^2} \right) \\
& - \frac{2 \sin \frac{M}{2} \cosh \frac{M}{2}}{\sinh M + \sin M} A \left(\frac{\cosh \frac{M}{2} \sin \frac{M}{2} - \sinh \frac{M}{2} \cos \frac{M}{2}}{M} \right) \\
& - \frac{2 \sin \frac{M}{2} \cosh \frac{M}{2}}{\sinh M + \sin M} B \left(\frac{\cosh M \sin M - \sinh M \cos M}{8M} \right) \\
& - \frac{2 \sin \frac{M}{2} \cosh \frac{M}{2}}{\sinh M + \sin M} C \left(-\frac{\cosh M \sin M}{8M} - \frac{\sinh M \cos M}{8M} + \frac{\sinh M}{4M} \right. \\
& \qquad \qquad \qquad \left. - \frac{1}{4} + \frac{\sin M}{4M} \right) \\
& - \frac{2 \sin \frac{M}{2} \cosh \frac{M}{2}}{\sinh M + \sin M} D \left(\frac{\sinh M \sin M - \cosh M \cos M}{16M} + \frac{\sinh M \cos M}{16M^2} \right. \\
& \qquad \qquad \qquad \left. - \frac{\sin^2 \frac{M}{2}}{4M} + \frac{1}{8M} - \frac{\sin M}{8M^2} \right) \\
& - \frac{2 \sin \frac{M}{2} \cosh \frac{M}{2}}{\sinh M + \sin M} E \left(-\frac{\cosh M \cos M - 2 \cosh M + \sinh M \sin M}{16M} \right. \\
& \qquad \qquad \qquad \left. + \frac{\cosh M \sin M - 2 \sinh M}{16M^2} \right) \\
& - \frac{2 \sin \frac{M}{2} \cosh \frac{M}{2}}{\sinh M + \sin M} A \left(\frac{\cosh \frac{M}{2} \sin \frac{M}{2} + \sinh \frac{M}{2} \cos \frac{M}{2}}{M} \right) \\
& - \frac{2 \sin \frac{M}{2} \cosh \frac{M}{2}}{\sinh M + \sin M} B \left(\frac{\cosh M \sin M + \sinh M \cos M + 2 \sinh M}{8M} \right. \\
& \qquad \qquad \qquad \left. + \frac{\sin M}{4M} + \frac{1}{4} \right) \\
& - \frac{2 \sin \frac{M}{2} \cosh \frac{M}{2}}{\sinh M + \sin M} C \left(\frac{\cosh M \sin M - \sinh M \cos M}{8M} \right) \\
& - \frac{2 \sin \frac{M}{2} \cosh \frac{M}{2}}{\sinh M + \sin M} D \left(\frac{\cosh M \cos M + 2 \cosh M + \sinh M \sin M}{16M} \right. \\
& \qquad \qquad \qquad \left. - \frac{\cosh M \sin M + 2 \sinh M}{16M^2} \right)
\end{aligned}$$

$$\begin{aligned}
& - \frac{2 \sin \frac{M}{2} \cosh \frac{M}{2}}{\sinh M + \sin M} E \left(\frac{\sinh M \sin M - \cosh M \cos M}{16M} + \frac{\sinh M \cos M}{16M^2} \right. \\
& \qquad \qquad \qquad \left. + \frac{\sin^2 \frac{M}{2}}{4M} - \frac{1}{8M} + \frac{\sin M}{8M^2} \right) \\
& - \frac{2 \sinh \frac{M}{2} \cos \frac{M}{2}}{\sinh M + \sin M} A \left(\frac{\cosh \frac{M}{2} \sin \frac{M}{2} + \sinh \frac{M}{2} \cos \frac{M}{2}}{M} \right) \\
& - \frac{2 \sinh \frac{M}{2} \cos \frac{M}{2}}{\sinh M + \sin M} B \left(\frac{\cosh M \sin M + \sinh M \cos M + 2 \sinh M}{8M} \right. \\
& \qquad \qquad \qquad \left. + \frac{\sin M}{4M} + \frac{1}{4} \right) \\
& - \frac{2 \sinh \frac{M}{2} \cos \frac{M}{2}}{\sinh M + \sin M} C \left(\frac{\cosh M \sin M - \sinh M \cos M}{8M} \right) \\
& - \frac{2 \sinh \frac{M}{2} \cos \frac{M}{2}}{\sinh M + \sin M} D \left(\frac{\cosh M \cos M + 2 \cosh M + \sinh M \sin M}{16M} \right. \\
& \qquad \qquad \qquad \left. - \frac{\cosh M \sin M + 2 \sinh M}{16M^2} \right) \\
& - \frac{2 \sinh \frac{M}{2} \cos \frac{M}{2}}{\sinh M + \sin M} E \left(\frac{\sinh M \sin M - \cosh M \cos M}{16M} + \frac{\sinh M \cos M}{16M^2} \right. \\
& \qquad \qquad \qquad \left. + \frac{\sin^2 \frac{M}{2}}{4M} - \frac{1}{8M} + \frac{\sin M}{8M^2} \right) \\
& + \frac{2 \sinh \frac{M}{2} \cos \frac{M}{2}}{\sinh M + \sin M} A \left(\frac{\cosh \frac{M}{2} \sin \frac{M}{2} - \sinh \frac{M}{2} \cos \frac{M}{2}}{M} \right) \\
& + \frac{2 \sinh \frac{M}{2} \cos \frac{M}{2}}{\sinh M + \sin M} B \left(\frac{\cosh M \sin M - \sinh M \cos M}{8M} \right) \\
& + \frac{2 \sinh \frac{M}{2} \cos \frac{M}{2}}{\sinh M + \sin M} C \left(-\frac{\cosh M \sin M}{8M} - \frac{\sinh M \cos M}{8M} + \frac{\sinh M}{4M} \right. \\
& \qquad \qquad \qquad \left. - \frac{1}{4} + \frac{\sin M}{4M} \right) \\
& + \frac{2 \sinh \frac{M}{2} \cos \frac{M}{2}}{\sinh M + \sin M} D \left(\frac{\sinh M \sin M - \cosh M \cos M}{16M} + \frac{\sinh M \cos M}{16M^2} \right. \\
& \qquad \qquad \qquad \left. - \frac{\sin^2 \frac{M}{2}}{4M} + \frac{1}{8M} - \frac{\sin M}{8M^2} \right) \\
& + \frac{2 \sinh \frac{M}{2} \cos \frac{M}{2}}{\sinh M + \sin M} E \left(-\frac{\cosh M \cos M - 2 \cosh M + \sinh M \sin M}{16M} \right)
\end{aligned}$$

$$\begin{aligned}
& + \frac{\sin^2 \frac{M}{2}}{4M} - \frac{1}{8M} + \frac{\sin M}{8M^2} \\
- \sinh \frac{M}{2} \cosh \frac{M}{2} 2EM^3 & \left(-\frac{\cosh M \cos M - 2 \cosh M + \sinh M \sin M}{16M} \right. \\
& \left. + \frac{\cosh M \sin M - 2 \sinh M}{16M^2} \right) \\
+ \sin \frac{M}{2} \cosh \frac{M}{2} 2BM^3 & \left(\frac{\cosh M \sin M - \sinh M \cos M}{8M} \right) \\
+ \sin \frac{M}{2} \cosh \frac{M}{2} 2BM^3 & \left(\frac{\sinh M \cos M + \cosh M \sin M + 2 \sinh M}{8M} \right. \\
& \left. - \frac{1}{4} - \frac{\sin M}{4M} \right) \\
- \sin \frac{M}{2} \cosh \frac{M}{2} 2CM^3 & \left(\frac{\sinh M \cos M + \cosh M \sin M + 2 \sinh M}{8M} \right. \\
& \left. - \frac{1}{4} - \frac{\sin M}{4M} \right) \\
+ \sin \frac{M}{2} \cosh \frac{M}{2} 2CM^3 & \left(\frac{\cosh M \sin M - \sinh M \cos M}{8M} \right) \\
+ \sin \frac{M}{2} \cosh \frac{M}{2} 6DM^2 & \left(\frac{\cosh M \sin M - \sinh M \cos M}{8M} \right) \\
+ \sin \frac{M}{2} \cosh \frac{M}{2} 2DM^3 & \left(\frac{\sinh M \sin M - \cosh M \cos M}{16M} + \frac{\sinh M \cos M}{16M^2} \right. \\
& \left. - \frac{\sin^2 \frac{M}{2}}{4M} + \frac{1}{8M} - \frac{\sin M}{8M^2} \right) \\
+ \sin \frac{M}{2} \cosh \frac{M}{2} 2DM^3 & \left(\frac{\cosh M \cos M + 2 \cosh M + \sinh M \sin M}{16M} \right. \\
& \left. - \frac{\cosh M \sin M + 2 \sinh M}{16M^2} \right) \\
- \sin \frac{M}{2} \cosh \frac{M}{2} 6EM^2 & \left(\frac{\sinh M \cos M + \cosh M \sin M + 2 \sinh M}{8M} \right. \\
& \left. - \frac{1}{4} - \frac{\sin M}{4M} \right) \\
- \sin \frac{M}{2} \cosh \frac{M}{2} 2EM^3 & \left(\frac{\cosh M \cos M + 2 \cosh M + \sinh M \sin M}{16M} \right)
\end{aligned}$$

$$\begin{aligned}
& - \frac{\cosh M \sin M + 2 \sinh M}{16M^2} \\
+ \sin \frac{M}{2} \cosh \frac{M}{2} 2EM^3 & \left(\frac{\sinh M \sin M - \cosh M \cos M}{16M} + \frac{\sinh M \cos M}{16M^2} \right. \\
& \left. - \frac{\sin^2 \frac{M}{2}}{4M} + \frac{1}{8M} - \frac{\sin M}{8M^2} \right).
\end{aligned} \tag{5.2.28}$$

From the expression (5.2.26), the minimum value of Ra_T/τ and the corresponding value of Ra_S can be found. This gives the location of the minimum in the small α limit to be

$$\begin{aligned}
Ra_T/\tau &= 3137.9, \\
Ra_S &= 1001.6\tau
\end{aligned} \tag{5.2.29}$$

This minimum point also corresponds to $M = 3.9779$.

We can compare these theoretical results of (5.2.29) with minima calculated from the full problem using the Runge-Kutta scheme of chapter 3 for a range of τ . These results for the full problem are shown in table 5.1. Both results in the limit of small α from the two independent methods indicate an exceptionally good agreement which are accurate to five significant places.

τ	Ra_{S_m}	Ra_{T_m}
0.1	100.16	313.79
0.01	10.016	31.379
0.001	1.0016	3.1379
0.0001	0.10016	0.31379
0.00001	0.010016	0.031379
0.000001	0.0010016	0.0031379

Table 5.1: The minimum values of Ra_T and Ra_S obtained for the full problem for different values of τ , using the Runge-Kutta scheme.

However, to the left of the stability boundary of the reduced model in figure 5.7, a vertical asymptote can be found in the limit of $Ra_T \rightarrow \infty$. This is determined by the theoretical expression of (5.2.26) written in terms of τ and the function H , i.e.

$$Ra_T = \tau H(M), \quad (5.2.30)$$

where H depends just on $M = \sqrt[4]{Ra_S/4\tau}$. The function $H(M)$ is given by

$$H(M) = \left[\frac{-4M^7(\sin M + \sinh M)}{fM^3(\sin M + \sinh M) + g} \right]^{\frac{1}{2}}. \quad (5.2.31)$$

We then set the denominator of (5.2.31) to zero and find numerically that the asymptote with $Ra_T \rightarrow \infty$ in this small α limit occurs at

$$M = 3.3460, \quad (5.2.32)$$

which translates to

$$Ra_S = 501.36\tau. \quad (5.2.33)$$

This value of Ra_S gives an upper bound to the vertical part of the stability curve on the left hand side for the full problem. The reason is that the vertical asymptote found here must lie to the right of the true full instability boundary. The solutions found here are marginally stable, and so cannot lie in the region of stability. This also contradicts the result of Thangam *et al.* who found a vertical instability boundary near $Ra_S = 10$. We will return to this value of Ra_S when discussing the vertical portion of the stability curve for the full problem in the following section.

The stability curves from the full model and the small α asymptotic of the reduced model show good agreement around the bottom of the curve in figure 5.7. It is clear from the analysis that only the interaction between the salinity concentration and the stream function play a role in the leading

order dynamics in this limit of small α and the temperature perturbation plays an insignificant role in this regime. The temperature is important only to establish the background salinity and velocity fields. This minor role in temperature is not due to a large difference in the diffusivities of salt and heat as this has not been mentioned in the analysis. The salinity no-flux boundary conditions allow large concentrations of salt to build up which are uniform across the slot. Therefore these concentration perturbations can only decay by diffusion in the vertical direction with a long time scale. Since the temperature perturbation is zero at the walls the time scale for its dissipation is essentially the diffusion time across the slot width. This is a much faster scale than the diffusion time for salinity. Alternatively, if different boundary conditions were imposed on the salinity, its concentration would vary across the slot at the leading order and so it would diffuse on a time scale based on the slot width. This gives a much shorter time scale and would significantly alter the above analysis.

5.3 Large Ra_T

The asymptotic in the limit of large thermal Rayleigh number corresponding to regime 3 in figure 5.1 will be examined in this section. A comparison between the asymptotic results and the full numerical solutions for this vertical boundary is shown in figure 5.11. These results are clearly to the left of the vertical boundary of the stability regime of Thangam, Zebib & Chen (1981) in figure 3.6. The full results indicate that this stability boundary continues a long distance upwards into the unstable regime as a local minimum in $\alpha-Ra_S$ plots.

In this regime with Ra_T increasing, the salt Rayleigh number is approximately constant and of order one while the vertical wave number is non-zero

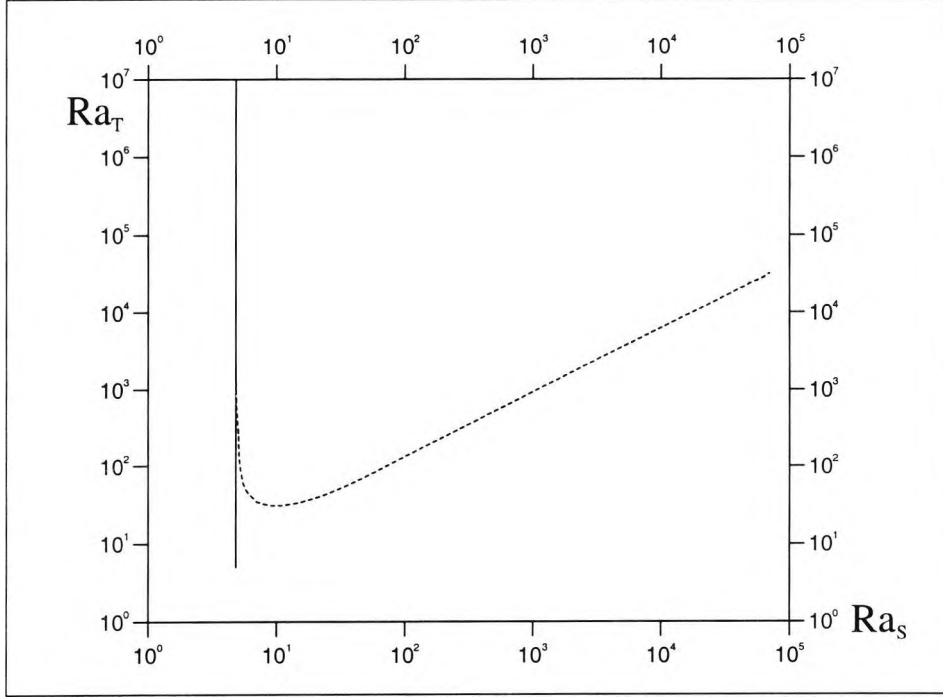


Figure 5.11: In the $Ra_T \gg 1$ limit of region 3, good agreement is found between the full and reduced results. Dashed line for the full model and solid for the asymptotic result.

and decays as Ra_T^{-1} . The leading order behaviour of this regime can be found by examining the balances in the full problem. With the choice of scaling for $\alpha = O(Ra_T^a)$, $\psi = O(1)$, $T = O(Ra_T^b)$, $S = O(Ra_T^c)$, $M = O(1)$, $\overline{w}_o = O(Ra_T)$, $\overline{T}_o = O(1)$ and $D\overline{S}_o = O(Ra_T)$, the full problem of (2.10.2) to (2.10.4) has terms of the following order in Ra_T :

$$\begin{aligned}
 & \begin{array}{cccccc}
 D^4\psi & - & 2\alpha^2 D^2\psi & + & \alpha^4\psi & - & \frac{i\alpha}{Pr}\overline{w}_o D^2\psi & + & \frac{i\alpha^3}{Pr}\overline{w}_o\psi \\
 \vdots & & \vdots & & \vdots & & \vdots & & \vdots \\
 O(Ra_T^0) & & O(Ra_T^{2a}) & & O(Ra_T^{4a}) & & O(Ra_T^{a+1}) & & O(Ra_T^{3a+1})
 \end{array} \\
 & + \frac{i\alpha}{Pr} D^2\overline{w}_o\psi - Ra_T DT + Ra_S DS = 0, \\
 & \begin{array}{ccc}
 \vdots & \vdots & \vdots \\
 O(Ra_T^{a+1}) & O(Ra_T^{1+b}) & O(Ra_T^c)
 \end{array} \tag{5.3.1}
 \end{aligned}$$

$$\begin{aligned}
 & \begin{array}{cccccc}
 D^2T & - & \alpha^2 T & + & i\alpha\psi & - & i\alpha\overline{w}_o T & = & 0, \\
 \vdots & & \vdots & & \vdots & & \vdots & & \\
 O(Ra_T^b) & & O(Ra_T^{2a+b}) & & O(Ra_T^a) & & O(Ra_T^{a+1+b}) & &
 \end{array} \tag{5.3.2}
 \end{aligned}$$

and

$$\begin{array}{cccccc}
\tau D^2 S & - & \tau \alpha^2 S & - & i\alpha D \overline{S}_o \psi & - & i\alpha \overline{w}_o S & - & D\psi & = & 0, \\
\vdots & & \\
O(Ra_T^c) & & O(Ra_T^{2a+c}) & & O(Ra_T^{a+1}) & & O(Ra_T^{1+a+c}) & & O(Ra_T^0) & &
\end{array} \tag{5.3.3}$$

where a , b and c are to be determined. We need to look at all possible balances in the above equations and see if the paired terms (or powers) are the leading order terms. By examining a from (5.3.1) to (5.3.3) we hope to find a suitable scaling to represent the reduced model for this large Ra_T regime.

First consider the case $a > 0$. The possible dominant terms are

$$\begin{array}{cccccc}
\alpha^4 \psi & + & \frac{i\alpha^3}{Pr} \overline{w}_o \psi & - & Ra_T DT & + & Ra_S DS & = & 0, \\
\vdots & & \vdots & & \vdots & & \vdots & & \\
O(Ra_T^{4a}) & & O(Ra_T^{1+3a}) & & O(Ra_T^{1+b}) & & O(Ra_T^c) & &
\end{array} \tag{5.3.4}$$

$$\begin{array}{cccccc}
-\alpha^2 T & + & i\alpha \psi & - & i\alpha \overline{w}_o T & = & 0, \\
\vdots & & \vdots & & \vdots & & \\
O(Ra_T^{b+2a}) & & O(Ra_T^a) & & O(Ra_T^{1+a+b}) & &
\end{array} \tag{5.3.5}$$

and

$$\begin{array}{cccccc}
-\tau \alpha^2 S & - & i\alpha D \overline{S}_o \psi & - & i\alpha \overline{w}_o S & = & 0. \\
\vdots & & \vdots & & \vdots & & \\
O(Ra_T^{c+2a}) & & O(Ra_T^{1+a}) & & O(Ra_T^{1+a+c}) & &
\end{array} \tag{5.3.6}$$

We will look at 3 combinations of the possible leading order balances in the salinity equation of (5.3.6). We first assume $1 + a = 1 + a + c$ is the leading order balance; then this gives $c = 0$. The next paired terms in the salinity give $c + 2a \leq 1 + a + c$ and so $a \leq 1$. If this condition with $c = 0$ and $a \leq 1$ is assumed in the stream function of (5.3.4) then this means $4a \leq 1 + 3a$ and so the leading order balance in ψ is $1 + 3a = 1 + b > 0$. Now the temperature

equation in (5.3.5) is divided by α which must be non-zero (otherwise solutions to the full perturbation equations do not exist). This gives

$$\begin{array}{rcccc} -\alpha T & + & i\psi & - & i\overline{w}_o T & = & 0, \\ \vdots & & \vdots & & \vdots & & \\ O(Ra_T^{b+a}) & & O(Ra_T^0) & & O(Ra_T^{1+b}) & & \end{array} \quad (5.3.7)$$

and the leading order balance in T is then $b + a = 1 + b$. Therefore this condition gives $a = 1$ and thereafter $b = 3a = 3$ while $c = 0$ as a potential scaling.

The second combination of the salinity terms to be balanced from (5.3.6) is $c + 2a = 1 + a$, indicating $c + a = 1$. Given that we have assumed $1 + a \geq 1 + a + c$ we see $c \leq 0$. Similarly $a \geq 1$ is given by $c + 2a \geq 1 + a + c$. With $c \leq 0$ and $a \geq 1$ in the stream function of (5.3.4), this means $4a \geq 1 + 3a$ and so the leading order balance in ψ gives $4a = 1 + b$ (> 0). If $4a = 1 + b$ is used in conjunction with the leading order balance in T from (5.3.7) to be $b + a = b + 1$, then the result is again $a = 1$, $b = 3$ and $c = 0$.

Finally, the last combination in (5.3.6) to be balanced is $c + 2a = 1 + a + c$. So $a = 1$ and then $c \leq 0$. This will mean the stream function has the leading order balance $4 = 1 + b > 0$ and this agrees with the balance for T in (5.3.7) to be $1 + b > 0$.

If the above scaling with powers $a = 1$, $b = 3$ and $c = 0$ is used for the asymptotic behaviour in this regime where $Ra_T \rightarrow \infty$ then $\alpha = O(Ra_T)$ and $T = O(Ra_T^3)$ so the temperature equation (5.3.7) reduces to

$$-\alpha T - i\overline{w}_o T = -T(\alpha + i\overline{w}_o) = 0. \quad (5.3.8)$$

This will have a solution if $T = 0$ since we know we only have solutions for $\alpha \neq 0$. Therefore this scaling fails and so a is not greater than 0.

With $a = 0$, the possible important terms are

$$\begin{array}{ccccc}
D^4\psi & - & 2\alpha^2 D^2\psi & + & \alpha^4\psi & - & \frac{i\alpha}{Pr}\overline{w}_o D^2\psi & + & \frac{i\alpha^3}{Pr}\overline{w}_o\psi \\
\vdots & & \vdots & & \vdots & & \vdots & & \vdots \\
O(Ra_T^0) & & O(Ra_T^0) & & O(Ra_T^0) & & O(Ra_T^1) & & O(Ra_T^1) \\
& & + & \frac{i\alpha}{Pr}D^2\overline{w}_o\psi & - & Ra_T DT & + & Ra_S DS & = 0, \\
& & \vdots & & \vdots & & \vdots & & \\
& & O(Ra_T^1) & & O(Ra_T^{1+b}) & & O(Ra_T^c) & &
\end{array} \tag{5.3.9}$$

$$\begin{array}{ccccccc}
D^2T & - & \alpha^2 T & + & i\alpha\psi & - & i\alpha\overline{w}_o T & = 0, \\
\vdots & & \vdots & & \vdots & & \vdots & \\
O(Ra_T^b) & & O(Ra_T^b) & & O(Ra_T^0) & & O(Ra_T^{1+b}) &
\end{array} \tag{5.3.10}$$

and

$$\begin{array}{ccccccccc}
\tau D^2 S & - & \tau \alpha^2 S & - & i\alpha D \overline{S}_o \psi & - & i\alpha \overline{w}_o S & - & D\psi & = 0. \\
\vdots & & \vdots & & \vdots & & \vdots & & \vdots & \\
O(Ra_T^c) & & O(Ra_T^c) & & O(Ra_T^1) & & O(Ra_T^{1+c}) & & O(Ra_T^0) &
\end{array} \tag{5.3.11}$$

It is easy to see from equation (5.3.11) that since $c < 1 + c$ then the leading order balance $1 = 1 + c$ in the S equation gives $c = 0$. If $c = 0$ is used in (5.3.9) for the stream function then $1 = 1 + b$ gives $b = 0$. With $b = 0$, there is no possible balance for which the temperature equation in (5.3.10) is satisfied. Therefore the result $a = b = c = 0$ is clearly invalid in the present slot problem.

Now $a < 0$ is the last possible form for the reduced model giving

$$\begin{array}{ccccccc}
D^4\psi & - & \frac{i\alpha}{Pr}\overline{w}_o D^2\psi & + & \frac{i\alpha}{Pr}D^2\overline{w}_o\psi & - & Ra_T DT & + & Ra_S DS & = 0, \\
\vdots & & \vdots & & \vdots & & \vdots & & \vdots & \\
O(Ra_T^0) & & O(Ra_T^{1+a}) & & O(Ra_T^{1+a}) & & O(Ra_T^{1+b}) & & O(Ra_T^c) &
\end{array} \tag{5.3.12}$$

$$\begin{array}{ccccccc}
D^2T & + & i\alpha\psi & - & i\alpha\overline{w}_oT & = & 0, \\
\vdots & & \vdots & & \vdots & & \\
O(Ra_T^b) & & O(Ra_T^a) & & O(Ra_T^{1+a+b}) & &
\end{array} \tag{5.3.13}$$

and

$$\begin{array}{ccccccc}
\tau D^2S & - & i\alpha D\overline{S}_o\psi & - & i\alpha\overline{w}_oS & - & D\psi & = & 0. \\
\vdots & & \vdots & & \vdots & & \vdots & & \\
O(Ra_T^c) & & O(Ra_T^{1+a}) & & O(Ra_T^{1+a+c}) & & O(Ra_T^0) & &
\end{array} \tag{5.3.14}$$

If the temperature equation in (5.3.13) is used assuming the balance $a = b$ then $a \geq 1 + a + b = 1 + 2a$ gives $a + 1 \leq 0$. Since $a + 1 \leq 0$ and $1 + a + c \leq c$ in (5.3.14), this gives the leading order balance in the S equation to be $c = 0$. As $a = 1 + a + b$ from the leading balance in (5.3.13) for the temperature terms, this yields $b = -1$. If the leading order balance in (5.3.12) for ψ is $0 = 1 + b$ then either $1 + a < 0$ giving $c = 0$, or $c < 0$ giving $1 + a = 0$ and so $a = -1$. This will give $a = -1$ and $c = 0$. Thus we have found the coefficients to be $a = -1$, $b = -1$ and $c = 0$ in order to give a suitable scaling for the reduced model in this regime:

$$\alpha = O(Ra_T^{-1}), \quad T = O(Ra_T^{-1}), \quad S = O(1) \quad \text{and} \quad \psi = O(1). \tag{5.3.15}$$

Profiles of the various terms in these governing equations in figures 5.12, 5.13 and 5.14 confirm the respective significant terms found in the equations for the stream function, temperature and salinity in (5.3.21) to (5.3.23) below. These curves can also be used as a means to determine the possible dominant terms found in this regime. The technique in plotting these curves across the slot has already been described in the previous section of large Ra_S asymptotic.

With the above scalings we can pose the large Ra_T expansion as:

$$\psi = \psi_0 + Ra_T^{-1}\psi_1 + \dots, \tag{5.3.16}$$

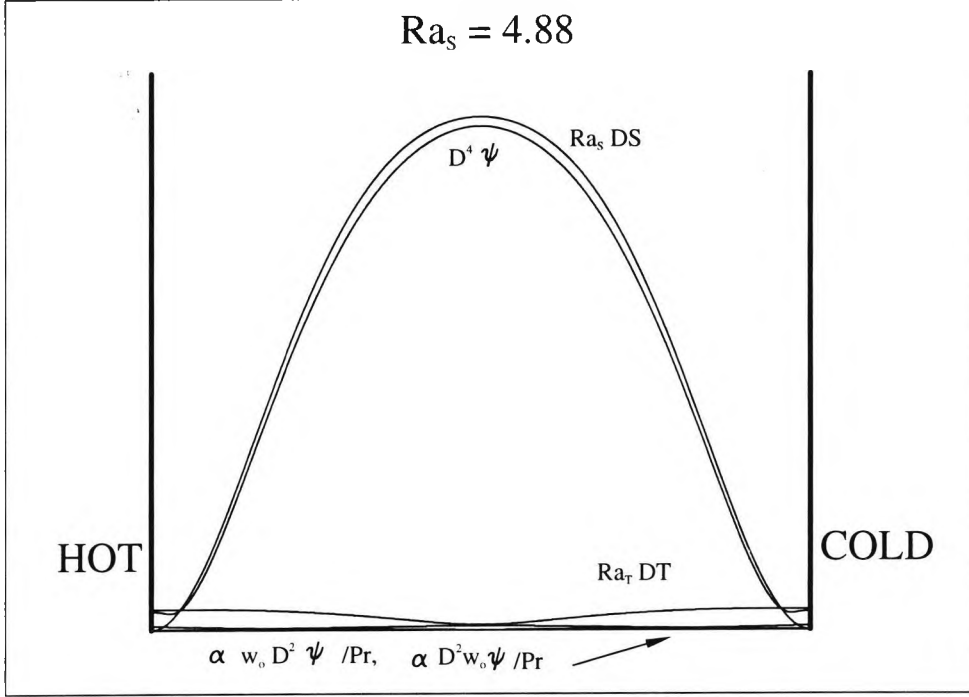


Figure 5.12: In region 3, these are the important terms found for the modulus of the stream function between the two walls in the limit of Ra_T is large.

$$T = Ra_T^{-1}T_0 + Ra_T^{-2}T_1 + \dots, \quad (5.3.17)$$

$$S = S_0 + Ra_T^{-1}S_1 + \dots, \quad (5.3.18)$$

and

$$Ra_S = Ra_{S_0} + Ra_T^{-1}Ra_{S_1} + \dots. \quad (5.3.19)$$

Noting that the background velocity and salinity gradient are proportional to Ra_T we express them as

$$\overline{w}_o = Ra_T \hat{w}_o, \quad D\overline{S}_o = Ra_T D\hat{S}_o / \tau. \quad (5.3.20)$$

Both \hat{w}_o and $D\hat{S}_o$ are dependent on x and $M = (Ra_S/4\tau)^{1/4}$ only. The vertical wave number is rescaled to give $\alpha = Ra_T^{-1}\hat{\alpha}$. This yields the system of leading order equations:

$$D^4\psi_0 - \frac{i\hat{\alpha}}{Pr} \left\{ \hat{w}_o D^2\psi_0 - D^2\hat{w}_o\psi_0 \right\} - DT_0 + Ra_{S_0}DS_0 = 0, \quad (5.3.21)$$

$$D^2T_0 + i\hat{\alpha}\psi_0 - i\hat{\alpha}\hat{w}_oT_0 = 0, \quad (5.3.22)$$

$$\tau D^2S_0 - i\hat{\alpha}D\hat{S}_o\psi_0/\tau - i\hat{\alpha}\hat{w}_oS_0 - D\psi_0 = 0, \quad (5.3.23)$$

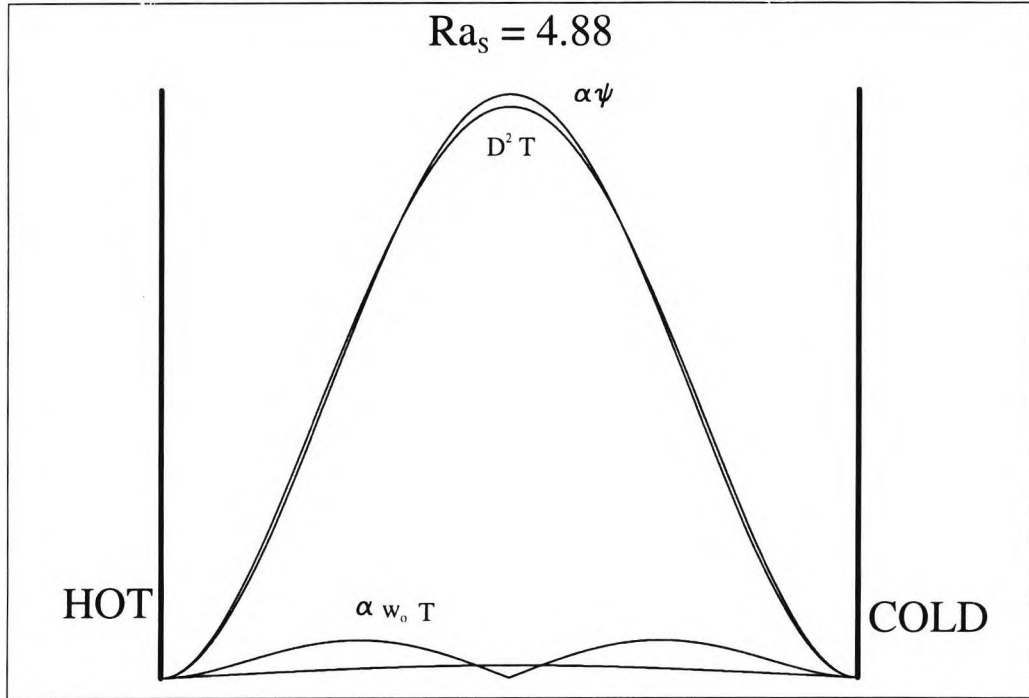


Figure 5.13: These are the modulus of the important temperature terms found in large Ra_T regime for the slot problem.

subject to boundary conditions

$$\psi_0 = D\psi_0 = T_0 = DS_0 = 0 \quad \text{on} \quad x = \pm 1/2. \quad (5.3.24)$$

This reduced model is similar to the full model except that Ra_T does not appear explicitly in these equations. These are solved using the Runge-Kutta scheme as previously used in the full problem. This gives the minimum value of Ra_{S_0} and the corresponding $\hat{\alpha}$. The minimum point was found to occur at

$$Ra_{S_0} = 4.7701, \quad \hat{\alpha} = 442.67. \quad (5.3.25)$$

The graph in figure 5.11 shows the solutions obtained for the full and reduced problems and the agreement is indeed good. The asymptotic results and the full numerical results agree as far down the vertical boundary as Ra_T reaching 3000 which can be seen in figure 5.15. The above scaling does not develop any singularity problems in these equations near this point as $Ra_T \rightarrow \infty$ and so the full problem was not too difficult to solve for large values of Ra_T .

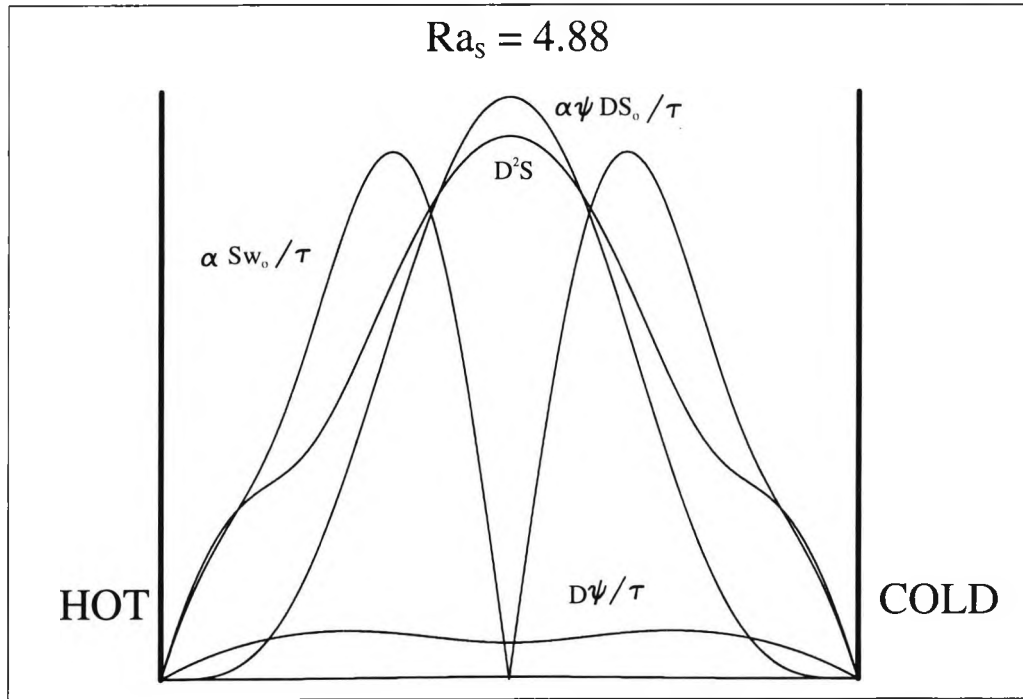


Figure 5.14: The modulus of the salinity terms found significant in the large Ra_T regime are shown from these curves plotted across the slot.

Unlike the previous two asymptotic regimes the dependency of Ra_{S_0} on Pr and τ is not clear. We can use the above reduced equations (5.3.21) to (5.3.23) to examine the asymptotic behaviour of this branch when a different diffusivity ratio is used. We would use hydrochloric acid (HCl) or copper sulphate ($CuSO_4$) instead of salt in this differentially-heated slot problem. The minimum values of Ra_{S_0} for the three solutes and the corresponding $\hat{\alpha}$ are shown in table 5.2. The results indicate that as τ decreases so does Ra_{S_0} and the corresponding wave number for the different solute.

solute	$\tau \times 10^{-2}$	Ra_{S_0}	$\hat{\alpha}$
HCl	2.2	10.90226	512.22265
NaCl	1.0	4.77011	442.67079
$CuSO_4$	0.35	1.61574	253.34107

Table 5.2: These are the minimum values found for Ra_{S_0} and $\hat{\alpha}$ in the limit of large Ra_T when an approximate value of τ is used for each solute.

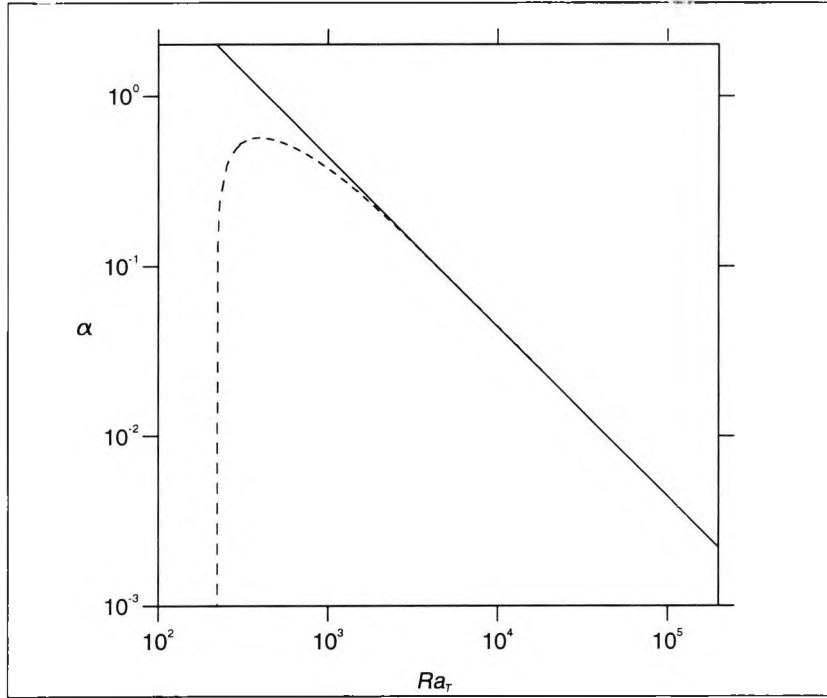


Figure 5.15: A graph of the vertical wave number, α , as a function of Ra_T is shown to give the comparison of the asymptotic behaviour (solid line) and the full numerical results (dashed line) for the large Ra_T limit.

Now both Pr and τ appear in (5.3.21) to (5.3.23) and it may seem necessary in practical terms to re-calculate the asymptotic behaviour of this regime every time a different fluid and/or a different solute is used. However, we can simplify these equations further if τ is assumed small. As $\tau \rightarrow 0$, we find the suitable scalings are $\psi_0 = O(1)$, $T_0 = O(\tau)$, $S_0 = O(\tau^{-1})$, $Ra_{S_0} = O(\tau)$ and $\hat{\alpha} = O(\tau)$. If we define new rescaled variables to be

$$\psi_0 = \psi_*, \quad T_0 = \tau T_*, \quad S_0 = \tau^{-1} S_*, \quad Ra_{S_0} = \tau Ra_{S_*}, \quad \hat{\alpha} = \tau \alpha_*, \quad (5.3.26)$$

then the leading set of equations is

$$D^4\psi_* + Ra_{S_*}DS_* = 0, \quad (5.3.27)$$

$$D^2T_* + i\alpha_*\psi_* = 0, \quad (5.3.28)$$

$$D^2S_* - i\alpha_*D\hat{S}_o\psi_* - i\alpha_*\hat{w}_oS_* - D\psi_* = 0, \quad (5.3.29)$$

with boundary conditions

$$\psi_* = D\psi_* = T_* = DS_* = 0 \quad \text{on} \quad x = \pm 1/2. \quad (5.3.30)$$

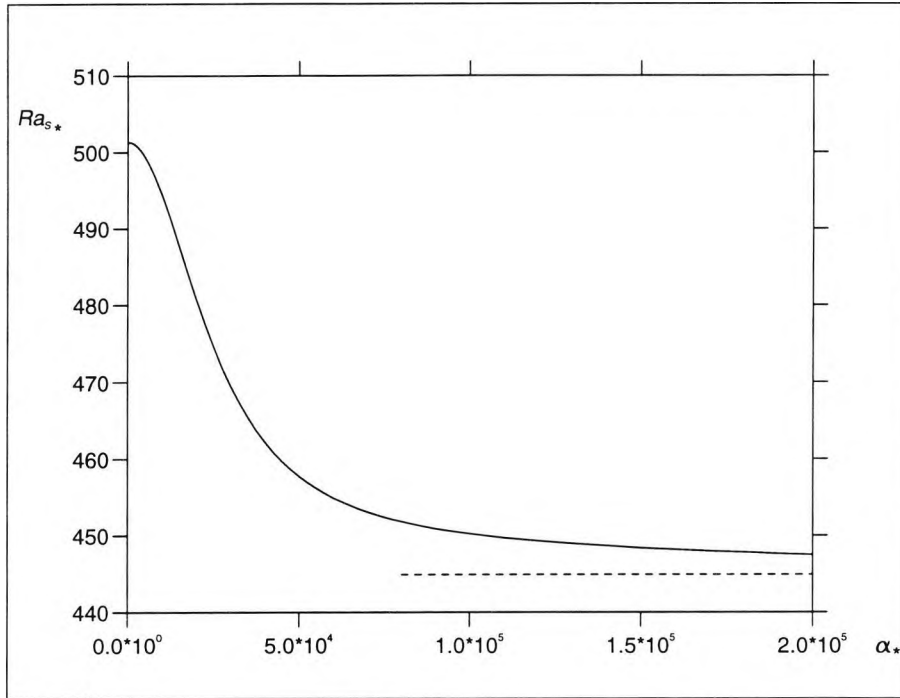


Figure 5.16: A graph of Ra_{S_*} as a function of α_* for the limit $\tau \rightarrow 0$, with the large α_* asymptote estimated at $Ra_{S_*} = 444.8$ as indicated by a dashed line.

It can be seen in the above leading order equations that the parameters Pr and τ are no longer visible. We only have to solve (5.3.27) and (5.3.29) to obtain the relationship between Ra_{S_*} and α_* . The results shown in figure 5.16 reveal that Ra_{S_*} has a maximum of 501.36 at the origin which slopes down towards an asymptote estimated to be at $Ra_{S_*} = 444.8$. Although a minimum can be found for Ra_{S_*} , there is no corresponding finite α_* . The maximum with $Ra_{S_*} = 501.36$ in the $\alpha_*-Ra_{S_*}$ plane has the same value as (5.2.33) found in the previous section for the vertical asymptote where the assumption for $\tau \rightarrow 0$ was not needed in the small α analysis. Since this value of Ra_S was previously found to give an upper bound for the stability boundary in this region, the vertical part of the full stability curve obtained here with $Pr = 6.7$ and $\tau = 0.01$ is lower than this value as anticipated.

The above results for the limit $\tau \rightarrow 0$ need to be carefully interpreted particularly when examining the large α_* behaviour in figure 5.16. When de-

riving the original large Ra_T equations (5.3.21) to (5.3.23), we have used one limiting process which made some assumptions about the relative magnitudes of the terms in the full problem. When the second limiting process is taken the additional assumptions have to be compatible with the first limiting process, in that the small terms neglected in the large Ra_T assumption would not become large with the additional small τ assumption. However, if we take a further limit $\alpha_* \rightarrow \infty$ this would then become incompatible with the earlier assumptions that $\alpha \rightarrow 0$ as $Ra_T \rightarrow \infty$ and $\alpha_* \rightarrow 0$ as $\tau \rightarrow 0$. This suggests the original assumptions will always provide a constraint on the maximum allowable size of α_* . Therefore, the limit $Ra_{S_*} \rightarrow 444.8$ may only be found when values of Ra_T and τ are extreme. This limit can provide a lower bound for the possible minimum values of Ra_{S_*} in this asymptotic regime. This is not too different in magnitude from an upper bound for the vertical boundary in this stability regime.

The most distinctive feature found in this large Ra_T regime is the vertical nature of the stability boundary in the Ra_S - Ra_T plane. This means as the temperature difference is increased or decreased for any given salinity gradient across the slot it will have no effect on the stability of the fluid, at least to leading order. This may seem surprising when both \hat{w}_o and $D\hat{S}_o$ are proportional to Ra_T and hence the temperature difference. Both the shear of the background flow and the horizontal salinity gradient are the potential driving forces for destabilisation in this regime. We can investigate their respective roles by multiplying \hat{w}_o and $D\hat{S}_o$ by some arbitrary factor in (5.3.21) and (5.3.23) and investigating the effect on the stability boundary. We found increasing the background velocity stabilises the flow while increasing the salinity gradient destabilises the flow. If the two parameters are increased by the same factor then there is little change in the location of the stability

boundary. We conclude that the instability in this large Ra_T regime is driven by the horizontal salinity gradient whereas the effect of the vertical shear is to stabilise the flow. This effect of shear suppressing double-diffusive convection has been shown by Linden (1974) in his study of the effect of shear on salt fingers.

5.4 Thermal Convection and Small Ra_S

The final part of the stability curve that we consider in this section is regime 5 of figure 5.1. These steady solutions correspond to the limit of $Ra_S \ll 1$ as well as the solution for $Ra_S = 0$ which is the thermal problem of a laterally heated slot. We have learnt from chapters 3 and 4 that non-oscillatory solutions for Ra_S below 2.0256 were found from the Galerkin approach but not from the original Runge-Kutta scheme. The reason for the failure in the Runge-Kutta scheme will be explained during the discussion of the asymptotic behaviour for this small Ra_S regime. However, when salinity dependence is removed from the linear system, the thermally driven problem across a vertical slot can be solved using the Runge-Kutta scheme. This thermal situation will be examined first.

From the steady-state background problem in (2.8.5) to (2.8.7), we can find the leading order behaviour for the background velocity so that the equations below are independent of S :

$$\frac{d^3 \overline{w}_o}{dx^3} + Ra_T \frac{d\overline{T}_o}{dx} = 0, \quad (5.4.1)$$

$$\frac{d^2 \overline{T}_o}{dx^2} = 0. \quad (5.4.2)$$

It is clear from (5.4.2) that a solution $\overline{T}_o = Ax + B$ with boundary conditions $\overline{T}_o = \pm 1/2$ on $x = \mp 1/2$, will give $A = -1$ and $B = 0$. Therefore the simple

solution $\overline{T}_o = -x$ can be substituted into (5.4.1) to give

$$\frac{d^3 \overline{w}_o}{dx^3} - Ra_T = 0, \quad (5.4.3)$$

and the leading order \overline{w}_o is an odd function given by

$$\overline{w}_o = Ra_T \frac{x^3}{6} - \frac{Ra_T}{24} x. \quad (5.4.4)$$

The leading order thermal problem consists of the stream function and the temperature equations only:

$$(D^2 - \alpha^2)^2 \psi - \frac{i\alpha}{Pr} \left\{ \overline{w}_o (D^2 - \alpha^2) \psi - D^2 \overline{w}_o \psi \right\} - Ra_T DT = 0, \quad (5.4.5)$$

$$(D^2 - \alpha^2)T + i\alpha(\psi - \overline{w}_o T) = 0, \quad (5.4.6)$$

with boundary conditions

$$\psi = D\psi = T = 0 \quad \text{at} \quad x = \pm 1/2. \quad (5.4.7)$$

The neutral stability curve can be calculated using the Runge-Kutta scheme as before. This curve is shown in figure 5.17. The minimum value found for Ra_T and the corresponding wave number are

$$Ra_T = 52\,715 \quad \text{and} \quad \alpha = 2.7671. \quad (5.4.8)$$

The study of stationary instabilities in a vertical slot by Vest & Arpaci (1969) showed that the critical Rayleigh number was approximately $7\,880 \times Pr$ for a wide range of Pr and would correspond to $Ra_T = 52\,796$ for $Pr = 6.7$ used here. Their result is valid to within a few percent for all Prandtl numbers. Clearly, this result is in good agreement with the result found in (5.4.8).

Next we consider what happens when there is a weak salinity gradient present in a slot. This is the case where the salt Rayleigh number is assumed to be small and we will examine the asymptotic behaviour in this limit of $Ra_S \ll 1$. We first pose the asymptotic expansions:

$$\psi = \psi_0 + Ra_S \psi_1 + \dots, \quad (5.4.9)$$

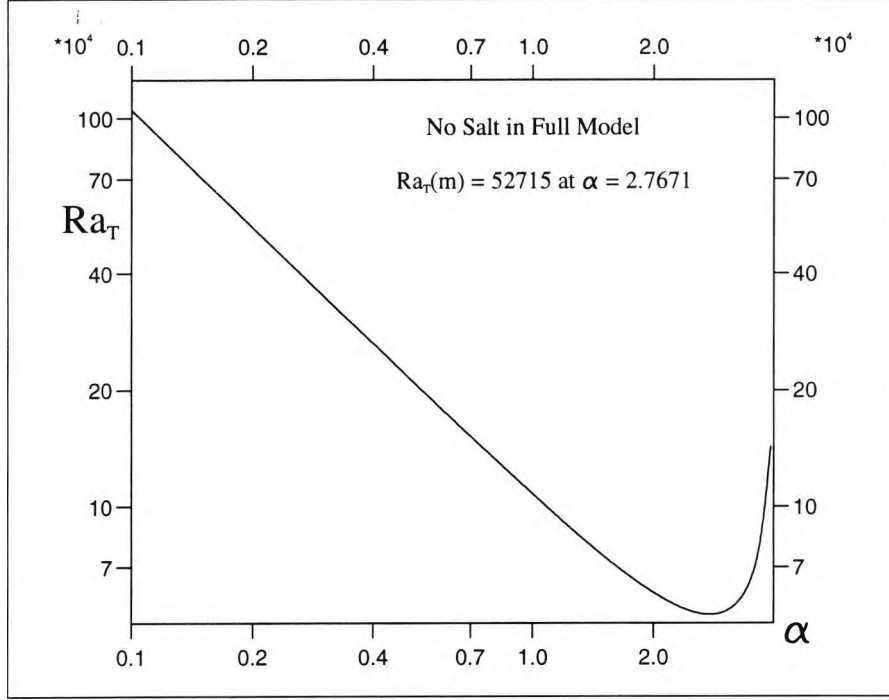


Figure 5.17: In the thermally driven case for a laterally heated slot, the minimum value of Ra_T is found with the corresponding α .

$$T = T_0 + Ra_S T_1 + \dots, \quad (5.4.10)$$

$$S = S_0 + Ra_S S_1 + \dots, \quad (5.4.11)$$

$$Ra_T = Ra_{T_0} + Ra_S Ra_{T_1} + \dots. \quad (5.4.12)$$

The leading order terms for the background state are

$$\begin{aligned} D\overline{S}_o &= \frac{-h_1(x)}{\tau} [Ra_{T_0} + Ra_S Ra_{T_1} + \dots] \\ &+ \frac{Ra_S h_2(x)}{\tau^2} [Ra_{T_0} + Ra_S Ra_{T_1} + \dots] + \dots, \end{aligned} \quad (5.4.13)$$

$$\begin{aligned} \overline{w}_o &= h_3(x) [Ra_{T_0} + Ra_S Ra_{T_1} + \dots] \\ &- \frac{Ra_S h_4(x)}{\tau} [Ra_{T_0} + Ra_S Ra_{T_1} + \dots] + \dots, \end{aligned} \quad (5.4.14)$$

$$\begin{aligned} D^2\overline{w}_o &= h_5(x) [Ra_{T_0} + Ra_S Ra_{T_1} + \dots] \\ &- \frac{Ra_S h_6(x)}{\tau} [Ra_{T_0} + Ra_S Ra_{T_1} + \dots] + \dots, \end{aligned} \quad (5.4.15)$$

where

$$h_1(x) = \frac{16x^4 - 8x^2 + 1}{384}, \quad (5.4.16)$$

$$h_2(x) = \frac{768x^8 - 1792x^6 + 3360x^4 - 1392x^2 + 163}{30965760}, \quad (5.4.17)$$

$$h_3(x) = \frac{x(4x^2 - 1)}{24}, \quad (5.4.18)$$

$$h_4(x) = \frac{x(4x^2 - 1)(16x^4 - 24x^2 + 29)}{322560}, \quad (5.4.19)$$

$$h_5(x) = x, \quad (5.4.20)$$

$$h_6(x) = \frac{x(48x^4 - 40x^2 + 15)}{5760}. \quad (5.4.21)$$

Substituting these expansions into the full stability equations of (2.10.2) to (2.10.4) will give the $O(1)$ and $O(Ra_S)$ problems where, as before, $\sigma = 0$ is assumed. The $O(1)$ problem will consider terms in the absence of Ra_S or a vertical salinity gradient and these leading order perturbation equations are:

$$(D^2 - \alpha^2)^2 \psi_0 - \frac{i\alpha}{Pr} h_3(x) Ra_{T_0} (D^2 - \alpha^2) \psi_0 + \frac{i\alpha}{Pr} h_5(x) Ra_{T_0} \psi_0 - Ra_{T_0} DT_0 = 0, \quad (5.4.22)$$

$$(D^2 - \alpha^2)T_0 + i\alpha\psi_0 - i\alpha h_3(x) Ra_{T_0} T_0 = 0, \quad (5.4.23)$$

$$\tau(D^2 - \alpha^2)S_0 + i\alpha \frac{h_1(x)}{\tau} Ra_{T_0} \psi_0 - i\alpha h_3(x) Ra_{T_0} S_0 - D\psi_0 = 0, \quad (5.4.24)$$

with boundary conditions

$$\psi_0 = D\psi_0 = T_0 = DS_0 = 0 \quad \text{on} \quad x = \pm 1/2. \quad (5.4.25)$$

Equations (5.4.22) and (5.4.23) are identical to the thermal problem in (5.4.5) and (5.4.6) that we solved earlier using the Runge-Kutta scheme, although different notations are used here. However, the above leading order salinity problem can only be solved in the same way as long as τ is larger than approximately 0.25 because for τ smaller than this value, boundary layers

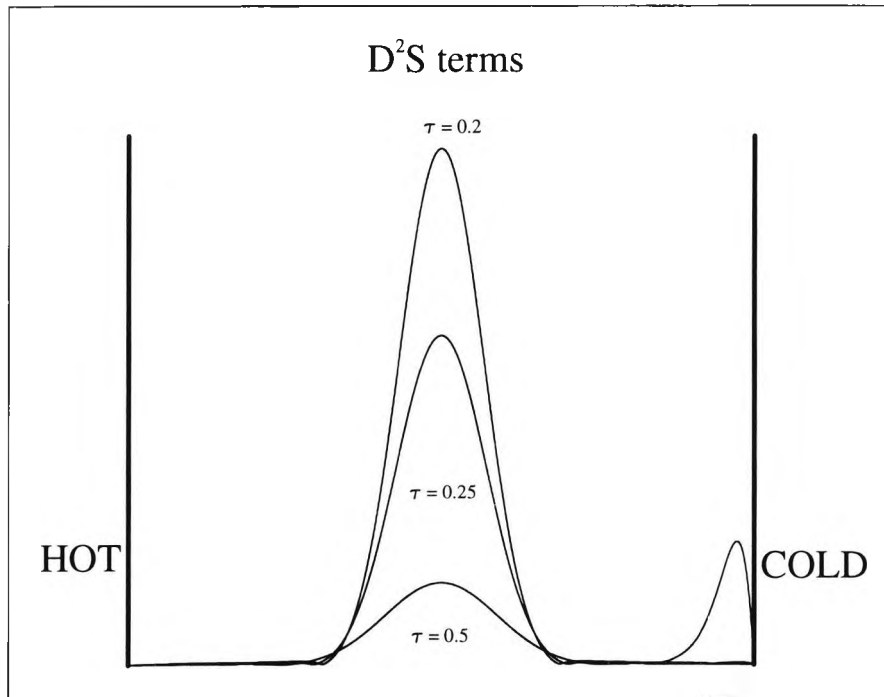


Figure 5.18: Plot of D^2S across the slot for the leading order problem in the $Ra_S \ll 1$ limit. As the diffusivity ratio, τ , becomes small, the Runge-Kutta scheme failed to produce solutions which satisfy all boundary conditions. In the case $\tau = 0.2$ the solution does not become zero at the right wall. This can be seen by the second peak in the solution.

develop both at the centre and at the walls of the slot. This boundary layer behaviour is discussed below. Figures 5.18, 5.19 and 5.20 illustrate the curves of the various salinity terms across the slot for different values of τ . When $\tau = 0.2$ there is a small peak in the curve near the right wall. In this case the Runge-Kutta scheme failed to produce solutions that satisfied the right boundary conditions. The solution always grew to large values at the right wall for whatever choice of boundary conditions at the left wall. These solutions are found using double precision arithmetic on the computer. By using quadruple precision, further progress could be made but still solutions could only be found down to $\tau = 0.1$.

Further examination in equation (5.4.24) shows that the factor $i\alpha h_3(x)Ra_{T_0}$ multiplying $\bar{\theta}_0$ has magnitude that changes from 0 at the walls and the centre to peaks of 117 000 in the regions adjacent to them. The behaviour of this

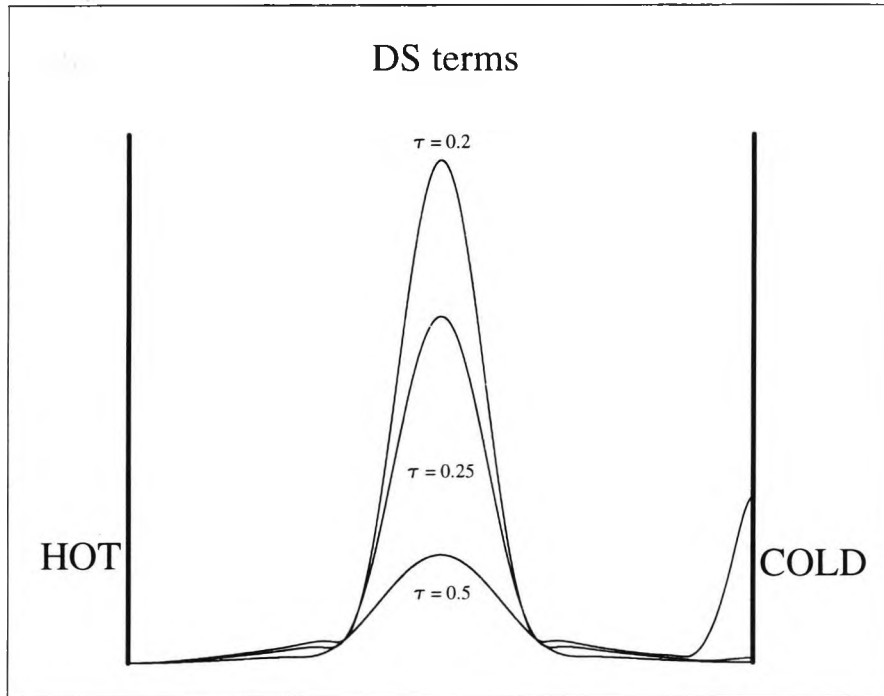


Figure 5.19: This is the same situation as figure 5.18, but this time plotting DS . The solutions grew to large values at the right wall when τ is approximately smaller than 0.25.

term across the slot can comparably be seen in figure 5.14 of the previous section with the curve labelled $\alpha S w_o / \tau$. This structure causes the salinity equation to become very stiff with a boundary layer behaviour developing at $x = 0$ and at the walls. This stiff behaviour of the salinity equation is the cause of the failure in the Runge-Kutta scheme. As the Runge-Kutta scheme failed to give solutions, the Galerkin approach of chapter 4 was used to find solutions for $\tau = 0.01$ in the presence of weak salinity gradient. This Galerkin approach is robust as long as the truncation level used is sufficiently large for the boundary layers to be resolved. It was only when the truncation level was set to $N = 72$ and $N = 96$ that solutions along this branch were satisfactorily resolved. Indeed, the functions used in the expansions of the Galerkin approach by Thangam, Zebib & Chen (1981) and used here have the advantage of approximately uniform resolution across the slot, enabling us to resolve the boundary layer found in the middle of the slot as well as those at the walls. Other schemes which use, for example, Chebyshev polynomi-

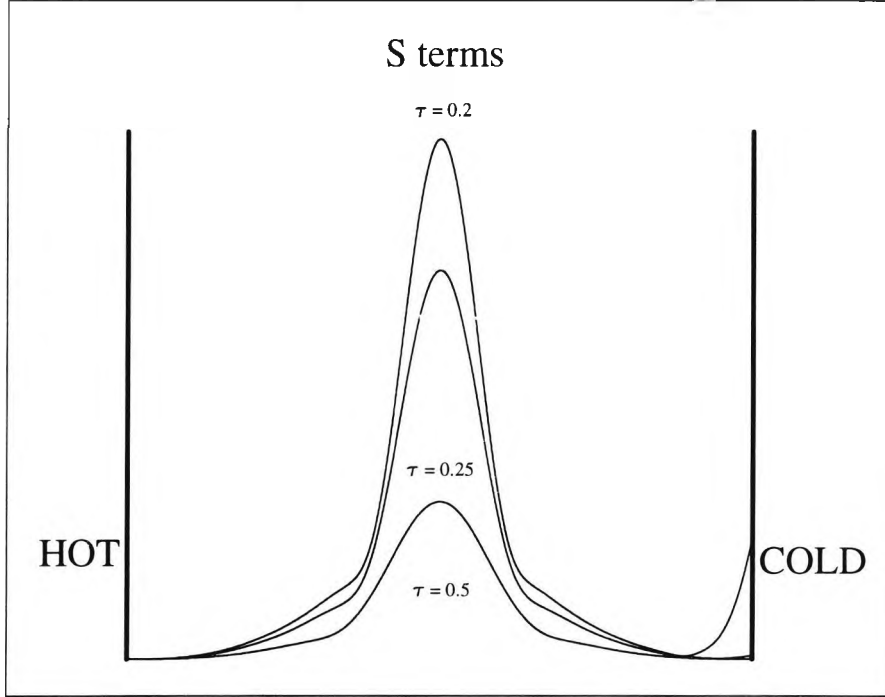


Figure 5.20: The same behaviour from D^2S and DS is observed in S . However, a sharp peak in the middle of the slot is a distinct feature found in all the curves of the salinity terms.

als concentrate the resolution near the walls and so may not be as appropriate.

In order to determine the next order perturbation for Ra_T , a solvability condition is applied to the $O(Ra_S)$ problem. The equations for ψ_1 and T_1 are

$$\begin{aligned}
 & (D^2 - \alpha^2)^2 \psi_1 - \frac{i\alpha}{Pr} h_3(x) Ra_{T_0} (D^2 - \alpha^2) \psi_1 + \frac{i\alpha}{Pr} h_5(x) Ra_{T_0} \psi_1 - Ra_{T_0} DT_1 \\
 &= \frac{i\alpha}{Pr} h_3(x) Ra_{T_1} (D^2 - \alpha^2) \psi_0 - \frac{i\alpha h_4(x)}{\tau Pr} Ra_{T_0} (D^2 - \alpha^2) \psi_0 \\
 & \quad - \frac{i\alpha}{Pr} h_5(x) Ra_{T_1} \psi_0 + \frac{i\alpha h_6(x)}{\tau Pr} Ra_{T_0} \psi_0 + Ra_{T_1} DT_0 - DS_0, \quad (5.4.26)
 \end{aligned}$$

$$(D^2 - \alpha^2) T_1 + i\alpha \psi_1 - i\alpha h_3(x) Ra_{T_0} T_1 = i\alpha h_3(x) Ra_{T_1} T_0 - i\alpha \frac{h_4(x)}{\tau} Ra_{T_0} T_0, \quad (5.4.27)$$

with boundary conditions

$$\psi_1 = D\psi_1 = T_1 = 0 \quad \text{on} \quad x = \pm 1/2. \quad (5.4.28)$$

Equations (5.4.26) and (5.4.27) do not, in general, have a solution. To find out

when a solution does exist we apply a solvability condition. This condition is obtained by finding the adjoints $\hat{\psi}$ and \hat{T} to ψ_0 and T_0 . These satisfy the adjoint problem

$$(D^2 - \alpha^2)^2 \hat{\psi} - \frac{i\alpha}{Pr} Ra_{T_0} h_3(x) D^2 \hat{\psi} + \frac{i\alpha^3}{Pr} Ra_{T_0} h_3(x) \hat{\psi} - \frac{2i\alpha}{Pr} Ra_{T_0} D h_3(x) D \hat{\psi} - \frac{i\alpha}{Pr} Ra_{T_0} D^2 h_3(x) \hat{\psi} + \frac{i\alpha}{Pr} Ra_{T_0} h_5(x) \hat{\psi} + i\alpha \hat{T} = 0, \quad (5.4.29)$$

$$D^2 \hat{T} - \alpha^2 \hat{T} - i\alpha Ra_{T_0} h_3(x) \hat{T} + Ra_{T_0} D \hat{\psi} = 0, \quad (5.4.30)$$

with boundary conditions

$$\hat{\psi} = D\hat{\psi} = \hat{T} = 0 \quad \text{on} \quad x = \pm 1/2. \quad (5.4.31)$$

Both equations (5.4.26) and (5.4.27) are multiplied by the corresponding complex conjugates of $\hat{\psi}$ and \hat{T} and the sum of these equations are then integrated from $x = -1/2$ to $x = 1/2$. The resulting solvability condition obtained for Ra_{T_1} , indicating the existence of a steady solution in the case of $Ra_S \rightarrow 0$ is

$$Ra_{T_1} = \frac{Ra_{T_0} \eta_1(\alpha, Pr, \tau) - \int_{-1/2}^{1/2} S_0 D \hat{\psi} dx}{\eta_2(\alpha, Pr, \tau)}, \quad (5.4.32)$$

where

$$\begin{aligned} \eta_1(\alpha, Pr, \tau) &= \frac{i\alpha}{\tau Pr} I_{\eta_1}(x) + \frac{2i\alpha}{\tau Pr} I_{\eta_2}(x) + \frac{i\alpha}{\tau Pr} I_{\eta_3}(x) \\ &\quad - \frac{i\alpha}{\tau Pr} I_{\eta_4}(x) + \frac{i\alpha}{\tau} I_{\eta_5}(x), \end{aligned} \quad (5.4.33)$$

and

$$\begin{aligned} \eta_2(\alpha, Pr, \tau) &= \frac{i\alpha}{Pr} J_{\eta_1}(x) + \frac{2i\alpha}{Pr} J_{\eta_2}(x) + \frac{i\alpha}{Pr} J_{\eta_3}(x) \\ &\quad - \frac{i\alpha}{Pr} J_{\eta_4}(x) - J_{\eta_5}(x) + i\alpha J_{\eta_6}(x). \end{aligned} \quad (5.4.34)$$

These $I_{\eta_{1,\dots,5}}(x)$ and $J_{\eta_{1,\dots,6}}(x)$ are integrals involving the adjoints as well as ψ_0 and T_0 . These integrals are

$$I_{\eta_1}(x) = \int_{-1/2}^{1/2} \psi_0 h_4(x) (D^2 - \alpha^2) \hat{\psi} dx, \quad (5.4.35)$$

$$I_{\eta_2}(x) = \int_{-1/2}^{1/2} \psi_0 D h_4(x) D \hat{\psi} dx, \quad (5.4.36)$$

$$I_{\eta_3}(x) = \int_{-1/2}^{1/2} \psi_0 D^2 h_4(x) \hat{\psi} dx, \quad (5.4.37)$$

$$I_{\eta_4}(x) = \int_{-1/2}^{1/2} \psi_0 h_6(x) \hat{\psi} dx, \quad (5.4.38)$$

$$I_{\eta_5}(x) = \int_{-1/2}^{1/2} T_0 h_4(x) \hat{T} dx, \quad (5.4.39)$$

and,

$$J_{\eta_1}(x) = \int_{-1/2}^{1/2} \psi_0 h_3(x) (D^2 - \alpha^2) \hat{\psi} dx, \quad (5.4.40)$$

$$J_{\eta_2}(x) = \int_{-1/2}^{1/2} \psi_0 D h_3(x) D \hat{\psi} dx, \quad (5.4.41)$$

$$J_{\eta_3}(x) = \int_{-1/2}^{1/2} \psi_0 D^2 h_3(x) \hat{\psi} dx, \quad (5.4.42)$$

$$J_{\eta_4}(x) = \int_{-1/2}^{1/2} \psi_0 h_5(x) \hat{\psi} dx, \quad (5.4.43)$$

$$J_{\eta_5}(x) = \int_{-1/2}^{1/2} T_0 D \hat{\psi} dx, \quad (5.4.44)$$

$$J_{\eta_6}(x) = \int_{-1/2}^{1/2} T_0 h_3(x) \hat{T} dx. \quad (5.4.45)$$

These can all be found numerically provided Ra_{T_0} , the adjoints $\hat{\psi}$ and \hat{T} , ψ_0 , T_0 , S_0 and their respective derivatives are known. The difficulty lies in finding the solution to S_0 , the $O(1)$ problem for the salinity equation. We have seen earlier that the Runge-Kutta scheme failed to find a solution which satisfied all the boundary conditions and so an approximate solution to the salinity equation was found by a matched asymptotic expansion. This ensures that the asymptotic behaviour calculated is independent of the Galerkin approach. The asymptotic approximation for S_0 is discussed below. We have found an asymptotic estimate of S_0 that matches almost perfectly with the real and imaginary numerics for S_0 as shown in figure 5.21. There are very

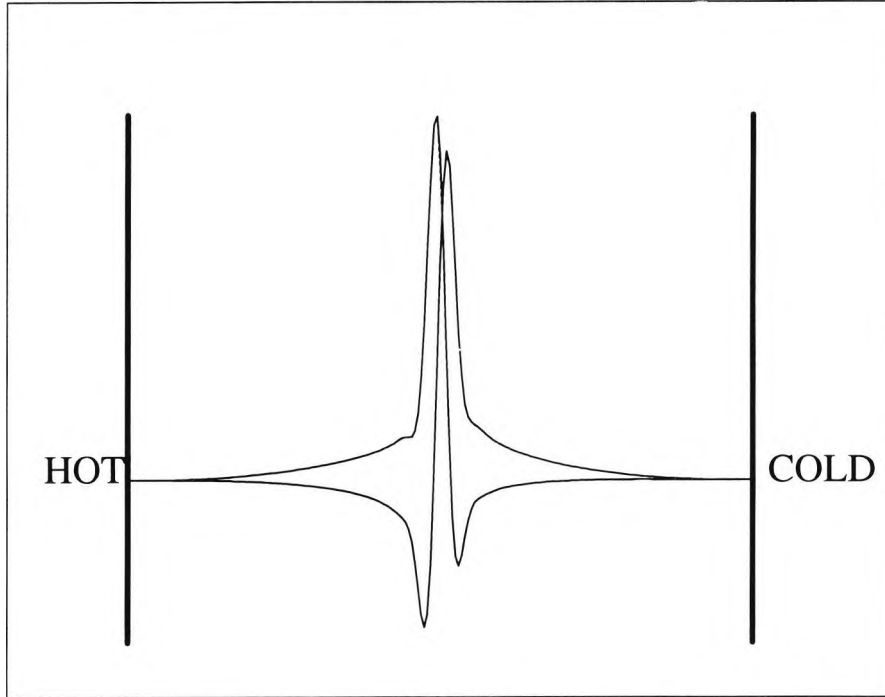


Figure 5.21: A comparison of the asymptotic estimate of the salinity equation in the limit of $Ra_S \ll 1$ (dashed line) with the solution found by the Galerkin approach with truncation $N = 96$ for $Ra_S = 0.001$ (solid line). The left highest peak is the imaginary part of S and the adjacent peak is the corresponding real part. The Galerkin results are barely distinguishable from the dashed line of the asymptotic.

small differences visible near $x = 0$ but the fit is good.

Here we derive the asymptotic approximation for S_0 . The leading order salinity equation is

$$(D^2 - \alpha^2)S_0 + i\alpha \frac{h_1(x)}{\tau^2} Ra_{T_0} \psi_0 - \frac{i\alpha}{\tau} h_3(x) Ra_{T_0} S_0 - \frac{D\psi_0}{\tau} = 0. \quad (5.4.46)$$

The factor $h_3(x)$ of the third term is the background velocity which leads to numerical problems as its magnitude is approximately of order 10^5 for $\tau = 0.01$. In order to cope with the problem arising from the large magnitude of this term, an approximate solution to this salinity equation is found by a matched asymptotic expansion in x . The structure of the solution consists of outer solutions away from the walls and the centre, and the inner boundary layer solutions at the walls and in the centre. This salinity equation can be

written in more general terms as

$$D^2 S_0 - (\alpha^2 + i\mu_0 x(4x^2 - 1))S_0 = \frac{D\psi_0}{\tau} - \frac{i\alpha}{\tau} D\overline{S}_o \psi_0, \quad (5.4.47)$$

with the no-flux boundary conditions

$$DS_0 = 0 \quad \text{on} \quad x = \pm 1/2, \quad (5.4.48)$$

where $\mu_0 \gg 1$ (here $\mu_0 = \alpha Ra_{T_0}/24\tau$), α is $O(1)$ and, both ψ_0 and $D\psi_0$ are some known functions of x . If x is not small or near $\pm 1/2$, then we obtain the leading order outer solution which takes the form

$$S_0 \approx \frac{i\alpha D\overline{S}_o \psi_0 - D\psi_0}{i\tau\mu_0 x(4x^2 - 1)}. \quad (5.4.49)$$

When x is small and near $\pm 1/2$ this approximation breaks down because the denominator of equation (5.4.49) tends to zero as $x \rightarrow \pm 1/2$ or $x \rightarrow 0$. The numerator also tends to zero as $x \rightarrow \pm 1/2$ and so there S_0 is relatively well behaved. However, as $x \rightarrow 0$ the numerator is non-zero and so this outer behaviour becomes singular near the centre of the slot. Thus we must find an inner solution for the region near $x = 0$. We look for a stretching of the form $X = \mu_0^\gamma x$ with $\gamma > 0$ for the inner layer near $x = 0$. If we substitute this inner variable X into (5.4.47) then it gives

$$\begin{aligned} \mu_0^{2\gamma} \frac{d^2 S_I}{dX^2} &= \left\{ \alpha^2 + i4\mu_0^{1-3\gamma} X^3 - i\mu_0^{1-\gamma} X \right\} S_I \\ &= \frac{D\psi_0(0)}{\tau} - \frac{i\alpha D\overline{S}_o(0)\psi_0(0)}{\tau} + O(\mu_0^{-\gamma}). \end{aligned} \quad (5.4.50)$$

Balancing powers of μ_0 gives either $2\gamma = 1 - \gamma$ or $2\gamma = 1 - 3\gamma$, and so $\gamma = 1/3$ or $1/5$ respectively. However, the choice $\gamma = 1/5$ does not work as the term $-i\mu_0^{1-\gamma} X S_I$ would dominate by itself. The appropriate horizontal length scale for the region near $x = 0$ is thus $O(\mu_0^{-1/3})$, and using the scaling $X = \mu_0^{1/3} x$ gives the leading order inner problem

$$\frac{d^2 S_I}{dX^2} + iX S_I = \mu_0^{-2/3} \left\{ \frac{D\psi_0(0)}{\tau} - \frac{i\alpha D\overline{S}_o(0)\psi_0(0)}{\tau} \right\} + O(\mu_0^{-1/3}), \quad (5.4.51)$$

where $\mu_0 = \alpha Ra_{T_0}/24\tau$. We look for a solution that decays as $X \rightarrow \pm\infty$. This leading order problem for the inner region does not have an exact solution when the right-hand side of (5.4.51) is non-zero. Therefore we find a numerical solution to the modified Airy's equation

$$Y''(X) + iXY(X) = 1. \quad (5.4.52)$$

This solution is obtained using the Runge-Kutta technique. The solution required is one that decays as $-i/X$ as $X \rightarrow \pm\infty$. This requires the real part of $Y(X)$ to be an even function of X and the imaginary part an odd function. By adjusting $Y(0)$ and $Y'(0)$, a solution to (5.4.52) was found which satisfied these criteria. The inner behaviour is made up of this solution multiplied by the right-hand side of (5.4.51) involving the leading order term of \overline{w}_o hidden in μ_0 and the values of $\psi_0(0)$ and $D\psi_0(0)$.

When both the outer solution from (5.4.49) and the inner solution from (5.4.51) are known, we can find a solution valid for all x . We find the inner approximation to the outer solution using

$$S_{IO}(x) = \frac{i\alpha D\overline{S}_o\psi_0(0) - D\psi_0(0)}{-i\tau\mu_0x}, \quad (5.4.53)$$

and so this gives a composite solution of the form

$$S_0(x) \approx S_O(x) + S_I(\mu_0^{-1/3}x) - S_{IO}(x), \quad (5.4.54)$$

where $S_O(x)$ is the outer solution from (5.4.49), $S_I(\mu_0^{-1/3}x)$ the inner solution from (5.4.51) and $S_{IO}(x)$ the singular behaviour from (5.4.53). This composite solution will be valid in most regions at leading order except for regions with the boundary layers near $x = \pm 1/2$ and the point at $x = 0$ where the value of $S_I(0)$ is used. Since the boundary conditions for ψ and $D\psi$ require them to decay to 0 at the walls, the boundary layers near $x = \pm 1/2$ are not important in the integration of the solvability condition for finding the

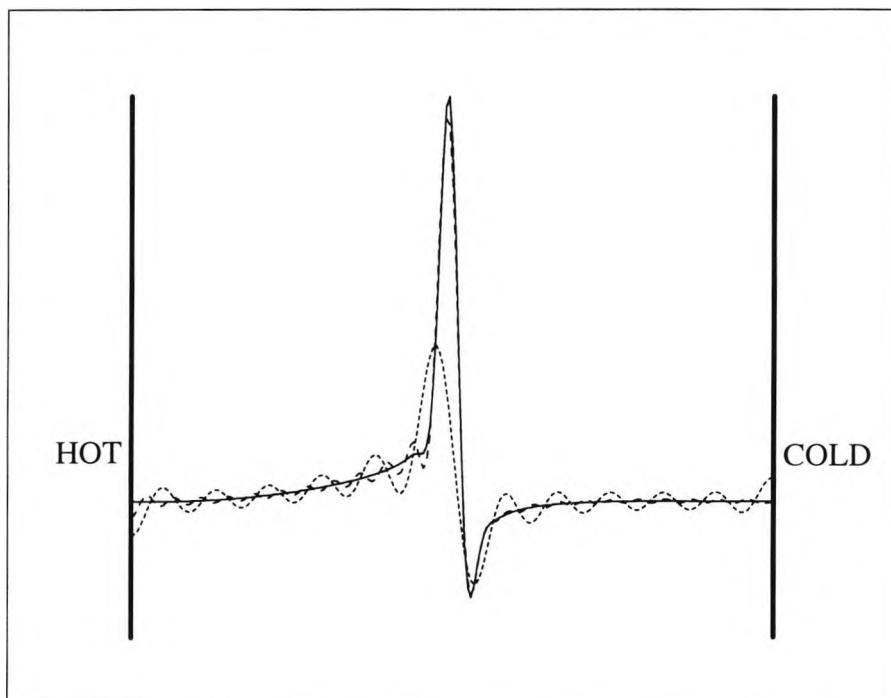


Figure 5.22: Plot of the estimate of the real part of S_0 (solid line) when compared with the Galerkin approach where the truncation levels are set to $N = 24, 48,$ and 96 (dashed lines).

approximation to Ra_{T_1} . Therefore these calculations are not discussed here. When the estimate to $S_0(x)$ of equation (5.4.54) is compared with the results found by the Galerkin approach of chapter 4 for the full problem, we found the results for $N = 24$ fail to resolve the peak at the centre of the slot while $N = 96$ gives good agreement. These results for different values of N can be observed in figure 5.22 for the real part of S_0 and in figure 5.23 for the corresponding imaginary part. Thangam *et al.* used $N = 30$, and so would not have resolved the region accurately. It is important to ensure the truncation level used is large enough to resolve the singular behaviour at $x = 0$. This will safeguard the risk of obtaining plausible incorrect results. The real and imaginary parts of S_0 in figures 5.21, 5.22 and 5.23 are not odd or even because the boundary condition used to define the scale of the perturbations, $\psi''(-1/2) = 1$, does not lead to such solutions. Multiplication by a suitable complex constant would make these real and imaginary parts have a definite

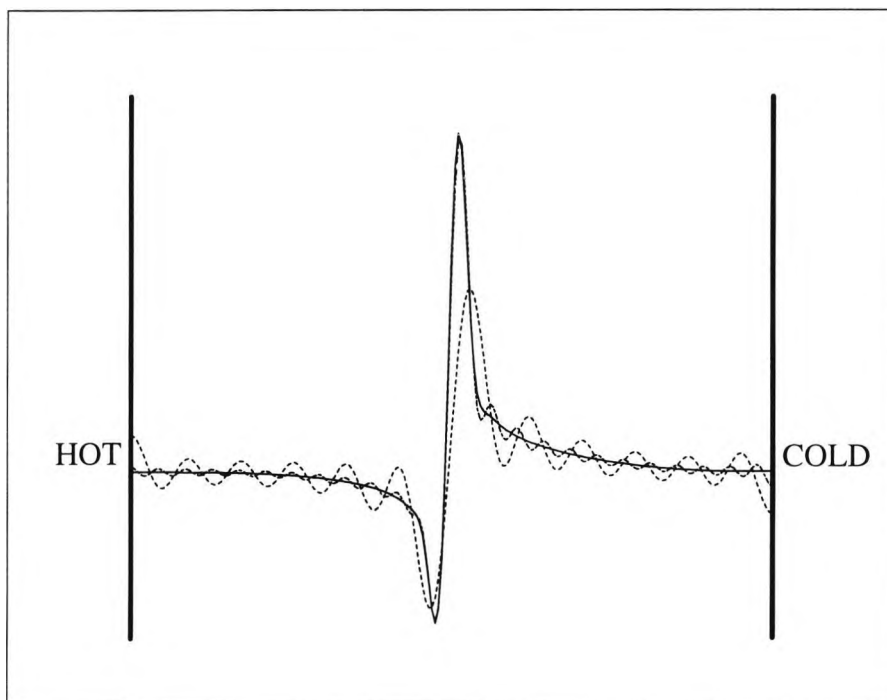


Figure 5.23: Plot of the corresponding imaginary part of S_0 as indicated in figure 5.22.

parity. This can be seen by the symmetry of the contour plots of ψ , T and S in figure 4.5 for the case $Ra_S = 0.1$.

The solvability condition derived in (5.4.32) for the next order of the thermal Rayleigh number can finally be calculated. The integrations to find η_1 , η_2 and in particular the one associated with S_0 , can now be determined. Taking the real and imaginary parts of equation (5.4.32), the value of Ra_{T_1} is evaluated numerically. With $Pr = 6.7$, $\tau = 0.01$ and $\alpha = 2.7671$ the marginally stable state has

$$Ra_{T_1} = 13886. \quad (5.4.55)$$

This gives the critical value of Ra_T as

$$Ra_T = 52715 + 13886 Ra_S + O(Ra_S^2). \quad (5.4.56)$$

These estimates are based on calculations using the Runge-Kutta scheme.

Similar results for the leading order perturbation to the thermal Rayleigh number can be obtained by looking at solutions to the full problem using the Galerkin approach. These are shown below in table 5.3. It can be seen that the estimate of Ra_{T_0} is accurate for all levels of truncation. This behaviour is expected since the leading order behaviour is merely the effect of a laterally heated slot with zero salinity concentration. There is no boundary layer structure involved in this case, and the solution is adequately resolved for all truncations. The next order perturbation, Ra_{T_1} , only starts to converge when the truncation level is set to $N = 72$ and $N = 96$. This estimate is slightly different from the result in (5.4.55). The difference is of the order that may be expected from the accuracy of the asymptotic expansions for $S_0(x)$. However, the estimate in (5.4.55) uses an approximate solution so perfect agreement cannot be expected.

N	Ra_{T_0}	Ra_{T_1}
24	52715.338	5785.872
48	52715.368	13311.849
72	52715.367	13713.527
96	52715.366	13713.722

Table 5.3: These estimates of Ra_{T_0} and Ra_{T_1} based on the results for $Ra_S = 0.01$ and 0.001 are found by the Galerkin approach for different truncation levels.

The result of Ra_{T_1} in (5.4.55) is for a fixed value of the vertical wave number that corresponds to the minimum of Ra_{T_0} . It is possible that the leading order perturbation for the wave number can be determined. We can expand Ra_{T_0} and Ra_{T_1} in Taylor series around α_0 , the critical value of α for the slot problem. This gives the critical value of α to be

$$\alpha = \alpha_0 - Ra_S \left(\frac{\partial Ra_{T_1}(\alpha_0)/\partial \alpha}{\partial^2 Ra_{T_0}(\alpha_0)/\partial \alpha^2} \right) + \dots \quad (5.4.57)$$

These derivatives are numerically calculated by the Runge-Kutta scheme, giving

$$\alpha = 2.7671 - 0.0525 Ra_S + O(Ra_S^2). \quad (5.4.58)$$

These estimates for α_0 and α_1 are compared to the Galerkin approach for the full problem and are shown in table 5.4. The agreement for α_0 is good at all levels but the estimate of α_1 only gives a reasonable agreement with the asymptotic prediction.

N	α_0	α_1
24	2.7670180	0.1092931
48	2.7670166	-0.0283445
72	2.7670166	-0.0543947
96	2.7670160	-0.0550332

Table 5.4: These estimates of α_0 and α_1 for different values of N are calculated by the Galerkin approach based on the results for $Ra_S = 0.01$ and 0.001 .

Finally, the comparison of the asymptotic results and the full results found by the Galerkin approach is shown in figure 5.24. This shows good agreement between the asymptotic and full results for small Ra_S . We would expect to see oscillatory solutions for Ra_S greater than 2 which has already been discussed in chapter 4.

We have now identified and analysed the four different asymptotic regimes on the stability boundary.

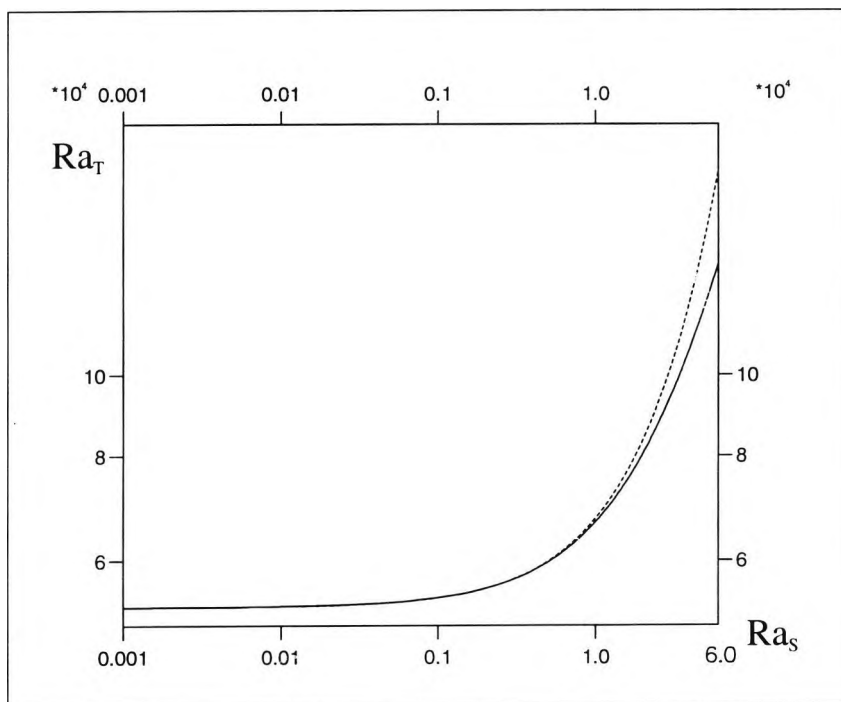


Figure 5.24: A comparison of the asymptotic behaviour (solid line) and the full results (dashed line) for the small Ra_s limit, indicating good agreement.

Chapter 6

Conclusion

We have investigated the linear stability of a stable, salt-stratified fluid confined in an infinite vertical slot subject to a lateral temperature difference between the two boundaries. This problem has previously been examined experimentally and theoretically for the case of a strong salinity gradient. The present work focuses on the marginal stability curve reported by Thangam, Zebib & Chen (1981) where several different stability boundaries, representing the numerical solutions of both stationary and oscillatory branches are given in the Ra_S - Ra_T plane. We did not reproduce their results but found their oscillatory solutions are erroneous in the region where Ra_S lies between 0.45 and 10. Our results have shown that in the region of $0.45 < Ra_S < 2.0256$ the initial instability is steady. This region is then joined by the curved section with oscillatory instability between $Ra_S = 2.0256$ and $Ra_S = 4.7703$. The next part of the boundary is almost vertical, sweeping down to a minimum near $Ra_S = 10$. Along this point of the boundary the initial instabilities are steady.

Two independent numerical schemes are used in our investigation to provide confirmation of the difference between our results and those of Thangam *et al.* The error in the earlier results was later verified by Young & Rosner

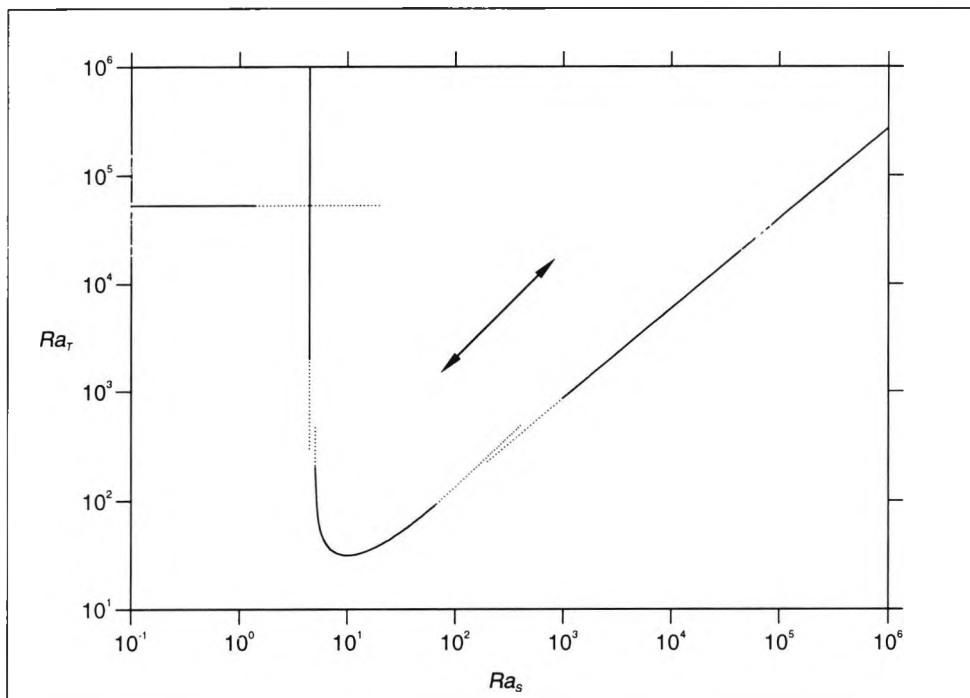


Figure 6.1: A schematic diagram showing the four different leading order asymptotic regimes considered here for $Pr = 6.7$ and $\tau = 0.01$. The position of the horizontal boundary at the left is a function of Pr . The other three boundaries move together in unison in the diagonal direction as τ varies. The oscillatory branch of instabilities is not shown.

(1998) in their recent publication with slightly different parameters. There is good indication that Thangam *et al.* did not use sufficient resolution in their Galerkin method and hence the solutions were underresolved for both the oscillatory and small Ra_S regions. One of the strengths of the Galerkin method is that it can produce solutions to difficult problems where, say, the Runge-Kutta method fails but its drawback is that it can produce plausible incorrect solutions.

We have identified four different asymptotic regimes for the stability boundaries. The leading order positions of these are shown in figure 6.1. These asymptotic results are also compared with those obtained numerically from the full problem with good agreement. Three of the asymptotic analyses are not previously found, the exception being the asymptotic limit of large Ra_S (Thorpe, Platt & Soulsby, 1969). Some possible physical explanations are

given for the observed stability characteristics of the four regimes. In the large Ra_S regime, the instabilities take the form of thin almost horizontal layers whose vertical scale is given by the Chen scale (Chen, Briggs & Wirtz, 1971). The mechanistic argument by Kerr (1989) for sidewall heating can also be applied to the instabilities in this regime, and the non-dimensional parameter Q which depends on the Chen scale and the width of the slot is the appropriate parameter for determining stability. Both length scales for the diffusion of temperature and salinity perturbations are the same and so both the temperature and salinity are important in the leading order behaviour for general Lewis number, τ . In the small wave number regime and the large Ra_T regime, the two length scales for diffusion of heat and salt are different. Heat diffuses on the scale of the slot width, while salt diffuses on the vertical scale of the instabilities. This scale is much larger than the slot width in these two regions. Since the time scale for the diffusion of salt is much greater than that of the heat the temperature perturbations diffuse away and are not important in the asymptotic analysis. The leading order dynamics only involve the interaction between the stream function and the salinity concentration.

One interesting part of the marginal stability boundary is covered in the large Ra_T regime. The instability in this regime is driven by the horizontal salinity gradient and stabilised by the vertical shear. Since this boundary is vertical in the Ra_S - Ra_T plane it may seem that it would play no significant role in real experiments where Ra_S is determined by the initial setup of an experiment. However, heat would in fact take some time to diffuse across the slot before establishing a linear horizontal temperature gradient. If the wall temperature is raised quickly then the effective instantaneous Rayleigh numbers will be governed by the distance that the heat has diffused into the fluid and not the slot width. Therefore, Ra_T will initially grow like $t^{3/2}$ and

Ra_S like t^2 where t is the time since the onset of heating. Thus the instantaneous values of Ra_T and Ra_S may evolve in such a way that they may cross the vertical boundary. In such cases the initial instability observed in experiments may be related to the instabilities on this portion of the boundary and not to those that may be anticipated from the final values of the Rayleigh numbers. Of course, the details of the instabilities and the stability boundary will be different in the evolving case than those found here for the steady background gradients and vertical velocity. However, one implication of this for experimenters is that in order to understand the instabilities observed it may be important to record not only the final Ra_T and Ra_S , but how the instantaneous values of the Rayleigh numbers evolved to this final state and their values when instabilities first appeared.

The need to monitor the evolution of Ra_T and Ra_S is also required in experiments where a salinity gradient is heated from a single vertical boundary. In these situations there are no steady background states (Kerr, 1991). In Tanny & Tsinober (1988) the evolving salt and thermal Rayleigh numbers were traced in their single boundary experiments as outlined above. The values of these Rayleigh numbers at the onset of instability are consistent with a stability boundary whose shape is similar to that of a vertical slot, with the vertical portion of the boundary playing an important role. Although the number of their experiments in this regime are not great and concentrated around the lower end of where the vertical boundary would be found. The testing of whether this boundary is vertical experimentally may be difficult as it would require rates of wall temperature increase much greater than Tanny & Tsinober were able to achieve. The destabilising salinity gradient and stabilising shear may provide insight into the first appearance of instabilities. The presence of transient vertical motions near the heated wall when there

was rapid heating was reported by Schladow, Thomas & Koseff (1992). The onset of instabilities could be associated with times when these initial velocities reduce in magnitude, thus reducing the stabilising effect of the shear. An investigation of this would be an interesting area for further research.

Our results have shown that the three stability boundaries in a slot represented by the asymptotic limits of large Ra_S , small wave number and large Ra_T are determined by the salt/heat diffusivity ratio, τ , for their positions in the $(\log - Ra_S, \log - Ra_T)$ plane. In the limit $\tau \rightarrow 0$ the curves in each case can be written in the form

$$F(Ra_T/\tau, Ra_S/\tau) = 0. \quad (6.1)$$

As τ varies, the positions of these three boundaries would move together in unison. This is illustrated schematically in figure 6.1 where the solid lines show the regions of the appropriate asymptotic regimes and the dashed lines showing their continuations. The arrow indicates the direction these three boundaries move in as τ varies. In the small Ra_S regime, the salinity gradient is weak and so this regime is essentially the thermally driven problem of a laterally heated slot. For Prandtl number, Pr , less than 12.7, Korpela, Gözüüm & Baxi (1973) showed that the initial instability is steady and the leading order result takes the form of $Ra_T = 7880 Pr$ (Vest & Arpaci, 1969). Hence, the position of this stability boundary for small Ra_S depends on the Prandtl number. For larger values of the Prandtl number, the initial instability is oscillatory and so the analysis included here is not appropriate.

The asymptotics given here cover most of the cases for marginal instabilities in a vertical slot. The small curved section that describes oscillatory instability is indicated by a dashed line on the marginal stability boundary of figure 5.1 for the case of water and common salt considered here. Young &

Rosner (1998) used three different values of τ , 0.1, 0.01 and 0.001. The size of the oscillatory region on the stability boundary did not change much with these changes in the parameter. Unfortunately, this oscillatory region does not seem to have an identifiable asymptotic behaviour and so its position on the stability boundary cannot be given in the same manner as other regimes for general values of τ and Pr . One possible interpretation of the origin of these oscillatory instabilities is that for $Pr < 12.7$ the instabilities are steady in a laterally heated slot with no salinity gradient, but for large Pr the onset of instabilities is oscillatory. Our analysis suggests that steady instability is stabilised by the salinity gradient but we could speculate that the oscillatory instability is destabilised. With Pr just below 12.7, it is possible that salinity gradient could make the oscillatory mode of instability more unstable than the mode of steady stability. This scenario seems to be appropriate based on some recent calculations by Kerr (private communication), and could be the subject of further examination.

The shape of the marginal stability curve reveals two important conditions for instability to occur in any given stratified solute. These conditions are based on how large are the salinity stratification and the temperature difference across the vertical slot. But as τ gets smaller, the two conditions become less stringent. For instance, if salt was replaced by protein as the solute in the slot problem then τ could be reduced by a hundredfold and so the temperature difference across the boundaries that could start convection would be a hundred times less than that necessary for stratification due to common salt. In the absence of any solute stratification, the heating required for the onset of cellular convection would be 100 000 more than that required for a protein gradient. The minimum temperature difference needed to cause convection with a vertical protein gradient could be as little as 10^{-4} °C in a

slot of width 1 cm, and so it is likely one would observe convection in the presence of any stratification, unless great care is taken to ensure a uniform temperature.

This analysis with the assumption of a steady state in an infinite channel cannot be applied extensively in all practical situations because channels have upper and lower ends. These impermeable ends will result in a background state that evolves with time even when no temperature difference is considered, although the slow diffusivity of salt does mean that the time for disturbances to diffuse from the end walls is long. However, it will always be difficult to solve the slot problem around these end regions both experimentally and analytically. The present analysis would be useful to the understanding of the core of a vertical cavity where the end effects are less important. Another possible problem with finite cavities is the limitation on the vertical wave number of instabilities. The limit of $\alpha \rightarrow 0$ implies disturbances of unbounded height. The heating required to develop convection cells of small but finite wave number is close to that found in the small α limit. The stability curves are shown to be very flat in figure 3.1 of chapter 3 for the $\alpha \rightarrow 0$ limit so convection would occur on a wide range of scales and so the small α limit is not too restrictive.

The work of this thesis has corrected some earlier erroneous results on the double-diffusive instabilities in a vertical slot. In addition, we hope it has shed some new light on the different modes of instability that make up the stability boundary which may open up new avenues for research into the problem of double-diffusive instabilities at a single boundary.

I am grateful to my supervisor, Dr. Oliver S. Kerr, who has unstintingly

helped to produce a joint paper based on this work entitled “ Double-diffusive instabilities in a vertical slot” which has recently been accepted for publication in the Journal of Fluid Mechanics.

Appendix A

Full Numerical Method

This appendix is related to chapter 3. The details in finding solutions to the full problem by the shooting method are given here. We propose to solve the full stability equations in (2.10.2) to (2.10.5) numerically using a fourth order Runge-Kutta scheme. The stream function, temperature and salinity are written in terms of their real and imaginary parts:

$$\psi(x) = \psi_r + i\psi_i, \quad T(x) = T_r + iT_i, \quad S(x) = S_r + iS_i. \quad (\text{A.1})$$

These x -dependent variables are substituted into the full problem where $\sigma_i = 0$ for steady instabilities. The real part of the system is

$$(D^2 - \alpha^2)^2\psi_r + \frac{\alpha}{Pr} \left\{ \bar{w}_o(D^2 - \alpha^2)\psi_i - D^2\bar{w}_o\psi_i \right\} - Ra_T DT_r + Ra_S DS_r = 0, \quad (\text{A.2})$$

$$(D^2 - \alpha^2)T_r - \alpha(\psi_i - \bar{w}_o T_i) = 0, \quad (\text{A.3})$$

$$\tau(D^2 - \alpha^2)S_r + \alpha\psi_i D\bar{S}_o + \alpha\bar{w}_o S_i - D\psi_r = 0, \quad (\text{A.4})$$

and the imaginary part gives

$$(D^2 - \alpha^2)^2\psi_i - \frac{\alpha}{Pr} \left\{ \bar{w}_o(D^2 - \alpha^2)\psi_r - D^2\bar{w}_o\psi_r \right\} - Ra_T DT_i + Ra_S DS_i = 0, \quad (\text{A.5})$$

$$(D^2 - \alpha^2)T_i + \alpha(\psi_r - \bar{w}_o T_r) = 0, \quad (\text{A.6})$$

$$\tau(D^2 - \alpha^2)S_i - \alpha\psi_r \overline{DS_o} - \alpha\overline{w_o}S_r - D\psi_i = 0, \quad (\text{A.7})$$

with the corresponding boundary conditions

$$\psi_r = \psi_i = D\psi_r = D\psi_i = DS_r = DS_i = T_r = T_i = 0 \quad \text{on} \quad x = \pm 1/2. \quad (\text{A.8})$$

To apply the Runge-Kutta scheme the higher order differential equations of the system are expressed in terms of first-order equations so that the numerical scheme solves $D\mathbf{y} = f(x, \mathbf{y})$ where \mathbf{y} is a vector representing the 16 elements in the full problem. To illustrate the idea, we shall write out the 16 elements in terms of y_1, \dots, y_{16} for (A.2) to (A.8). The stream function elements are

$$\begin{aligned} y_1 &= \psi_r & y_2 &= \psi_i, \\ y_3 &= D\psi_r = Dy_1, & y_4 &= D\psi_i = Dy_2, \\ y_5 &= D^2\psi_r = Dy_3, & y_6 &= D^2\psi_i = Dy_4, \\ y_7 &= D^3\psi_r = Dy_5, & y_8 &= D^3\psi_i = Dy_6, \end{aligned} \quad (\text{A.9})$$

the salinity elements are:

$$\begin{aligned} y_9 &= S_r & y_{10} &= S_i, \\ y_{11} &= DS_r = Dy_9, & y_{12} &= DS_i = Dy_{10}, \end{aligned} \quad (\text{A.10})$$

and the temperature elements are:

$$\begin{aligned} y_{13} &= T_r & y_{14} &= T_i, \\ y_{15} &= DT_r = Dy_{13}, & y_{16} &= DT_i = Dy_{14}, \end{aligned} \quad (\text{A.11})$$

with the boundary conditions

$$y_1 = y_2 = y_3 = y_4 = y_{11} = y_{12} = y_{13} = y_{14} = 0, \quad (\text{A.12})$$

on $x = \pm 1/2$. The above elements, y_1, \dots, y_{16} , are used to define the following 16 functions:

$$f_1 = y_3, \quad (\text{A.13})$$

$$f_2 = y_4, \quad (\text{A.14})$$

$$f_3 = y_5, \quad (\text{A.15})$$

$$f_4 = y_6, \quad (\text{A.16})$$

$$f_5 = y_7, \quad (\text{A.17})$$

$$f_6 = y_8, \quad (\text{A.18})$$

$$f_7 = 2\alpha^2 y_5 - \alpha^4 y_1 - \frac{\alpha}{Pr} \bar{w}_o y_6 + \frac{\alpha^3 \bar{w}_o}{Pr} y_2 + \frac{\alpha}{Pr} y_2 D^2 \bar{w}_o + Ra_T y_{15} - Ra_S y_{11}, \quad (\text{A.19})$$

$$f_8 = 2\alpha^2 y_6 - \alpha^4 y_2 + \frac{\alpha}{Pr} \bar{w}_o y_5 - \frac{\alpha^3 \bar{w}_o}{Pr} y_1 - \frac{\alpha}{Pr} y_1 D^2 \bar{w}_o + Ra_T y_{16} - Ra_S y_{12}, \quad (\text{A.20})$$

$$f_9 = y_{11}, \quad (\text{A.21})$$

$$f_{10} = y_{12}, \quad (\text{A.22})$$

$$f_{11} = \alpha^2 y_9 - \frac{1}{\tau} [\alpha D \bar{S}_o y_2 + \alpha \bar{w}_o y_{10} - y_3], \quad (\text{A.23})$$

$$f_{12} = \alpha^2 y_{10} + \frac{1}{\tau} [\alpha D \bar{S}_o y_1 + \alpha \bar{w}_o y_9 + y_4], \quad (\text{A.24})$$

$$f_{13} = y_{15}, \quad (\text{A.25})$$

$$f_{14} = y_{16}, \quad (\text{A.26})$$

$$f_{15} = \alpha^2 y_{13} + \alpha y_2 - \alpha \bar{w}_o y_{14}, \quad (\text{A.27})$$

$$f_{16} = \alpha^2 y_{14} - \alpha y_1 + \alpha \bar{w}_o y_{13}. \quad (\text{A.28})$$

These 16 functions are used in the four-stage formula of (3.1.1) with step size taken to be $dx = 5 \times 10^{-4}$ across the interval $x = -1/2$ to $x = 1/2$. We need to specify the choice of boundary conditions on the left wall so that solutions obtained will satisfy the boundary conditions on the right wall. This can be achieved by using the iterative process of the shooting method. This uses matrix manipulation to get the first six boundary conditions to zero before satisfying the last two boundary conditions by varying the physical parameters of the problem using the secant method.

We shall first specify the choice of the boundary conditions on the left

wall. Since the problem is linear and $\psi = T = S = 0$ is always a solution, we can force a non-zero solution if we set $D^2\psi = 1$. Therefore the 8 fixed boundary conditions on $x = -1/2$ are

$$\begin{aligned} y_1 &= 0, & y_2 &= 0, \\ y_3 &= 0, & y_4 &= 0, \\ y_{11} &= 0, & y_{12} &= 0, \\ y_{13} &= 0, & y_{14} &= 0, \end{aligned} \tag{A.29}$$

leaving the choices for others to be

$$\begin{aligned} y_5 &= 1, & y_6 &= 0, \\ y_7 &= u_1, & y_8 &= u_2, \\ y_9 &= u_3, & y_{10} &= u_4, \\ y_{15} &= u_5, & y_{16} &= u_6, \end{aligned} \tag{A.30}$$

where u_1, \dots, u_6 are the 6 free boundary conditions on the left wall to be determined. If we integrate across the slot for some choice of our free u_i we determine the values of y_i at the right boundary, say v_1, \dots, v_{16} . For fixed $Ra_S, Ra_T, \alpha, \tau, Pr$ and σ_i these depend on the free u_i according to

$$\mathbf{P}' = A'\mathbf{u} + \mathbf{z}', \tag{A.31}$$

where

$$\mathbf{P}'(\mathbf{u}) = (v_1, v_2, \dots, v_{16})^t, \tag{A.32}$$

$$\mathbf{u} = (u_1, u_2, \dots, u_6)^t, \tag{A.33}$$

$$\mathbf{z}' = (z_1, z_2, \dots, z_{16})^t, \tag{A.34}$$

Here A' and \mathbf{z}' are a matrix and vector whose entries are not yet determined. We will restrict ourselves, say, to the first 6 of the right boundary conditions that we require to be zero, defining

$$\mathbf{P}(\mathbf{u}) = A\mathbf{u} + \mathbf{z}, \tag{A.35}$$

where

$$\mathbf{P} = (v_1, v_2, v_3, v_4, v_{11}, v_{12})^t, \quad (\text{A.36})$$

$$\mathbf{z} = (z_1, z_2, z_3, z_4, z_{11}, z_{12})^t, \quad (\text{A.37})$$

and A is a (6×6) matrix representing the coefficient of the vector \mathbf{u} . We can vary the values of \mathbf{u} to find both the vector \mathbf{z} and matrix A . From (A.35) we see $\mathbf{z} = \mathbf{P}(\mathbf{0})$. Then by further setting $u_i = 1$ with the other $u_j = 0$ for $i = 1, \dots, 6$ in turn, we can determine all the matrix elements in A .

In principle we can now find \mathbf{u} that sets $\mathbf{P}(\mathbf{u})$ to zero by solving

$$\mathbf{u} = -A^{-1}\mathbf{z}. \quad (\text{A.38})$$

However, calculations showed that on calculating $\mathbf{P}(\mathbf{0})$ very large terms were found which resulted in significant rounding errors and loss of accuracy. Instead this method was adapted to use an initial guess for \mathbf{u} , say \mathbf{u}_o , which may be provided by the above method. If we let

$$\mathbf{z} = \mathbf{P}(\mathbf{u}_o), \quad (\text{A.39})$$

then we use calculations of $\mathbf{P}(\mathbf{u}_o + \delta\mathbf{u})$ to estimate the matrix A in a similar manner as before such that

$$\mathbf{P}(\mathbf{u}_o + \delta\mathbf{u}) = A\delta\mathbf{u} + \mathbf{z}. \quad (\text{A.40})$$

Then

$$\delta\mathbf{u} = -A^{-1}\mathbf{z}. \quad (\text{A.41})$$

This then gave a better estimate for $\mathbf{u} = \mathbf{u}_o + \delta\mathbf{u}$ that sets the right boundary conditions to zero.

When looking at the steady case the symmetry of the problem ensures that if we can set one of the remaining right boundary conditions to zero the

other condition becomes zero at the same time. Thus for the steady case we set one of the conditions to zero using the secant method. This method is based on drawing a straight line between two good guesses of Ra_T , namely Ra_{T_1} and Ra_{T_2} , and getting a better guess given by

$$Ra_T = \frac{v(Ra_{T_2})Ra_{T_1} - v(Ra_{T_1})Ra_{T_2}}{v(Ra_{T_2}) - v(Ra_{T_1})}. \quad (\text{A.42})$$

where the boundary condition v is a function of the Rayleigh number Ra_T . When converged this value of Ra_T will produce steady solutions that set the two remaining right boundary conditions to zero (strictly speaking, they cannot be identically zero therefore the iterative process depends on the choice of tolerance level, a choice of say, tolerance = 1×10^{-8} seems sufficient for obtaining accurate solutions in most cases).

When the problem with $\sigma_i \neq 0$ is considered then Broyden's algorithm of chapter 3 is substituted in place of the secant method.

The marginal state can be determined by fitting a parabola to three solutions and using this to give an estimate of the minimum. This parabola technique depends on three paired guesses of Ra_T and α which give the approximate equation

$$Ra_T \approx A * Ra_{T_1} + B * Ra_{T_2} + C * Ra_{T_3}, \quad (\text{A.43})$$

where A , B , C are functions of α defined by

$$A = \frac{(\alpha - \alpha_2)(\alpha - \alpha_3)}{(\alpha_1 - \alpha_2)(\alpha_1 - \alpha_3)}, \quad (\text{A.44})$$

$$B = \frac{(\alpha - \alpha_1)(\alpha - \alpha_3)}{(\alpha_2 - \alpha_1)(\alpha_2 - \alpha_3)}, \quad (\text{A.45})$$

$$C = \frac{(\alpha - \alpha_1)(\alpha - \alpha_2)}{(\alpha_3 - \alpha_1)(\alpha_3 - \alpha_2)}. \quad (\text{A.46})$$

Differentiating (A.43) with respect to α and solving to find where the gradient is zero gives an estimate of the critical value of Ra_T at this lowest point and the corresponding α_m which is

$$\alpha_m = \frac{Ra_{T_1}(\alpha_2^2 - \alpha_3^2) + Ra_{T_2}(\alpha_3^2 - \alpha_1^2) + Ra_{T_3}(\alpha_1^2 - \alpha_2^2)}{2[Ra_{T_1}(\alpha_2 - \alpha_3) + Ra_{T_2}(\alpha_3 - \alpha_1) + Ra_{T_3}(\alpha_1 - \alpha_2)]}. \quad (\text{A.47})$$

This estimate can be used to give an iterative scheme which converges to the true minimum.

For any given value of Ra_S , this scheme gives the minimum value of Ra_T with the corresponding α . When the stability boundary becomes parallel to the vertical axis, this scheme breaks down. In this case we fix Ra_T instead of Ra_S and look for a minimum value of Ra_S with the corresponding α .

It is unfortunate that oscillatory modes could not be found using this numerical scheme with Broyden's algorithm (see the accompanied section of chapter 3). But on the other hand, it was able to provide confirmation of some non-steady solutions that were found by the Galerkin method.

Appendix B

Galerkin Approach

This appendix will be divided into 5 sections for the purpose of evaluating those integrals from the linear system of algebraic equations (4.1.12), (4.1.13) and (4.1.38) to (4.1.41) in chapter 4. The relevant background states are those obtained in chapter 2.

The first section gives details about the orthogonal properties of the functions used in the expansions of the stream function, temperature and salinity in (4.1.1) to (4.1.3). The next three sections respectively give the 24 integrals for ψ , the 8 integrals for T and the 12 integrals for S . The final section contains the general expressions of those 'abbreviated integrals', e.g. $P1a(a, b)$, $S2i(a, b)$, $T3b(a, b, c, d)$ and so on. These integrals are found in the last three sections. For example, integral H_1 in the second section involves $P1a(\mu_{2m-1}, \mu_{2m-1})$, the definition of $P1a$ contains two arbitrary parameters a and b and these are replaced by the appropriate values of μ as required in the integration.

B.1 Orthogonal Properties

For the stream function:

$$\int_{-1/2}^{1/2} \psi_{2m-1}^2 dx = 1, \quad (\text{B.1.1})$$

$$\int_{-1/2}^{1/2} \psi_{2m-1} \psi_{2n-1} dx = 0 \quad (n \neq m), \quad (\text{B.1.2})$$

$$\int_{-1/2}^{1/2} \psi_{2m}^2 dx = 1, \quad (\text{B.1.3})$$

$$\int_{-1/2}^{1/2} \psi_{2m} \psi_{2n} dx = 0 \quad (n \neq m), \quad (\text{B.1.4})$$

and

$$\int_{-1/2}^{1/2} \psi_{2m-1} \psi_{2n} dx = 0 \quad (\forall n, m). \quad (\text{B.1.5})$$

For the temperature:

$$\int_{-1/2}^{1/2} T_{2m-1}^2 dx = \frac{1}{2}, \quad (\text{B.1.6})$$

$$\int_{-1/2}^{1/2} T_{2m-1} T_{2n-1} dx = 0 \quad (n \neq m), \quad (\text{B.1.7})$$

$$\int_{-1/2}^{1/2} T_{2m}^2 dx = \frac{1}{2}, \quad (\text{B.1.8})$$

$$\int_{-1/2}^{1/2} T_{2m} T_{2n} dx = 0 \quad (n \neq m), \quad (\text{B.1.9})$$

and

$$\int_{-1/2}^{1/2} T_{2m-1} T_{2n} dx = 0 \quad (\forall n, m). \quad (\text{B.1.10})$$

For the salinity:

$$\int_{-1/2}^{1/2} S_{2m-1}^2 dx = \frac{1}{2}, \quad (\text{B.1.11})$$

$$\int_{-1/2}^{1/2} S_{2m-1} S_{2n-1} dx = 0 \quad (n \neq m), \quad (\text{B.1.12})$$

$$\int_{-1/2}^{1/2} S_{2m}^2 dx = \frac{1}{2}, \quad (\text{B.1.13})$$

$$\int_{-1/2}^{1/2} S_{2m} S_{2n} dx = 0 \quad (n \neq m), \quad (\text{B.1.14})$$

and

$$\int_{-1/2}^{1/2} S_{2m-1} S_{2n} dx = 0 \quad (\forall n, m). \quad (\text{B.1.15})$$

B.2 Integrals for ψ

The parameters μ_{2n-1} and μ_{2n} are the positive roots of the integrals of ψ , T and S :

$$\tanh \frac{1}{2}\mu_{2n-1} + \tan \frac{1}{2}\mu_{2n-1} = 0, \quad (\text{B.2.1})$$

$$\coth \frac{1}{2}\mu_{2n} - \cot \frac{1}{2}\mu_{2n} = 0, \quad (\text{B.2.2})$$

and the parameter M is given by

$$M = \left(\frac{Ra_S}{4\tau} \right)^{1/4}. \quad (\text{B.2.3})$$

For the integrals involving the even function in ψ :

$$\begin{aligned} H_1 &= \int_{-1/2}^{1/2} \left(\frac{\cosh \mu_{2m-1}x}{\cosh \frac{1}{2}\mu_{2m-1}} + \frac{\cos \mu_{2m-1}x}{\cos \frac{1}{2}\mu_{2m-1}} \right) \left(\frac{\cosh \mu_{2m-1}x}{\cosh \frac{1}{2}\mu_{2m-1}} - \frac{\cos \mu_{2m-1}x}{\cos \frac{1}{2}\mu_{2m-1}} \right) dx \\ &= \frac{P1a(\mu_{2m-1}, \mu_{2m-1})}{\cosh^2 \frac{1}{2}\mu_{2m-1}} - \frac{S2i(\mu_{2m-1}, \mu_{2m-1})}{\cos^2 \frac{1}{2}\mu_{2m-1}}. \end{aligned} \quad (\text{B.2.4})$$

$$\begin{aligned} H_2 &= \int_{-1/2}^{1/2} \bar{w}_o \left(\frac{\sinh \mu_{2m}x}{\sinh \frac{1}{2}\mu_{2m}} + \frac{\sin \mu_{2m}x}{\sin \frac{1}{2}\mu_{2m}} \right) \left(\frac{\cosh \mu_{2m-1}x}{\cosh \frac{1}{2}\mu_{2m-1}} - \frac{\cos \mu_{2m-1}x}{\cos \frac{1}{2}\mu_{2m-1}} \right) dx \\ &= \frac{Ra_T \sinh \frac{1}{2}M \cos \frac{1}{2}M P3ef(M, M, \mu_{2m}, \mu_{2m-1})}{M^3(\sin M + \sinh M) \sinh \frac{1}{2}\mu_{2m} \cosh \frac{1}{2}\mu_{2m-1}} \\ &\quad - \frac{Ra_T \cosh \frac{1}{2}M \sin \frac{1}{2}M P4ef(M, M, \mu_{2m}, \mu_{2m-1})}{M^3(\sin M + \sinh M) \sinh \frac{1}{2}\mu_{2m} \cosh \frac{1}{2}\mu_{2m-1}} \\ &\quad - \frac{Ra_T \sinh \frac{1}{2}M \cos \frac{1}{2}M S2cd(\mu_{2m}, M, M, \mu_{2m-1})}{M^3(\sin M + \sinh M) \sinh \frac{1}{2}\mu_{2m} \cos \frac{1}{2}\mu_{2m-1}} \\ &\quad + \frac{Ra_T \cosh \frac{1}{2}M \sin \frac{1}{2}M P5de(M, M, \mu_{2m}, \mu_{2m-1})}{M^3(\sin M + \sinh M) \sinh \frac{1}{2}\mu_{2m} \cos \frac{1}{2}\mu_{2m-1}} \\ &\quad + \frac{Ra_T \sinh \frac{1}{2}M \cos \frac{1}{2}M P6de(M, M, \mu_{2m}, \mu_{2m-1})}{M^3(\sin M + \sinh M) \sin \frac{1}{2}\mu_{2m} \cosh \frac{1}{2}\mu_{2m-1}} \\ &\quad - \frac{Ra_T \cosh \frac{1}{2}M \sin \frac{1}{2}M S2cd(M, \mu_{2m}, \mu_{2m-1}, M)}{M^3(\sin M + \sinh M) \sin \frac{1}{2}\mu_{2m} \cosh \frac{1}{2}\mu_{2m-1}} \end{aligned}$$

$$\begin{aligned}
& - \frac{Ra_T \sinh \frac{1}{2}M \cos \frac{1}{2}M T3b(M, M, \mu_{2m}, \mu_{2m-1})}{M^3(\sin M + \sinh M) \sin \frac{1}{2}\mu_{2m} \cos \frac{1}{2}\mu_{2m-1}} \\
& + \frac{Ra_T \cosh \frac{1}{2}M \sin \frac{1}{2}M T3c(M, M, \mu_{2m}, \mu_{2m-1})}{M^3(\sin M + \sinh M) \sin \frac{1}{2}\mu_{2m} \cos \frac{1}{2}\mu_{2m-1}}. \tag{B.2.5}
\end{aligned}$$

$$\begin{aligned}
H_3 &= \int_{-1/2}^{1/2} \frac{1}{\bar{w}_o} \left(\frac{\sinh \mu_{2m}x}{\sinh \frac{1}{2}\mu_{2m}} - \frac{\sin \mu_{2m}x}{\sin \frac{1}{2}\mu_{2m}} \right) \left(\frac{\cosh \mu_{2m-1}x}{\cosh \frac{1}{2}\mu_{2m-1}} - \frac{\cos \mu_{2m-1}x}{\cos \frac{1}{2}\mu_{2m-1}} \right) dx \\
&= \frac{Ra_T \sinh \frac{1}{2}M \cos \frac{1}{2}M P3ef(M, M, \mu_{2m}, \mu_{2m-1})}{M^3(\sin M + \sinh M) \sinh \frac{1}{2}\mu_{2m} \cosh \frac{1}{2}\mu_{2m-1}} \\
& - \frac{Ra_T \cosh \frac{1}{2}M \sin \frac{1}{2}M P4ef(M, M, \mu_{2m}, \mu_{2m-1})}{M^3(\sin M + \sinh M) \sinh \frac{1}{2}\mu_{2m} \cosh \frac{1}{2}\mu_{2m-1}} \\
& - \frac{Ra_T \sinh \frac{1}{2}M \cos \frac{1}{2}M S2cd(\mu_{2m}, M, M, \mu_{2m-1})}{M^3(\sin M + \sinh M) \sinh \frac{1}{2}\mu_{2m} \cos \frac{1}{2}\mu_{2m-1}} \\
& + \frac{Ra_T \cosh \frac{1}{2}M \sin \frac{1}{2}M P5de(M, M, \mu_{2m}, \mu_{2m-1})}{M^3(\sin M + \sinh M) \sinh \frac{1}{2}\mu_{2m} \cos \frac{1}{2}\mu_{2m-1}} \\
& - \frac{Ra_T \sinh \frac{1}{2}M \cos \frac{1}{2}M P6de(M, M, \mu_{2m}, \mu_{2m-1})}{M^3(\sin M + \sinh M) \sin \frac{1}{2}\mu_{2m} \cosh \frac{1}{2}\mu_{2m-1}} \\
& + \frac{Ra_T \cosh \frac{1}{2}M \sin \frac{1}{2}M S2cd(M, \mu_{2m}, \mu_{2m-1}, M)}{M^3(\sin M + \sinh M) \sin \frac{1}{2}\mu_{2m} \cosh \frac{1}{2}\mu_{2m-1}} \\
& + \frac{Ra_T \sinh \frac{1}{2}M \cos \frac{1}{2}M T3b(M, M, \mu_{2m}, \mu_{2m-1})}{M^3(\sin M + \sinh M) \sin \frac{1}{2}\mu_{2m} \cos \frac{1}{2}\mu_{2m-1}} \\
& - \frac{Ra_T \cosh \frac{1}{2}M \sin \frac{1}{2}M T3c(M, M, \mu_{2m}, \mu_{2m-1})}{M^3(\sin M + \sinh M) \sin \frac{1}{2}\mu_{2m} \cos \frac{1}{2}\mu_{2m-1}}. \tag{B.2.6}
\end{aligned}$$

$$\begin{aligned}
H_4 &= \int_{-1/2}^{1/2} D^2 \bar{w}_o \left(\frac{\sinh \mu_{2m}x}{\sinh \frac{1}{2}\mu_{2m}} - \frac{\sin \mu_{2m}x}{\sin \frac{1}{2}\mu_{2m}} \right) \left(\frac{\cosh \mu_{2m-1}x}{\cosh \frac{1}{2}\mu_{2m-1}} - \frac{\cos \mu_{2m-1}x}{\cos \frac{1}{2}\mu_{2m-1}} \right) dx \\
&= \frac{2Ra_T \sinh \frac{1}{2}M \cos \frac{1}{2}M P4ef(M, M, \mu_{2m}, \mu_{2m-1})}{M(\sin M + \sinh M) \sinh \frac{1}{2}\mu_{2m} \cosh \frac{1}{2}\mu_{2m-1}} \\
& + \frac{2Ra_T \cosh \frac{1}{2}M \sin \frac{1}{2}M P3ef(M, M, \mu_{2m}, \mu_{2m-1})}{M(\sin M + \sinh M) \sinh \frac{1}{2}\mu_{2m} \cosh \frac{1}{2}\mu_{2m-1}}
\end{aligned}$$

$$\begin{aligned}
& - \frac{2Ra_T \sinh \frac{1}{2}M \cos \frac{1}{2}M P5de(M, M, \mu_{2m}, \mu_{2m-1})}{M(\sin M + \sinh M) \sinh \frac{1}{2}\mu_{2m} \cos \frac{1}{2}\mu_{2m-1}} \\
& - \frac{2Ra_T \cosh \frac{1}{2}M \sin \frac{1}{2}M S2cd(\mu_{2m}, M, M, \mu_{2m-1})}{M(\sin M + \sinh M) \sinh \frac{1}{2}\mu_{2m} \cos \frac{1}{2}\mu_{2m-1}} \\
& - \frac{2Ra_T \sinh \frac{1}{2}M \cos \frac{1}{2}M S2cd(M, \mu_{2m}, \mu_{2m-1}, M)}{M(\sin M + \sinh M) \sin \frac{1}{2}\mu_{2m} \cosh \frac{1}{2}\mu_{2m-1}} \\
& - \frac{2Ra_T \cosh \frac{1}{2}M \sin \frac{1}{2}M P6de(M, M, \mu_{2m}, \mu_{2m-1})}{M(\sin M + \sinh M) \sin \frac{1}{2}\mu_{2m} \cosh \frac{1}{2}\mu_{2m-1}} \\
& + \frac{2Ra_T \sinh \frac{1}{2}M \cos \frac{1}{2}M T3c(M, M, \mu_{2m}, \mu_{2m-1})}{M(\sin M + \sinh M) \sin \frac{1}{2}\mu_{2m} \cos \frac{1}{2}\mu_{2m-1}} \\
& + \frac{2Ra_T \cosh \frac{1}{2}M \sin \frac{1}{2}M T3b(M, M, \mu_{2m}, \mu_{2m-1})}{M(\sin M + \sinh M) \sin \frac{1}{2}\mu_{2m} \cos \frac{1}{2}\mu_{2m-1}}. \tag{B.2.7}
\end{aligned}$$

$$\begin{aligned}
H_5 &= \int_{-1/2}^{1/2} \cos(2m)\pi x \left(\frac{\cosh \mu_{2m-1}x}{\cosh \frac{1}{2}\mu_{2m-1}} - \frac{\cos \mu_{2m-1}x}{\cos \frac{1}{2}\mu_{2m-1}} \right) dx \\
&= \frac{S2a(\mu_{2m-1}, 2m\pi)}{\cosh \frac{1}{2}\mu_{2m-1}} - \frac{S2i(2m\pi, \mu_{2m-1})}{\cos \frac{1}{2}\mu_{2m-1}}. \tag{B.2.8}
\end{aligned}$$

$$\begin{aligned}
H_6 &= \int_{-1/2}^{1/2} \cos(2m-1)\pi x \left(\frac{\cosh \mu_{2m-1}x}{\cosh \frac{1}{2}\mu_{2m-1}} - \frac{\cos \mu_{2m-1}x}{\cos \frac{1}{2}\mu_{2m-1}} \right) dx \\
&= \frac{S2a(\mu_{2m-1}, (2m-1)\pi)}{\cosh \frac{1}{2}\mu_{2m-1}} - \frac{S2i((2m-1)\pi, \mu_{2m-1})}{\cos \frac{1}{2}\mu_{2m-1}}. \tag{B.2.9}
\end{aligned}$$

$$\begin{aligned}
H_7 &= \int_{-1/2}^{1/2} \left(\frac{\cosh \mu_{2n-1}x}{\cosh \frac{1}{2}\mu_{2n-1}} + \frac{\cos \mu_{2n-1}x}{\cos \frac{1}{2}\mu_{2n-1}} \right) \left(\frac{\cosh \mu_{2m-1}x}{\cosh \frac{1}{2}\mu_{2m-1}} - \frac{\cos \mu_{2m-1}x}{\cos \frac{1}{2}\mu_{2m-1}} \right) dx \\
&= \frac{P1a(\mu_{2n-1}, \mu_{2m-1})}{\cosh \frac{1}{2}\mu_{2n-1} \cosh \frac{1}{2}\mu_{2m-1}} - \frac{S2a(\mu_{2n-1}, \mu_{2m-1})}{\cosh \frac{1}{2}\mu_{2n-1} \cos \frac{1}{2}\mu_{2m-1}} \\
&+ \frac{S2a(\mu_{2m-1}, \mu_{2n-1})}{\cos \frac{1}{2}\mu_{2n-1} \cosh \frac{1}{2}\mu_{2m-1}} - \frac{S2i(\mu_{2n-1}, \mu_{2m-1})}{\cos \frac{1}{2}\mu_{2n-1} \cos \frac{1}{2}\mu_{2m-1}}. \tag{B.2.10}
\end{aligned}$$

$$H_8 = \int_{-1/2}^{1/2} \overline{w}_o \left(\frac{\sinh \mu_{2n}x}{\sinh \frac{1}{2}\mu_{2n}} + \frac{\sin \mu_{2n}x}{\sin \frac{1}{2}\mu_{2n}} \right) \left(\frac{\cosh \mu_{2m-1}x}{\cosh \frac{1}{2}\mu_{2m-1}} - \frac{\cos \mu_{2m-1}x}{\cos \frac{1}{2}\mu_{2m-1}} \right) dx$$

$$\begin{aligned}
&= \frac{Ra_T \sinh \frac{1}{2}M \cos \frac{1}{2}M P3ef(M, M, \mu_{2n}, \mu_{2m-1})}{M^3(\sin M + \sinh M) \sinh \frac{1}{2}\mu_{2n} \cosh \frac{1}{2}\mu_{2m-1}} \\
&\quad - \frac{Ra_T \cosh \frac{1}{2}M \sin \frac{1}{2}M P4ef(M, M, \mu_{2n}, \mu_{2m-1})}{M^3(\sin M + \sinh M) \sinh \frac{1}{2}\mu_{2n} \cosh \frac{1}{2}\mu_{2m-1}} \\
&\quad - \frac{Ra_T \sinh \frac{1}{2}M \cos \frac{1}{2}M S2cd(\mu_{2n}, M, M, \mu_{2m-1})}{M^3(\sin M + \sinh M) \sinh \frac{1}{2}\mu_{2n} \cos \frac{1}{2}\mu_{2m-1}} \\
&\quad + \frac{Ra_T \cosh \frac{1}{2}M \sin \frac{1}{2}M P5de(M, M, \mu_{2n}, \mu_{2m-1})}{M^3(\sin M + \sinh M) \sinh \frac{1}{2}\mu_{2n} \cos \frac{1}{2}\mu_{2m-1}} \\
&\quad + \frac{Ra_T \sinh \frac{1}{2}M \cos \frac{1}{2}M P6de(M, M, \mu_{2n}, \mu_{2m-1})}{M^3(\sin M + \sinh M) \sin \frac{1}{2}\mu_{2n} \cosh \frac{1}{2}\mu_{2m-1}} \\
&\quad - \frac{Ra_T \cosh \frac{1}{2}M \sin \frac{1}{2}M S2cd(M, \mu_{2n}, \mu_{2m-1}, M)}{M^3(\sin M + \sinh M) \sin \frac{1}{2}\mu_{2n} \cosh \frac{1}{2}\mu_{2m-1}} \\
&\quad - \frac{Ra_T \sinh \frac{1}{2}M \cos \frac{1}{2}M T3b(M, M, \mu_{2n}, \mu_{2m-1})}{M^3(\sin M + \sinh M) \sin \frac{1}{2}\mu_{2n} \cos \frac{1}{2}\mu_{2m-1}} \\
&\quad + \frac{Ra_T \cosh \frac{1}{2}M \sin \frac{1}{2}M T3c(M, M, \mu_{2n}, \mu_{2m-1})}{M^3(\sin M + \sinh M) \sin \frac{1}{2}\mu_{2n} \cos \frac{1}{2}\mu_{2m-1}} \tag{B.2.11}
\end{aligned}$$

$$\begin{aligned}
H_9 &= \int_{-1/2}^{1/2} \bar{w}_o \left(\frac{\sinh \mu_{2n}x}{\sinh \frac{1}{2}\mu_{2n}} - \frac{\sin \mu_{2n}x}{\sin \frac{1}{2}\mu_{2n}} \right) \left(\frac{\cosh \mu_{2m-1}x}{\cosh \frac{1}{2}\mu_{2m-1}} - \frac{\cos \mu_{2m-1}x}{\cos \frac{1}{2}\mu_{2m-1}} \right) dx \\
&= \frac{Ra_T \sinh \frac{1}{2}M \cos \frac{1}{2}M P3ef(M, M, \mu_{2n}, \mu_{2m-1})}{M^3(\sin M + \sinh M) \sinh \frac{1}{2}\mu_{2n} \cosh \frac{1}{2}\mu_{2m-1}} \\
&\quad - \frac{Ra_T \cosh \frac{1}{2}M \sin \frac{1}{2}M P4ef(M, M, \mu_{2n}, \mu_{2m-1})}{M^3(\sin M + \sinh M) \sinh \frac{1}{2}\mu_{2n} \cosh \frac{1}{2}\mu_{2m-1}} \\
&\quad - \frac{Ra_T \sinh \frac{1}{2}M \cos \frac{1}{2}M S2cd(\mu_{2n}, M, M, \mu_{2m-1})}{M^3(\sin M + \sinh M) \sinh \frac{1}{2}\mu_{2n} \cos \frac{1}{2}\mu_{2m-1}} \\
&\quad + \frac{Ra_T \cosh \frac{1}{2}M \sin \frac{1}{2}M P5de(M, M, \mu_{2n}, \mu_{2m-1})}{M^3(\sin M + \sinh M) \sinh \frac{1}{2}\mu_{2n} \cos \frac{1}{2}\mu_{2m-1}} \\
&\quad - \frac{Ra_T \sinh \frac{1}{2}M \cos \frac{1}{2}M P6de(M, M, \mu_{2n}, \mu_{2m-1})}{M^3(\sin M + \sinh M) \sin \frac{1}{2}\mu_{2n} \cosh \frac{1}{2}\mu_{2m-1}}
\end{aligned}$$

$$\begin{aligned}
& + \frac{Ra_T \cosh \frac{1}{2}M \sin \frac{1}{2}M S2cd(M, \mu_{2n}, \mu_{2m-1}, M)}{M^3(\sin M + \sinh M) \sin \frac{1}{2}\mu_{2n} \cosh \frac{1}{2}\mu_{2m-1}} \\
& + \frac{Ra_T \sinh \frac{1}{2}M \cos \frac{1}{2}M T3b(M, M, \mu_{2n}, \mu_{2m-1})}{M^3(\sin M + \sinh M) \sin \frac{1}{2}\mu_{2n} \cos \frac{1}{2}\mu_{2m-1}} \\
& - \frac{Ra_T \cosh \frac{1}{2}M \sin \frac{1}{2}M T3c(M, M, \mu_{2n}, \mu_{2m-1})}{M^3(\sin M + \sinh M) \sin \frac{1}{2}\mu_{2n} \cos \frac{1}{2}\mu_{2m-1}}. \tag{B.2.12}
\end{aligned}$$

$$\begin{aligned}
H_{10} & = \int_{-1/2}^{1/2} D^2 \overline{w}_o \left(\frac{\sinh \mu_{2n} x}{\sinh \frac{1}{2}\mu_{2n}} - \frac{\sin \mu_{2n} x}{\sin \frac{1}{2}\mu_{2n}} \right) \left(\frac{\cosh \mu_{2m-1} x}{\cosh \frac{1}{2}\mu_{2m-1}} - \frac{\cos \mu_{2m-1} x}{\cos \frac{1}{2}\mu_{2m-1}} \right) dx \\
& = \frac{2Ra_T \sinh \frac{1}{2}M \cos \frac{1}{2}M P4ef(M, M, \mu_{2n}, \mu_{2m-1})}{M(\sin M + \sinh M) \sinh \frac{1}{2}\mu_{2n} \cosh \frac{1}{2}\mu_{2m-1}} \\
& + \frac{2Ra_T \cosh \frac{1}{2}M \sin \frac{1}{2}M P3ef(M, M, \mu_{2n}, \mu_{2m-1})}{M(\sin M + \sinh M) \sinh \frac{1}{2}\mu_{2n} \cosh \frac{1}{2}\mu_{2m-1}} \\
& - \frac{2Ra_T \sinh \frac{1}{2}M \cos \frac{1}{2}M P5de(M, M, \mu_{2n}, \mu_{2m-1})}{M(\sin M + \sinh M) \sinh \frac{1}{2}\mu_{2n} \cos \frac{1}{2}\mu_{2m-1}} \\
& - \frac{2Ra_T \cosh \frac{1}{2}M \sin \frac{1}{2}M S2cd(\mu_{2n}, M, M, \mu_{2m-1})}{M(\sin M + \sinh M) \sinh \frac{1}{2}\mu_{2n} \cos \frac{1}{2}\mu_{2m-1}} \\
& - \frac{2Ra_T \sinh \frac{1}{2}M \cos \frac{1}{2}M S2cd(M, \mu_{2n}, \mu_{2m-1}, M)}{M(\sin M + \sinh M) \sin \frac{1}{2}\mu_{2n} \cosh \frac{1}{2}\mu_{2m-1}} \\
& - \frac{2Ra_T \cosh \frac{1}{2}M \sin \frac{1}{2}M P6de(M, M, \mu_{2n}, \mu_{2m-1})}{M(\sin M + \sinh M) \sin \frac{1}{2}\mu_{2n} \cosh \frac{1}{2}\mu_{2m-1}} \\
& + \frac{2Ra_T \sinh \frac{1}{2}M \cos \frac{1}{2}M T3c(M, M, \mu_{2n}, \mu_{2m-1})}{M(\sin M + \sinh M) \sin \frac{1}{2}\mu_{2n} \cos \frac{1}{2}\mu_{2m-1}} \\
& + \frac{2Ra_T \cosh \frac{1}{2}M \sin \frac{1}{2}M T3b(M, M, \mu_{2n}, \mu_{2m-1})}{M(\sin M + \sinh M) \sin \frac{1}{2}\mu_{2n} \cos \frac{1}{2}\mu_{2m-1}}. \tag{B.2.13}
\end{aligned}$$

$$\begin{aligned}
H_{11} & = \int_{-1/2}^{1/2} \cos(2n)\pi x \left(\frac{\cosh \mu_{2m-1} x}{\cosh \frac{1}{2}\mu_{2m-1}} - \frac{\cos \mu_{2m-1} x}{\cos \frac{1}{2}\mu_{2m-1}} \right) dx \\
& = \frac{S2a(\mu_{2m-1}, 2n\pi)}{\cosh \frac{1}{2}\mu_{2m-1}} - \frac{S2i(2n\pi, \mu_{2m-1})}{\cos \frac{1}{2}\mu_{2m-1}}. \tag{B.2.14}
\end{aligned}$$

$$\begin{aligned}
H_{12} &= \int_{-1/2}^{1/2} \cos(2n-1)\pi x \left(\frac{\cosh \mu_{2m-1}x}{\cosh \frac{1}{2}\mu_{2m-1}} - \frac{\cos \mu_{2m-1}x}{\cos \frac{1}{2}\mu_{2m-1}} \right) dx \\
&= \frac{S2a(\mu_{2m-1}, (2n-1)\pi)}{\cosh \frac{1}{2}\mu_{2m-1}} - \frac{S2i((2n-1)\pi, \mu_{2m-1})}{\cos \frac{1}{2}\mu_{2m-1}}. \quad (\text{B.2.15})
\end{aligned}$$

For the integrals involving the odd function in ψ :

$$\begin{aligned}
H_{13} &= \int_{-1/2}^{1/2} \bar{w}_o \left(\frac{\cosh \mu_{2m-1}x}{\cosh \frac{1}{2}\mu_{2m-1}} + \frac{\cos \mu_{2m-1}x}{\cos \frac{1}{2}\mu_{2m-1}} \right) \left(\frac{\sinh \mu_{2m}x}{\sinh \frac{1}{2}\mu_{2m}} - \frac{\sin \mu_{2m}x}{\sin \frac{1}{2}\mu_{2m}} \right) dx \\
&= \frac{Ra_T \sinh \frac{1}{2}M \cos \frac{1}{2}M P3ef(M, M, \mu_{2m}, \mu_{2m-1})}{M^3(\sin M + \sinh M) \sinh \frac{1}{2}\mu_{2m} \cosh \frac{1}{2}\mu_{2m-1}} \\
&\quad - \frac{Ra_T \cosh \frac{1}{2}M \sin \frac{1}{2}M P4ef(M, M, \mu_{2m}, \mu_{2m-1})}{M^3(\sin M + \sinh M) \sinh \frac{1}{2}\mu_{2m} \cosh \frac{1}{2}\mu_{2m-1}} \\
&\quad + \frac{Ra_T \sinh \frac{1}{2}M \cos \frac{1}{2}M S2cd(\mu_{2m}, M, M, \mu_{2m-1})}{M^3(\sin M + \sinh M) \sinh \frac{1}{2}\mu_{2m} \cos \frac{1}{2}\mu_{2m-1}} \\
&\quad - \frac{Ra_T \cosh \frac{1}{2}M \sin \frac{1}{2}M P5de(M, M, \mu_{2m}, \mu_{2m-1})}{M^3(\sin M + \sinh M) \sinh \frac{1}{2}\mu_{2m} \cos \frac{1}{2}\mu_{2m-1}} \\
&\quad - \frac{Ra_T \sinh \frac{1}{2}M \cos \frac{1}{2}M P6de(M, M, \mu_{2m}, \mu_{2m-1})}{M^3(\sin M + \sinh M) \sin \frac{1}{2}\mu_{2m} \cosh \frac{1}{2}\mu_{2m-1}} \\
&\quad + \frac{Ra_T \cosh \frac{1}{2}M \sin \frac{1}{2}M S2cd(M, \mu_{2m}, \mu_{2m-1}, M)}{M^3(\sin M + \sinh M) \sin \frac{1}{2}\mu_{2m} \cosh \frac{1}{2}\mu_{2m-1}} \\
&\quad - \frac{Ra_T \sinh \frac{1}{2}M \cos \frac{1}{2}M T3b(M, M, \mu_{2m}, \mu_{2m-1})}{M^3(\sin M + \sinh M) \sin \frac{1}{2}\mu_{2m} \cos \frac{1}{2}\mu_{2m-1}} \\
&\quad + \frac{Ra_T \cosh \frac{1}{2}M \sin \frac{1}{2}M T3c(M, M, \mu_{2m}, \mu_{2m-1})}{M^3(\sin M + \sinh M) \sin \frac{1}{2}\mu_{2m} \cos \frac{1}{2}\mu_{2m-1}}. \quad (\text{B.2.16})
\end{aligned}$$

$$\begin{aligned}
H_{14} &= \int_{-1/2}^{1/2} \left(\frac{\sinh \mu_{2m}x}{\sinh \frac{1}{2}\mu_{2m}} + \frac{\sin \mu_{2m}x}{\sin \frac{1}{2}\mu_{2m}} \right) \left(\frac{\sinh \mu_{2m}x}{\sinh \frac{1}{2}\mu_{2m}} - \frac{\sin \mu_{2m}x}{\sin \frac{1}{2}\mu_{2m}} \right) dx \\
&= \frac{P7(\mu_{2m}, \mu_{2m})}{\sinh^2 \frac{1}{2}\mu_{2m}} - \frac{S4f(\mu_{2m}, \mu_{2m})}{\sin^2 \frac{1}{2}\mu_{2m}}. \quad (\text{B.2.17})
\end{aligned}$$

$$H_{15} = \int_{-1/2}^{1/2} \bar{w}_o \left(\frac{\cosh \mu_{2m-1}x}{\cosh \frac{1}{2}\mu_{2m-1}} - \frac{\cos \mu_{2m-1}x}{\cos \frac{1}{2}\mu_{2m-1}} \right) \left(\frac{\sinh \mu_{2m}x}{\sinh \frac{1}{2}\mu_{2m}} - \frac{\sin \mu_{2m}x}{\sin \frac{1}{2}\mu_{2m}} \right) dx$$

$$\begin{aligned}
&= \int_{-1/2}^{1/2} \overline{w}_o \left(\frac{\sinh \mu_{2m} x}{\sinh \frac{1}{2} \mu_{2m}} - \frac{\sin \mu_{2m} x}{\sin \frac{1}{2} \mu_{2m}} \right) \left(\frac{\cosh \mu_{2m-1} x}{\cosh \frac{1}{2} \mu_{2m-1}} - \frac{\cos \mu_{2m-1} x}{\cos \frac{1}{2} \mu_{2m-1}} \right) dx \\
&= H_3. \tag{B.2.18}
\end{aligned}$$

$$\begin{aligned}
H_{16} &= \int_{-1/2}^{1/2} D^2 \overline{w}_o \left(\frac{\cosh \mu_{2m-1} x}{\cosh \frac{1}{2} \mu_{2m-1}} - \frac{\cos \mu_{2m-1} x}{\cos \frac{1}{2} \mu_{2m-1}} \right) \left(\frac{\sinh \mu_{2m} x}{\sinh \frac{1}{2} \mu_{2m}} - \frac{\sin \mu_{2m} x}{\sin \frac{1}{2} \mu_{2m}} \right) dx \\
&= \int_{-1/2}^{1/2} D^2 \overline{w}_o \left(\frac{\sinh \mu_{2m} x}{\sinh \frac{1}{2} \mu_{2m}} - \frac{\sin \mu_{2m} x}{\sin \frac{1}{2} \mu_{2m}} \right) \left(\frac{\cosh \mu_{2m-1} x}{\cosh \frac{1}{2} \mu_{2m-1}} - \frac{\cos \mu_{2m-1} x}{\cos \frac{1}{2} \mu_{2m-1}} \right) dx \\
&= \overline{H}_4. \tag{B.2.19}
\end{aligned}$$

$$\begin{aligned}
H_{17} &= \int_{-1/2}^{1/2} \sin(2m-1)\pi x \left(\frac{\sinh \mu_{2m} x}{\sinh \frac{1}{2} \mu_{2m}} - \frac{\sin \mu_{2m} x}{\sin \frac{1}{2} \mu_{2m}} \right) dx \\
&= \frac{S4a(\mu_{2m}, (2m-1)\pi)}{\sinh \frac{1}{2} \mu_{2m}} - \frac{S4f((2m-1)\pi, \mu_{2m})}{\sin \frac{1}{2} \mu_{2m}}. \tag{B.2.20}
\end{aligned}$$

$$\begin{aligned}
H_{18} &= \int_{-1/2}^{1/2} \sin 2(m-1)\pi x \left(\frac{\sinh \mu_{2m} x}{\sinh \frac{1}{2} \mu_{2m}} - \frac{\sin \mu_{2m} x}{\sin \frac{1}{2} \mu_{2m}} \right) dx \\
&= \frac{S4a(\mu_{2m}, 2(m-1)\pi)}{\sinh \frac{1}{2} \mu_{2m}} - \frac{S4f(2(m-1)\pi, \mu_{2m})}{\sin \frac{1}{2} \mu_{2m}}. \tag{B.2.21}
\end{aligned}$$

$$\begin{aligned}
H_{19} &= \int_{-1/2}^{1/2} \overline{w}_o \left(\frac{\cosh \mu_{2n-1} x}{\cosh \frac{1}{2} \mu_{2n-1}} + \frac{\cos \mu_{2n-1} x}{\cos \frac{1}{2} \mu_{2n-1}} \right) \left(\frac{\sinh \mu_{2m} x}{\sinh \frac{1}{2} \mu_{2m}} - \frac{\sin \mu_{2m} x}{\sin \frac{1}{2} \mu_{2m}} \right) dx \\
&= \frac{Ra_T \sinh \frac{1}{2} M \cos \frac{1}{2} M P3ef(M, M, \mu_{2m}, \mu_{2n-1})}{M^3 (\sin M + \sinh M) \sinh \frac{1}{2} \mu_{2m} \cosh \frac{1}{2} \mu_{2n-1}} \\
&\quad - \frac{Ra_T \cosh \frac{1}{2} M \sin \frac{1}{2} M P4ef(M, M, \mu_{2m}, \mu_{2n-1})}{M^3 (\sin M + \sinh M) \sinh \frac{1}{2} \mu_{2m} \cosh \frac{1}{2} \mu_{2n-1}} \\
&\quad + \frac{Ra_T \sinh \frac{1}{2} M \cos \frac{1}{2} M S2cd(\mu_{2m}, M, M, \mu_{2n-1})}{M^3 (\sin M + \sinh M) \sinh \frac{1}{2} \mu_{2m} \cos \frac{1}{2} \mu_{2n-1}} \\
&\quad - \frac{Ra_T \cosh \frac{1}{2} M \sin \frac{1}{2} M P5de(M, M, \mu_{2m}, \mu_{2n-1})}{M^3 (\sin M + \sinh M) \sinh \frac{1}{2} \mu_{2m} \cos \frac{1}{2} \mu_{2n-1}}
\end{aligned}$$

$$\begin{aligned}
& - \frac{Ra_T \sinh \frac{1}{2}M \cos \frac{1}{2}M P6de(M, M, \mu_{2m}, \mu_{2n-1})}{M^3(\sin M + \sinh M) \sin \frac{1}{2}\mu_{2m} \cosh \frac{1}{2}\mu_{2n-1}} \\
& + \frac{Ra_T \cosh \frac{1}{2}M \sin \frac{1}{2}M S2cd(M, \mu_{2m}, \mu_{2n-1}, M)}{M^3(\sin M + \sinh M) \sin \frac{1}{2}\mu_{2m} \cosh \frac{1}{2}\mu_{2n-1}} \\
& - \frac{Ra_T \sinh \frac{1}{2}M \cos \frac{1}{2}M T3b(M, M, \mu_{2m}, \mu_{2n-1})}{M^3(\sin M + \sinh M) \sin \frac{1}{2}\mu_{2m} \cos \frac{1}{2}\mu_{2n-1}} \\
& + \frac{Ra_T \cosh \frac{1}{2}M \sin \frac{1}{2}M T3c(M, M, \mu_{2m}, \mu_{2n-1})}{M^3(\sin M + \sinh M) \sin \frac{1}{2}\mu_{2m} \cos \frac{1}{2}\mu_{2n-1}}. \tag{B.2.22}
\end{aligned}$$

$$\begin{aligned}
H_{20} &= \int_{-1/2}^{1/2} \left(\frac{\sinh \mu_{2n}x}{\sinh \frac{1}{2}\mu_{2n}} + \frac{\sin \mu_{2n}x}{\sin \frac{1}{2}\mu_{2n}} \right) \left(\frac{\sinh \mu_{2m}x}{\sinh \frac{1}{2}\mu_{2m}} - \frac{\sin \mu_{2m}x}{\sin \frac{1}{2}\mu_{2m}} \right) dx \\
&= \frac{P7(\mu_{2n}, \mu_{2m})}{\sinh \frac{1}{2}\mu_{2n} \sinh \frac{1}{2}\mu_{2m}} - \frac{S4a(\mu_{2n}, \mu_{2m})}{\sinh \frac{1}{2}\mu_{2n} \sin \frac{1}{2}\mu_{2m}} \\
&\quad + \frac{S4a(\mu_{2m}, \mu_{2n})}{\sin \frac{1}{2}\mu_{2n} \sinh \frac{1}{2}\mu_{2m}} - \frac{S4f(\mu_{2n}, \mu_{2m})}{\sin \frac{1}{2}\mu_{2n} \sin \frac{1}{2}\mu_{2m}}. \tag{B.2.23}
\end{aligned}$$

$$\begin{aligned}
H_{21} &= \int_{-1/2}^{1/2} \overline{w}_0 \left(\frac{\cosh \mu_{2n-1}x}{\cosh \frac{1}{2}\mu_{2n-1}} - \frac{\cos \mu_{2n-1}x}{\cos \frac{1}{2}\mu_{2n-1}} \right) \left(\frac{\sinh \mu_{2m}x}{\sinh \frac{1}{2}\mu_{2m}} - \frac{\sin \mu_{2m}x}{\sin \frac{1}{2}\mu_{2m}} \right) dx \\
&= \frac{Ra_T \sinh \frac{1}{2}M \cos \frac{1}{2}M P3ef(M, M, \mu_{2m}, \mu_{2n-1})}{M^3(\sin M + \sinh M) \sinh \frac{1}{2}\mu_{2m} \cosh \frac{1}{2}\mu_{2n-1}} \\
&\quad - \frac{Ra_T \cosh \frac{1}{2}M \sin \frac{1}{2}M P4ef(M, M, \mu_{2m}, \mu_{2n-1})}{M^3(\sin M + \sinh M) \sinh \frac{1}{2}\mu_{2m} \cosh \frac{1}{2}\mu_{2n-1}} \\
&\quad - \frac{Ra_T \sinh \frac{1}{2}M \cos \frac{1}{2}M S2cd(\mu_{2m}, M, M, \mu_{2n-1})}{M^3(\sin M + \sinh M) \sinh \frac{1}{2}\mu_{2m} \cos \frac{1}{2}\mu_{2n-1}} \\
&\quad + \frac{Ra_T \cosh \frac{1}{2}M \sin \frac{1}{2}M P5de(M, M, \mu_{2m}, \mu_{2n-1})}{M^3(\sin M + \sinh M) \sinh \frac{1}{2}\mu_{2m} \cos \frac{1}{2}\mu_{2n-1}} \\
&\quad - \frac{Ra_T \sinh \frac{1}{2}M \cos \frac{1}{2}M P6de(M, M, \mu_{2m}, \mu_{2n-1})}{M^3(\sin M + \sinh M) \sin \frac{1}{2}\mu_{2m} \cosh \frac{1}{2}\mu_{2n-1}} \\
&\quad + \frac{Ra_T \cosh \frac{1}{2}M \sin \frac{1}{2}M S2cd(M, \mu_{2m}, \mu_{2n-1}, M)}{M^3(\sin M + \sinh M) \sin \frac{1}{2}\mu_{2m} \cosh \frac{1}{2}\mu_{2n-1}}
\end{aligned}$$

$$\begin{aligned}
& + \frac{Ra_T \sinh \frac{1}{2}M \cos \frac{1}{2}M T3b(M, M, \mu_{2m}, \mu_{2n-1})}{M^3(\sin M + \sinh M) \sin \frac{1}{2}\mu_{2m} \cos \frac{1}{2}\mu_{2n-1}} \\
& - \frac{Ra_T \cosh \frac{1}{2}M \sin \frac{1}{2}M T3c(M, M, \mu_{2m}, \mu_{2n-1})}{M^3(\sin M + \sinh M) \sin \frac{1}{2}\mu_{2m} \cos \frac{1}{2}\mu_{2n-1}}. \tag{B.2.24}
\end{aligned}$$

$$\begin{aligned}
H_{22} &= \int_{-1/2}^{1/2} D^2 \bar{w}_o \left(\frac{\cosh \mu_{2n-1}x}{\cosh \frac{1}{2}\mu_{2n-1}} - \frac{\cos \mu_{2n-1}x}{\cos \frac{1}{2}\mu_{2n-1}} \right) \left(\frac{\sinh \mu_{2m}x}{\sinh \frac{1}{2}\mu_{2m}} - \frac{\sin \mu_{2m}x}{\sin \frac{1}{2}\mu_{2m}} \right) dx \\
&= \frac{2\bar{R}a_T \sinh \frac{1}{2}M \cos \frac{1}{2}M P4ef(M, M, \mu_{2m}, \mu_{2n-1})}{M(\sin M + \sinh M) \sinh \frac{1}{2}\mu_{2m} \cosh \frac{1}{2}\mu_{2n-1}} \\
&+ \frac{2Ra_T \cosh \frac{1}{2}M \sin \frac{1}{2}M P3ef(M, M, \mu_{2m}, \mu_{2n-1})}{M(\sin M + \sinh M) \sinh \frac{1}{2}\mu_{2m} \cosh \frac{1}{2}\mu_{2n-1}} \\
&- \frac{2Ra_T \sinh \frac{1}{2}M \cos \frac{1}{2}M P5de(M, M, \mu_{2m}, \mu_{2n-1})}{M(\sin M + \sinh M) \sinh \frac{1}{2}\mu_{2m} \cos \frac{1}{2}\mu_{2n-1}} \\
&- \frac{2Ra_T \cosh \frac{1}{2}M \sin \frac{1}{2}M S2cd(\mu_{2m}, M, M, \mu_{2n-1})}{M(\sin M + \sinh M) \sinh \frac{1}{2}\mu_{2m} \cos \frac{1}{2}\mu_{2n-1}} \\
&- \frac{2Ra_T \sinh \frac{1}{2}M \cos \frac{1}{2}M S2cd(M, \mu_{2m}, \mu_{2n-1}, M)}{M(\sin M + \sinh M) \sin \frac{1}{2}\mu_{2m} \cosh \frac{1}{2}\mu_{2n-1}} \\
&- \frac{2Ra_T \cosh \frac{1}{2}M \sin \frac{1}{2}M P6de(M, M, \mu_{2m}, \mu_{2n-1})}{M(\sin M + \sinh M) \sin \frac{1}{2}\mu_{2m} \cosh \frac{1}{2}\mu_{2n-1}} \\
&+ \frac{2Ra_T \sinh \frac{1}{2}M \cos \frac{1}{2}M T3c(M, M, \mu_{2m}, \mu_{2n-1})}{M(\sin M + \sinh M) \sin \frac{1}{2}\mu_{2m} \cos \frac{1}{2}\mu_{2n-1}} \\
&+ \frac{2Ra_T \cosh \frac{1}{2}M \sin \frac{1}{2}M T3b(M, M, \mu_{2m}, \mu_{2n-1})}{M(\sin M + \sinh M) \sin \frac{1}{2}\mu_{2m} \cos \frac{1}{2}\mu_{2n-1}}. \tag{B.2.25}
\end{aligned}$$

$$\begin{aligned}
H_{23} &= \int_{-1/2}^{1/2} \sin(2n-1)\pi x \left(\frac{\sinh \mu_{2m}x}{\sinh \frac{1}{2}\mu_{2m}} - \frac{\sin \mu_{2m}x}{\sin \frac{1}{2}\mu_{2m}} \right) dx \\
&= \frac{S4a(\mu_{2m}, (2n-1)\pi)}{\sinh \frac{1}{2}\mu_{2m}} - \frac{S4f((2n-1)\pi, \mu_{2m})}{\sin \frac{1}{2}\mu_{2m}}. \tag{B.2.26}
\end{aligned}$$

$$H_{24} = \int_{-1/2}^{1/2} \sin 2(n-1)\pi x \left(\frac{\sinh \mu_{2m}x}{\sinh \frac{1}{2}\mu_{2m}} - \frac{\sin \mu_{2m}x}{\sin \frac{1}{2}\mu_{2m}} \right) dx$$

$$= \frac{S4a(\mu_{2m}, 2(n-1)\pi)}{\sinh \frac{1}{2}\mu_{2m}} - \frac{S4f(2(n-1)\pi, \mu_{2m})}{\sin \frac{1}{2}\mu_{2m}}. \quad (\text{B.2.27})$$

B.3 Integrals for T

For the integrals involving the even function in T :

$$\begin{aligned} F_1 &= \int_{-1/2}^{1/2} \left(\frac{\cosh \mu_{2m-1}x}{\cosh \frac{1}{2}\mu_{2m-1}} - \frac{\cos \mu_{2m-1}x}{\cos \frac{1}{2}\mu_{2m-1}} \right) \cos(2m-1)\pi x dx \\ &= \frac{-2\pi(2m-1)(-1)^m}{\pi^2(2m-1)^2 + \mu_{2m-1}^2} - \frac{\sin[\pi(m-\frac{1}{2}) + \frac{1}{2}\mu_{2m-1}]}{\cos \frac{1}{2}\mu_{2m-1}[\pi(2m-1) + \mu_{2m-1}]} \\ &= \frac{\sin[\pi(m-\frac{1}{2}) - \frac{1}{2}\mu_{2m-1}]}{\cos \frac{1}{2}\mu_{2m-1}[\pi(2m-1) - \mu_{2m-1}]}. \end{aligned} \quad (\text{B.3.1})$$

$$\begin{aligned} F_2 &= \int_{-1/2}^{1/2} \bar{w}_o \sin(2m)\pi x \cos(2m-1)\pi x dx \\ &= \frac{Ra_T \sinh \frac{1}{2}M \cos \frac{1}{2}M T3b(M, M, 2m\pi, (2m-1)\pi)}{M^3(\sin M + \sinh M)} \\ &= \frac{Ra_T \cosh \frac{1}{2}M \sin \frac{1}{2}M T3c(M, M, 2m\pi, (2m-1)\pi)}{M^3(\sin M + \sinh M)}. \end{aligned} \quad (\text{B.3.2})$$

$$\begin{aligned} F_3 &= \int_{-1/2}^{1/2} \left(\frac{\cosh \mu_{2n-1}x}{\cosh \frac{1}{2}\mu_{2n-1}} - \frac{\cos \mu_{2n-1}x}{\cos \frac{1}{2}\mu_{2n-1}} \right) \cos(2m-1)\pi x dx \\ &= \frac{-2\pi(2m-1)(-1)^m}{\pi^2(2m-1)^2 + \mu_{2n-1}^2} - \frac{\sin[\pi(m-\frac{1}{2}) + \frac{1}{2}\mu_{2n-1}]}{\cos \frac{1}{2}\mu_{2n-1}[\pi(2m-1) + \mu_{2n-1}]} \\ &= \frac{\sin[\pi(m-\frac{1}{2}) - \frac{1}{2}\mu_{2n-1}]}{\cos \frac{1}{2}\mu_{2n-1}[\pi(2m-1) - \mu_{2n-1}]}. \end{aligned} \quad (\text{B.3.3})$$

$$\begin{aligned} F_4 &= \int_{-1/2}^{1/2} \bar{w}_o \sin(2n)\pi x \cos(2m-1)\pi x dx \\ &= \frac{Ra_T \sinh \frac{1}{2}M \cos \frac{1}{2}M T3b(M, M, 2n\pi, (2m-1)\pi)}{M^3(\sin M + \sinh M)} \\ &= \frac{Ra_T \cosh \frac{1}{2}M \sin \frac{1}{2}M T3c(M, M, 2n\pi, (2m-1)\pi)}{M^3(\sin M + \sinh M)}. \end{aligned} \quad (\text{B.3.4})$$

For the integrals involving the odd function in T :

$$\begin{aligned}
 F_5 &= \int_{-1/2}^{1/2} \left(\frac{\sinh \mu_{2m} x}{\sinh \frac{1}{2} \mu_{2m}} - \frac{\sin \mu_{2m} x}{\sin \frac{1}{2} \mu_{2m}} \right) \sin(2m)\pi x \, dx \\
 &= \frac{-4\pi m(-1)^m}{4\pi^2 m^2 + \mu_{2m}^2} - \frac{\sin[\pi m - \frac{1}{2} \mu_{2m}]}{\sin \frac{1}{2} \mu_{2m} [2\pi m - \mu_{2m}]} \\
 &\quad + \frac{\sin[\pi m + \frac{1}{2} \mu_{2m}]}{\sin \frac{1}{2} \mu_{2m} [2\pi m + \mu_{2m}]} \tag{B.3.5}
 \end{aligned}$$

$$\begin{aligned}
 F_6 &= \int_{-1/2}^{1/2} \bar{w}_o \cos(2m-1)\pi x \sin(2m)\pi x \, dx \\
 &= F_2. \tag{B.3.6}
 \end{aligned}$$

$$\begin{aligned}
 F_7 &= \int_{-1/2}^{1/2} \left(\frac{\sinh \mu_{2n} x}{\sinh \frac{1}{2} \mu_{2n}} - \frac{\sin \mu_{2n} x}{\sin \frac{1}{2} \mu_{2n}} \right) \sin(2m)\pi x \, dx \\
 &= \frac{-4\pi m(-1)^m}{4\pi^2 m^2 + \mu_{2n}^2} - \frac{\sin[\pi m - \frac{1}{2} \mu_{2n}]}{\sin \frac{1}{2} \mu_{2n} [2\pi m - \mu_{2n}]} \\
 &\quad + \frac{\sin[\pi m + \frac{1}{2} \mu_{2n}]}{\sin \frac{1}{2} \mu_{2n} [2\pi m + \mu_{2n}]} \tag{B.3.7}
 \end{aligned}$$

$$\begin{aligned}
 F_8 &= \int_{-1/2}^{1/2} \bar{w}_o \cos(2n-1)\pi x \sin(2m)\pi x \, dx \\
 &= \frac{Ra_T \sinh \frac{1}{2} M \cos \frac{1}{2} M T3b(M, M, 2m\pi, (2n-1)\pi)}{M^3(\sin M + \sinh M)} \\
 &\quad - \frac{Ra_T \cosh \frac{1}{2} M \sin \frac{1}{2} M T3c(M, M, 2m\pi, (2n-1)\pi)}{M^3(\sin M + \sinh M)}. \tag{B.3.8}
 \end{aligned}$$

B.4 Integrals for S

The parameters λ_1 and λ_2 used in the S integrals are

$$\begin{aligned}
 \lambda_1 &= \sin \frac{1}{2} M \cosh \frac{1}{2} M - \sinh \frac{1}{2} M \cos \frac{1}{2} M, \\
 \lambda_2 &= \sin \frac{1}{2} M \cosh \frac{1}{2} M + \sinh \frac{1}{2} M \cos \frac{1}{2} M. \tag{B.4.1}
 \end{aligned}$$

For the integrals involving the even function in S :

$$\begin{aligned}
G_1 &= \int_{-1/2}^{1/2} D\overline{S}_o \left(\frac{\cosh \mu_{2m-1}x}{\cosh \frac{1}{2}\mu_{2m-1}} - \frac{\cos \mu_{2m-1}x}{\cos \frac{1}{2}\mu_{2m-1}} \right) \cos 2(m-1)\pi x dx \\
&= - \frac{Ra_T S2a(\mu_{2m-1}, 2(m-1)\pi)}{Ra_S \cosh \frac{1}{2}\mu_{2m-1}} \\
&\quad + \frac{Ra_T 2\lambda_1 S2cd(M, M, \mu_{2m-1}, 2(m-1)\pi)}{Ra_S (\sin M + \sinh M) \cosh \frac{1}{2}\mu_{2m-1}} \\
&\quad + \frac{Ra_T 2\lambda_2 S2gh(M, M, \mu_{2m-1}, 2(m-1)\pi)}{Ra_S (\sin M + \sinh M) \cosh \frac{1}{2}\mu_{2m-1}} \\
&\quad + \frac{Ra_T S2i(\mu_{2m-1}, 2(m-1)\pi)}{Ra_S \cos \frac{1}{2}\mu_{2m-1}} \\
&\quad - \frac{Ra_T 2\lambda_1 T3c(M, \mu_{2m-1}, M, 2(m-1)\pi)}{Ra_S (\sin M + \sinh M) \cos \frac{1}{2}\mu_{2m-1}} \\
&\quad - \frac{Ra_T 2\lambda_2 S2k(M, M, \mu_{2m-1}, 2(m-1)\pi)}{Ra_S (\sin M + \sinh M) \cos \frac{1}{2}\mu_{2m-1}}. \tag{B.4.2}
\end{aligned}$$

$$\begin{aligned}
G_2 &= \int_{-1/2}^{1/2} \overline{w}_o \sin(2m-1)\pi x \cos 2(m-1)\pi x dx \\
&= \frac{Ra_T \sinh \frac{1}{2}M \cos \frac{1}{2}M T3b(M, M, (2m-1)\pi, 2(m-1)\pi)}{M^3 (\sin M + \sinh M)} \\
&\quad - \frac{Ra_T \cosh \frac{1}{2}M \sin \frac{1}{2}M T3c(M, M, (2m-1)\pi, 2(m-1)\pi)}{M^3 (\sin M + \sinh M)}. \tag{B.4.3}
\end{aligned}$$

$$\begin{aligned}
G_3 &= \int_{-1/2}^{1/2} \left(\frac{\cosh \mu_{2m}x}{\sinh \frac{1}{2}\mu_{2m}} - \frac{\cos \mu_{2m}x}{\sin \frac{1}{2}\mu_{2m}} \right) \cos 2(m-1)\pi x dx \\
&= \frac{S2a(\mu_{2m}, 2(m-1)\pi)}{\sinh \frac{1}{2}\mu_{2m}} - \frac{S2i(\mu_{2m}, 2(m-1)\pi)}{\sin \frac{1}{2}\mu_{2m}}. \tag{B.4.4}
\end{aligned}$$

$$G_4 = \int_{-1/2}^{1/2} D\overline{S}_o \left(\frac{\cosh \mu_{2n-1}x}{\cosh \frac{1}{2}\mu_{2n-1}} - \frac{\cos \mu_{2n-1}x}{\cos \frac{1}{2}\mu_{2n-1}} \right) \cos 2(m-1)\pi x dx$$

$$\begin{aligned}
&= -\frac{Ra_T S2a(\mu_{2n-1}, 2(m-1)\pi)}{Ra_S \cosh \frac{1}{2}\mu_{2n-1}} \\
&+ \frac{Ra_T 2\lambda_1 S2cd(M, M, \mu_{2n-1}, 2(m-1)\pi)}{Ra_S (\sin M + \sinh M) \cosh \frac{1}{2}\mu_{2n-1}} \\
&+ \frac{Ra_T 2\lambda_2 S2gh(M, M, \mu_{2n-1}, 2(m-1)\pi)}{Ra_S (\sin M + \sinh M) \cosh \frac{1}{2}\mu_{2n-1}} \\
&+ \frac{Ra_T S2i(\mu_{2n-1}, 2(m-1)\pi)}{Ra_S \cos \frac{1}{2}\mu_{2n-1}} \\
&- \frac{Ra_T 2\lambda_1 T3c(M, \mu_{2n-1}, M, 2(m-1)\pi)}{Ra_S (\sin M + \sinh M) \cos \frac{1}{2}\mu_{2n-1}} \\
&- \frac{Ra_T 2\lambda_2 S2k(M, M, \mu_{2n-1}, 2(m-1)\pi)}{Ra_S (\sin M + \sinh M) \cos \frac{1}{2}\mu_{2n-1}}. \tag{B.4.5}
\end{aligned}$$

$$\begin{aligned}
G_5 &= \int_{-1/2}^{1/2} \bar{w}_o \sin(2n-1)\pi x \cos 2(m-1)\pi x dx \\
&= \frac{Ra_T \sinh \frac{1}{2}M \cos \frac{1}{2}M T3b(M, M, (2n-1)\pi, 2(m-1)\pi)}{M^3 (\sin M + \sinh M)} \\
&- \frac{Ra_T \cosh \frac{1}{2}M \sin \frac{1}{2}M T3c(M, M, (2n-1)\pi, 2(m-1)\pi)}{M^3 (\sin M + \sinh M)}. \tag{B.4.6}
\end{aligned}$$

$$\begin{aligned}
G_6 &= \int_{-1/2}^{1/2} \left(\frac{\cosh \mu_{2n}x}{\sinh \frac{1}{2}\mu_{2n}} - \frac{\cos \mu_{2n}x}{\sin \frac{1}{2}\mu_{2n}} \right) \cos 2(m-1)\pi x dx \\
&= \frac{S2a(\mu_{2n}, 2(m-1)\pi)}{\sinh \frac{1}{2}\mu_{2n}} = \frac{S2i(\mu_{2n}, 2(m-1)\pi)}{\sin \frac{1}{2}\mu_{2n}}. \tag{B.4.7}
\end{aligned}$$

For the integrals involving the odd function in S :

$$\begin{aligned}
G_7 &= \int_{-1/2}^{1/2} D\bar{S}_o \left(\frac{\sinh \mu_{2m}x}{\sinh \frac{1}{2}\mu_{2m}} - \frac{\sin \mu_{2m}x}{\sin \frac{1}{2}\mu_{2m}} \right) \sin(2m-1)\pi x dx \\
&= -\frac{Ra_T S4a(\mu_{2m}, (2m-1)\pi)}{Ra_S \sinh \frac{1}{2}\mu_{2m}}
\end{aligned}$$

$$\begin{aligned}
& + \frac{Ra_T 2\lambda_1 S4de(M, M, \mu_{2m}, (2m-1)\pi)}{Ra_S(\sin M + \sinh M) \sinh \frac{1}{2}\mu_{2m}} \\
& + \frac{Ra_T 2\lambda_2 S2cd(\mu_{2m}, (2m-1)\pi, M, M)}{Ra_S(\sin M + \sinh M) \sinh \frac{1}{2}\mu_{2m}} \\
& + \frac{Ra_T S4f(\mu_{2m}, (2m-1)\pi)}{Ra_S \sin \frac{1}{2}\mu_{2m}} \\
& - \frac{Ra_T 2\lambda_1 S4h(M, M, \mu_{2m}, (2m-1)\pi)}{Ra_S(\sin M + \sinh M) \sin \frac{1}{2}\mu_{2m}} \\
& - \frac{Ra_T 2\lambda_2 T3b(M, \mu_{2m}, (2m-1)\pi, M)}{Ra_S(\sin M + \sinh M) \sin \frac{1}{2}\mu_{2m}}. \tag{B.4.8}
\end{aligned}$$

$$\begin{aligned}
G_8 & = \int_{-1/2}^{1/2} \overline{w}_o \cos 2(m-1)\pi x \sin(2m-1)\pi x dx \\
& = \frac{Ra_T \sinh \frac{1}{2}M \cos \frac{1}{2}M T3b(M, M, (2m-1)\pi, 2(m-1)\pi)}{M^3(\sin M + \sinh M)} \\
& \quad - \frac{Ra_T \cosh \frac{1}{2}M \sin \frac{1}{2}M T3c(M, M, (2m-1)\pi, 2(m-1)\pi)}{M^3(\sin M + \sinh M)}. \tag{B.4.9}
\end{aligned}$$

$$\begin{aligned}
G_9 & = \int_{-1/2}^{1/2} \left(\frac{\sinh \mu_{2m-1}x}{\cosh \frac{1}{2}\mu_{2m-1}} + \frac{\sin \mu_{2m-1}x}{\cos \frac{1}{2}\mu_{2m-1}} \right) \sin(2m-1)\pi x dx \\
& = \frac{S4a(\mu_{2m-1}, (2m-1)\pi)}{\cosh \frac{1}{2}\mu_{2m-1}} + \frac{S4f(\mu_{2m-1}, (2m-1)\pi)}{\cos \frac{1}{2}\mu_{2m-1}}. \tag{B.4.10}
\end{aligned}$$

$$\begin{aligned}
G_{10} & = \int_{-1/2}^{1/2} D\overline{S}_o \left(\frac{\sinh \mu_{2n}x}{\sinh \frac{1}{2}\mu_{2n}} - \frac{\sin \mu_{2n}x}{\sin \frac{1}{2}\mu_{2n}} \right) \sin(2m-1)\pi x dx \\
& = - \frac{Ra_T S4a(\mu_{2n}, (2m-1)\pi)}{Ra_S \sinh \frac{1}{2}\mu_{2n}} \\
& \quad + \frac{Ra_T 2\lambda_1 S4de(M, M, \mu_{2n}, (2m-1)\pi)}{Ra_S(\sin M + \sinh M) \sinh \frac{1}{2}\mu_{2n}} \\
& \quad + \frac{Ra_T 2\lambda_2 S2cd(\mu_{2n}, (2m-1)\pi, M, M)}{Ra_S(\sin M + \sinh M) \sinh \frac{1}{2}\mu_{2n}}
\end{aligned}$$

$$\begin{aligned}
& + \frac{Ra_T S4f(\mu_{2n}, (2m-1)\pi)}{Ra_S \sin \frac{1}{2}\mu_{2n}} \\
& - \frac{Ra_T 2\lambda_1 S4h(M, M, \mu_{2n}, (2m-1)\pi)}{Ra_S (\sin M + \sinh M) \sin \frac{1}{2}\mu_{2n}} \\
& - \frac{Ra_T 2\lambda_2 T3b(M, \mu_{2n}, (2m-1)\pi, M)}{Ra_S (\sin M + \sinh M) \sin \frac{1}{2}\mu_{2n}}. \tag{B.4.11}
\end{aligned}$$

$$\begin{aligned}
G_{11} &= \int_{-1/2}^{1/2} \bar{w}_o \cos 2(n-1)\pi x \sin(2m-1)\pi x dx \\
&= \frac{Ra_T \sinh \frac{1}{2}M \cos \frac{1}{2}M T3b(M, M, (2m-1)\pi, 2(n-1)\pi)}{M^3 (\sin M + \sinh M)} \\
&\quad - \frac{Ra_T \cosh \frac{1}{2}M \sin \frac{1}{2}M T3c(M, M, (2m-1)\pi, 2(n-1)\pi)}{M^3 (\sin M + \sinh M)}. \tag{B.4.12}
\end{aligned}$$

$$\begin{aligned}
G_{12} &= \int_{-1/2}^{1/2} \left(\frac{\sinh \mu_{2n-1} x}{\cosh \frac{1}{2}\mu_{2n-1}} + \frac{\sin \mu_{2n-1} x}{\cos \frac{1}{2}\mu_{2n-1}} \right) \sin(2m-1)\pi x dx \\
&= \frac{S4a(\mu_{2n-1}, (2m-1)\pi)}{\cosh \frac{1}{2}\mu_{2n-1}} + \frac{S4f(\mu_{2n-1}, (2m-1)\pi)}{\cos \frac{1}{2}\mu_{2n-1}}. \tag{B.4.13}
\end{aligned}$$

B.5 Abbreviated Integrals

$$\begin{aligned}
T3b(a, b, c, d) &= \int_{-1/2}^{1/2} \cosh ax \sin bx \sin cx \cos dx dx = \\
& - \frac{a \cos \frac{1}{2}(b+c+d) \sinh \frac{1}{2}a}{2[a^2 + (b+c+d)^2]} - \frac{(b+c+d) \sin \frac{1}{2}(b+c+d) \cosh \frac{1}{2}a}{2[a^2 + (b+c+d)^2]} \\
& - \frac{a \cos \frac{1}{2}(b+c-d) \sinh \frac{1}{2}a}{2[a^2 + (b+c-d)^2]} - \frac{(b+c-d) \sin \frac{1}{2}(b+c-d) \cosh \frac{1}{2}a}{2[a^2 + (b+c-d)^2]} \\
& + \frac{a \cos \frac{1}{2}(b-c+d) \sinh \frac{1}{2}a}{2[a^2 + (b-c+d)^2]} + \frac{(b-c+d) \sin \frac{1}{2}(b-c+d) \cosh \frac{1}{2}a}{2[a^2 + (b-c+d)^2]} \\
& + \frac{a \cos \frac{1}{2}(b-c-d) \sinh \frac{1}{2}a}{2[a^2 + (b-c-d)^2]} + \frac{(b-c-d) \sin \frac{1}{2}(b-c-d) \cosh \frac{1}{2}a}{2[a^2 + (b-c-d)^2]}. \tag{B.5.1}
\end{aligned}$$

$$\begin{aligned}
T3c(a, b, c, d) &= \int_{-1/2}^{1/2} \sinh ax \cos bx \sin cx \cos dx \, dx = \\
&- \frac{(b+c+d) \cos \frac{1}{2}(b+c+d) \sinh \frac{1}{2}a}{2[a^2 + (b+c+d)^2]} + \frac{a \sin \frac{1}{2}(b+c+d) \cosh \frac{1}{2}a}{2[a^2 + (b+c+d)^2]} \\
&- \frac{(b+c-d) \cos \frac{1}{2}(b+c-d) \sinh \frac{1}{2}a}{2[a^2 + (b+c-d)^2]} + \frac{a \sin \frac{1}{2}(b+c-d) \cosh \frac{1}{2}a}{2[a^2 + (b+c-d)^2]} \\
&+ \frac{(b-c+d) \cos \frac{1}{2}(b-c+d) \sinh \frac{1}{2}a}{2[a^2 + (b-c+d)^2]} - \frac{a \sin \frac{1}{2}(b-c+d) \cosh \frac{1}{2}a}{2[a^2 + (b-c+d)^2]} \\
&+ \frac{(b-c-d) \cos \frac{1}{2}(b-c-d) \sinh \frac{1}{2}a}{2[a^2 + (b-c-d)^2]} - \frac{a \sin \frac{1}{2}(b-c-d) \cosh \frac{1}{2}a}{2[a^2 + (b-c-d)^2]}.
\end{aligned} \tag{B.5.2}$$

$$\begin{aligned}
S2a(a, b) &= \int_{-1/2}^{1/2} \cosh ax \cos bx \, dx \\
&= \frac{2[a \cos \frac{1}{2}b \sinh \frac{1}{2}a + b \sin \frac{1}{2}b \cosh \frac{1}{2}a]}{a^2 + b^2}.
\end{aligned} \tag{B.5.3}$$

$$\begin{aligned}
S2cd(a, b, c, d) &= \int_{-1/2}^{1/2} \sinh ax \sin bx \cosh cx \cos dx \, dx \\
&= \frac{(\cosh \frac{1}{2}a - \sinh \frac{1}{2}a)(\cosh \frac{1}{2}c + \sinh \frac{1}{2}c)[(b+d) \cos \frac{1}{2}(b+d) + (a-c) \sin \frac{1}{2}(b+d)]}{4(a^2 - 2ac + b^2 + 2bd + c^2 + d^2)} \\
&+ \frac{(\cosh \frac{1}{2}a - \sinh \frac{1}{2}a)(\cosh \frac{1}{2}c + \sinh \frac{1}{2}c)[(b-d) \cos \frac{1}{2}(b-d) + (a-c) \sin \frac{1}{2}(b-d)]}{4(c^2 - 2ac + b^2 - 2bd + c^2 + d^2)} \\
&+ \frac{(\cosh \frac{1}{2}a - \sinh \frac{1}{2}a)(\cosh \frac{1}{2}c - \sinh \frac{1}{2}c)[(b+d) \cos \frac{1}{2}(b+d) + (a+c) \sin \frac{1}{2}(b+d)]}{4(a^2 + 2ac + b^2 + 2bd + c^2 + d^2)} \\
&+ \frac{(\cosh \frac{1}{2}a - \sinh \frac{1}{2}a)(\cosh \frac{1}{2}c - \sinh \frac{1}{2}c)[(b-d) \cos \frac{1}{2}(b-d) + (a+c) \sin \frac{1}{2}(b-d)]}{4(a^2 + 2ac + b^2 - 2bd + c^2 + d^2)} \\
&- \frac{(\cosh \frac{1}{2}a + \sinh \frac{1}{2}a)(\cosh \frac{1}{2}c + \sinh \frac{1}{2}c)[(b+d) \cos \frac{1}{2}(b+d) - (a+c) \sin \frac{1}{2}(b+d)]}{4(a^2 + 2ac + b^2 + 2bd + c^2 + d^2)} \\
&- \frac{(\cosh \frac{1}{2}a + \sinh \frac{1}{2}a)(\cosh \frac{1}{2}c + \sinh \frac{1}{2}c)[(b-d) \cos \frac{1}{2}(b-d) - (a+c) \sin \frac{1}{2}(b-d)]}{4(c^2 + 2ac + b^2 - 2bd + c^2 + d^2)}.
\end{aligned}$$

$$\begin{aligned}
& \frac{(\cosh \frac{1}{2}a + \sinh \frac{1}{2}c)(\cosh \frac{1}{2}c - \sinh \frac{1}{2}c)[(b+d)\cos \frac{1}{2}(b+d) + (c-a)\sin \frac{1}{2}(b+d)]}{4(a^2 - 2ac + b^2 + 2bd + c^2 + d^2)} \\
& - \frac{(\cosh \frac{1}{2}a + \sinh \frac{1}{2}a)(\cosh \frac{1}{2}c - \sinh \frac{1}{2}c)[(b-d)\cos \frac{1}{2}(b-d) + (c-a)\sin \frac{1}{2}(b-d)]}{4(a^2 - 2ac + b^2 - 2bd + c^2 + d^2)}.
\end{aligned} \tag{B.5.4}$$

If $a \neq b$,

$$\begin{aligned}
S2i(a, b) &= \int_{-1/2}^{1/2} \cos ax \cos bx \, dx \\
&= \frac{\sin \frac{1}{2}(a+b)}{a+b} + \frac{\sin \frac{1}{2}(a-b)}{a-b},
\end{aligned}$$

$$S2i(a, a) = \frac{\sin a}{2a} + \frac{1}{2}. \tag{B.5.5}$$

$$\begin{aligned}
S2gh(a, b, c, d) &= \int_{-1/2}^{1/2} \cosh ax \cos bx \cosh cx \cos dx \, dx \\
&= \frac{(\cosh \frac{1}{2}a + \sinh \frac{1}{2}a)(\cosh \frac{1}{2}c + \sinh \frac{1}{2}c)[(a+c)\cos \frac{1}{2}(b+d) + (b+d)\sin \frac{1}{2}(b+d)]}{4(a^2 + 2ac + b^2 + 2bd + c^2 + d^2)} \\
&+ \frac{(\cosh \frac{1}{2}a + \sinh \frac{1}{2}a)(\cosh \frac{1}{2}c + \sinh \frac{1}{2}c)[(a+c)\cos \frac{1}{2}(b-d) + (b-d)\sin \frac{1}{2}(b-d)]}{4(a^2 + 2ac + b^2 - 2bd + c^2 + d^2)} \\
&+ \frac{(\cosh \frac{1}{2}a + \sinh \frac{1}{2}a)(\cosh \frac{1}{2}c - \sinh \frac{1}{2}c)[(a-c)\cos \frac{1}{2}(b+d) + (b+d)\sin \frac{1}{2}(b+d)]}{4(a^2 - 2ac + b^2 + 2bd + c^2 + d^2)} \\
&+ \frac{(\cosh \frac{1}{2}a + \sinh \frac{1}{2}a)(\cosh \frac{1}{2}c - \sinh \frac{1}{2}c)[(a-c)\cos \frac{1}{2}(b-d) + (b-d)\sin \frac{1}{2}(b-d)]}{4(a^2 - 2ac + b^2 - 2bd + c^2 + d^2)} \\
&- \frac{(\cosh \frac{1}{2}a - \sinh \frac{1}{2}a)(\cosh \frac{1}{2}c + \sinh \frac{1}{2}c)[(a-c)\cos \frac{1}{2}(b+d) - (b+d)\sin \frac{1}{2}(b+d)]}{4(a^2 - 2ac + b^2 + 2bd + c^2 + d^2)} \\
&- \frac{(\cosh \frac{1}{2}a - \sinh \frac{1}{2}a)(\cosh \frac{1}{2}c + \sinh \frac{1}{2}c)[(a-c)\cos \frac{1}{2}(b-d) + (d-b)\sin \frac{1}{2}(b-d)]}{4(a^2 - 2ac + b^2 - 2bd + c^2 + d^2)} \\
&- \frac{(\cosh \frac{1}{2}a - \sinh \frac{1}{2}a)(\cosh \frac{1}{2}c - \sinh \frac{1}{2}c)[(a+c)\cos \frac{1}{2}(b+d) - (b+d)\sin \frac{1}{2}(b+d)]}{4(a^2 + 2ac + b^2 + 2bd + c^2 + d^2)}
\end{aligned}$$

$$\frac{(\cosh \frac{1}{2}a - \sinh \frac{1}{2}a)(\cosh \frac{1}{2}c - \sinh \frac{1}{2}c)[(a+c)\cos \frac{1}{2}(b-d) + (d-b)\sin \frac{1}{2}(b-d)]}{4(a^2 + 2ac + b^2 - 2bd + c^2 + d^2)} \quad (\text{B.5.6})$$

$$\begin{aligned} S2k(a, b, c, d) &= \int_{-1/2}^{1/2} \cosh ax \cos bx \cos cx \cos dx \, dx = \\ &= \frac{a \cos \frac{1}{2}(b+c+d) \sinh \frac{1}{2}a}{2[a^2 + (b+c+d)^2]} + \frac{(b+c+d) \sin \frac{1}{2}(b+c+d) \cosh \frac{1}{2}a}{2[a^2 + (b+c+d)^2]} \\ &+ \frac{a \cos \frac{1}{2}(b+c-d) \sinh \frac{1}{2}a}{2[a^2 + (b+c-d)^2]} + \frac{(b+c-d) \sin \frac{1}{2}(b+c-d) \cosh \frac{1}{2}a}{2[a^2 + (b+c-d)^2]} \\ &+ \frac{a \cos \frac{1}{2}(b-c+d) \sinh \frac{1}{2}a}{2[a^2 + (b-c+d)^2]} + \frac{(b-c+d) \sin \frac{1}{2}(b-c+d) \cosh \frac{1}{2}a}{2[a^2 + (b-c+d)^2]} \\ &+ \frac{a \cos \frac{1}{2}(b-c-d) \sinh \frac{1}{2}a}{2[a^2 + (b-c-d)^2]} + \frac{(b-c-d) \sin \frac{1}{2}(b-c-d) \cosh \frac{1}{2}a}{2[a^2 + (b-c-d)^2]} \end{aligned} \quad (\text{B.5.7})$$

$$\begin{aligned} S4a(a, b) &= \int_{-1/2}^{1/2} \sinh ax \sin bx \, dx \\ &= \frac{2a \sin \frac{1}{2}b \cosh \frac{1}{2}a}{a^2 + b^2} - \frac{2b \cos \frac{1}{2}b \sinh \frac{1}{2}a}{a^2 + b^2} \end{aligned} \quad (\text{B.5.8})$$

$$\begin{aligned} S4de(a, b, c, d) &= \int_{-1/2}^{1/2} \sinh ax \sin bx \sinh cx \sin dx \, dx \\ &= \frac{(\cosh \frac{1}{2}a + \sinh \frac{1}{2}a)(\cosh \frac{1}{2}c - \sinh \frac{1}{2}c)[(a-c)\cos \frac{1}{2}(b+d) + (b+d)\sin \frac{1}{2}(b+d)]}{4(a^2 - 2ac + b^2 + 2bd + c^2 + d^2)} \\ &+ \frac{(\cosh \frac{1}{2}a + \sinh \frac{1}{2}a)(\cosh \frac{1}{2}c - \sinh \frac{1}{2}c)[(c-a)\cos \frac{1}{2}(b-d) + (d-b)\sin \frac{1}{2}(b-d)]}{4(a^2 - 2ac + b^2 - 2bd + c^2 + d^2)} \\ &- \frac{(\cosh \frac{1}{2}a + \sinh \frac{1}{2}a)(\cosh \frac{1}{2}c + \sinh \frac{1}{2}c)[(a+c)\cos \frac{1}{2}(b+d) + (b+d)\sin \frac{1}{2}(b+d)]}{4(a^2 + 2ac + b^2 + 2bd + c^2 + d^2)} \\ &- \frac{(\cosh \frac{1}{2}a + \sinh \frac{1}{2}a)(\cosh \frac{1}{2}c + \sinh \frac{1}{2}c)[(d-b)\sin \frac{1}{2}(b-d) - (a+c)\cos \frac{1}{2}(b-d)]}{4(a^2 + 2ac + b^2 - 2bd + c^2 + d^2)} \\ &+ \frac{(\cosh \frac{1}{2}a - \sinh \frac{1}{2}a)(\cosh \frac{1}{2}c - \sinh \frac{1}{2}c)[(a+c)\cos \frac{1}{2}(b+d) - (b+d)\sin \frac{1}{2}(b+d)]}{4(a^2 + 2ac + b^2 + 2bd + c^2 + d^2)} \end{aligned}$$

$$\begin{aligned}
& + \frac{(\cosh \frac{1}{2}a - \sinh \frac{1}{2}a)(\cosh \frac{1}{2}c - \sinh \frac{1}{2}c)[(b-d) \sin \frac{1}{2}(b-d) - (a+c) \cos \frac{1}{2}(b-d)]}{4(a^2 + 2ac + b^2 - 2bd + c^2 + d^2)} \\
& - \frac{(\cosh \frac{1}{2}a - \sinh \frac{1}{2}a)(\cosh \frac{1}{2}c + \sinh \frac{1}{2}c)[(a-c) \cos \frac{1}{2}(b+d) - (b+d) \sin \frac{1}{2}(b+d)]}{4(a^2 - 2ac + b^2 + 2bd + c^2 + d^2)} \\
& - \frac{(\cosh \frac{1}{2}a - \sinh \frac{1}{2}a)(\cosh \frac{1}{2}c + \sinh \frac{1}{2}c)[(c-a) \cos \frac{1}{2}(b-d) + (b-d) \sin \frac{1}{2}(b-d)]}{4(a^2 - 2ac + b^2 - 2bd + c^2 + d^2)}.
\end{aligned} \tag{B.5.9}$$

If $a \neq b$,

$$\begin{aligned}
S4f(a, b) &= \int_{-1/2}^{1/2} \sin ax \sin bx \, dx \\
&= \frac{\sin \frac{1}{2}(a-b)}{a-b} - \frac{\sin \frac{1}{2}(a+b)}{a+b}, \\
S4f(a, a) &= \frac{1}{2} - \frac{\sin a}{2a}.
\end{aligned} \tag{B.5.10}$$

$$\begin{aligned}
S4h(a, b, c, d) &= \int_{-1/2}^{1/2} \sinh ax \sin bx \sin cx \sin dx \, dx = \\
& \frac{(b+c+d) \cos \frac{1}{2}(b+c+d) \sinh \frac{1}{2}a}{2[a^2 + (b+c+d)^2]} - \frac{a \sin \frac{1}{2}(b+c+d) \cosh \frac{1}{2}a}{2[a^2 + (b+c+d)^2]} \\
& - \frac{(b+c-d) \cos \frac{1}{2}(b+c-d) \sinh \frac{1}{2}a}{2[a^2 + (b+c-d)^2]} + \frac{a \sin \frac{1}{2}(b+c-d) \cosh \frac{1}{2}a}{2[a^2 + (b+c-d)^2]} \\
& - \frac{(b-c+d) \cos \frac{1}{2}(b-c+d) \sinh \frac{1}{2}a}{2[a^2 + (b-c+d)^2]} + \frac{a \sin \frac{1}{2}(b-c+d) \cosh \frac{1}{2}a}{2[a^2 + (b-c+d)^2]} \\
& + \frac{(b-c-d) \cos \frac{1}{2}(b-c-d) \sinh \frac{1}{2}a}{2[a^2 + (b-c-d)^2]} - \frac{a \sin \frac{1}{2}(b-c-d) \cosh \frac{1}{2}a}{2[a^2 + (b-c-d)^2]}.
\end{aligned} \tag{B.5.11}$$

If $a \neq b$,

$$P1a(a, b) = \int_{-1/2}^{1/2} \cosh ax \cosh bx \, dx$$

$$\begin{aligned}
&= \frac{(\cosh \frac{1}{2}a + \sinh \frac{1}{2}a)(\cosh \frac{1}{2}b + \sinh \frac{1}{2}b)}{2(a+b)} + \frac{(\cosh \frac{1}{2}a + \sinh \frac{1}{2}a)(\cosh \frac{1}{2}b - \sinh \frac{1}{2}b)}{2(a-b)} \\
&- \frac{(\cosh \frac{1}{2}a - \sinh \frac{1}{2}a)(\cosh \frac{1}{2}b + \sinh \frac{1}{2}b)}{2(a-b)} - \frac{(\cosh \frac{1}{2}a - \sinh \frac{1}{2}a)(\cosh \frac{1}{2}b - \sinh \frac{1}{2}b)}{2(a+b)}, \\
P1a(a, a) &= \frac{(\cosh \frac{1}{2}a + \sinh \frac{1}{2}a)^2}{4a} + \frac{1}{2} - \frac{(\cosh \frac{1}{2}a - \sinh \frac{1}{2}a)^2}{4a}. \tag{B.5.12}
\end{aligned}$$

$$\begin{aligned}
P3ef(a, b, c, d) &= \int_{-1/2}^{1/2} \cosh ax \sin bx \sinh cx \cosh dx \, dx \\
&= \frac{(\cosh \frac{1}{2}a + \sinh \frac{1}{2}a)(\cosh \frac{1}{2}c - \sinh \frac{1}{2}c)(\cosh \frac{1}{2}d + \sinh \frac{1}{2}d)b \cos \frac{1}{2}b}{4(a^2 + 2a(d-c) + b^2 + c^2 - 2cd + d^2)} \\
&- \frac{(\cosh \frac{1}{2}a + \sinh \frac{1}{2}a)(\cosh \frac{1}{2}c - \sinh \frac{1}{2}c)(\cosh \frac{1}{2}d + \sinh \frac{1}{2}d)(a-c+d) \sin \frac{1}{2}b}{4(a^2 + 2a(d-c) + b^2 + c^2 - 2cd + d^2)} \\
&+ \frac{(\cosh \frac{1}{2}a + \sinh \frac{1}{2}a)(\cosh \frac{1}{2}c - \sinh \frac{1}{2}c)(\cosh \frac{1}{2}d - \sinh \frac{1}{2}d)b \cos \frac{1}{2}b}{4(a^2 - 2a(c+d) + b^2 + c^2 + 2cd + d^2)} \\
&- \frac{(\cosh \frac{1}{2}a + \sinh \frac{1}{2}a)(\cosh \frac{1}{2}c - \sinh \frac{1}{2}c)(\cosh \frac{1}{2}d - \sinh \frac{1}{2}d)(a-c-d) \sin \frac{1}{2}b}{4(a^2 - 2a(c+d) + b^2 + c^2 + 2cd + d^2)} \\
&- \frac{(\cosh \frac{1}{2}a + \sinh \frac{1}{2}a)(\cosh \frac{1}{2}c + \sinh \frac{1}{2}c)(\cosh \frac{1}{2}d + \sinh \frac{1}{2}d)b \cos \frac{1}{2}b}{4(a^2 + 2a(c+d) + b^2 + c^2 + 2cd + d^2)} \\
&+ \frac{(\cosh \frac{1}{2}a + \sinh \frac{1}{2}a)(\cosh \frac{1}{2}c + \sinh \frac{1}{2}c)(\cosh \frac{1}{2}d + \sinh \frac{1}{2}d)(a+c+d) \sin \frac{1}{2}b}{4(a^2 + 2a(c+d) + b^2 + c^2 + 2cd + d^2)} \\
&- \frac{(\cosh \frac{1}{2}a + \sinh \frac{1}{2}a)(\cosh \frac{1}{2}c + \sinh \frac{1}{2}c)(\cosh \frac{1}{2}d - \sinh \frac{1}{2}d)b \cos \frac{1}{2}b}{4(a^2 + 2a(c-d) + b^2 + c^2 - 2cd + d^2)} \\
&+ \frac{(\cosh \frac{1}{2}a + \sinh \frac{1}{2}a)(\cosh \frac{1}{2}c + \sinh \frac{1}{2}c)(\cosh \frac{1}{2}d - \sinh \frac{1}{2}d)(a+c-d) \sin \frac{1}{2}b}{4(a^2 + 2a(c-d) + b^2 + c^2 - 2cd + d^2)} \\
&+ \frac{(\cosh \frac{1}{2}a - \sinh \frac{1}{2}a)(\cosh \frac{1}{2}c - \sinh \frac{1}{2}c)(\cosh \frac{1}{2}d + \sinh \frac{1}{2}d)b \cos \frac{1}{2}b}{4(a^2 + 2a(c-d) + b^2 + c^2 - 2cd + d^2)} \\
&+ \frac{(\cosh \frac{1}{2}a - \sinh \frac{1}{2}a)(\cosh \frac{1}{2}c - \sinh \frac{1}{2}c)(\cosh \frac{1}{2}d + \sinh \frac{1}{2}d)(a+c-d) \sin \frac{1}{2}b}{4(a^2 + 2a(c-d) + b^2 + c^2 - 2cd + d^2)}
\end{aligned}$$

$$\begin{aligned}
& + \frac{(\cosh \frac{1}{2}a - \sinh \frac{1}{2}a)(\cosh \frac{1}{2}c - \sinh \frac{1}{2}c)(\cosh \frac{1}{2}d - \sinh \frac{1}{2}d)b \cos \frac{1}{2}b}{4(a^2 + 2a(c+d) + b^2 + c^2 + 2cd + d^2)} \\
& + \frac{(\cosh \frac{1}{2}a - \sinh \frac{1}{2}a)(\cosh \frac{1}{2}c - \sinh \frac{1}{2}c)(\cosh \frac{1}{2}d - \sinh \frac{1}{2}d)(a+c+d) \sin \frac{1}{2}b}{4(a^2 + 2a(c+d) + b^2 + c^2 + 2cd + d^2)} \\
& - \frac{(\cosh \frac{1}{2}a - \sinh \frac{1}{2}a)(\cosh \frac{1}{2}c + \sinh \frac{1}{2}c)(\cosh \frac{1}{2}d + \sinh \frac{1}{2}d)b \cos \frac{1}{2}b}{4(a^2 - 2a(c+d) + b^2 + c^2 + 2cd + d^2)} \\
& - \frac{(\cosh \frac{1}{2}a - \sinh \frac{1}{2}a)(\cosh \frac{1}{2}c + \sinh \frac{1}{2}c)(\cosh \frac{1}{2}d + \sinh \frac{1}{2}d)(a-c-d) \sin \frac{1}{2}b}{4(a^2 - 2a(c+d) + b^2 + c^2 + 2cd + d^2)} \\
& - \frac{(\cosh \frac{1}{2}a - \sinh \frac{1}{2}a)(\cosh \frac{1}{2}c + \sinh \frac{1}{2}c)(\cosh \frac{1}{2}d - \sinh \frac{1}{2}d)(a-c+d) \sin \frac{1}{2}b}{4(a^2 + 2a(d-c) + b^2 + c^2 - 2cd + d^2)} \\
& - \frac{(\cosh \frac{1}{2}a - \sinh \frac{1}{2}a)(\cosh \frac{1}{2}c + \sinh \frac{1}{2}c)(\cosh \frac{1}{2}d - \sinh \frac{1}{2}d)b \cos \frac{1}{2}b}{4(a^2 + 2a(d-c) + b^2 + c^2 - 2cd + d^2)}. \quad (\text{B.5.13})
\end{aligned}$$

$$\begin{aligned}
P4ef(a, b, c, d) &= \int_{-1/2}^{1/2} \sinh ax \cos bx \sinh cx \cosh dx \, dx \\
&= \frac{(\cosh \frac{1}{2}a + \sinh \frac{1}{2}a)(\cosh \frac{1}{2}c + \sinh \frac{1}{2}c)(\cosh \frac{1}{2}d + \sinh \frac{1}{2}d)(a+c+d) \cos \frac{1}{2}b}{4(a^2 + 2a(c+d) + b^2 + c^2 + 2cd + d^2)} \\
&+ \frac{(\cosh \frac{1}{2}a + \sinh \frac{1}{2}a)(\cosh \frac{1}{2}c + \sinh \frac{1}{2}c)(\cosh \frac{1}{2}d + \sinh \frac{1}{2}d)b \sin \frac{1}{2}b}{4(a^2 + 2a(c+d) + b^2 + c^2 + 2cd + d^2)} \\
&+ \frac{(\cosh \frac{1}{2}a + \sinh \frac{1}{2}a)(\cosh \frac{1}{2}c + \sinh \frac{1}{2}c)(\cosh \frac{1}{2}d - \sinh \frac{1}{2}d)(a+c-d) \cos \frac{1}{2}b}{4(a^2 + 2a(c-d) + b^2 + c^2 - 2cd + d^2)} \\
&+ \frac{(\cosh \frac{1}{2}a + \sinh \frac{1}{2}a)(\cosh \frac{1}{2}c + \sinh \frac{1}{2}c)(\cosh \frac{1}{2}d - \sinh \frac{1}{2}d)b \sin \frac{1}{2}b}{4(a^2 + 2a(c-d) + b^2 + c^2 - 2cd + d^2)} \\
&- \frac{(\cosh \frac{1}{2}a + \sinh \frac{1}{2}a)(\cosh \frac{1}{2}c - \sinh \frac{1}{2}c)(\cosh \frac{1}{2}d + \sinh \frac{1}{2}d)(a-c+d) \cos \frac{1}{2}b}{4(a^2 + 2a(d-c) + b^2 + c^2 - 2cd + d^2)} \\
&- \frac{(\cosh \frac{1}{2}a + \sinh \frac{1}{2}a)(\cosh \frac{1}{2}c - \sinh \frac{1}{2}c)(\cosh \frac{1}{2}d + \sinh \frac{1}{2}d)b \sin \frac{1}{2}b}{4(a^2 + 2a(d-c) + b^2 + c^2 - 2cd + d^2)} \\
&- \frac{(\cosh \frac{1}{2}a + \sinh \frac{1}{2}a)(\cosh \frac{1}{2}c - \sinh \frac{1}{2}c)(\cosh \frac{1}{2}d - \sinh \frac{1}{2}d)(a-c-d) \cos \frac{1}{2}b}{4(a^2 - 2a(c+d) + b^2 + c^2 + 2cd + d^2)}
\end{aligned}$$

$$\begin{aligned}
& - \frac{(\cosh \frac{1}{2}a + \sinh \frac{1}{2}a)(\cosh \frac{1}{2}c - \sinh \frac{1}{2}c)(\cosh \frac{1}{2}d - \sinh \frac{1}{2}d)b \sin \frac{1}{2}b}{4(a^2 - 2a(c+d) + b^2 + c^2 + 2cd + d^2)} \\
& + \frac{(\cosh \frac{1}{2}a - \sinh \frac{1}{2}a)(\cosh \frac{1}{2}c + \sinh \frac{1}{2}c)(\cosh \frac{1}{2}d + \sinh \frac{1}{2}d)(a - c - d) \cos \frac{1}{2}b}{4(a^2 - 2a(c+d) + b^2 + c^2 + 2cd + d^2)} \\
& - \frac{(\cosh \frac{1}{2}a - \sinh \frac{1}{2}a)(\cosh \frac{1}{2}c + \sinh \frac{1}{2}c)(\cosh \frac{1}{2}d + \sinh \frac{1}{2}d)b \sin \frac{1}{2}b}{4(a^2 - 2a(c+d) + b^2 + c^2 + 2cd + d^2)} \\
& + \frac{(\cosh \frac{1}{2}a - \sinh \frac{1}{2}a)(\cosh \frac{1}{2}c + \sinh \frac{1}{2}c)(\cosh \frac{1}{2}d - \sinh \frac{1}{2}d)(a - c + d) \cos \frac{1}{2}b}{4(a^2 + 2a(d-c) + b^2 + c^2 - 2cd + d^2)} \\
& - \frac{(\cosh \frac{1}{2}a - \sinh \frac{1}{2}a)(\cosh \frac{1}{2}c + \sinh \frac{1}{2}c)(\cosh \frac{1}{2}d - \sinh \frac{1}{2}d)b \sin \frac{1}{2}b}{4(a^2 + 2a(d-c) + b^2 + c^2 - 2cd + d^2)} \\
& - \frac{(\cosh \frac{1}{2}a - \sinh \frac{1}{2}a)(\cosh \frac{1}{2}c - \sinh \frac{1}{2}c)(\cosh \frac{1}{2}d + \sinh \frac{1}{2}d)(a + c - d) \cos \frac{1}{2}b}{4(a^2 + 2a(c-d) + b^2 + c^2 - 2cd + d^2)} \\
& + \frac{(\cosh \frac{1}{2}a - \sinh \frac{1}{2}a)(\cosh \frac{1}{2}c - \sinh \frac{1}{2}c)(\cosh \frac{1}{2}d + \sinh \frac{1}{2}d)b \sin \frac{1}{2}b}{4(a^2 + 2a(c-d) + b^2 + c^2 - 2cd + d^2)} \\
& - \frac{(\cosh \frac{1}{2}a - \sinh \frac{1}{2}a)(\cosh \frac{1}{2}c - \sinh \frac{1}{2}c)(\cosh \frac{1}{2}d - \sinh \frac{1}{2}d)(a + c + d) \cos \frac{1}{2}b}{4(a^2 + 2a(c+d) + b^2 + c^2 + 2cd + d^2)} \\
& + \frac{(\cosh \frac{1}{2}a - \sinh \frac{1}{2}a)(\cosh \frac{1}{2}c - \sinh \frac{1}{2}c)(\cosh \frac{1}{2}d - \sinh \frac{1}{2}d)b \sin \frac{1}{2}b}{4(a^2 + 2a(c+d) + b^2 + c^2 + 2cd + d^2)}. \quad (\text{B.5.14})
\end{aligned}$$

$$\begin{aligned}
P5de(a, b, c, d) &= \int_{-1/2}^{1/2} \sinh ax \cos bx \sinh cx \cos dx \, dx \\
&= \frac{(\cosh \frac{1}{2}a + \sinh \frac{1}{2}a)(\cosh \frac{1}{2}c + \sinh \frac{1}{2}c)(a + c) \cos \frac{1}{2}(b + d)}{4(a^2 + 2ac + b^2 + 2bd + c^2 + d^2)} \\
&+ \frac{(\cosh \frac{1}{2}a + \sinh \frac{1}{2}a)(\cosh \frac{1}{2}c + \sinh \frac{1}{2}c)(b + d) \sin \frac{1}{2}(b + d)}{4(a^2 + 2ac + b^2 + 2bd + c^2 + d^2)} \\
&+ \frac{(\cosh \frac{1}{2}a + \sinh \frac{1}{2}a)(\cosh \frac{1}{2}c + \sinh \frac{1}{2}c)(a + c) \cos \frac{1}{2}(b - d)}{4(a^2 + 2ac + b^2 - 2bd + c^2 + d^2)} \\
&+ \frac{(\cosh \frac{1}{2}a + \sinh \frac{1}{2}a)(\cosh \frac{1}{2}c + \sinh \frac{1}{2}c)(b - d) \sin \frac{1}{2}(b - d)}{4(a^2 + 2ac + b^2 - 2bd + c^2 + d^2)}
\end{aligned}$$

$$\begin{aligned}
& - \frac{(\cosh \frac{1}{2}a + \sinh \frac{1}{2}a)(\cosh \frac{1}{2}c - \sinh \frac{1}{2}c)(a - c) \cos \frac{1}{2}(b + d)}{4(a^2 - 2ac + b^2 + 2bd + c^2 + d^2)} \\
& - \frac{(\cosh \frac{1}{2}a + \sinh \frac{1}{2}a)(\cosh \frac{1}{2}c - \sinh \frac{1}{2}c)(b + d) \sin \frac{1}{2}(b + d)}{4(a^2 - 2ac + b^2 + 2bd + c^2 + d^2)} \\
& - \frac{(\cosh \frac{1}{2}a + \sinh \frac{1}{2}a)(\cosh \frac{1}{2}c - \sinh \frac{1}{2}c)(a - c) \cos \frac{1}{2}(b - d)}{4(a^2 - 2ac + b^2 - 2bd + c^2 + d^2)} \\
& - \frac{(\cosh \frac{1}{2}a + \sinh \frac{1}{2}a)(\cosh \frac{1}{2}c - \sinh \frac{1}{2}c)(b - d) \sin \frac{1}{2}(b - d)}{4(a^2 - 2ac + b^2 - 2bd + c^2 + d^2)} \\
& + \frac{(\cosh \frac{1}{2}a - \sinh \frac{1}{2}a)(\cosh \frac{1}{2}c + \sinh \frac{1}{2}c)(a - c) \cos \frac{1}{2}(b + d)}{4(a^2 - 2ac + b^2 + 2bd + c^2 + d^2)} \\
& - \frac{(\cosh \frac{1}{2}a - \sinh \frac{1}{2}a)(\cosh \frac{1}{2}c + \sinh \frac{1}{2}c)(b + d) \sin \frac{1}{2}(b + d)}{4(a^2 - 2ac + b^2 + 2bd + c^2 + d^2)} \\
& + \frac{(\cosh \frac{1}{2}a - \sinh \frac{1}{2}a)(\cosh \frac{1}{2}c + \sinh \frac{1}{2}c)(a - c) \cos \frac{1}{2}(b - d)}{4(a^2 - 2ac + b^2 - 2bd + c^2 + d^2)} \\
& + \frac{(\cosh \frac{1}{2}a - \sinh \frac{1}{2}a)(\cosh \frac{1}{2}c + \sinh \frac{1}{2}c)(d - b) \sin \frac{1}{2}(b - d)}{4(a^2 - 2ac + b^2 - 2bd + c^2 + d^2)} \\
& - \frac{(\cosh \frac{1}{2}a - \sinh \frac{1}{2}a)(\cosh \frac{1}{2}c - \sinh \frac{1}{2}c)(a + c) \cos \frac{1}{2}(b + d)}{4(a^2 + 2ac + b^2 + 2bd + c^2 + d^2)} \\
& + \frac{(\cosh \frac{1}{2}a - \sinh \frac{1}{2}a)(\cosh \frac{1}{2}c - \sinh \frac{1}{2}c)(b + d) \sin \frac{1}{2}(b + d)}{4(a^2 + 2ac + b^2 + 2bd + c^2 + d^2)} \\
& - \frac{(\cosh \frac{1}{2}a - \sinh \frac{1}{2}a)(\cosh \frac{1}{2}c - \sinh \frac{1}{2}c)(a + c) \cos \frac{1}{2}(b - d)}{4(a^2 + 2ac + b^2 - 2bd + c^2 + d^2)} \\
& - \frac{(\cosh \frac{1}{2}a - \sinh \frac{1}{2}a)(\cosh \frac{1}{2}c - \sinh \frac{1}{2}c)(d - b) \sin \frac{1}{2}(b - d)}{4(a^2 + 2ac + b^2 - 2bd + c^2 + d^2)}.
\end{aligned}
\tag{B.5.15}$$

$$P6de(a, b, c, d) = \int_{-1/2}^{1/2} \cosh ax \sin bx \sin cx \cosh dx \, dx$$

$$\begin{aligned}
&= \frac{(\cosh \frac{1}{2}a - \sinh \frac{1}{2}a)(\cosh \frac{1}{2}d + \sinh \frac{1}{2}d)(a - d) \cos \frac{1}{2}(b + c)}{4(a^2 - 2ad + b^2 + 2bc + c^2 + d^2)} \\
&- \frac{(\cosh \frac{1}{2}a - \sinh \frac{1}{2}a)(\cosh \frac{1}{2}d + \sinh \frac{1}{2}d)(b + c) \sin \frac{1}{2}(b + c)}{4(a^2 - 2ad + b^2 + 2bc + c^2 + d^2)} \\
&+ \frac{(\cosh \frac{1}{2}a - \sinh \frac{1}{2}a)(\cosh \frac{1}{2}d + \sinh \frac{1}{2}d)(d - a) \cos \frac{1}{2}(b - c)}{4(a^2 - 2ad + b^2 - 2bc + c^2 + d^2)} \\
&+ \frac{(\cosh \frac{1}{2}a - \sinh \frac{1}{2}a)(\cosh \frac{1}{2}d + \sinh \frac{1}{2}d)(b - c) \sin \frac{1}{2}(b - c)}{4(a^2 - 2ad + b^2 - 2bc + c^2 + d^2)} \\
&+ \frac{(\cosh \frac{1}{2}a - \sinh \frac{1}{2}a)(\cosh \frac{1}{2}d - \sinh \frac{1}{2}d)(a + d) \cos \frac{1}{2}(b + c)}{4(a^2 + 2ad + b^2 + 2bc + c^2 + d^2)} \\
&- \frac{(\cosh \frac{1}{2}a - \sinh \frac{1}{2}a)(\cosh \frac{1}{2}d - \sinh \frac{1}{2}d)(b + c) \sin \frac{1}{2}(b + c)}{4(a^2 + 2ad + b^2 + 2bc + c^2 + d^2)} \\
&- \frac{(\cosh \frac{1}{2}a - \sinh \frac{1}{2}a)(\cosh \frac{1}{2}d - \sinh \frac{1}{2}d)(a + d) \cos \frac{1}{2}(b - c)}{4(a^2 + 2ad + b^2 - 2bc + c^2 + d^2)} \\
&+ \frac{(\cosh \frac{1}{2}a - \sinh \frac{1}{2}a)(\cosh \frac{1}{2}d - \sinh \frac{1}{2}d)(b - c) \sin \frac{1}{2}(b - c)}{4(a^2 + 2ad + b^2 - 2bc + c^2 + d^2)} \\
&- \frac{(\cosh \frac{1}{2}a + \sinh \frac{1}{2}a)(\cosh \frac{1}{2}d + \sinh \frac{1}{2}d)(a + d) \cos \frac{1}{2}(b + c)}{4(a^2 + 2ad + b^2 + 2bc + c^2 + d^2)} \\
&- \frac{(\cosh \frac{1}{2}a + \sinh \frac{1}{2}a)(\cosh \frac{1}{2}d + \sinh \frac{1}{2}d)(b + c) \sin \frac{1}{2}(b + c)}{4(a^2 + 2ad + b^2 + 2bc + c^2 + d^2)} \\
&+ \frac{(\cosh \frac{1}{2}a + \sinh \frac{1}{2}a)(\cosh \frac{1}{2}d + \sinh \frac{1}{2}d)(a + d) \cos \frac{1}{2}(b - c)}{4(a^2 + 2ad + b^2 - 2bc + c^2 + d^2)} \\
&- \frac{(\cosh \frac{1}{2}a + \sinh \frac{1}{2}a)(\cosh \frac{1}{2}d + \sinh \frac{1}{2}d)(c - b) \sin \frac{1}{2}(b - c)}{4(a^2 + 2ad + b^2 - 2bc + c^2 + d^2)} \\
&- \frac{(\cosh \frac{1}{2}a + \sinh \frac{1}{2}a)(\cosh \frac{1}{2}d - \sinh \frac{1}{2}d)(a - d) \cos \frac{1}{2}(b + c)}{4(a^2 - 2ad + b^2 + 2bc + c^2 + d^2)} \\
&- \frac{(\cosh \frac{1}{2}a + \sinh \frac{1}{2}a)(\cosh \frac{1}{2}d - \sinh \frac{1}{2}d)(b + c) \sin \frac{1}{2}(b + c)}{4(a^2 - 2ad + b^2 + 2bc + c^2 + d^2)}
\end{aligned}$$

$$\begin{aligned}
&= \frac{(\cosh \frac{1}{2}a + \sinh \frac{1}{2}a)(\cosh \frac{1}{2}d - \sinh \frac{1}{2}d)(d - a) \cos \frac{1}{2}(b - c)}{4(a^2 - 2ad + b^2 - 2bc + c^2 + d^2)} \\
&= \frac{(\cosh \frac{1}{2}a + \sinh \frac{1}{2}a)(\cosh \frac{1}{2}d - \sinh \frac{1}{2}d)(c - b) \sin \frac{1}{2}(b - c)}{4(a^2 - 2ad + b^2 - 2bc + c^2 + d^2)} \quad (\text{B.5.16})
\end{aligned}$$

If $a \neq b$,

$$\begin{aligned}
P7(a, b) &= \int_{-1/2}^{1/2} \sinh ax \sinh bx \, dx \\
&= \frac{(\cosh \frac{1}{2}a + \sinh \frac{1}{2}a)(\cosh \frac{1}{2}b + \sinh \frac{1}{2}b)}{2(a + b)} + \frac{(\cosh \frac{1}{2}a + \sinh \frac{1}{2}a)(\cosh \frac{1}{2}b - \sinh \frac{1}{2}b)}{2(b - a)} \\
&+ \frac{(\cosh \frac{1}{2}a - \sinh \frac{1}{2}a)(\cosh \frac{1}{2}b + \sinh \frac{1}{2}b)}{2(a - b)} - \frac{(\cosh \frac{1}{2}a - \sinh \frac{1}{2}a)(\cosh \frac{1}{2}b - \sinh \frac{1}{2}b)}{2(a + b)}, \\
P7(a, a) &= \frac{(\cosh \frac{1}{2}a + \sinh \frac{1}{2}a)^2}{4a} - \frac{1}{2} - \frac{(\cosh \frac{1}{2}a - \sinh \frac{1}{2}a)^2}{4a}. \quad (\text{B.5.17})
\end{aligned}$$

Appendix C

Small α

This appendix refers to the small α asymptotics section of chapter 5 which is divided into three parts. The first part looks into the solution of ψ_0 . The next two parts evaluate the two integrals from equation (5.2.24) in order to give the two expressions for $f(Ra_S, \tau)$ and $g(Ra_S, \tau)$.

C.1 Solution ψ_0

From the leading order problem we derived a fifth-order differential equation in order to find a solution to ψ_0 . The method used in solving this inhomogeneous ordinary differential equation

$$D^5\psi_0 + \frac{Ra_S}{\tau}D\psi_0 = -i\frac{Ra_S}{\tau}\overline{w_o}(x)S_{-1}, \quad (\text{C.1.1})$$

is more tedious than complicated. We first express ψ_0 , bearing in mind it is an even function, into two parts: the complementary function, $\psi_{0_{CF}}$, and the particular integral, $\psi_{0_{PI}}$:

$$\psi_{0_{CF}} = A' + B' \cosh(Mx) \cos(Mx) + C' \sinh(Mx) \sin(Mx), \quad (\text{C.1.2})$$

$$\psi_{0_{PI}} = D'x \sinh(Mx) \cos(Mx) + E'x \cosh(Mx) \sin(Mx). \quad (\text{C.1.3})$$

Substituting (C.1.3) into the left of (C.1.1) gives,

$$D^5 \psi_{0_{PI}} + \frac{Ra_S}{\tau} D \psi_{0_{PI}} = - 16D' M^4 \sinh(Mx) \cos(Mx) - 16E' M^4 \cosh(Mx) \sin(Mx). \quad (C.1.4)$$

Similarly we express the right of (C.1.1) using the background state of \overline{w}_o from (2.8.23) giving,

$$-i \frac{Ra_S}{\tau} \overline{w}_o S_{-1} = \frac{i4MS_{-1}Ra_T}{(\sinh M + \sin M)} \left\{ - \cosh(Mx) \sin(Mx) \sinh\left(\frac{M}{2}\right) \cos\left(\frac{M}{2}\right) + \cos(Mx) \sinh(Mx) \sin\left(\frac{M}{2}\right) \cosh\left(\frac{M}{2}\right) \right\}. \quad (C.1.5)$$

Comparing similar terms from (C.1.4) and (C.1.5) we obtain

$$D' = \frac{-i S_{-1} Ra_T \sin \frac{M}{2} \cosh \frac{M}{2}}{4 M^3 (\sin M + \sinh M)}, \quad (C.1.6)$$

and

$$E' = \frac{i S_{-1} Ra_T \sinh \frac{M}{2} \cos \frac{M}{2}}{4 M^3 (\sin M + \sinh M)}. \quad (C.1.7)$$

From the boundary conditions $\psi_0 = \psi_0^i = \psi_0^{iv} = 0$ on $x = \pm \frac{1}{2}$, we get

$$\begin{aligned} \psi_0(\pm 1/2) &= A' + B' \cosh \frac{M}{2} \cos \frac{M}{2} + C' \sinh \frac{M}{2} \sin \frac{M}{2} \\ &+ \psi_{0_{PI}}(\pm 1/2) = 0, \end{aligned} \quad (C.1.8)$$

$$\begin{aligned} \psi_0^i(\pm 1/2) &= B' M \sinh \frac{M}{2} \cos \frac{M}{2} - B' M \cosh \frac{M}{2} \sin \frac{M}{2} \\ &+ C' M \cosh \frac{M}{2} \sin \frac{M}{2} + C' M \sinh \frac{M}{2} \cos \frac{M}{2} \\ &+ \psi_{0_{PI}}^i(\pm 1/2) = 0, \end{aligned} \quad (C.1.9)$$

$$\begin{aligned} \psi_0^{iv}(\pm 1/2) &= -4B' M^4 \cosh \frac{M}{2} \cos \frac{M}{2} - 4C' M^4 \sinh \frac{M}{2} \sin \frac{M}{2} \\ &+ \psi_{0_{PI}}^{iv}(\pm 1/2) = 0, \end{aligned} \quad (C.1.10)$$

where

$$\psi_{0_{PI}}(\pm 1/2) = \frac{D'}{2} \sinh \frac{M}{2} \cos \frac{M}{2} + \frac{E'}{2} \cosh \frac{M}{2} \sin \frac{M}{2}, \quad (\text{C.1.11})$$

$$\begin{aligned} \psi_{0_{PI}}^i(\pm 1/2) &= D' \sinh \frac{M}{2} \cos \frac{M}{2} + \frac{D'}{2} M \cosh \frac{M}{2} \cos \frac{M}{2} \\ &\quad - \frac{D'}{2} M \sinh \frac{M}{2} \sin \frac{M}{2} + E' \cosh \frac{M}{2} \sin \frac{M}{2} \\ &\quad + \frac{E'}{2} M \sinh \frac{M}{2} \sin \frac{M}{2} + \frac{E'}{2} M \cosh \frac{M}{2} \cos \frac{M}{2}, \end{aligned} \quad (\text{C.1.12})$$

and,

$$\begin{aligned} \psi_{0_{PI}}^{iv}(\pm 1/2) &= -8D'M^3 \sinh \frac{M}{2} \sin \frac{M}{2} - 8D'M^3 \cosh \frac{M}{2} \cos \frac{M}{2} \\ &\quad - 2D'M^4 \sinh \frac{M}{2} \cos \frac{M}{2} + 8E'M^3 \cosh \frac{M}{2} \cos \frac{M}{2} \\ &\quad - 8E'M^3 \sinh \frac{M}{2} \sin \frac{M}{2} - 2E'M^4 \cosh \frac{M}{2} \sin \frac{M}{2}. \end{aligned} \quad (\text{C.1.13})$$

Substituting the values of D' and E' into the above gives

$$\psi_{0_{PI}}(\pm 1/2) = 0, \quad (\text{C.1.14})$$

$$\psi_{0_{PI}}^i(\pm 1/2) = \frac{iS_{-1}Ra_T(\sinh M - \sin M)}{16M^2(\sin M + \sinh M)}, \quad (\text{C.1.15})$$

and

$$\psi_{0_{PI}}^{iv}(\pm 1/2) = iS_{-1}Ra_T. \quad (\text{C.1.16})$$

Hence

$$A' = -\frac{\psi_{0_{PI}}^{iv}(\pm 1/2)}{4M^4} = -\frac{iS_{-1}Ra_T}{4M^4}, \quad (\text{C.1.17})$$

$$\begin{aligned} B' &= \frac{\psi_{0_{PI}}^{iv}(\pm 1/2)}{4M^4 \cosh \frac{M}{2} \cos \frac{M}{2}} - \frac{C' \sinh \frac{M}{2} \sin \frac{M}{2}}{\cosh \frac{M}{2} \cos \frac{M}{2}} \\ &= \frac{iS_{-1}Ra_T \left[4(\sinh M + \sin M)^2 - \sinh \frac{M}{2} \sin \frac{M}{2} C_1 \right]}{16M^4(\sinh M + \sin M)^2 \cosh \frac{M}{2} \cos \frac{M}{2}}, \end{aligned} \quad (\text{C.1.18})$$

and

$$\begin{aligned}
C' &= \frac{\psi_{0_{PI}}^{iv}(\pm 1/2) \cosh \frac{M}{2} \sin \frac{M}{2} - \psi_{0_{PI}}^{iv}(\pm 1/2) \sinh \frac{M}{2} \cos \frac{M}{2}}{2M^4(\sinh M + \sin M)} \\
&\quad - \frac{\psi_{0_{PI}}^i(\pm 1/2) 4M^3 \cosh \frac{M}{2} \cos \frac{M}{2}}{2M^4(\sinh M + \sin M)} \\
&= \frac{iS_{-1} Ra_T C_1}{16M^4(\sinh M + \sin M)^2}, \tag{C.1.19}
\end{aligned}$$

where

$$\begin{aligned}
C_1 &= 8 \cos \frac{M}{2} \cosh \frac{M}{2} - 4 \cos \frac{3M}{2} \cosh \frac{M}{2} \\
&\quad + 4 \sin \frac{M}{2} \sinh \frac{3M}{2} - 4 \sin \frac{3M}{2} \sinh \frac{M}{2} \\
&\quad - 4 \cos \frac{M}{2} \cosh \frac{3M}{2} - M \cos \frac{M}{2} \sinh \frac{3M}{2} \\
&\quad - M \cos \frac{M}{2} \sinh \frac{M}{2} + M \sin \frac{3M}{2} \cosh \frac{M}{2} \\
&\quad + M \sin \frac{M}{2} \cosh \frac{M}{2}. \tag{C.1.20}
\end{aligned}$$

C.2 Function $f(Ra_S, \tau)$

In this section we integrate all the terms in the full salinity equation across the slot. One of the contributions is

$$\int_{-1/2}^{1/2} i \alpha D\overline{S}_o \psi_0 dx, \tag{C.2.1}$$

where the function $f(Ra_S, \tau)$ is obtained. We first concentrate on the terms for the background salinity gradient and the leading order ψ_0 . This requires the solution to ψ_0 from (5.2.16) and the background state of $D\overline{S}_o$ from (2.8.22). This contains a series of integrals involving the combinations of hyperbolic and trigonometric expressions giving,

$$\int_{-1/2}^{1/2} D\overline{S}_o \psi_0 dx = \int_{-1/2}^{1/2} \frac{-iS_{-1} Ra_T^2}{4\tau M^4} [\Phi_1 - 2\Phi_2] dx, \tag{C.2.2}$$

where

$$\begin{aligned}\Phi_1 = & A + B \cosh(Mx) \cos(Mx) + C \sinh(Mx) \sin(Mx) \\ & + Dx \sinh(Mx) \cos(Mx) + Ex \cosh(Mx) \sin(Mx), \quad (\text{C.2.3})\end{aligned}$$

and

$$\begin{aligned}\Phi_2 = & \frac{\Phi_1}{\sinh M + \sin M} \left\{ \sin \frac{M}{2} \cosh \frac{M}{2} \sinh(Mx) \sin(Mx) \right. \\ & + \sin \frac{M}{2} \cosh \frac{M}{2} \cosh(Mx) \cos(Mx) \\ & + \sinh \frac{M}{2} \cos \frac{M}{2} \cosh(Mx) \cos(Mx) \\ & \left. - \sinh \frac{M}{2} \cos \frac{M}{2} \sinh(Mx) \sin(Mx) \right\}. \quad (\text{C.2.4})\end{aligned}$$

Hence the required integral gives

$$\begin{aligned}& \int_{-1/2}^{1/2} i \alpha D \bar{S}_o \psi_0 dx \\ = & - \frac{i \alpha \cdot i S_{-1} Ra_T^2}{4\tau M^4} \int_{-1/2}^{1/2} (\Phi_1 - 2\Phi_2) dx \\ = & \frac{\alpha S_{-1} Ra_T^2}{4\tau M^4} f(Ra_S, \tau), \quad (\text{C.2.5})\end{aligned}$$

where

$$\begin{aligned}f(Ra_S, \tau) = & \int_{-1/2}^{1/2} (\Phi_1 - 2\Phi_2) dx \\ = & A + BI_1 + CI_2 + DI_3 + EI_4 \\ & - \frac{2 \sin \frac{M}{2} \cosh \frac{M}{2}}{\sinh M + \sin M} \left\{ \begin{array}{l} AI'_1 + BI'_2 + CI'_3 + DI'_4 + EI'_5 \\ + AI'_6 + BI'_7 + CI'_2 + DI'_8 + EI'_9 \end{array} \right\} \\ & - \frac{2 \sinh \frac{M}{2} \cos \frac{M}{2}}{\sinh M + \sin M} \left\{ \begin{array}{l} AI'_6 + BI'_7 + CI'_2 + DI'_8 + EI'_9 \\ - AI'_1 - BI'_2 - CI'_3 - DI'_4 - EI'_5 \end{array} \right\}, \quad (\text{C.2.6})\end{aligned}$$

The expressions of $I_{1,\dots,4}, I'_{1,\dots,11}$ are given later in this appendix. The corresponding determinants are the same as those expressions already seen in (5.2.17) for A, B, C, D and E which are applied both in this part and the next.

C.3 Function $g(Ra_S, \tau)$

Here we look at the second contribution resulting from the integration of the full salinity equation across the slot and the integral

$$\int_{-1/2}^{1/2} i \alpha \bar{w}_o S_0 dx, \quad (\text{C.3.1})$$

from which the function $g(Ra_S, \tau)$ is obtained. We first consider the background velocity and the leading order S_0 in the integral. This can be rearranged using $D^4\psi_0 + Ra_S DS_0 = 0$ and gives

$$\int_{-1/2}^{1/2} \bar{w}_o S_0 dx = \int_{-1/2}^{1/2} \frac{-1}{Ra_S} (\bar{w}_o D^3\psi_0) dx. \quad (\text{C.3.2})$$

But

$$\begin{aligned} D^3\psi_0 = & i S_{-1} Ra_T \left\{ -2BM^3 \cosh(Mx) \sin(Mx) - 2BM^3 \sinh(Mx) \cos(Mx) \right. \\ & + 2CM^3 \sinh(Mx) \cos(Mx) - 2CM^3 \cosh(Mx) \sin(Mx) \\ & - 6DM^2 \cosh(Mx) \sin(Mx) - 2DM^3 x \sinh(Mx) \sin(Mx) \\ & - 2DM^3 x \cosh(Mx) \cos(Mx) + 6EM^2 \sinh(Mx) \cos(Mx) \\ & \left. + 2EM^3 x \cosh(Mx) \cos(Mx) - 2EM^3 x \sinh(Mx) \sin(Mx) \right\}, \end{aligned} \quad (\text{C.3.3})$$

and

$$\bar{w}_o = \frac{Ra_T (\cosh Mx \sin Mx \sinh \frac{M}{2} \cos \frac{M}{2} - \cos Mx \sinh Mx \sin \frac{M}{2} \cosh \frac{M}{2})}{M^3 (\sin M + \sinh M)}. \quad (\text{C.3.4})$$

We multiply $D^3\psi_0$ with \overline{w}_o and then integrate across the slot. Again this produces a sequence of hyperbolic and trigonometric expressions. These are evaluated to give

$$\begin{aligned} \frac{-1}{Ra_S} \int_{-1/2}^{1/2} \overline{w}_o D^3\psi_0 dx &= \frac{-iS_{-1}Ra_T^2}{Ra_S M^3(\sin M + \sinh M)} \\ &\quad \left[\sinh \frac{M}{2} \cos \frac{M}{2} X_o + \sin \frac{M}{2} \cosh \frac{M}{2} y_o \right], \end{aligned} \quad (C.3.5)$$

where

$$\begin{aligned} X_o &= -2BM^3(I'_{10} + I'_2) + 2CM^3(I'_2 - I'_{10}) \\ &\quad - 6DM^2(I'_{10}) - 2DM^3(I'_5 + I'_9) \\ &\quad + 6EM^2(I'_2) + 2EM^3(I'_9 - I'_5), \end{aligned} \quad (C.3.6)$$

and

$$\begin{aligned} y_o &= 2BM^3(I'_2 + I'_{11}) - 2CM^3(I'_{11} - I'_2) \\ &\quad + 6DM^2(I'_2) + 2DM^3(I'_4 + I'_8) \\ &\quad - 6EM^2(I'_{11}) - 2EM^3(I'_8 - I'_4). \end{aligned} \quad (C.3.7)$$

Hence the required integral gives

$$\begin{aligned} &\int_{-1/2}^{1/2} i \alpha \overline{w}_o S_0 dx \\ &= -\frac{i\alpha \cdot iS_{-1}Ra_T^2 \left[\sinh \frac{M}{2} \cos \frac{M}{2} X_o + \sin \frac{M}{2} \cosh \frac{M}{2} y_o \right]}{Ra_S M^3(\sinh M + \sin M)} \\ &= \frac{\alpha S_{-1} Ra_T^2 g(Ra_S, \tau)}{Ra_S M^3(\sin M + \sinh M)}, \end{aligned} \quad (C.3.8)$$

where

$$g(Ra_S, \tau) = \sinh \frac{M}{2} \cos \frac{M}{2} X_o + \sin \frac{M}{2} \cosh \frac{M}{2} y_o. \quad (C.3.9)$$

Finally the above integrals for $I_{1,\dots,4}$ and $I'_{1,\dots,11}$ are now evaluated as follows:

$$\begin{aligned} I_1 &= \int_{-1/2}^{1/2} \cosh(Mx) \cos(Mx) dx \\ &= \frac{\cosh \frac{M}{2} \sin \frac{M}{2} + \sinh \frac{M}{2} \cos \frac{M}{2}}{M}, \end{aligned} \quad (\text{C.3.10})$$

$$\begin{aligned} I_2 &= \int_{-1/2}^{1/2} \sinh(Mx) \sin(Mx) dx \\ &= \frac{\cosh \frac{M}{2} \sin \frac{M}{2} - \sinh \frac{M}{2} \cos \frac{M}{2}}{M}, \end{aligned} \quad (\text{C.3.11})$$

$$\begin{aligned} I_3 &= \int_{-1/2}^{1/2} x \sinh(Mx) \cos(Mx) dx \\ &= \frac{\cosh \frac{M}{2} \cos \frac{M}{2} + \sinh \frac{M}{2} \sin \frac{M}{2}}{2M} - \frac{\cosh \frac{M}{2} \sin \frac{M}{2}}{M^2}, \end{aligned} \quad (\text{C.3.12})$$

$$\begin{aligned} I_4 &= \int_{-1/2}^{1/2} x \cosh(Mx) \sin(Mx) dx \\ &= \frac{-\cosh \frac{M}{2} \cos \frac{M}{2} + \sinh \frac{M}{2} \sin \frac{M}{2}}{2M} + \frac{\sinh \frac{M}{2} \cos \frac{M}{2}}{M^2}, \end{aligned} \quad (\text{C.3.13})$$

$$\begin{aligned} I'_1 &= \int_{-1/2}^{1/2} \sinh(Mx) \sin(Mx) dx \\ &= \frac{\cosh \frac{M}{2} \sin \frac{M}{2} - \sinh \frac{M}{2} \cos \frac{M}{2}}{M} \\ &= I_2, \end{aligned} \quad (\text{C.3.14})$$

$$\begin{aligned} I'_2 &= \int_{-1/2}^{1/2} \sinh(Mx) \sin(Mx) \cosh(Mx) \cos(Mx) dx \\ &= \frac{\cosh M \sin M - \sinh M \cos M}{8M}, \end{aligned} \quad (\text{C.3.15})$$

$$\begin{aligned} I'_3 &= \int_{-1/2}^{1/2} \sinh^2(Mx) \sin^2(Mx) dx \\ &= -\frac{\cosh M \sin M}{8M} - \frac{\sinh M \cos M}{8M} \\ &\quad + \frac{\sinh M}{4M} - \frac{1}{4} + \frac{\sin M}{4M}, \end{aligned} \quad (\text{C.3.16})$$

$$\begin{aligned}
I'_4 &= \int_{-1/2}^{1/2} x \sinh^2(Mx) \sin(Mx) \cos(Mx) dx \\
&= \frac{\sinh M \sin M - \cosh M \cos M}{16M} + \frac{\sinh \frac{M}{2} \cos \frac{M}{2}}{16M^2} \\
&\quad - \frac{\sin^2 \frac{M}{2}}{4M} + \frac{1}{8M} - \frac{\sin M}{8M^2}, \tag{C.3.17}
\end{aligned}$$

$$\begin{aligned}
I'_5 &= \int_{-1/2}^{1/2} x \sinh(Mx) \cosh(Mx) \sin^2(Mx) dx \\
&= -\frac{\cosh M \cos M - 2 \cosh M + \sinh M \sin M}{16M} \tag{C.3.18}
\end{aligned}$$

$$+ \frac{\cosh M \sin M - 2 \sinh M}{16M^2}, \tag{C.3.19}$$

$$\begin{aligned}
I'_6 &= \int_{-1/2}^{1/2} \cosh(Mx) \cos(Mx) dx \\
&= \frac{\cosh \frac{M}{2} \sin \frac{M}{2} + \sinh \frac{M}{2} \cos \frac{M}{2}}{M} \\
&= I_1, \tag{C.3.20}
\end{aligned}$$

$$\begin{aligned}
I'_7 &= \int_{-1/2}^{1/2} \cosh^2(Mx) \cos^2(Mx) dx \\
&= \frac{\cosh M \sin M + \sinh M \cos M + 2 \sinh M}{8M} \\
&\quad + \frac{\sin M}{4M} + \frac{1}{4}, \tag{C.3.21}
\end{aligned}$$

$$\begin{aligned}
I'_8 &= \int_{-1/2}^{1/2} x \sinh(Mx) \cosh(Mx) \cos^2(Mx) dx \\
&= \frac{\cosh M \cos M + 2 \cosh M + \sinh M \sin M}{16M} \tag{C.3.22}
\end{aligned}$$

$$- \frac{\cosh M \sin M + 2 \sinh M}{16M^2}, \tag{C.3.23}$$

$$I'_9 = \int_{-1/2}^{1/2} x \cosh^2(Mx) \sin(Mx) \cos(Mx) dx$$

$$\begin{aligned}
&= \frac{\sinh M \sin M - \cosh M \cos M}{16M} + \frac{\sinh M \cos M}{16M^2} \\
&\quad + \frac{\sin^2 \frac{M}{2}}{4M} - \frac{1}{8M} + \frac{\sin M}{8M^2}, \tag{C.3.24}
\end{aligned}$$

$$\begin{aligned}
I'_{10} &= \int_{-1/2}^{1/2} \cosh^2(Mx) \sin^2(Mx) dx \\
&= -\frac{\sinh M \cos M}{8M} - \frac{\cosh M \sin M}{8M} \\
&\quad + \frac{\sinh M}{4M} + \frac{1}{4} - \frac{\sin M}{4M}, \tag{C.3.25}
\end{aligned}$$

and,

$$\begin{aligned}
I'_{11} &= \int_{-1/2}^{1/2} \sinh^2(Mx) \cos^2(Mx) dx \\
&= \frac{\sinh M \cos M + \cosh M \sin M + 2 \sinh M}{8M} \\
&\quad - \frac{1}{4} - \frac{\sin M}{4M}. \tag{C.3.26}
\end{aligned}$$

References

- Baines, P.G. & Gill, A.E. 1969 On thermohaline convection with linear gradients. *J. Fluid Mech.* **37**, 289–306.
- Batchelor, G.K. 1954 Heat transfer by free convection across a closed cavity between vertical boundaries at different temperatures. *Quart. J. Appl. Math.* **12**, 209–233.
- Batchelor, G.K. 1967 *An introduction to Fluid Dynamics*. Cambridge University Press.
- Bergholz, R.F. 1978 Instability of steady natural convection in a vertical fluid layer. *J. Fluid Mech.* **84**, 743–768.
- Brandt, A. & Fernando, H.J.S. 1996 *Double-diffusive Convection*. American Geophysical Union.
- Burden, R.L., Faires, J.D. & Reynolds, A.C. 1981 *Numerical Analysis* (second edition). Prindle, Weber & Schmidt.
- Chen, C.F. 1975 Double-diffusive convection in an inclined slot. *J. Fluid Mech.* **72**, 721–729.
- Chen, C.F., Briggs, R.A. & Wirtz, D.G. 1971 Stability of thermal convection in a salinity gradient due to lateral heating. *Intl. J. Heat Mass Transfer* **14**, 57–65.
- Chen, C.F. & Sandford, R.D. 1977 Stability of time-dependent double diffusive convection in an inclined slot. *J. Fluid Mech.* **83**, 83–95.
- Chen, C.F. & Skok, W.W. 1974 Cellular convection in a salinity gradient along a heated inclined wall. *International Journal of Heat and Mass Transfer*, **17**, 51–60.
- Chen, C.F. & Wong, S.B. 1974 Double-diffusive convection along a sloping wall. *Bull. Am. Phys. Soc.* **19**, 1153.
- Chereskin, T.K. & Linden, P.F. 1986 The effect of rotation on intrusions produced by heating a salinity gradient. *Deep-Sea Res.* **33**, 305–322.
- Daniels, P.G. 1987 Convection in a vertical slot. *J. Fluid Mech.* **176**, 419–441.
- Gill, A.E. & Kirkham, C.C. 1970 A note on the stability of convection in a vertical slot. *J. Fluid Mech.* **42**, 125.
- Hart, J.E. 1971 On sideways diffusive instability. *J. Fluid Mech.* **49**, 279–288.

- Hart, J.E. 1973 Finite amplitude sideways diffusive convection. *J. Fluid Mech.* **59**, 47–64.
- Holyer, J.Y. 1983 Double-diffusive interleaving due to horizontal gradients. *J. Fluid Mech.* **137**, 347–362.
- Holyer, J.Y., Jones, T.J., Priestly, M.G. & Williams, N.J. 1987 The effect of vertical temperature and salinity gradients on double-diffusive interleaving. *Deep-Sea Res.* **34**, 517–530.
- Huppert, H.E. 1990 The fluid mechanics of solidification. *J. Fluid Mech.* **212**, 209–240.
- Huppert, H.E. & Josberger, E.G. 1980 The melting of ice in cold stratified water. *Journal of Physical Oceanography* **10**, 953–969.
- Huppert, H.E., Kerr, R.C. & Hallworth, M.A. 1984 Heating or cooling a stable compositional gradient from side. *International Journal of Heat and Mass Transfer.* **27**, 1395–1401.
- Huppert, H.E. & Turner, J.S. 1980 Ice blocks melting into a salinity gradient. *J. Fluid Mech.* **100**, 367–384.
- Huppert, H.E. & Turner, J.S. 1981 Double-diffusive convection. *J. Fluid Mech.* **106**, 299–329.
- Jevons, W.S. 1857 On the cirrous form of cloud. London, Edinburgh, Dublin *Philos. Mag. J. Sci. Ser. 4*, **14**, 22–35.
- Kerr, O.S. 1989 Heating a salinity gradient from a vertical sidewall: linear theory. *J. Fluid Mech.* **207**, 323–352.
- Kerr, O.S. 1990 Heating a salinity gradient from a vertical sidewall: non-linear theory. *J. Fluid Mech.* **217**, 529–546.
- Kerr, O.S. 1991 Double-diffusive instabilities at a sloping boundary. *J. Fluid Mech.* **225**, 333–354.
- Kerr, O.S. 1995 The effect of rotation on double-diffusive convection in a laterally heated vertical slot. *J. Fluid Mech.* **301**, 345–370.
- Kerr, O.S. 1996 Double-diffusive instabilities at a vertical boundary. In *Double-Diffusive Convection* (ed. A. Brandt & J. Fernando) American Geophysical Union, 105–113.
- Korpela, S.A., Gözüüm, D. & Baxi, C.B. 1973 On the stability of the conduction regime of natural convection in a vertical slot. *Int. J. Heat Mass Transfer* **16**, 1683–1690.

- Linden, P.F. 1974 Salt fingers in a steady shear flow. *Geophys. Fluid Dyn.* **6**, 1–27.
- Linden, P.F. & Weber, J.E. 1977 The formation of layers in a double diffusive system with a sloping boundary. *J. Fluid Mech.* **81**, 757–773.
- McDougall, T.J. 1985 Double-diffusive interleaving I. Linear stability analysis. *J. Phys. Oceanogr.* **15**, 1532–1541.
- Mizushima, J. & Gotoh, K. 1976 The stability of natural convection in a vertical fluid layer. *J. Fluid Mech.* **73**, 65–75.
- Narusawa, J., & Suzukawa, Y. 1981 Experimental study of double-diffusive cellular convection due to a uniform lateral heat flux. *J. Fluid Mech.* **113**, 387–405.
- Nield, D.A. 1967 The thermohaline Rayleigh-Jeffreys problem. *J. Fluid Mech.* **29**, 545–558.
- Niino, H. 1986 A linear theory of double-diffusive horizontal intrusions in a temperature-salinity front. *J. Fluid Mech.* **171**, 71–100.
- Paliwal, R.C. 1979 Double-diffusive convective instability in an inclined fluid layer, Ph.D. thesis, Department of Mechanical, Industrial and Aerospace Engineering, Rutgers University.
- Paliwal, R.C. & Chen, C.F. 1980 Double-diffusive instability in an inclined fluid layer. Part 1. Experimental investigations. *J. Fluid Mech.* **98**, 755–768.
- Paliwal, R.C. & Chen, C.F. 1980 Double-diffusive instability in an inclined fluid layer. Part 2. Stability analysis. *J. Fluid Mech.* **98**, 769–785.
- Rayleigh, Lord 1883 Investigation of the character of the equilibrium of an incompressible heavy fluid of variable density. *Proc. London Math. Soc.* **14**, 170–177.
- Ruddick, B.R. 1992 Intrusive mixing in a Mediterranean salt lens: intrusion slopes and dynamical mechanisms. *J. Phys. Oceanogr.*, **22**, 1274–1285.
- Ruddick, E.R. & Turner, J.S. 1979 The vertical length scale of double-diffusive intrusions. *Deep-Sea Res.* **26A**, 903–913.
- Schladow, S.G., Thomas, E. & Koseff, J.R. 1992 The dynamics of intrusions into a thermohaline stratification. *J. Fluid Mech.* **236**, 127–165.
- Schmitt, R.W. 1994 Double Diffusion in Oceanography. *Annu. Rev. Fluid Mech.* **26**, 255–285.

- Stern, M.E. 1960 The 'salt fountain' and thermohaline convection. *Tellus*. **12**, 172-175.
- Stern, M.E. 1967 Lateral mixing of water masses. *Deep-Sea Res.* **14**, 747-753.
- Stommel, H., Arons, A.B. & Blanchard, D. 1956 An oceanographical curiosity: the perpetual salt fountain. *Deep-Sea Res.* **3**, 152-153.
- Tait, R.I. & Howe, M.R. 1968 Some observations of thermohaline stratification in the deep ocean. *Deep-Sea Res.* **15**, 275-280.
- Tait, R.I. & Howe, M.R. 1971 Thermohaline staircase. *Nature*, **231**, 178-179.
- Tanny, J. & Tsinober, A.B. 1988 The dynamics and structure of double-diffusive layers in sidewall-heating experiments. *J. Fluid Mech.* **196**, 135-156.
- Tanny, J. & Tsinober, A.B. 1989 On the behaviour of a system of double diffusive layers during its evolution. *Phys. Fluids A* **1**, 606-609.
- Thangam, S., Zebib, A. & Chen, C.F. 1981 Transition from shear to sideways diffusive instability in a vertical slot. *J. Fluid Mech.* **112**, 151-160.
- Thorpe, S.A., Hutt, P.K. & Soulsby, R. 1969 The effects of horizontal gradients on thermohaline convection. *J. Fluid Mech.* **38**, 375-400.
- Turner, J.S. 1974 Double-diffusive phenomena. *Annu. Rev. Fluid Mech.* **6**, 37-56.
- Toole, J.M. & Georgi, D.T. 1981 On the dynamics and effects of double-diffusively driven intrusions. *Prog. Oceanogr.* **10**, 123-145.
- Turner, J.S. & Chen, C.F. 1974 Two-dimensional effects in double-diffusive convection. *J. Fluid Mech.* **63**, 577-592.
- Veronis, G. 1965 On finite amplitude instability in thermohaline convection. *J. Mar. Res.* **23**, 1-17.
- Vest, C.M. & Arapci, V.A. 1969 Stability of natural convection in a vertical slot. *J. Fluid Mech.* **36**, 1-15.
- Walin, G. 1964 Note on the stability of water stratified by both salt and heat. *Tellus*. **16**, 389-393.
- Walsh, D. & Ruddick, B. 1994 Double-diffusive interleaving: the influence of non-constant diffusivities. *J. Phys. Oceanogr.* **25**, 348-358.

- Williams, A.J. 1974 Salt fingers observed in the Mediterranean outflow. *Science* **185**, 941–943.
- Williams, A.J. 1981 The role of double-diffusion in a Gulf Stream frontal intrusion. *Journal of Geophysical Research* **86**, 1917–1928.
- Yoshida, J., Nagashima, H. & Niino, H. 1989 The behaviour of double-diffusive intrusions in a rotating system. *J. Geo-phys. Res.* **94**, 4923–4937.
- Young, Y. & Rosner, R. 1998 Linear and weakly nonlinear analysis of doubly-diffusive vertical slot convection. *Phys. Rev. E* **57**, 5554–5563.